

---

# **Development and Function of Monoaminergic Systems in the Brain of Zebrafish**

-  
Entwicklung und Funktion monoaminerger Systeme im  
Zebrafischgehirn

---



Doctoral Thesis for a Doctoral Degree  
at the Graduate School of Life Sciences,  
Julius-Maximilians University Würzburg,  
Section: Neuroscience

submitted by

**Isabel Reuter**

from  
Saarburg

Würzburg 2019



Submitted on:

-----  
*Office stamp*

Date of Public Defense:

-----

Date of Receipt of Certificates:

-----

### **Members of the Thesis Committee:**

Chairperson:

**Prof. Dr. Manfred Gessler**

*Department of Developmental Biochemistry  
Biocentre  
University of Würzburg*

Primary supervisor:

**Prof. Dr. Klaus-Peter Lesch**

*Department of Molecular Psychiatry  
Centre for Mental Health  
University Hospital of Würzburg*

2<sup>nd</sup> supervisor:

**Prof. Dr. Dr. Manfred Scharl**

*Department of Physiological Chemistry  
Biocentre  
University of Würzburg*

3<sup>rd</sup> supervisor:

**Prof. Dr. Marcel Romanos**

*Department of Child and Adolescent Psychiatry  
Centre for Mental Health  
University Hospital of Würzburg*

4<sup>th</sup> supervisor:

**Dr. Christina Lillesaar**

*Department of Child and Adolescent Psychiatry  
Centre for Mental Health  
University Hospital of Würzburg*



---

## Table of contents

<b>TABLE OF CONTENTS</b>	<b>1</b>
<b>SUMMARY [EN]</b>	<b>5</b>
<b>ZUSAMMENFASSUNG [GER]</b>	<b>7</b>
<b>INTRODUCTION</b>	<b>10</b>
Part one – Establishing the early zebrafish CNS	10
<i>Gastrulation</i>	10
<i>Neural induction and neurulation</i>	12
<i>Longitudinal zones and the prosomeric model of neural tube development</i>	14
<i>Neurogenesis</i>	17
Part two – Development and neuroanatomical comparisons of the hypothalamus	21
Part three – Development of the monoaminergic system in the CNS of zebrafish	27
<i>Functions, behaviours and evolution of monoamines</i>	27
<i>Whole genome duplication in the context of 5-HT and DA metabolism</i>	28
<i>Wired and volume transmission</i>	30
<i>Neuroanatomical distribution of serotonergic and dopaminergic cell clusters</i>	34
<i>Dopaminergic and serotonergic gene regulatory networks</i>	36
<i>Cerebrospinal fluid-contacting cells and hypothalamic serotonergic clusters</i>	40
<i>The Fgf-signalling pathway and the ligand Fgf3</i>	42
<b>AIMS OF THE THESIS</b>	<b>46</b>
<b>MATERIALS AND METHODS</b>	<b>49</b>
Fish husbandry and embryo preparation	49
Genotyping	49
<i>fgf3</i> and <i>tph1a</i> impairment strategies	50
Labelling proliferating cells in S phase	55
Cell death assays	56

---

Immunohistochemistry	57
Whole-mount RNA <i>in situ</i> hybridisation	58
Cryosections	59
3D structural protein models of Fgf3	60
Sample preparation, RNA library generation and analysis of the hypothalamic transcriptome	60
Imaging, measurements, cell quantifications and figure preparation	63
Statistical analysis	64
<b>RESULTS</b>	<b>65</b>
Characterisation of <i>fgf3</i> expression and impact on <i>etv5b</i> in the hypothalamus	65
Fgf3 regulates caudal hypothalamic monoaminergic CSF-c cell development	70
Neuroendocrine cells expressing <i>avp</i> depend on Fgf3 whereas neuroendocrine cells expressing <i>oxl</i> and <i>cort</i> do not	80
Impairment of <i>fgf3</i> leads to a smaller hypothalamus	83
Fgf3 ensures proliferation, survival and serotonergic lineage commitment of caudal hypothalamic cells	87
Impaired Fgf3 isoforms of mutants and morphants are probably still able to interact with Fgf receptors	92
The analysed genes of the hypothalamic transcriptome display small expression alterations after <i>fgf3</i> impairment	93
<i>tph1a</i> impairment strategies to explore the function of serotonergic CSF-c cells in the hypothalamus	98
<b>SUMMARY CHART OF RESULTS</b>	<b>103</b>
<b>DISCUSSION</b>	<b>104</b>
Caudal hypothalamic Fgf3 regulates the expression of the ETS-domain transcription factor <i>etv5b</i> in the developing hypothalamus	104
Monoaminergic CSF-c and <i>avp</i> expressing cells of the caudal hypothalamus are highly dependent on Fgf3 activity	107
Fgf3 regulates the proliferation of serotonergic progenitors in the caudal hypothalamus	112
Assessing the effects of the three <i>fgf3</i> impairment strategies on Fgf3 activity in the hypothalamus	114

---

First steps toward understanding the functions of serotonergic CSF-c cells of the hypothalamus	117
<b>CONCLUSION</b>	<b>119</b>
<b>REFERENCES</b>	<b>122</b>
<b>APPENDIX</b>	<b>134</b>
Abbreviations	134
Recipes and protocols	136
<i>Solutions and buffers</i>	136
<i>Genotyping by PCR</i>	139
<i>Injections</i>	140
<i>Morpholino validation</i>	141
<i>CRISPR/Cas9 strategy</i>	144
<i>BrdU labelling</i>	161
<i>Acridine Orange staining</i>	162
<i>Immunohistochemistry</i>	163
<i>DIG/fluor labelling of RNA probe for in situ hybridisation</i>	168
<i>Whole-mount RNA in situ hybridisation</i>	170
<i>Cryosections</i>	175
<i>Sample preparation for RNA sequencing</i>	177
Publication list	178
Curriculum Vitae	179
Acknowledgement/ Danksagung [ger]	182
Affidavit [en]	184
Eidesstattliche Erklärung [ger]	184

---

*A considerable part of the results of the presented work has been published in Reuter et al. (2019).*

---



## Summary [en]

This thesis explores the development of monoaminergic systems in the central nervous system (CNS) of zebrafish. The serotonergic cells of the hypothalamus pose the main focus of the present work. Most vertebrates except for mammals possess serotonin (5-HT) synthesising cells in more than one region of the CNS. In zebrafish such regions are, e.g. the hypothalamus, the raphe nuclei and the spinal cord. Serotonin functions as a neurotransmitter and neuromodulator in the CNS. Presumably due to its neuromodulatory tasks hypothalamic serotonergic cells are in contact with the cerebrospinal fluid (CSF), which expands the field of potential serotonergic targets tremendously. This highlights that serotonergic CSF-contacting (CSF-c) cells are vital for the execution of many functions and behaviours. Further, the hypothalamic serotonergic clusters constitute the largest population of serotonergic cells in the CNS of zebrafish. Together, these facts emphasise the need to understand the development and function of serotonergic CSF-c cells in the hypothalamus. Few studies have dealt with this subject, hence, information about the development of these cells is scarce. The zinc-finger transcription factor *fezf2*, and Fibroblast growth factor (Fgf)-signalling via the ETS-domain transcription factor *etv5b* are known to regulate serotonergic cell development in the hypothalamus (Bosco et al., 2013; Rink and Guo, 2004). However, the main Fgf ligand responsible for this mediation has not been determined prior to this work. The present thesis identifies Fgf3 as a crucial Fgf ligand. To achieve this result three independent strategies to impair Fgf3 activity have been applied to zebrafish embryos: the *fgf3*<sup>t24152</sup> mutant, an *fgf3* morpholino-based knock-down and the CRISPR/Cas9 technique. The investigations show that Fgf3 regulates the development of monoaminergic CSF-c cells in the hypothalamus. Additionally, Fgf3 impacts on cells expressing the peptide hormone *arginine vasopressin* (*avp*). Most interestingly, the requirement for Fgf3 by these cells follows a caudo-rostral gradient with a higher dependence on Fgf3 by caudal cells. This also seems to be the case for dopaminergic

---

CSF-c cells in the hypothalamus (Koch et al., 2014). Moreover, *etv5b* a downstream target of Fgf-signalling is demonstrated to be under the control of Fgf3. With regard to serotonergic CSF-c cell development, it is shown that *fgf3* is expressed several hours before *tph1a* and 5-HT (Bellipanni et al., 2002; Bosco et al., 2013). Together with the result that the hypothalamus is already smaller before mature serotonergic CSF-c cells appear, this argues for an early impact of Fgf3 on serotonergic specification. This hypothesis is supported by several findings in this study: the universal decrease of proliferating cells in the hypothalamus and simultaneous increase of cell death after *fgf3* impairment. Complementary cell fate experiments confirm that proliferating serotonergic progenitors need Fgf3 to commit serotonergic specification. Further, these results corroborate findings of an earlier study stating that hypothalamic serotonergic progenitors require Fgf-signalling via *etv5b* to maintain the progenitor pool (Bosco et al., 2013). Additionally, the transcriptome of the hypothalamus has been analysed and 13 previously overlooked transcripts of Fgf ligands are expressed at developmental stages. The transcriptome analysis provides evidence for a self-compensatory mechanism of *fgf3* since expression of *fgf3* is upregulated as a consequence of its own impairment. Moreover, the Fgf-signalling pathway appears to be mildly affected by *fgf3* manipulation. Together, Fgf-signalling and especially Fgf3 are established to be of critical importance during hypothalamic development with effects on serotonergic, dopaminergic CSF-c and *avp* expressing cells. Furthermore, this thesis provides two strategies to impair the *tph1a* gene. Both strategies will facilitate investigations regarding the function of hypothalamic serotonergic CSF-c cells. Finally, the presented findings in this study provide insights into the emergence of the posterior recess region of the hypothalamus, thereby, contributing to the understanding of the evolution of the vertebrate hypothalamus.

---

## Zusammenfassung [ger]

Die vorliegende Dissertation untersucht die Entwicklung und Funktion monoaminerger Systeme im Zebrafischgehirn. Hierzu konzentriert sich die Studie hauptsächlich auf die serotonergen Zellen des Hypothalamus. Die meisten Vertebraten, außer Säugetiere, besitzen Serotonin (5-HT)-synthetisierende Zellen in mehr als einer Region im zentralen Nervensystem (ZNS). Solche Zellen lassen sich in Zebrafischen unter anderem im Hypothalamus, den Raphe Kernen und dem Rückenmark finden. Im ZNS agiert 5-HT als Neurotransmitter und als Neuromodulator. Es wird vermutet, dass, aufgrund der neuromodulatorischen Aufgaben des 5-HT, serotonerge Zellen mit ihren Vorsätzen mit der Cerebrospinalflüssigkeit (CSF) in Kontakt stehen, wodurch der Wirkungsbereich dieser Zellen enorm vergrößert wird. Dies betont den weitläufigen Einfluss serotonerger CSF-kontaktierender (CSF-k) Zellen auf vielfältige Funktionen und Verhalten. Zudem bilden serotonerge Zellen des Hypothalamus die größte serotonerge Zellpopulation im ZNS des Zebrafisches. Zusammengefasst heben diese Fakten die Notwendigkeit hervor, die Entwicklung und die Funktion serotonerger Zellen im Hypothalamus genauer zu verstehen. Nur wenige Studien haben sich dieser Thematik bisher angenommen, weshalb Erkenntnisse über diese Zellen rar sind. Bereits bekannt ist, dass der Zinkfinger-Transkriptionsfaktor *fezf2* und der Fibroblasten-Wachstumsfaktor (Fgf)-Signaltransduktionsweg über den ETS-Domäne-Transkriptionsfaktor *etv5b* Einfluss auf die Entwicklung serotonerger CSF-k Zellen des Hypothalamus nehmen (Bosco et al., 2013; Rink and Guo, 2004). Allerdings ist der Fgf-Ligand, der die Entwicklung serotonerger CSF-k Zellen reguliert, noch nicht bekannt. Die vorliegende Arbeit identifiziert Fgf3 als einen Schlüsselliganden in diesem Zusammenhang. Hierfür wurden drei unabhängige Strategien zur Beeinträchtigung der Fgf3-Aktivität in Zebrafischembryos angewendet: die *fgf3*<sup>t24152</sup> Mutante, ein Morpholino-basierter *fgf3* Gen-Knockdown und die CRISPR/Cas9-Methodik. Die

---

durchgeführten Untersuchungen zeigen, dass Fgf3 die Entwicklung monoaminerger CSF-k Zellen des Hypothalamus maßgeblich reguliert. Zusätzlich beeinflusst Fgf3 auch die Genexpression des Peptidhormons *arginine vasopressin (avp)* in dieser Region. Interessanterweise sind caudale *avp* exprimierende Zellen abhängiger von Fgf3 als rostrale. Dies scheint auch der Fall für dopaminerge Zellpopulationen des Hypothalamus zu sein (Koch et al., 2014). Des Weiteren wird demonstriert, dass Fgf3 über den Fgf-Signalweg die Expression von *etv5b* kontrolliert. Bezüglich der Entwicklung serotonerger CSF-k Zellen wird gezeigt, dass die *fgf3* Expression bereits einige Stunden vor *tph1a* und 5-HT im caudalen Hypothalamus vorhanden ist (Bellipanni et al., 2002; Bosco et al., 2013). Zusammen mit dem Ergebnis, dass die *nkx2.4b* Expressionsdomäne, die zur Kenntlichmachung des Hypothalamus verwendet wurde, ebenfalls in früheren Entwicklungsstadien eine verringerte Größe aufweist, führt dies zu der Annahme, dass Fgf3 Auswirkungen auf die serotonerge Zellspezifikation hat. Diese Hypothese wird durch folgende Beobachtungen in dieser Arbeit unterstützt: Proliferierende Zellen des gesamten caudalen Hypothalamus sind mehrheitlich reduziert nachdem *fgf3* beeinträchtigt wurde, gleichzeitig ist der Zelltod erhöht. Des Weiteren wird gezeigt, dass serotonerge Vorläuferzellen Fgf3 benötigen, um einer serotonergen Spezialisierung zu folgen. Die beschriebenen Beobachtungen untermauern die Ergebnisse einer früheren Studie, wonach der Fgf-Signalweg und *etv5b* wichtige Rollen für die Erhaltung der Proliferation von serotonergen Vorläuferzellen einnehmen (Bosco et al., 2013). Zusätzlich werden durch die durchgeführte Transkriptomanalyse 13 zuvor übersehene Fgf Liganden identifiziert, die im Hypothalamus exprimiert werden. Die Transkriptomanalyse zeigt zudem, dass die Beeinträchtigung von *fgf3* zu einer Zunahme der *fgf3* Transkript Anzahl führt, weshalb ein Selbstkompensationsmechanismus von *fgf3* vorzuliegen scheint. Komponenten des Fgf-Signalweges unterliegen geringen Veränderungen nach der Manipulation von *fgf3*. Zusammenfassend wird in dieser Dissertation der Ligand Fgf3 als essentieller Faktor für die Entwicklung des Hypothalamus etabliert. Dies wird durch die Fgf3 Abhängigkeit von serotonergen, dopaminergen CSF-k und *avp*

---

exprimierenden Zellen in dieser Region bestätigt. Des Weiteren werden in dieser Arbeit zwei Strategien für die Beeinträchtigung von *tph1a* präsentiert, die Untersuchungen bezüglich der Funktion serotonerger CSF-k Zellen des Hypothalamus ermöglichen. Abschließend erlauben die Ergebnisse neue Einblicke in die Entwicklung der Region um den posterioren Ventrikelrezess des Hypothalamus. Dies trägt dazu bei, das Verständnis über die Evolution des Hypothalamus von Vertebraten zu erweitern.

---

## Introduction

### Part one – Establishing the early zebrafish CNS

#### Gastrulation

Embryogenesis is a process largely conserved in vertebrate evolution. It follows an array of well-timed positional cues that determine the brain bauplan of each species (Vernier, 2017). Embryogenesis can be subdivided into cleavage, blastula phase, gastrulation, neurulation, somitogenesis and organogenesis. On a microscopic scale, however, species-specific differences exist and their impact becomes more prominent as embryogenesis advances (Lupo et al., 2006; Muñoz-Sanjuán and Brivanlou, 2002; Stern, 2005; Wilson and Edlund, 2001). For the purpose of understanding the hypothalamic development in zebrafish, the following paragraphs focus entirely on zebrafish embryogenesis. Physiology and morphology of the adult hypothalamus are described, and neuroanatomical comparisons of the adult hypothalamus are drawn between teleosts and other vertebrates or invertebrates.

During zebrafish development the process of gastrulation leads to the generation of primary germ layers and the embryonic axis by four morphogenetic cell movements termed epiboly, involution, convergence and extension (Fig. 1; Webb and Miller, 2006). The first cell movement is epiboly, which has already started at blastula stages when the embryo consisted of four parts – yolk, yolk syncytial layer, deep cell layer and enveloping cell layer (Webb and Miller, 2006). Epiboly describes the continuous spreading of the three cell populations surrounding the yolk toward the vegetal pole. Upon reaching the embryonic equator marking the 50% epiboly stage gastrulation commences, which includes the three types of morphogenetic cell movements mentioned above (Fig. 1A). At the beginning of gastrulation the primary germ layers – ectoderm (Woo and Fraser, 1995), endoderm and mesoderm (Warga and Nüsslein-

---

Volhard, 1999) – start developing from the deep cells (Webb and Miller, 2006). The deep cells are sandwiched between the enveloping cell layer on the outside and the yolk syncytial layer on the inside of the blastoderm. The first time deep cells internalise, they form the germ ring, thereby, generating the epiblast (later ectoderm) on the outside and the hypoblast (later mesoderm and endoderm) on the inside of the embryo (Kimmel et al., 1990) (Fig. 1A). Together with the germ ring the shield appears marking the future dorsal side of the embryo (Fig. 1B). The shield acts as the dorsal axis organiser, a primary organiser of embryogenesis playing a pivotal role in neural induction and patterning. It leads involuted cells to migrate anterior-ward by convergence and extension movements (Webb and Miller, 2006; Woo and Fraser, 1995). The dorsal axis organiser or shield in fish has varying names depending on the species. For example, in amphibians this structure is called the Spemann-Mangold organiser after the researchers who first discovered its function. The Spemann-Mangold organiser denotes the dorsal lip of the blastopore in amphibians (Spemann and Mangold, 1924). In birds, reptiles and mammals the equivalent is termed the primitive node, however, in birds the organiser can also be called Hensen's node, after the researcher who first described it in birds (Boettger et al., 2001).

At the shield stage the neural plate is induced from cells of the thin dorsal epiblast cell layer, which start converging to the dorsal midline where they become neural progenitors (Woo and Fraser, 1995). By the 90% epiboly stage most of these cells have converged to the dorsal midline where the neural plate is manifesting throughout the bud stage, which concludes gastrulation (Fig. 1C) (Araya et al., 2016; Concha and Adams, 1998; Webb and Miller, 2006).

---

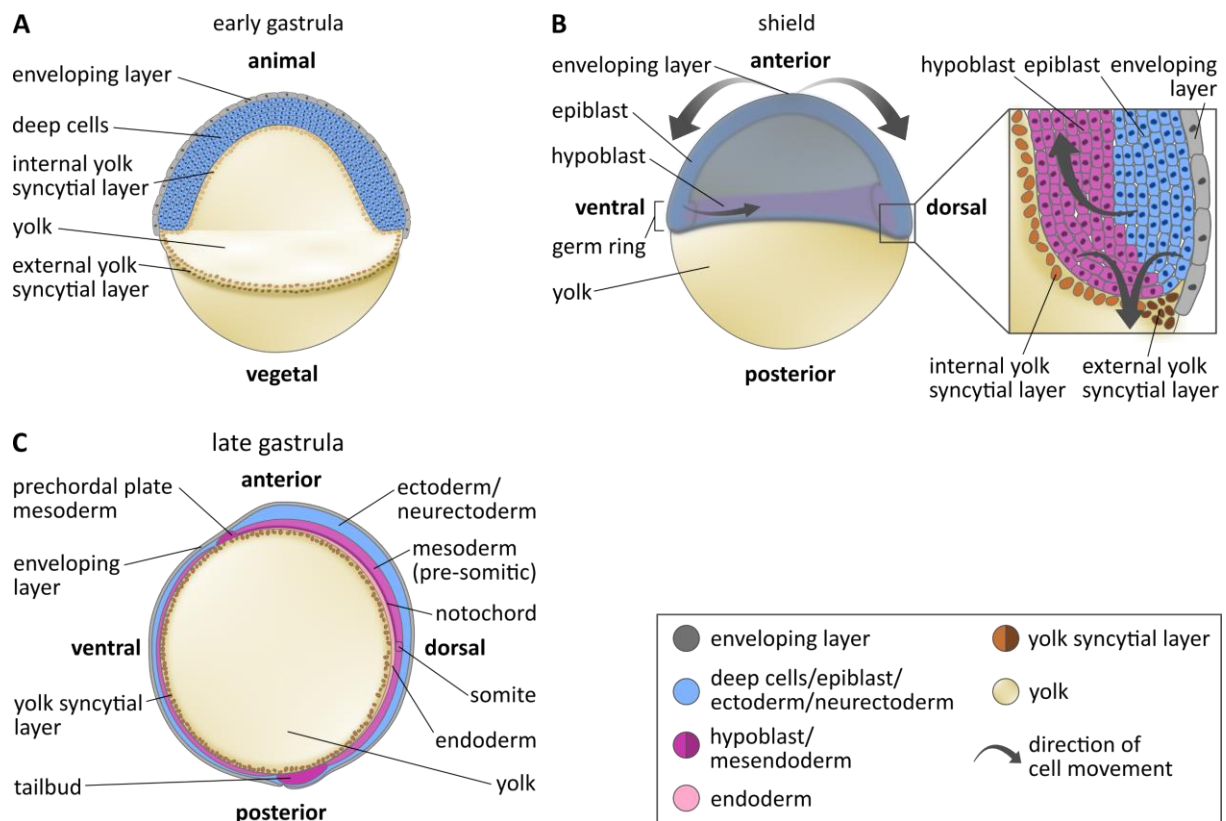


**Fig. 1: Gastrulation of the zebrafish embryo.** Depicted are schemes of early gastrula (**A**, partial sagittal section), shield (**B**, side view) and late gastrula stages (**C**, sagittal section). The enveloping layer in **B** is depicted as transparent grey layer to fully visualise interior structures. The arrows pointing toward posterior outline the direction of epibolic cell movements by enveloping cells. The arrow pointing toward dorsal shows the direction epiblast cells converge. Magnification in **B** shows a sagittal view of the shield area. Here, the arrow pointing toward anterior depicts the direction epiblast cells convolute and ingress to form the hypoblast combined with the direction of extension of the hypoblast. The arrows pointing toward posterior highlight the direction of extension of non-convoluting epiblast and hypoblast cells. Based on Gilbert (2014), Keller et al. (2008) and Kimmel et al. (1991).

## Neural induction and neurulation

Concomitant with the onset of somitogenesis, the early phase of neurulation starts at 10 hours post fertilisation (hpf) in zebrafish (Araya et al., 2016; Lowery and Sive, 2004; Woo and Fraser, 1995). During the neurulation process the neural plate progenitors located most medially are first folding inward forming the neural keel (~13 hpf), thereby, adopting a ventral fate. Only after the medially located cells have involuted, the more laterally located neural plate progenitors converge to the dorsal midline



where they involute as well. Thereby, these cells adopt a dorsal fate marking the generation of the neural rod (~15-17 hpf). After this initial process of dorso-ventral patterning the neural tube manifests and closes completely by 18 hpf.

The process of neural induction at the beginning of neurulation can be explained by two models. The default model of neural induction (Muñoz-Sanjuán and Brivanlou, 2002) states that cells of the epiblast will always adopt a neural fate by default unless Bone morphogenic proteins (Bmps) are present to promote an ectodermal fate instead (Wilson and Houart, 2004). Bmp antagonists (e.g. Chordin, Follistatin, Noggin) are secreted during gastrulation by the shield and later on by shield-derived prechordal plate mesoderm, which is located underneath the neural plate (Fig. 2A). Thus, Bmp antagonists ensure the maintenance of low levels of Bmps in the neural plate region. According to the two-signal-model, first, the ectoderm develops into the anterior-most neural tissues during the activation step followed by the transformation step, which leads to the generation of posterior neural tissues (Nieuwkoop, 1952). However, neural induction is a complex process of possibly undefinable starting point reflecting a continuum of events. Thus, already at blastula stages Fgf and Wingless-related integration site (Wnt)-signalling in the medial and lateral epiblast may instruct prospective neural and epidermal cells, respectively, of their fates (Delaune et al., 2005; Stern, 2005; Streit and Stern, 1999; Wilson and Edlund, 2001; Wilson et al., 2000). After the neural plate is induced, the anterior-posterior axis is specified in two steps (Fig. 2B,C): firstly, at early gastrulation Wnt and Fgf signals inhibit anteriorising, head-specifying signals (e.g. *otx2*, *cyp2*) in the posterior neural plate; secondly, at late gastrulation the accumulation of retinoic acid activates posteriorising genes (e.g. *hoxb1*). Thereby, head specifying signals are further confined to their final anterior position in the embryo while posteriorisation continues (Gilbert, 2014; Koshida et al., 2002; Kudoh et al., 2002).

---

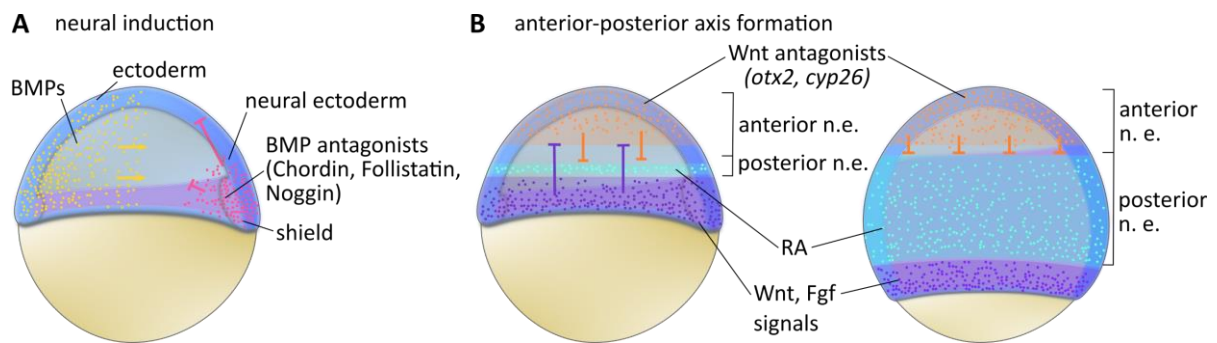


**Fig. 2: Neural induction and anterior-posterior axis formation.** **A** Neural ectoderm is induced by Bmp antagonists (Chordin, Follistatin, Noggin) (pink) expressed by the shield and later shield-derived prechordal plate. Bmp antagonists migrate anterior-ward. Thereby, Bmps (yellow) from the ectoderm are inhibited. **B** Anterior-posterior axis formation of neural ectoderm at shield (left) and 90% epiboly (right) stages. At the shield stage Wnt and Fgf signals (purple) inhibit anteriorising, head-specifying Wnt antagonists (*otx2*, *cyp26*) (orange) confining them anteriorly. Additionally, Wnt antagonists inhibit retinoic acid signalling (RA, light blue), thereby, the growth of posterior neural ectoderm. At 90% epiboly the embryonic margin has migrated further posteriorly enabling retinoic acid expression in the neural ectoderm, in turn, activating posteriorising genes. n.e., neural ectoderm. Modified from Gilbert (2014).

### Longitudinal zones and the prosomeric model of neural tube development

By the time the neural tube closes a hollow lumen has been generated. The lumen is filled with CSF and constitutes the first rudiment of the ventricular system of the CNS. Meanwhile, the neural tube develops longitudinal zones and at its most anterior position where the brain manifests also transverse zones (Mueller and Wullimann, 2015; Puelles and Rubenstein, 2003). The longitudinal zones – floor, basal, alar and roof plate – have been described by His in 1888 and range from the ventral to the dorsal neural tube, respectively. Floor and roof plates constitute secondary signalling centres. The floor plate is induced by Sonic hedgehog (Shh)-signalling from the notochord (Strähle et al., 2004) whereas the roof plate receives BMP-signalling from the ectoderm/epidermis (Araya et al., 2016; Beccari et al., 2013). After induction, both plates maintain their respective Shh or Bmp morphogen signalling activity. As a consequence, Shh- and Bmp-signalling gradients establish throughout the basal and alar plates, respectively. The fact that Shh and Bmp signals are received in a time- and

concentration-dependent manner results on the one hand in the differential expression of transcription factors (Beccari et al., 2013). On the other hand, it results in the activation of specific combinations of transcription factors. By this regionalisation process distinct dorso-ventral neuronal cell types are generated. Ventral interneurons and motor neurons both relay motor output and dorsal interneurons relay sensory information (Briscoe and Ericson, 1999).

After neural tube closure, the anterior-most neurectoderm enlarges to form three initially balloon-shaped morphogenetic units called neuromeres – the prosencephalon, the mesencephalon and the rhombencephalon (Vernier, 2017). These three neuromeres are each subdivided dorso-ventrally into longitudinal zones. With the introduction of the prosomeric model by Puelles and Rubenstein (1993; 2003; 2015) an additional antero-posterior subdivision into transverse zones is proposed (Fig. 3). These zones are called neuromeres and can be subdivided according to their neuroanatomical position into prosomeres, mesomeres and rhombomeres. A rudimentary neuromeric model has already been described by Orr (1887). The modern version of the prosomeric model stresses particularly how the basal-alar plate boundary is defined and proceeds in the prosencephalon. Consequently, this entails changes to the neuroanatomical classification of prosencephalic structures. According to the modern prosomeric model, the prosencephalon is subdivided into four transverse zones: prosomeres 1-3 constituting the diencephalon, and the secondary prosencephalon comprising telencephalon, optic recess region and hypothalamus (Affaticati et al., 2015). Each transverse zone consists, dorso-ventrally, of all four longitudinal zones. Further, the prosomeric model defines the hypothalamus as the basal (and floor) complement to the alar (and roof) positioned telencephalon and optic recess region. The views of the prosomeric model, particularly, the deflection of the neural axis in the prosencephalon and the resulting shift of the basal-alar boundary challenge the views of the previously established columnar model, first proposed by Herrick (1910). Therein, the hypothalamus has been regarded as the ventral part of the diencephalon (Kuhlenbeck, 1973; Puelles, 2019). The re-introduction of the prosomeric model dates back to the

---

1980s when molecular markers have first been discovered and used to define subregions of the brain (Puelles and Rubenstein, 2015; Puelles, 2019). This allowed genetic expression patterns to be revealed (e.g. *Shh*) that, especially, in the prosencephalon diverged from the established columnar borders. Henceforth, the columnar model has been frequently criticised and questioned (Hauptmann and Gerster, 2000; Puelles, 2019).

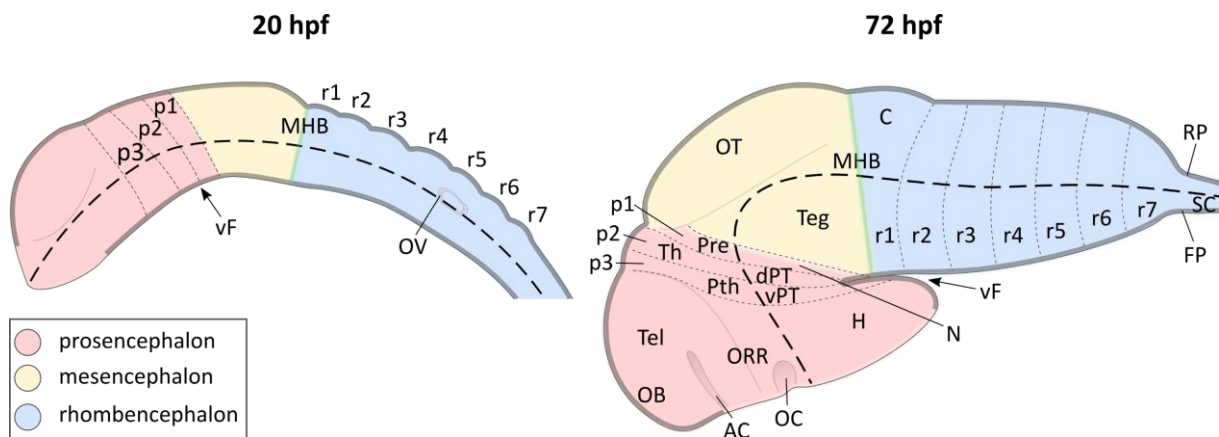


**Fig. 3: Prosomeric model adapted for zebrafish at 20 and 72 hpf.** According to the prosomeric model the hypothalamus can be described as the basal complement of the alar telencephalon and optic recess region since these three structures develop most anteriorly (20 hpf) and are placed opposite to each other from a rostro-caudal perspective (72 hpf). Therefore, telencephalic, optic recess and hypothalamic regions constitute the secondary prosencephalon. This is due to the bending of the neural axis at the ventral region where the dorsal part of the posterior tuberculum will develop (20 hpf). As a result of the roughly 90° bend, the ventral fissure emerges positioning the hypothalamus as one of the anterior-most structures at the ventral (caudal) end of the brain below di-, mes- and rhombencephalon (72 hpf). Prosencephalon, mesencephalon and rhombencephalon are depicted in red, yellow and blue, respectively. Mid-hindbrain boundary is indicated in green. Black dashed line indicates the border of basal and alar plates, terminating anteriorly near the optic commissure. Prosomeres 1-3 form the diencephalon and are separated into corresponding basal and alar structures. Anterior to the left. AC, anterior commissure; C, cerebellum; dPT, dorsal part of posterior tuberculum; FP, floor plate; H, Hypothalamus; MHB, mid-hindbrain boundary; N, region of the nucleus of medial longitudinal fascicle; OB, olfactory bulb; OC, optic commissure; ORR, optic recess region; OT, optic tectum; OV, otic vesicle; p1-3, prosomere 1-3; Pre, pretectum; Pth, prethalamus; r1-7, rhombomere 1-7; RP, roof plate; SC, spinal cord; Teg, tegmentum; Tel, telencephalon; Th, thalamus; vF, ventral fissure; vPT, ventral part of posterior tuberculum. Based on Affaticati et al. (2015), Mueller and Wullimann (2015), Puelles (2019), Puelles and Rubenstein (2015), Tropepe and Sive (2003) and Wullimann and Puelles (1999).

## Neurogenesis

The cellular process underlying these morphogenetic events that substantially shape the CNS and the neural cell types therein is neurogenesis. Neurogenesis begins at neural plate stages, continues throughout embryonic life, and in some regions of the CNS, e.g. the caudal hypothalamus (Duncan et al., 2016) even into adulthood (Alunni et al., 2013; Stigloher et al., 2008). Primary neurogenesis in zebrafish and other anamniotes involves the generation of primary neurons with long axons serving as scaffolds to guide migrating cells (Fig. 4A) (Blader et al., 1997; Chitnis and Kuwada, 1990; Haddon et al., 1998; Kimmel et al., 1991).

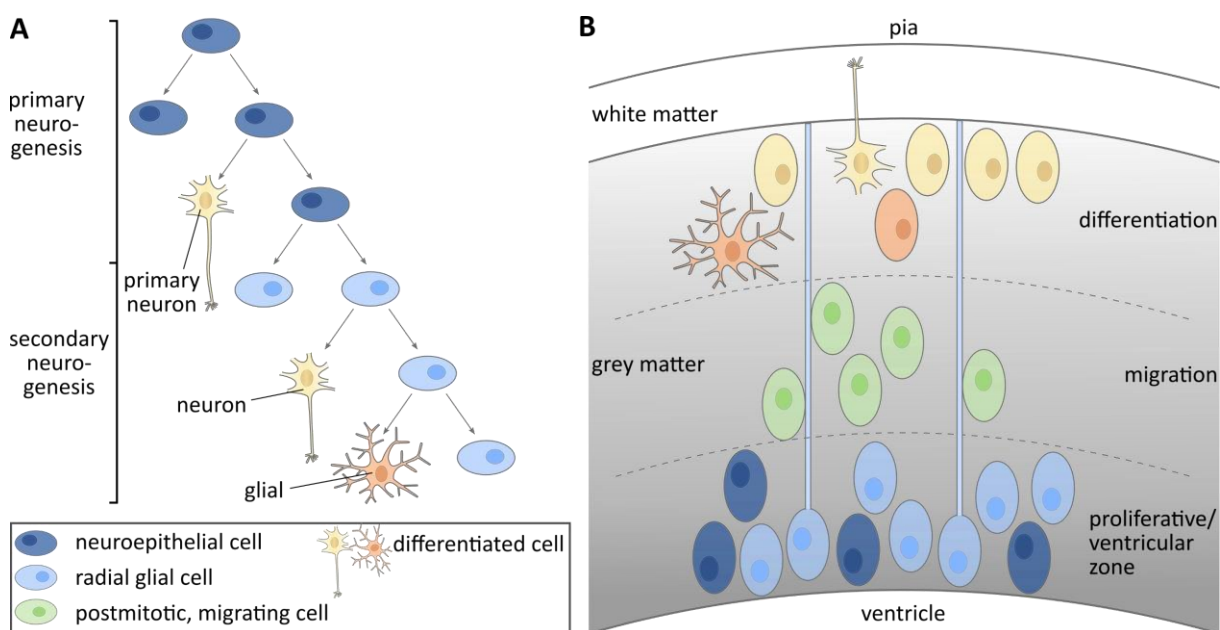


**Fig. 4: Primary and secondary neurogenesis in zebrafish.** **A** Symmetric proliferative and asymmetric differentiative cell divisions of neuroepithelial cells (dark blue) regulated by proneural genes at primary neurogenesis. Generation of primary neurons leads to axon scaffolds used for guidance of migrating cells. A burst of asymmetric cell divisions producing radial glial cells (light blue) launches secondary neurogenesis. Under the control of proneural genes radial glial cells first undergo a neurogenic phase producing neurons (yellow) followed by a gliogenic phase producing glial cells (orange). **B** Schematic representation of secondary neurogenesis. Neuroepithelial cells (dark blue) and therefrom derived radial glial cells (light blue) reside in the ventricular/proliferative zone and face the ventricle with their apical side. Radial glial cells can develop long processes that transverse the grey matter and anchor in the basal lamina. The process provides guidance for migrating postmitotic cells (green) on the way to their designated destination where they fully differentiate (yellow/orange). Based on Götz and Huttner (2005) and Mueller and Wullmann (2015).

In zebrafish the starting point of secondary neurogenesis is variable and elusively placed at the end of embryogenesis before hatching at 48 hpf. During secondary neurogenesis a more refined higher-order neural circuitry replaces the primary scaffolds by generating neuromodulatory monoaminergic circuits, neuroendocrine and excitatory/inhibitory regulatory systems, which form the majority of the later CNS mass (Mueller and Wullimann, 2015; Alunni et al., 2013).

Simultaneously with the development of the neural plate, initially a single cell layer, early neural progenitors called neuroepithelial cells (multipotent neural stem cells) develop at 10 hpf (Bally-Cuif and Hammerschmidt, 2003; Chitnis and Kuwada, 1990; Stigloher et al., 2008). Neuroepithelial cells are located at progenitor pool sites along the neural plate. To commit to a neural cell fate a proneural gene set of basic helix-loop-helix transcription factors (e.g. *neurogenin* (Blader et al., 1997) and *acheate-scute* family members) inherent to neuroepithelial cells is activated outside of the progenitor pool zone while inside proneural gene expression is inhibited (Alunni et al., 2013; Bertrand et al., 2002; Stigloher et al., 2008). Thus, the cells outside of the progenitor pool zone start to differentiate while cells located inside the progenitor pool zone remain undifferentiated. The responsible process is based on creating a disequilibrium of proneural gene activity in neighbouring neuroepithelial cells via Notch/Delta-signalling. A neuroepithelial cell A expressing more proneural genes than a neighbouring neuroepithelial cell B commits to a neural fate. Thereby, lateral inhibition via Notch-signalling by cell A inhibits proneural gene activity in the neighbouring cell B. Consequently, cell B does not commit to a neural fate and stays a multipotent neural stem cell. This process is critical in predetermining position and timing of proliferation, migration and differentiation of neural cell types during neurogenesis.

At the onset of secondary neurogenesis around the hatching period proliferation becomes restricted to proliferative zones around the ventricles (Wullimann and Puelles, 1999). At this point, the grey matter can be subdivided into three layers ranging from the ventricle to the periphery (Fig. 4B) (Mueller and Wullimann, 2015).

---

The cells in those layers can be labelled according to their maturation status. Proliferative ventricular zone cells are labelled by, e.g. proliferating cell nuclear antigen (PCNA) or *notch1a*. Newly determined postmitotic neural precursors migrate to the periphery in the direction of the pial surface and express *neurod1*. Lastly, differentiating cells that have arrived at their final destination can be identified by the expression of Hu proteins. The neurogenetic process leading to the emergence of these cell types begins with a burst of asymmetric neuroepithelial cell divisions. Consequently, more fate-restricted neural progenitors – radial glial cells – are generated in large quantities. They are committed to a neural cell fate (beginning with neurons, later astrocytes, oligodendrocytes, ependymal cells) (Götz and Huttner, 2005). Neuroepithelial and radial glial cells face the ventricle with their apical cell surface (Mueller and Wullimann, 2015). The nuclei of radial glial cells migrate periodically with the cell cycle phases from the apical beginning to the end of the ventricular zone. The basal processes of radial glial cells traverse the grey matter and connect to the basal lamina, which enables radial-glial guided migration. The processes of the radial glial cells are used as scaffolds by newly determined postmitotic neural precursors to find their designated destination for differentiation. In addition to radial migration, another mechanism of cell movement is tangential migration (Wullimann, 2009). Cells using this type of migration move parallel to the ventricular and pial surfaces in contrast to cells that use radial-glial migration. Cells most likely using tangential migration are found in the telencephalon (Wullimann, 2009). More precisely, they are supposed to be located in the dorsal subpallium where they migrate toward the pallium. Another example can be found in the dorsal rhombic lip (Köster and Fraser, 2001). Here, cells first move anteriorly toward the mid-hindbrain boundary. After changing direction, they move ventrally parallel to the mid-hindbrain boundary. Finally, they settle in the ventral brainstem underneath the cerebellum concluding migration.

The fate of a postmitotic cell is determined by a specific set of extrinsic factors such as morphogens and neurotrophic factors, and intrinsic factors such as transcription

---

factors (Livesey and Cepko, 2001). The interplay of these components as well as the cells appearance in time and space commit the non-dividing cell to a distinct lineage (Appel et al., 1995; Briscoe and Ericson, 1999; Kapsimali et al., 2004; Muthu et al., 2016). In general, radial glial cells first undergo a neurogenic phase producing neurons followed by a gliogenic phase producing glial cells. This process controlled by proneural genes highlights perfectly how meticulously timed events are during neurogenesis to compose an intricate network of cells that grows and self-renews throughout a life time (Grandel et al., 2006).

---



## **Part two – Development and neuroanatomical comparisons of the hypothalamus**

Regarding hypothalamic induction, it is likely that the hypothalamus as one of the anterior-most structures of the CNS develops early on (Woo and Fraser, 1995; Xie and Dorsky, 2017). Hence, hypothalamic development is in accordance with both neural induction models – the default and the two-signal model. Shortly after gastrulation ends around 10 hpf when the neural plate adopts a rostroventral fate, the hypothalamic primordium is induced. At this time expression of the hypothalamic marker *nkx2.4b* can be observed for the first time (Kapsimali et al., 2004). To ensure the correct position and size of the prospective hypothalamus Wnts (e.g. Wnt8 (Lekven et al., 2001), Wnt8b (Kim et al., 2002; Russek-Blum et al., 2008)), Wnt-signalling pathway components (e.g. *frizzled8a* (Kim et al., 2002; Russek-Blum et al., 2008)) and targets (e.g. *lef1* (Lee et al., 2006)) are met by Wnt antagonists (e.g. *dickkopf1* (Shinya et al., 2000), *axin1* (Kapsimali et al., 2004)). Wnts in the posterior neurectoderm and paraxial mesoderm (somites) promote posteriorisation, i.e. hindbrain fate. Whereas Wnt antagonists expressed in the anterior neurectoderm promote anteriorisation (Fig. 5) (Xie and Dorsky, 2017). Thus, a Wnt gradient is established, which is required for anterior-posterior hypothalamic regionalisation. In zebrafish, the neural plate is ventralised by Nodal and Shh signals, which induce the entire ventral CNS. Nodal and Shh originate from the axial mesoderm (prechordal plate, notochord). The hypothalamus as all anterior-most structures of the brain is induced by prechordal plate signals. Nodal signals, a subset of the Transforming growth factor beta (TGF $\beta$ ) superfamily, are required to activate expression of Shh (Lupo et al., 2006; Mathieu et al., 2002; Müller et al., 2000; Rohr et al., 2001; Varga et al., 2001).

---

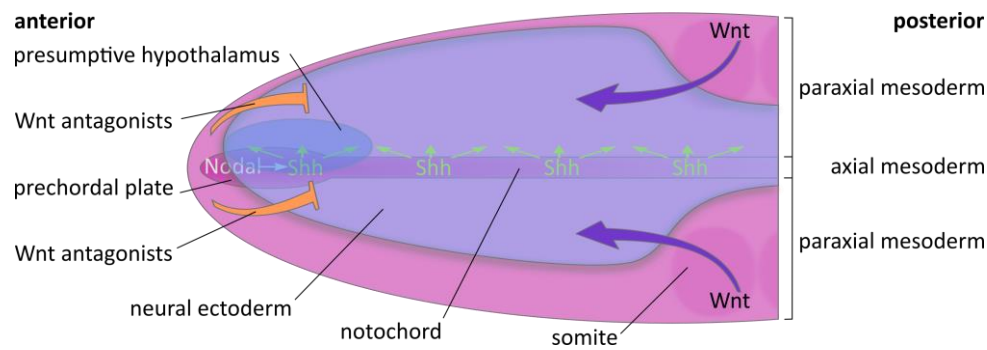


**Fig. 5: Hypothalamic induction in zebrafish.** Around the beginning of somitogenesis Wnt (purple) and Wnt antagonists (e.g. *dickkopf1*, *axin1*) (orange) in the neural ectoderm (light blue) determine the position of the hypothalamus (dark blue) on the anterior-posterior axis. Nodal signalling (white) from the prechordal plate activates Shh (green) expression along the notochord. Thus, Nodal and Shh induce the ventral CNS above including the hypothalamus. Dorsal view, anterior to the left. Modified from Xie and Dorsky (2017).

Regionalisation and patterning of the hypothalamus into neuronal clusters is preceded by the establishment of axonal scaffolds of primary neurons originating in the anterior prosencephalon between 14 and 24 hpf (Chitnis and Kuwada, 1990; Lewis and Eisen, 2003; Ross et al., 1992). Some primary neurons are part of the nucleus of the dorsolateral tract of the postoptic commissure (nTPOC) (also known as ventro-rostral cluster). Their axons form the dorsolateral tract of the postoptic commissure (TPOC), a scaffold guiding other axon tracts along the ventral diencephalon into the tegmentum. At 24 hpf cells of the nTPOC project axons rostrally to connect the left and right side of the neural tube by forming the optic commissure (Bak and Fraser, 2003; Ross et al., 1992). At 26 hpf GABAergic cells can be found in lateral and ventral clusters of the optic commissure neurons (Patel et al., 1994). The differentiation of this first group of neurons is likely to be regulated by the Notch/proneural network in zebrafish (Ware et al., 2014). However, further evidence is required as to which morphogens activate the Notch/proneural network, thus, initial neuronal differentiation in the early hypothalamus (Ware et al., 2014).

To be able to fully comprehend the neuroanatomy of the hypothalamus at late embryonic stages its physiology must be considered. Especially when regarding the

neuroendocrine functions of the hypothalamus, a broader look at the regions surrounding the hypothalamus must be taken (see Fig. 3, 6; Table 1). For this purpose, the optic recess region and the ventral part of the posterior tuberculum are considered in addition to the periventricular hypothalamus (Fig. 6). Subsequently, all three structures are referred to as the hypothalamic field.

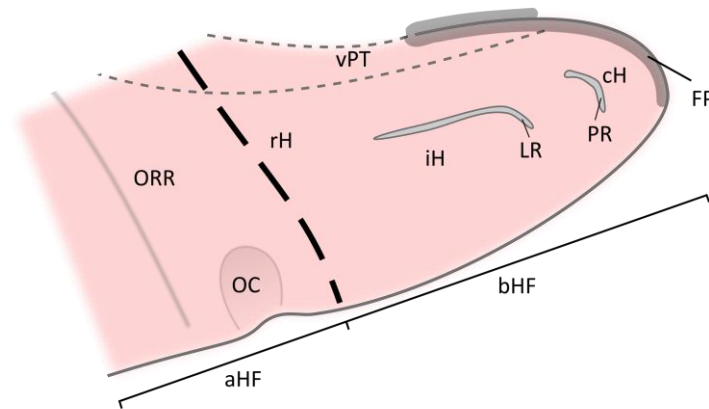


**Fig. 6: Anatomy of the hypothalamic field of zebrafish at 72 hpf.** The hypothalamic field includes the optic recess region (ORR) and the ventral part of the posterior tuberculum (vPT) in addition to the periventricular hypothalamus (rH, iH, cH). Black dashed line indicates the border of basal and alar plates terminating anteriorly at the optic commissure according to the prosomeric model. aHF, alar hypothalamic field; bHF, basal hypothalamic field; cH, caudal zone of the periventricular hypothalamus/caudal hypothalamus; FP, floor plate; iH, intermediate zone of the periventricular hypothalamus/intermediate hypothalamus; LR, lateral recess; OC, optic commissure; ORR, optic recess region; PR, posterior recess; rH, rostral zone of the periventricular hypothalamus/rostral hypothalamus. Based on Affaticati et al. (2015), Baeuml et al. (2019) and Biran et al. (2015).

In zebrafish the optic recess region has formerly been known as the preoptic region forming the alar part of the hypothalamus, thus, being 'hypothalamic' (Mueller and Wullimann, 2015; Wullimann et al., 1996). Therefore, the secondary prosencephalon has been viewed to consist of the telencephalon and the hypothalamus (Puelles and Rubenstein, 2003). However, recently the preoptic region has been proposed to be an independent morphogenetic entity termed optic recess region (Affaticati et al., 2015; Vernier, 2017). Thus, the secondary prosencephalon contains three entities as opposed to the previous two – the telencephalon, the optic recess region and the hypothalamus.

This neuroanatomical classification is also proposed for tetrapods. Here, the preoptic region has been regarded as part of the telencephalon. Now, the preoptic region together with the area defining the alar hypothalamus forms the optic recess region in tetrapods, which is regarded as independent morphogenetic entity. This view improves on the vertebrate prosomeric model by Puelles and Rubenstein in such a manner that it fits the teleost neuroanatomy as well as the tetrapod neuroanatomy (Puelles and Rubenstein, 2015; Yamamoto and Bloch, 2017). The main difference to Puelles' and Rubenstein's prosomeric model is the additional incorporation of ventricle-based teleost data in the model proposed by Affaticati et al. (2015). As opposed to the expression-based prosomeric model proposed by Puelles and Rubenstein (2015), which is mostly based on data from chicken and mouse.

In zebrafish the neuroanatomical classification of the ventral part of the posterior tuberculum has recently been adapted (Biran et al., 2015). Now, the area is part of the hypothalamus proper. Thus, it becomes easier to imagine, these regions – the optic recess region and the ventral part of the posterior tuberculum – are tightly cooperating with the hypothalamus proper when it comes to its physiology (Affaticati et al., 2015; Biran et al., 2015; Puelles and Rubenstein, 2015; Vernier, 2017).

Some parts of the adult hypothalamic field of zebrafish are neuroanatomically conserved between a range of species including members of the annelid phylum as well as species of the vertebrate phylum. Other hypothalamic field regions are found to be unique to teleosts (Biran et al., 2015; Tessmar-Raible et al., 2007). The neurosecretory centre of the medial forebrain – the prospective hypothalamic field – of zebrafish corresponds to the medial prostomial region of the annelid *Platynereis dumerilii* (Tessmar-Raible et al., 2007). This structure develops into the paired cerebral ganglia, the equivalent to the forebrain. Both fish and annelid regions co-express orthologues of the hypothalamic transcription factors *nkx2.1*, *rx* and *vax* during development. In addition, the medial forebrain regions of both species house *avp* expressing photoreceptors. Both findings argue for a conserved molecular anatomy of

---

the prospective medial forebrain region including evidence for an ancient peptide hormone population located therein.

Within the vertebrate phylum the neurosecretory preoptic area (part of the optic recess region) and the ventral zone of the periventricular hypothalamus (also known as the nucleus lateralis tuberis) of zebrafish are presumed to be homologous to the mouse's paraventricular nucleus and arcuate nucleus, respectively, based on expression data of neuropeptides reviewed in Biran et al. (2015) (Table 1). Similarly, mouse and zebrafish share orthologous transcription factors such as *otp*, *sim1/arnt2* and *nr5a1*, which impact on the specification of these neuropeptides. They are expressed in conserved hypothalamic domains. To regulate hypothalamic development, hence, ensure correct patterning and positioning of cell populations these transcription factors require activation by extrinsic factors such as Shh, Nodal, Wnt, Wnt antagonists as mentioned above.

Table 1: Neuropeptides expressed in the respective neuroanatomic region of the hypothalamic field of zebrafish.

Neuroanatomic region	Expressed neuropeptide
Neurosecretory preoptic region	Oxytocin Arginine-vasopressin Somatostatin Corticotropin-releasing hormone
Ventral zone of the periventricular hypothalamus (nucleus lateralis tuberis)	Neurokinin B Growth hormone-releasing hormone $\alpha$ -Melanocyte-stimulating hormone Kisspeptin Agouti-related peptide
Ventral part of the posterior tuberculum	Arginine-vasopressin Corticotropin-releasing hormone Neurokinin B Catecholamines
Based on Biran et al. (2015).	

A unique region to amniotes, apparently not present in teleosts, is the median eminence that connects the tuberal hypothalamus to the anterior lobe of the hypophysis (adenohypophysis) (Vernier, 2017). Consequently, hypothalamic hormones are released in the median eminence of amniotes where they are transported by the blood to the adenohypophysis. In teleosts cells of the adenohypophysis are directly innervated by hypothalamic neuroendocrine cells.

The most caudally located structure of the mammalian hypothalamus is the mammillary body (Vernier, 2017). This structure is a unique feature of their clade whereas the posterior recess and the surrounding caudal hypothalamus represent a unique region found only in teleosts (Vernier, 2017; Xavier et al., 2017). By focussing on monoaminergic cells, which are abundantly expressed in the caudal hypothalamus of zebrafish, this study aims to understand their development in teleosts by elucidating the lineage specific genetic network responsible for their generation.

---

## **Part three – Development of the monoaminergic system in the CNS of zebrafish**

### Functions, behaviours and evolution of monoamines

The monoaminergic system of the CNS is an immense network of ancient origin. It is best regarded as a collection of highly intricate circuitries impacting on a plethora of functions and behaviours. In general, the best-known neural function of, e.g. serotonin (5-hydroxytryptamine, 5-HT) is as mood stabiliser in the adult brain (Jenkins et al., 2016). 5-HT had first been characterised and named serotonin in 1948 (Rapport et al., 1948) even though its initial discovery in enterochromaffin cells of the gastrointestinal system had been achieved in 1937 (Erspamer and Vialli, 1937). Then, it had been called enteramine, which has been succeeded by the name it still carries today. In addition to its function in the adult brain, 5-HT is also implicated in a number of developmental processes in the CNS such as cell division, neuronal migration, cell differentiation and synaptogenesis (Gaspar et al., 2003). The behaviours that monoamines impact on are studied in zebrafish and include, e.g. locomotion, reward behaviour, learning and memory, aggression, anxiety and circadian rhythmicity (Norton and Bally-Cuif, 2010; Lillesaar, 2011; Lau et al., 2006; Peitsaro et al., 2003; Brustein et al., 2003; Filby et al., 2010; Maximino et al., 2010; Versteeg et al., 2015).

Monoamines act as neurotransmitters and neuromodulators. They are classically subdivided into three groups: (1) the catecholamines: dopamine (DA), noradrenalin and adrenalin; (2) the indolamines: 5-HT and melatonin; (3) the imidazoleamine: histamine. The diversity of species using monoamines as neurotransmitters to relay information is enormous. It ranges from the simplest nervous nets of cnidarians (e.g. the sea pen *Renilla koellikeri* (Umbriaco et al., 1990), the fresh-water polyp *Hydra vulgaris* (Carlberg, 1992)) to the most interwoven nervous systems of bilaterians such as chordates (e.g. the lancelet *Branchiostoma lanceolatum* (Moret et al., 2004), zebrafish and rodents (Lillesaar and Gaspar, 2019)). Cnidarians and bilaterians are sister clades,

---

which diverged ~555 million years ago in the Cambrian or even earlier in precambrian periods (Cunningham et al., 2017; Moroz and Kohn, 2016). Yet today, they all share the same monoamines. Therefore, monoamines are evolutionarily conserved (Ryan et al., 2013). During this long evolutionary history diverse taxa emerged and developed species-specific differences in morphology and physiology regarding their monoaminergic systems. One of those species is the zebrafish and its serotonergic and dopaminergic systems, the development of which are the main focus of this study. Certain unique characteristics to the zebrafish serotonergic and dopaminergic systems emerged during the course of evolution, which is the subject of the following paragraph.

#### Whole genome duplication in the context of 5-HT and DA metabolism

Serotonergic and dopaminergic cells can be identified by a set of biosynthesis and neurotransmission markers. Some of which both monoamines share. In zebrafish the genes encoding these markers often vary in the number of copies, i.e. paralogues when comparing them to, e.g. orthologues of mammalian species. The reason for this dates back to the base of the teleost radiation ~345 million years ago when, most likely, a whole genome duplication event took place (Furutani-Seiki and Wittbrodt, 2004). Generally, the ancestral deuterostome genome supposedly underwent two whole genome duplications to evolve into the vertebrate genome (1-2-4 rule) (Meyer and Schartl, 1999). Within vertebrates, teleosts phylogenetically belong to ray-finned fish (Actinopterygii), the sister class of lobe-finned fish (Sarcopterygii) that mammals belong to. Ray-finned and lobe-finned fish diverged before the whole genome duplication of teleosts. Therefore, this additional duplication did not affect mammals. Yet it explains the existence of up to eight paralogues of a gene in the zebrafish genome (1-2-4-8 rule) whereas mammalian species may only have four paralogues of the same gene. Single gene duplications or duplication of clusters of genes are additional evolutionary mechanisms that influence the number of gene copies in a species. Some

---



gene copies can be without function (non-functionalisation) and, as a consequence, lost during evolution. These mechanisms account for gene copy numbers not following the 1-2-4-8 rule (Furutani-Seiki and Wittbrodt, 2004; Meyer and Schartl, 1999). Other paralogous genes may adopt a new function (neo-functionalisation). Some genes may have copies that carry out only parts of the gene's function, yet together, complement each other (sub-functionalisation).

The types of functionalisation described above can be well illustrated in the case of monoaminergic marker genes of zebrafish (Table 2).

Table 2: Serotonergic and dopaminergic marker genes of zebrafish.

Serotonergic markers		Monoaminergic markers		Dopaminergic markers	
Gene name	Paralogues	Gene name	Paralogues	Gene name	Paralogues
<i>tryptophan hydroxylase</i>	<i>tph1a</i> <i>tph1b</i> <i>tph2</i>	<i>dopa decarboxylase</i>	<i>ddc</i>	<i>tyrosine hydroxylase</i>	<i>th1</i> <i>th2</i>
<i>5-HT transporter</i>	<i>slc6a4a/serta</i> <i>slc6a4b/sertb</i>	<i>GTP cyclohydrolase</i>	<i>gch1</i> <i>gch2</i>	<i>DA transporter</i>	<i>slc6a3/dat</i>
		<i>monoamine oxidase</i>	<i>mao</i>		
		<i>vesicular monoamine transporter</i>	<i>slc18a2/vmat2</i>		

Listed are all paralogues of a gene irrespective of their presence in the CNS. Based on references in the text and data on zfin.org.

Generally, the biosynthesis of 5-HT and DA involves three enzymes, one of which they share. The first enzyme in 5-HT biosynthesis is tryptophan hydroxylase (Tph) (Fitzpatrick, 1999). It is the rate-limiting enzyme and catalyses the reaction of the amino acid tryptophan to 5-hydroxy-tryptophan (5-HTP). The enzyme responsible for the rate-limiting reaction in DA biosynthesis is tyrosine hydroxylase (Th). Th catalyses the reaction of the amino acid tyrosine to L-3,4-dihydroxyphenylalanine (L-DOPA).

Both aromatic amino acid hydroxylases (Tph, Th) require a cofactor which is synthesised by a GTP cyclohydrolase 1 (Gch1) (Pelletier et al., 2001; Thöny et al., 2000). The last biosynthesis enzyme is dopa decarboxylase (Ddc), which the 5-HT and DA metabolic pathways share (Christenson et al., 1972). It catalyses the reactions of 5-HTP and L-DOPA producing 5-HT and DA, respectively. The synthesised 5-HT and DA are both degraded by a monoamine oxidase (Mao) to 5-Hydroxyindoleacetic acid (5-HIAA) and 3,4-Dihydroxyphenylacetic acid (DOPAC).

Zebrafish possess three *tph* genes – *tph1a*, *tph1b* and *tph2*, all of which are expressed in the CNS (Table 2) (Bellipanni et al., 2002; Lillesaar et al., 2007; Teraoka et al., 2004). In contrast, rodents have two genes – *Tph1* and *Tph2*. *Tph1* is mainly found in the periphery whereas *Tph2* is expressed in the CNS throughout life and predominantly responsible for the maintenance of serotonergic neurotransmission (Gutknecht et al., 2009; Nakamura et al., 2006). Thus, the *tph* genes pose an example of the described functionalisations of orthologous genes of different species. Apart from the *tph* genes, zebrafish possess two *th* paralogues – *th1* and *th2*, of which both are expressed in the CNS, and one copy of *ddc* and *mao* (Table 2) (Anichtchik et al., 2006; Candy and Collet, 2005; Filippi et al., 2007; Kaslin and Panula, 2001; Yamamoto et al., 2010; 2011). Rodents express only *Th1* and have likely lost the *Th2* gene. *Ddc* is the only gene copy in rodents. However, rodents express two paralogues of *Mao* – *Maoa* and *Maob*. The zebrafish *mao* gene shares 69% sequence homology with both rodent *Maoa* and *Maob* paralogues. Yet it functionally resembles MAO A more, which mainly metabolises 5-HT (Sallinen et al., 2009a).

### Wired and volume transmission

In their capacity as neuromodulators monoamines can act over longer distances on target cells located throughout the entire CNS. The concept of long-distance communication is called volume transmission and contrasts point-to-point communication, the essence of wired transmission (Fuxe et al., 2007). Apart from

---

---

chemical synapses, wired transmission occurs at electrical synapses, i.e. gap-junctions and close membrane juxta-positions (Nagy et al., 2004). These transmission concepts are based on two theories of intercellular communication, which competed with each other at the time: Cajal's neuron doctrine and Golgi's theory of the diffuse nerve networks (Ramón y Cajal, 1909; Shepherd, 2015). On Cajal's neuron doctrine Sherrington's classical synaptic transmission is based, which is the earliest and most common example for wired transmission (Sherrington, 1906). While the discovery of wired transmission preceded the establishment of Golgi's intercellular communication theory (Agnati et al., 1986), volume transmission poses the evolutionary older type of communication (Fuxe et al., 2007; De-Miguel and Fuxe, 2012). Converging evidence from the sea mollusc *Aplysia californica* (Branton et al., 1978; Mayeri et al., 1985) and ultra-structural observations of junctional and non-junctional monoaminergic varicosities from rats (Descarries et al., 1975; Descarries and Mechawar, 2000) has paved the way toward the current understanding of volume transmission. Volume transmission is characterised by chemical and physical signals which pass through the extracellular space and CSF using energy gradients (Agnati et al., 2006; De-Miguel and Fuxe, 2012; Fuxe et al., 2007). In the CSF this process is vector-assisted. Chemical signals include neuromodulators, neurotransmitters, neurotrophic factors, ions, gases and enzymes. Physical signals represent electrotonic currents and temperature gradients. Sources of these signals are synaptic spill-over of vesicular release, extra-synaptic vesicular release, non-junctional varicosities, ion currents, constitutive release, gaseous transmitters and reverse functioning of uptake mechanisms (see Fig. 3 in Agnati et al. (2006)). The secreted signals are distributed in the extracellular space using concentration, electric, or thermal gradients, bulk flow hydrostatic pressure or bulk flow osmotic pressure. Transmitted signals interact with receiving cells using receptors, enzymes, ion channels or temperature sensitive receptors. Additionally, signals can be received via membrane polarisation or as temperature-dependent chemical reaction. Thus, volume transmission is a slow and omnidirectional process of high divergence and plasticity, which includes neuronal-neuronal, neuronal-glial

---

and glial-glial communication. In contrast, wired transmission is a fast and directed process between fixed structures.

During classical wired transmission 5-HT and DA neurotransmitter vesicles are transported to the presynaptic membrane by a vesicular monoamine transporter Slc18a2, formerly Vmat2, for release into the synaptic cleft (Table 2) (Wen et al., 2008; Yamamoto et al., 2011). Within the synaptic cleft 5-HT diffuses to interact with 5-HT receptors. 5-HT receptors are diverse and categorised in seven recognised families (Hoyer et al., 2002; Nichols and Nichols, 2008). 5-HT receptor 3 family members are ligand-gated ion-channels with homology to the nicotinic type of acetylcholine receptors. All other 5-HT receptors represent G-protein coupled receptors. This allows an additional classification according to the G-proteins the receptors primarily interact with for signalling –  $G_{i/o}$ ,  $G_s$  or  $G_q$ . 5-HT receptor families 1 and 5 belong to  $G_{i/o}$ -protein coupled receptors, which inhibit adenylyl cyclase activity, thus, decrease the production of cyclic adenosine monophosphate (cAMP). On the other hand,  $G_s$ -coupled receptors stimulate cAMP production and include the 5-HT receptor families 4, 6 and 7. The impact of  $G_{i/o}$  and  $G_s$ -protein coupled receptors on cAMP activity affects cAMP targets that regulate amongst others calcium influx, membrane excitability and gene expression. Members of the 5-HT receptor family 2 are coupled to  $G_q$ -proteins, which lead to either an activation of protein kinase C or/and an intracellular calcium influx. DA receptors represent also G-protein coupled receptors and are split into two families (Yamamoto et al., 2015). DA receptor 1 family members are coupled to  $G_s$ -proteins and DA receptor 2 family members are bound to  $G_{i/o}$ -proteins. Finally, the released 5-HT and DA are taken up by 5-HT and DA transporters, respectively, clearing the synaptic cleft. After 5-HT and DA have been transported back inside the presynapse, they are inactivated by Mao or repackaged into vesicles, ready to be released again.

Of the 22 5-HT receptor genes found so far in zebrafish few have been studied in a neurobiological context (Table 3). Among them are three paralogues of the 5-HT receptor 1 family – *htr1aa*, *htr1ab* and *htr1d* (Norton et al., 2008) and the 5-HT receptor

---

2c (Schneider et al., 2012). Currently, a total of 14 DA receptor genes are reported in zebrafish (Table 3) (Fredriksson and Schiöth, 2005; Panula et al., 2010; Shontz et al., 2018; Yamamoto et al., 2015). Further, two paralogues of the 5-HT transporter gene – *slc6a4a* and *slc6a4b*, formerly *serta* and *sertb* – are expressed in zebrafish (Table 2) (Norton et al., 2008; Wang et al., 2006). One *slc6a3* gene, formerly *dat*, codes for the DA transporter (Yamamoto et al., 2010).

Table 3: 5-HT and DA receptors, coupled G-proteins and zebrafish gene paralogues.

5-HT receptors			G-proteins	DA receptors		
Family	Subtype	Gene name		Family	Subtype	Gene name
5-HT receptor 1 family	5-HTR1A	<i>htr1aa</i> <i>htr1ab</i>	G <sub>i/o</sub>	DA receptor 2 family	DARD2	<i>drd2a</i> <i>drd2b</i> <i>drd2l</i>
	5-HTR1B	<i>htr1b</i>			DARD3	<i>drd3</i> <i>drd4a</i> <i>drd4b</i> <i>drd4rs</i>
	5-HTR1D	<i>htr1d</i>				
	5-HTR1F	<i>htr1fa</i> <i>htr1fb</i>				
5-HT receptor 5 family	5-HTR5A	<i>htr5aa</i> <i>htr5ab</i>				
5-HT receptor 4 family	5-HTR4	<i>htr4</i>	G <sub>s</sub>	DA receptor 1 family	DARD1A	<i>drd1aa</i> <i>drd1ab</i> <i>drd1ba</i> <i>drd1bb</i> <i>drd1ca</i> <i>drd1cb</i> <i>drd1e</i>
5-HT receptor 6 family	5-HTR6	<i>htr6</i> <i>htr7a</i> <i>htr7al</i>			DARD1B	
5-HT receptor 7 family	5-HTR7	<i>htr7b</i> <i>htr7c</i> <i>htr7d</i>			DARD1C	
					DARD1E	
5-HT receptor 2 family	5-HTR2A	<i>htr2aa</i> <i>htr2ab</i>	G <sub>q</sub>			
	5-HTR2B	<i>htr2b</i>				
	5-HTR2C	<i>htr2cl1</i> <i>htr2cl2</i>				
5-HT receptor 3 family	5-HTR3	<i>htr3a</i> <i>htr3b</i>	Ligand-gated ion channel			

Listed are all paralogues of a gene irrespective of their presence in the CNS. Based on references in the text and data on zfin.org.

---

## Neuroanatomical distribution of serotonergic and dopaminergic cell clusters

---

The serotonergic system poses quite a formidable subject when it comes to its evolution and development, so does the dopaminergic system (Hay-Schmidt, 2000; Yamamoto and Vernier, 2011). Within bilaterians there appear to have developed two serotonergic systems, one inherent to spiralian protostomes the other inherent to deuterostome-like invertebrates (Hay-Schmidt, 2000). The latter has been proposed to be the one the vertebrate serotonergic system is derived of. The vertebrate serotonergic system of the CNS is separated into several cell clusters. One irregularity, however, pose placental mammals, a from an evolutionary viewpoint young vertebrate group. Here, serotonergic cells are with few possible exceptions (Ballion et al., 2002; Ugrumov et al., 1989) restricted to the raphe nuclei of the hindbrain (Dahlström and Fuxe, 1964; Gaspar and Lillesaar, 2012). For instance, mice have two raphe clusters, which are split into nine subclusters (B1-B9) (Dahlström and Fuxe, 1964; Gaspar and Lillesaar, 2012; Lillesaar and Gaspar, 2019). More commonly, in non-placental vertebrates such as fish, amphibians, reptiles, birds and monotremes serotonergic clusters are distributed throughout the di- and rhombencephalon and along the spinal cord (Lillesaar, 2011; Manger et al., 2002; Montgomery et al., 2016; Sako et al., 1986; Ueda et al., 1984; Ueda et al., 1983). For instance, in lamprey 23 serotonergic clusters are defined (Pierre et al., 1992) and adult zebrafish have nine (Kaslin and Panula, 2001). In postembryonic zebrafish neuroanatomical regions where cells express either *tph1a* or *tph2*, hence, synthesise 5-HT include from anterior to posterior: the hypothalamic field, pineal gland, pretectum, raphe nuclei and spinal cord (Fig. 7) (Bellipanni et al., 2002; Kaslin and Panula, 2001; Lillesaar, 2011; McLean and Fetcho, 2004). *tph1b* is expressed at earlier stages in the pineal gland and the optic recess region (Bellipanni et al., 2002), thus, omitted in Fig. 7.

Apart from the serotonergic populations, the vertebrate dopaminergic system of the CNS consists of multiple cell clusters as well. Generally, the nomenclature is based on the catecholaminergic system. Thus, it includes dopaminergic, noradrenergic and

---

---

adrenergic clusters and has first been described for the rat brain before becoming widely accepted (Dahlström and Fuxe, 1964; Hökfelt, 1984). According to this nomenclature dopaminergic and noradrenergic clusters are labelled in a caudal-rostral direction from A1-A17 and adrenergic clusters from C1-C3. Dopaminergic cell clusters are usually located in the diencephalon/midbrain (A8-A10), the hypothalamic field (A11-A15, A17) and the olfactory bulb (A16), which reflects prosomeric neuroanatomical views (Smeets and González, 2000; Yamamoto and Vernier, 2011). Comparative approaches show that the position of dopaminergic cell clusters can vary substantially between vertebrate species, which makes the identification of homologous clusters difficult (Yamamoto and Vernier, 2011). In embryonic zebrafish at 72 hpf Th1 cell clusters are found in the olfactory bulb, subpallium, hypothalamic field, ventral prethalamus, pretectum, locus coeruleus, area postrema and medulla oblongata (Fig. 7) (Holzschuh et al., 2001; Panula et al., 2010; Rink and Wullimann, 2002). Since noradrenalin and adrenalin are synthesised from DA, Th1 is a marker for all catecholamines. However, most of the named regions are truly dopaminergic except for the rhombencephalic clusters where DA occurs merely as metabolic intermediate until noradrenalin biosynthesis is completed (Alunni et al., 2013; Panula et al., 2010; Yamamoto et al., 2010; Holzschuh et al., 2001). *th2* expression is weakly detectable at 24 hpf in a few cells of the optic recess region (Chen et al., 2009; Panula et al., 2010). At 4 days post fertilisation (dpf) *th2* expression becomes clearly visible in the hypothalamic field clusters, thus, it is not shown in Fig. 7 (Chen et al., 2009; Panula et al., 2010; Reuter et al., 2019). Even though *th2* expressing cells are found in close vicinity to serotonergic cells, they are not coexpressed and there is compelling evidence that *th2* is only involved in catecholaminergic metabolism (Chen et al., 2016; Xavier et al., 2017). Taken together, truly dopaminergic cell clusters are distributed in the rostral brain ranging from the prosencephalon to the mid-hindbrain boundary in teleosts. This is largely in line with the distribution of dopaminergic cell clusters found in mammals, birds and amphibians (Yamamoto and Vernier, 2011).

---

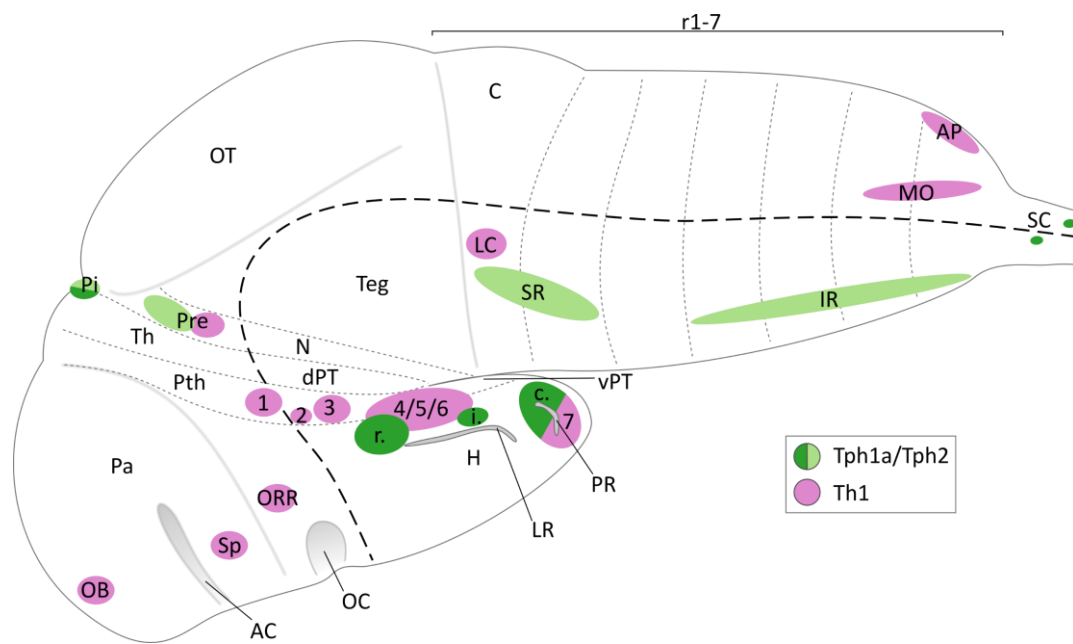


**Fig. 7: Monoaminergic cell clusters of the brain of zebrafish at 72 hpf.** Displayed are serotonergic cell clusters expressing *tph1a* (dark green) and *tph2* (light green) and dopaminergic cell clusters expressing *th1* (magenta) at 72 hpf. Serotonergic hypothalamic clusters are indicated according to their anatomic position in the periventricular hypothalamus (r., i., c.). Catecholaminergic clusters located in the hypothalamic field are numbered rostrally to caudally in ascending order from 1-7 according to Rink and Wullmann (2002). Note, overlapping clusters in the scheme only represent similar expression regions not coexpression. AC, anterior commissure; AP, area postrema; C, cerebellum; c., caudal zone of the periventricular hypothalamus; dPT, dorsal part of posterior tuberculum; H, hypothalamus; i., intermediate nucleus of the hypothalamus; IR, inferior raphe; LC, locus coeruleus; MO, medulla oblongata; N, region of the nucleus of medial longitudinal fascicle; OB, olfactory bulb; OC, optic commissure; ORR, optic recess region; OT, optic tectum; Pa, Pallium; Pi, pineal gland; Pre, pretectum; Pth, prethalamus; r., rostral zone of the periventricular hypothalamus; r1-7, rhombomere 1-7; SC, spinal cord; Sp, subpallium; SR, superior raphe; Teg, tegmentum; Th, thalamus; vPT, ventral part of posterior tuberculum. Based on Alunni et al. (2013), Kaslin and Panula (2001), Lillesaar et al. (2007), Panula et al. (2010) and Rink and Wullmann (2002).

### Dopaminergic and serotonergic gene regulatory networks

Among serotonergic and dopaminergic clusters of the CNS a large heterogeneity of neuronal subtypes develops (Rink and Guo, 2004; Rink and Wullmann, 2001). It indicates that a variety of complex genetic specification mechanisms are at work during neurogenesis of these clusters. It is even conceivable that a unique gene regulatory network installs each serotonergic and dopaminergic cell cluster, which strikingly all converge to establish a homogenous serotonergic or dopaminergic



identity. The ontogeny of the dopaminergic cell cluster of the hypothalamic field and the serotonergic cell clusters of the raphe nuclei is well investigated in zebrafish (Fig. 8A, B).

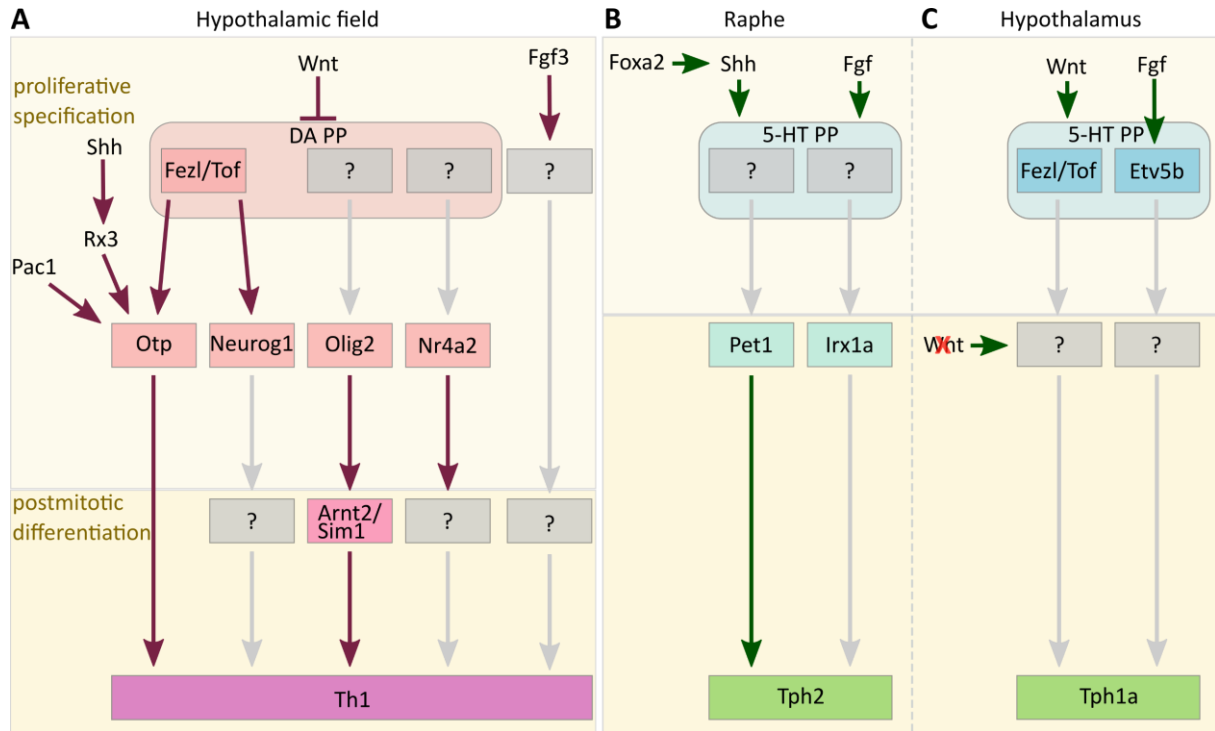


**Fig. 8: Monoaminergic gene regulatory networks in zebrafish.** **A** Gene cascade generating dopaminergic cells of hypothalamic field clusters. **B, C** Gene cascade generating serotonergic cells of raphe and hypothalamic clusters, respectively. Grey boxes indicate one or multiple unknown factors. Note that the zebrafish raphe network in **B** focuses only on genes investigated in zebrafish. Many genes that are part of the mammalian raphe serotonergic network (see text) are pending to be experimentally verified in zebrafish. Thus, they may still be part of the zebrafish raphe serotonergic network but are excluded from the present scheme for the time being. In **C** *Fezf2/Tof* is presumed to act in a similar fashion on serotonergic cell proliferation as on dopaminergic cell proliferation in **A**, even though data for serotonergic experiments is obtained from 6 dpf and adult zebrafish (Rink and Guo, 2004). PP, progenitor pool. Based on Alunni et al. (2013), Bosco et al. (2013), Cheng et al. (2007), Fernandes et al. (2013), Koch et al. (2014), Lillesaar et al. (2007), Löhr et al. (2009), Muthu et al. (2016), Norton et al. (2005), Rink and Guo (2004), Teraoka et al. (2004) and Wang et al. (2013).

Nodal, Shh and Wnt signals induce the ventral CNS, thereby, also the earliest dopaminergic progenitors of the hypothalamic field (Kapsimali et al., 2004; Mathieu et al., 2002; Yamamoto and Vernier, 2011). At early gastrulation Wnt activity

(Wnt8b/Lef1) delimits a dopaminergic progenitor pool within the rudiments of the neural plate that later develops into the basal prosencephalon (Alunni et al., 2013; Russek-Blum et al., 2008; Lee et al., 2006). The proliferative specification of dopaminergic progenitors depends at least partly on the expression of *fezf2/tof* (Levkowitz et al., 2003). During somitogenesis *neurogenin1* and *otp* expression, which is controlled by Fezf2/Tof, is observed in dopaminergic precursors (Blechman et al., 2007; Jeong et al., 2006; Ryu et al., 2007). At the same stage *olig2* and *nr4a2* are expressed in other dopaminergic progenitors whose upstream regulators are yet to be determined (Blin et al., 2008; Borodovsky et al., 2009; Luo et al., 2008). Interestingly, *lmx1b*, which is expressed around the same time as *neurogenin1*, *nr4a2*, *olig2* and *otp*, only impacts on the development of dopaminergic cells of cluster DC 1 in the hypothalamic field (Filippi et al., 2007). At 14-16 hpf cells start to exit the cell cycle and former *olig2* expression is substituted by *arnt2/sim1* expression in postmitotic progenitors. When *otp* expressing dopaminergic progenitors exit the cell cycle they express *arnt2* and *sim1*. Both transcription factors act in parallel to but also synergistically with *otp* to promote dopaminergic cell differentiation (Löhr et al., 2009). Apart from the events triggered by Wnt-signalling, *otp* expression is also depending on Shh-signalling that controls the expression of the transcription factor *rx3* (Muthu et al., 2016). In case *rx3* is absent *otp* expression is reduced causing a loss of dopaminergic cells in clusters DC 1 and 2. The dopaminergic network has been studied in most detail among the monoaminergic genetic networks in zebrafish, yet investigations into the raphe and hypothalamic serotonergic genetic networks have been undertaken as well. The key-genes regulating raphe serotonergic cell development are known in zebrafish even though the majority of the investigations has been carried out in other vertebrate model organisms. In zebrafish early proliferative specification of serotonergic progenitors in the raphe clusters is under the control of Fgf and Shh signals (Teraoka et al., 2004), of which Shh is regulated by *foxa2* (Fig. 8B) (Norton et al., 2005). Only after serotonergic progenitors have exited the cell cycle the Iroquois homeodomain factor *irx1a* impacts on the differentiation of *tph2* expressing raphe cells (Cheng et al., 2007).

---

---

Whether this relationship is direct or indirect remains to be investigated. The Ets-domain transcription factor *fev* (*pet1*) is a prominent postmitotic marker of serotonergic raphe clusters that precedes *tph2* expression by five hours (Lillesaar et al., 2007). Thus, *fev* (*pet1*) is required for the final maturation process. In contrast to *tph2*, *fev* (*pet1*) is only expressed in the raphe clusters suggesting a heterogeneity between genetic networks even within *tph2* expressing clusters. Lineage tracing of *fev* (*pet1*) cells demonstrated that serotonergic precursors of the superior raphe clusters originate from a progenitor pool at the mid-hindbrain boundary at late gastrulation. In addition, the axonal projections of *fev* (*pet1*) cells have been thoroughly investigated in zebrafish and compared to mammalian serotonergic raphe projections (Lillesaar et al., 2009). Combining these results with further observations gathered from different vertebrate models renders more components that are involved in the regulatory transcriptional network controlling the development of raphe serotonergic clusters (Deneris and Gaspar, 2018; Deneris and Wyler, 2012; Flames and Hobert, 2011; Kiyasova and Gaspar, 2011). A primary gene regulatory network consisting of *Ascl1*, *Nkx2.2*, *Nkx6.1* in addition to *Foxa2* promotes the commitment of proliferating ventral neural tube progenitors to the serotonergic lineage (Briscoe and Ericson, 1999; Jacob et al., 2007; Jacob et al., 2009; Jensen et al., 2008; Norton et al., 2005; Pattyn et al., 2004; Pattyn et al., 2003). After exiting the cell cycle a postmitotic network is in place involving a small number of transcription factors – *Gata2*, *Gata3*, *Insm1*, *Lmx1b*, *Fev* (*Pet1*) – with minor alterations along the rostro-caudal axis (Cheng et al., 2007; Craven et al., 2004; Ding et al., 2003; Hendricks et al., 1999; Jacob et al., 2009; van Doorninck et al., 1999). However, the mentioned factors are most essential and regulate genes with functions in 5-HT metabolism, packaging and transport. This complex network impressively demonstrates the value that combined research of different fields, in this case model organisms, has for our understanding of development, evolution and life itself.

Unfortunately, the ontogeny and regulatory transcriptional network of the hypothalamic serotonergic clusters of zebrafish have been the subject of only a few studies so far (Fig. 8C). Hence, the precise combination of signalling and transcription

---

factors required in time and space is largely elusive as is the degree of evolutionary conservation and general function of these clusters. The current state of knowledge is that the development of hypothalamic serotonergic clusters depends on Wnt-signalling (Wang et al., 2013) and the expression of the transcription factors *fezf2/tof* (Rink and Guo, 2004) and *etv5b* (Bosco et al., 2013). *fezf2/tof* is induced by Wnt antagonists (Hashimoto et al., 2000) and is also important for dopaminergic cell ontogeny in the hypothalamus as mentioned above (Alunni et al., 2013; Jeong et al., 2007; Levkowitz et al., 2003; Rink and Guo, 2004). *etv5b* is a downstream target of Fgf-signalling, which is implicated in the generation of hypothalamic serotonergic clusters as is outlined in more detail below (Bosco et al., 2013).

#### Cerebrospinal fluid-contacting cells and hypothalamic serotonergic clusters

This study focuses on the ontogeny of hypothalamic serotonergic CSF-c cells. Generally, CSF-c cells line the ventricular walls of the brain and the central canal of the spinal cord with one ciliated process protruding into the CSF (Orts-Del'Immagine and Wyart, 2017). The earliest description matching these general observations has been obtained from studies of retina neurons of frogs, salamanders and newts (Landolt, 1871). Reports of the first quarter of the 20<sup>th</sup> century show that neurons of the same description line the central canal. The spinal cord CSF-c cells have been named Kolmer-Agduhr cells according to the two researchers who described them almost at the same time (Agduhr, 1922; Kolmer, 1921). Their studies of CSF-c cells involved around 100 vertebrate species and show that all possess CSF-c cells. Thus, CSF-c are a conserved feature among vertebrates. Later, the term 'CSF-c cells' is established for the first time to describe cells of the paraventricular organ (Vigh et al., 1969). The processes of these cells protrude into the third ventricle. The morphology of CSF-c cells is diverse (Vigh and Vigh-Teichmann, 1998; Vigh et al., 2004). They can be bipolar or multipolar cells and either the dendritic or the axonal process is in contact with the CSF. This process usually displays cilia. In addition, CSF-c cells can have neuronal but also glial

---

---

properties and are immunoreactive for monoamines, peptide hormones, neurohormones and neurotransmitters (Jalalvand et al., 2016; Vigh and Vigh-Teichmann, 1998). Due to these characteristics CSF-c cells may present an important cell type that communicates via volume transmission (Vigh et al., 2004). The function of CSF-c cells has long been speculated about and only recently roles in mechanosensation and pH sensation could be experimentally validated for hypothalamic and spinal cord CSF-c cells (Djenoune et al., 2014; Jalalvand et al., 2018). In zebrafish spinal cord CSF-c cells modulate spinal central pattern organisers by sensing spinal bending, which impacts on locomotion (Böhm et al., 2016; Fidelin et al., 2015). Serotonergic intraspinal neurons are implicated in regulating the activity of the locomotor network (Montgomery et al., 2016; 2018). The function and ontogeny of hypothalamic CSF-c cells is still a matter of discovery in zebrafish. So far, the organisation of hypothalamic CSF-c cells containing DA and 5-HT, respectively, has been compared between zebrafish, *Xenopus laevis* and chicken (Xavier et al., 2017). Hypothalamic serotonergic CSF-c cells are concentrated around the third ventricle including lateral and posterior recesses, the latter being a unique ventricular structure of teleosts. This study investigates the development of caudal hypothalamic serotonergic CSF-c cells. The hypothalamic serotonergic population can be anatomically subdivided into three clusters, the anterior/rostral, intermediate and posterior/caudal cluster (Fig. 9) (Kaslin and Panula, 2001). Rostral and intermediate clusters are located around the lateral recess and the caudal cluster surrounds the posterior recess (Kaslin and Panula, 2001; Xavier et al., 2017). In all three clusters *tph1a* and 5-HT are co-localised (Bellipanni et al., 2002) demonstrating that the cells of these clusters not only contain 5-HT but actively synthesise it. Moreover, the complete range of serotonergic marker genes is expressed including *slc6a4b* (*sertb*), *slc18a2* (*vmat2*), *mao* and *ddc* (Anichtchik et al., 2006; Lillesaar et al., 2007; Norton et al., 2008; Sallinen et al., 2009b; Yamamoto and Vernier, 2011). The first postmitotic cells that are *tph1a*- and 5-HT-positive can be detected around 48 hpf in the rostral cluster (Bellipanni et al., 2002;

---

Panula et al., 2010) and around 62 hpf in the intermediate and caudal clusters (Bosco et al., 2013; McLean and Fetcho, 2004; Panula et al., 2010).

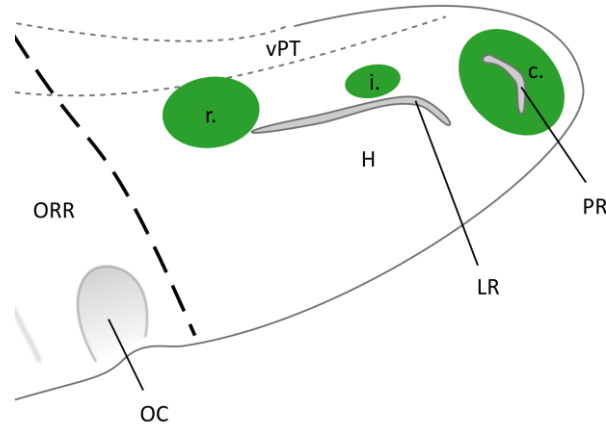


**Fig. 9: Serotonergic population of the periventricular hypothalamus of zebrafish.** Indicated (green) are the rostral (r.), intermediate (i.) and the caudal (c.) serotonergic cluster. r./i. clusters surround the lateral recess (LR) and c. cluster the posterior recess (PR) of the third ventricle. Black dashed line indicates alar-basal boundary. c., caudal cluster of the periventricular hypothalamus; i., intermediate cluster of the periventricular hypothalamus; H; hypothalamus; OC, optic commissure; ORR, optic recess region; r., rostral cluster of the periventricular hypothalamus; vPT, ventral part of posterior tuberculum. Based on Kaslin and Panula (2001) and Xavier et al. (2017).

### The Fgf-signalling pathway and the ligand Fgf3

As described above early proliferating hypothalamic progenitors are under the control of Nodal, Shh, Bmp, Wnt and Fgf signals as these signalling molecules are key factors defining the ventral CNS (Kapsimali et al., 2004; Mathieu et al., 2002; Muthu et al., 2016; Xie and Dorsky, 2017). Thus, some (or all) may play a role in the generation of hypothalamic serotonergic CSF-c cells. Focussing on Fgf-signalling, three Fgf-signalling pathways exist according to which Fgf ligands are categorised – the canonical, the non-canonical and the intracellular Fgfs (Mason, 2007). These three major categories are usually split into seven subfamilies. Therein, roughly 24 vertebrate *fgf* genes are distributed with varying numbers of orthologues depending on the species (Mason, 2007; Ornitz and Itoh, 2015; Oulion et al., 2012). Fgf3, which is

---

the most relevant ligand for the present work, has been the most difficult Fgf to place into a subfamily. According to phylogenetic analyses Fgf3 is commonly supposed to be a member of subfamily 7 whereas its genomic location shares higher similarity to subfamily 4 members (Itoh, 2007; Ornitz and Itoh, 2015). An altogether new categorisation creates an eighth subfamily for only Fgf3 (Oulion et al., 2012). This proposition is based on a tandem duplication event of a single *fgf3/4/5/6* gene in a presumptive chordate ancestor resulting into an *fgf3* and an *fgf4/5/6* gene. The remaining *fgfs* are supposed to be products of the two vertebrate specific whole genome duplications. Regardless of the specific subfamily, Fgf3 belongs to the category of canonical ligands (Ornitz and Itoh, 2015). The canonical Fgf-signalling pathway is extracellularly activated by the dimerisation of an Fgf ligand and an Fgf receptor (Itoh, 2007; Itoh and Ornitz, 2011; Mason, 2007; Ornitz and Itoh, 2015). This leads to a phosphorylation of the intracellular tyrosine kinase, which is bound to the receptor. Subsequently, adaptor protein complexes form at distinct tyrosine residues resulting in the activation of Ras-Mapk, P13K, Akt, Plc $\gamma$  and Stat intracellular signalling pathways. These pathways target a multitude of genes that are involved in cell motility, cell survival, cell proliferation and differentiation, stress response and Fgf-feedback inhibition (Ornitz and Itoh, 2015; Thisse and Thisse, 2005; Tsai et al., 2011). During early embryogenesis Fgf-signalling is known to be important for CNS development at least at two significant stages (Dono, 2003). Both stages are mentioned in detail above (Part One, neural induction) and include an early role of Fgf-signalling at blastula stages (Wilson et al., 2000) and during anterior-posterior patterning of the neural plate when Fgf-signalling promotes a posterior neural fate (Koshida et al., 2002; Pownall et al., 1996; Storey et al., 1998). Additionally, Fgf-signalling is needed for neuronal differentiation in the spinal cord (del Corral et al., 2002).

Taking a closer look at zebrafish, for which 31 *fgf* genes and five *fgf receptor* genes are currently listed (Itoh, 2007; Kanehisa, 2000; Ornitz and Itoh, 2015 and zfin.org). Amongst others the *fgf3* gene has been described for zebrafish (Kiefer et al., 1996). It consists of three exons with exactly the same splice locations of mouse and human

---

orthologues. The translated sequence is 256 amino acids long and has a conserved internal region of 155 amino acids whereas the N- and C-terminal regions are less conserved. Expression of *fgf3* in the CNS has been analysed for gastrula and early somite stages where it is confined to the prosencephalon, the mid-hindbrain boundary and the rhombencephalon (Raible and Brand, 2001). At later somite stages telencephalic expression decreases drastically while mid-hindbrain boundary expression persists. Simultaneously, a new expression domain occurs at the presumptive hypothalamus and at the optic stalk (Walshe and Mason, 2003). This pattern continues at 30 hpf. At 33 hpf until 48 hpf *fgf3* transcripts are restricted to the caudal hypothalamus while optic stalk expression continues (Liu et al., 2013). Functionally, Fgf3 is involved in inner ear development, which requires Fgf3 expression of rhombencephalic cells (Léger and Brand, 2002; Maroon et al., 2002). Fgf ligands, pathway genes and downstream targets are found in the zebrafish hypothalamus and the hypophysis (Bosco et al., 2013; Herzog et al., 2004; Jackman et al., 2004; Liu et al., 2013; Raible and Brand, 2001; Topp et al., 2008). Here, Fgf3 from the neurohypophysis affects axon guidance of cells expressing the peptide hormone *arginine vasopressin (avp)* (Liu et al., 2013). Further, Fgf3 is essential for adenohypophysis survival (Herzog et al., 2004) and for dopaminergic lineage specification of hypothalamic field clusters (Fig. 8A) (Koch et al., 2014). Since serotonergic CSF-c cells are located in the same hypothalamic areas as some dopaminergic clusters this may argue for a similar involvement of Fgf-signalling in the serotonergic lineage specification. The dependence of hypothalamic serotonergic clusters on Fgf-signalling during early specification is demonstrated in Bosco et al. (2013) and Teraoka et al. (2004). One particular downstream target activated by Fgf-signalling via the Ras-Mapk pathway is the ETS-domain transcription factor *etv5b*. This factor is regulating the proliferation of serotonergic progenitors (Fig. 8C) (Bosco et al., 2013). *etv5b* knock-down leads to a significant reduction of serotonergic CSF-c cells in the intermediate and caudal hypothalamic clusters. Functionally, *etv5b* indirectly regulates the cell cycle properties of serotonergic progenitors keeping them in a

---



proliferative state, thereby, maintaining the progenitor pool. Bosco et al. (2013) suggest a possible involvement of Fgf3 and/or Fgf8a in the development of caudal hypothalamic serotonergic clusters. This thesis aims to uncover novel experimental evidence for this hypothesis.

---

### Aims of the thesis

The main focus of this thesis was to investigate and possibly establish a link highlighting the dependence of hypothalamic serotonergic and dopaminergic CSF-c cells on Fgf3 during zebrafish development. Work toward this aim included a tempo-spatial expression analysis of *fgf3* in the hypothalamus to verify caudal hypothalamic *fgf3* expression at the time when serotonergic progenitors were proliferating. Additionally, double whole-mount *in situ* hybridisations of *fgf3* with respective hypothalamic markers *rx3* and *emx2*, Fgf-signalling feedback regulator *dusp6* and downstream target *etv5b* were carried out. This complemented the characterisation of *fgf3* expression. The spatial relation of *fgf3* expressing cells to *dusp6* and *etv5b* expressing cells, respectively, highlighted its possible role as a morphogen.

In order to be able to establish or confirm Fgf3 as a critical factor in hypothalamic serotonergic and dopaminergic CSF-c cell development (Koch et al., 2014), respectively, three independent strategies to impact on Fgf3 activity were applied: the *fgf3*<sup>t24152</sup> ENU mutant (*lia*), a morpholino-based knock-down of *fgf3* and the CRISPR/Cas9 technique. At first, the morpholino knock-down and CRISPR/Cas9 knock-out had to be generated and established whereas the *fgf3*<sup>t24152</sup> ENU mutant (*lia*) was obtained elsewhere (Herzog et al., 2004). By comparing the expression patterns of *fgf3* and *etv5b* it seemed likely that *etv5b* was a downstream target of *fgf3*. To test for this an expression analysis of *etv5b* was performed in *fgf3*<sup>t24152</sup> mutants and *fgf3* morphants. Next, all three *fgf3* impairment strategies were applied in parallel, for each of which immunohistochemistry was used to reveal 5-HT- and TH1-reactive CSF-c cells. Subsequently, immunoreactive 5-HT and TH1 CSF-c cells were counted for each strategy and statistically analysed. A significant reduction of caudal serotonergic and dopaminergic CSF-c cells was observed. To investigate whether the Fgf3 dependence was specific to monoaminergic cells in the hypothalamus or included other cell populations, three neuroendocrine cell types were analysed in *fgf3*<sup>t24152</sup> mutants and

---

---

*fgf3* morphants by whole-mount *in situ* hybridisation. The analysed peptide hormones included *oxytocin* (*oxt*), *avp* and *cortistatin* (*cort*), formerly, *somatostatin3* (*sst3*). The cells of relevant neuroendocrine clusters were counted and statistically analysed. Investigated *avp* expressing cells were depending on Fgf3, while *oxt* and *cort* expressing cells did not.

The observed loss of monoaminergic and *avp* expressing cells as a consequence of *fgf3* impairment suggested that the size of the hypothalamus may be smaller in *fgf3* impaired embryos. Thus, the expression pattern of the hypothalamic marker *nkx2.4b* was revealed by *in situ* hybridisation at three developmental stages critical during serotonergic cell specification. The *nkx2.4b* expression domain was used to visually outline the hypothalamus. A method for semi-automatic measurements of the expression domain was established and carried out from ventral and lateral viewpoints. Thus, a 2D impression of the possible changes to the developing hypothalamus could be obtained.

To mechanistically explain the loss of serotonergic CSF-c cells after *fgf3* impairment two cell death assays, a proliferation and a cell fate assay were performed at stages when serotonergic progenitors were proliferating. This would provide necessary information as to whether loss of serotonergic CSF-c cells: firstly, increased cell death; secondly, could be caused by an early depletion of the serotonergic progenitor pool; thirdly, could be due to a fate change of serotonergic progenitors, i.e. they committed to another cell lineage.

3D protein models of *fgf3*<sup>t24152</sup> mutant and *fgf3* morphant amino acid sequences were generated to evaluate the likelihood of ligand-receptor interactions of the impaired Fgf3 isoforms. This allowed for a better understanding of the severity of the individual phenotypes displayed by either mutants or morphants.

In order to find new candidates involved in hypothalamic serotonergic cell generation and to gain a better understanding of hypothalamic development the transcriptomes of the hypothalamus of wild types and *fgf3*<sup>t24152</sup> mutants were analysed at different developmental stages. The hypothalamic transcriptome facilitated insights into the

---

regulation of the Fgf3-signalling pathway. The focus was placed on the Ras-Mapk intracellular signalling components since *etv5b* is a known target of the Erk protein kinase.

Finally, the first steps were taken toward understanding the function of hypothalamic serotonergic clusters in non-placental vertebrates. To unravel the function of this enigmatic cell cluster a morpholino-based knock-down and a CRISPR/Cas9 knock-out of *tph1a* were prepared. By extension the investigations of this thesis may render clues regarding the evolution of the posterior recess region of the hypothalamus for future studies.

---

## Materials and methods

For detailed protocols see Annex.

### Fish husbandry and embryo preparation

Experiments were carried out using two zebrafish (*Danio rerio*) strains, either AB/AB wild types or the *fgf3*<sup>t24152</sup> N-ethyl-N-nitrosourea mutant (*lia*) in a Tü/Tü background (Herzog et al., 2004). Fish husbandry followed animal welfare regulations by the District Government of Lower Franconia, Germany. Embryos were raised and maintained in Danieau's solution. To suppress pigmentation of the skin 0.2 mM 1-phenyl-2-thiourea were added to the Danieau's solution after the first 24 hours of development for the time of subsequent rearing. Embryos were raised in petri dishes that contained medium and were stored in an incubator set to 28 °C and a 14/10 h light/dark cycle. Embryo stages were determined using the method described in Kimmel et al. (1995). For fixation embryos were dechorionated and transferred to 4% paraformaldehyde in phosphate buffered saline (PBS) solution, in which they were incubated for 24 h at 4°C. Subsequently, embryos were dehydrated in increasing concentrations (25%, 50%, 75% and 100%) of methanol in PBS with 20% Tween 20 (PBT). Finally, they were stored in 100% methanol at -20°C.

### Genotyping

All embryos expressing the *fgf3*<sup>t24152</sup> allele and their wild type siblings were genotyped. Before genotyping, embryos were kept in 100% methanol solution. To prepare

---

embryos for genotyping they were dried from the 100% methanol solution and pre-treated with proteinase K (Roche) for 4 h at 55°C. This denatured all proteins, thus, the endogenous genomic DNA (gDNA) of the respective embryos could be accessed. Genotyping was performed by PCR on all embryos using HiDi SNP DNA Polymerase (Genaxxon Bioscience). This allowed an allele specific discrimination of the genomic region containing the *fgf3*<sup>124152</sup> point mutation. This mutation includes a DNA base transition from G to A. To discriminate between the mutant and the wild type allele two PCR reactions were prepared for every embryo that needed genotyping. Both reactions were set apart from each other by using different forward primers. The reverse primer was the same in both reactions (reverse primer: 5' TGCCGCTGACTCTCTCTAAG 3'). The two forward primer sequences were almost identical apart from the last nucleotide at the 3' end, which was either a G, thereby, specific to the wild type allele (forward primer wild type: 5' GCCAGTTCTAAAAGGCAGTGG 3') or an A, thereby, specific to the mutant allele (forward primer mutant: 5' GCCAGTTCTAAAAGGCAGTGA 3'). In case an embryo had a wild type genotype (+/+) the PCR reaction containing the wild type forward primer gave a positive result whereas the PCR reaction with the mutant forward primer was negative. An embryo with a homozygous mutant genotype (-/-) had a negative PCR result in the wild type PCR reaction yet a positive PCR result in the mutant PCR reaction. In case an embryo had a heterozygous genotype (+/-) the wild type and the mutant PCR reactions were positive.

### ***fgf3* and *tph1a* impairment strategies**

#### Morpholino strategy

Two genes – *fgf3* and *tph1a* – were knocked-down by morpholinos designed by Gene Tools. Knock-down of *fgf3* was achieved using a morpholino targeting the splice donor site at exon 2/intron 2 (Fig. 10; Table 4).

---

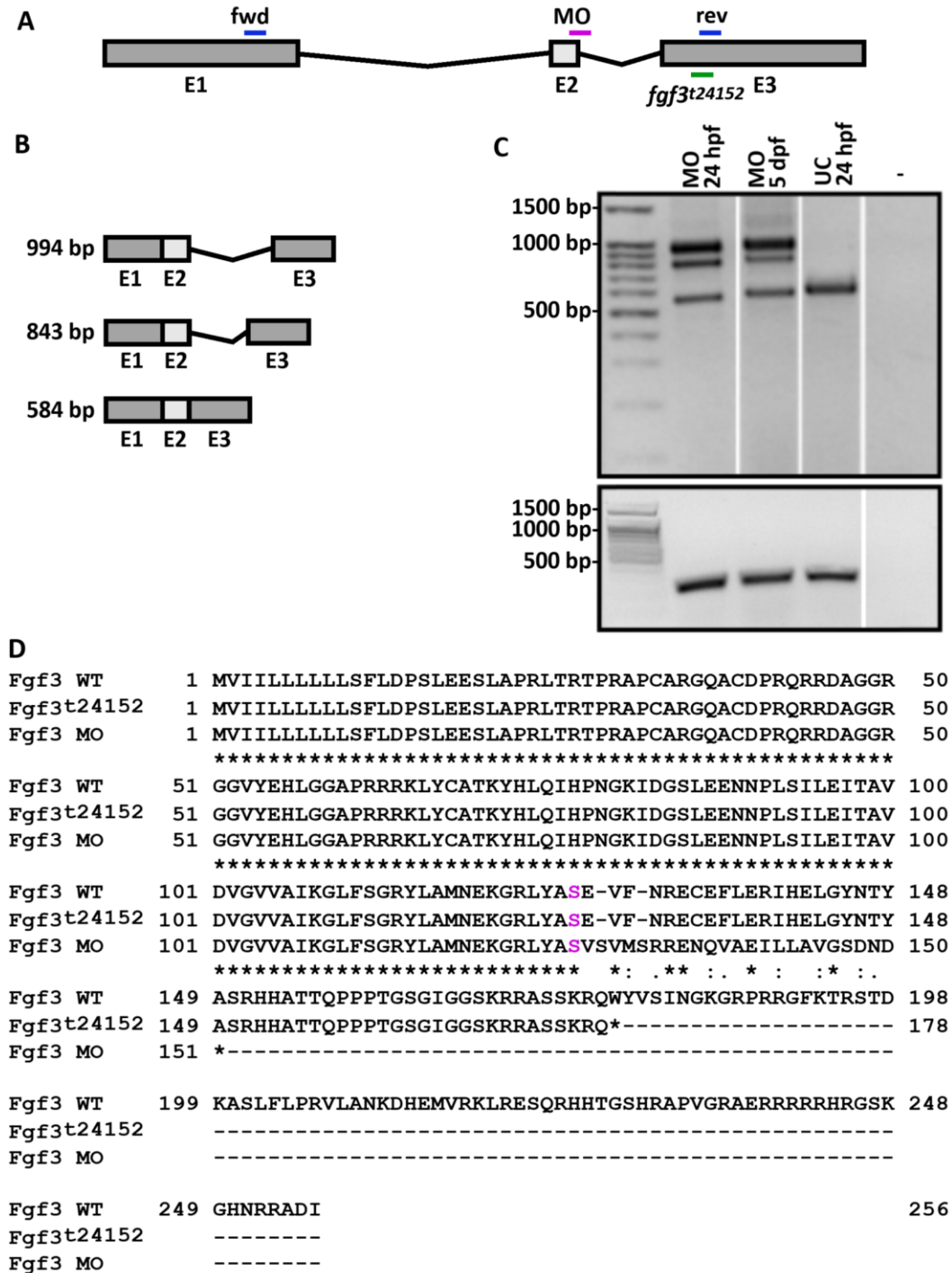


**Fig. 10: *fgf3* morpholino knock-down efficiency and amino acid sequence alignment of wild type, mutant and morphant Fgf3.** **A** Scheme of *fgf3* gene. Locations of splice morpholino target site (MO, magenta), forward (fwd) and reverse (rev) primers (blue) detecting morphant splice forms, and *fgf3*<sup>t24152</sup> point mutation (green) are highlighted. **B** Scheme represents detected splice products of *fgf3* after morpholino injections and RT-PCR. **C** Obtained RT-PCR products of morphants at 24 hpf and 5 dpf, uninjected control (UC) siblings at 24 hpf and water control (-) for *fgf3* (upper gel) and  $\beta$ -actin (lower gel). *fgf3* morphant product bands at 843 and 994 bp corresponded to a partial intron 2 inclusion due to a cryptic splice site and a complete inclusion of intron 2, respectively. **D** Amino acid sequence alignment of wild type (WT), *fgf3*<sup>t24152</sup> mutant and morphant (MO) Fgf3. Due to a G to A transition point mutation the *fgf3*<sup>t24152</sup> mutation results in a premature stop after amino acid 177 (Q) with a remaining 69% of the wild type protein sequence. After *fgf3* morpholino injections both splice forms generate a nonsense sequence after amino acid 127 (S, magenta) and a stop after amino acid 150 (D) leaving 50% of the wild type protein sequence intact. Modified from Reuter et al. (2019).

For the *tph1a* gene two knock-downs were created for which splice blocking morpholinos were designed to target the splice donor sites at the exon 3/intron 3 and at the exon 4/intron 4 boundaries, respectively (Fig. 27; Table 4).

Table 4: Designed splice-blocking morpholinos by Gene Tools and respective forward and reverse primers for *fgf3* and *tph1a* genes.

	<i>fgf3</i> exon 2 (5'-3')	<i>tph1a</i> exon 3 (5'-3')	<i>tph1a</i> exon 4 (5'-3')
<b>MO</b>	CCCGACGTGACATAACACTTACTGA	AAAAGACATTCATACCGCTTTCCTC	ACGGTAAAGTTATCCCACTTACAGG
<b>Primer fwd</b>	AGCTTCTTGGATCCGAGTTTGG	TCTTCAGAGACAGGCCGGG	CGACAGCAACCGTGAACAAC
<b>Primer rev</b>	TCACACTCTCGGTTGAAGACT	CATACATCAGCACGCGGTTC	AGCCAAGTCTGCAAAGTACT

Approximately 4.2 nl of 0.5 mM *fgf3* morpholino solution or 0.25 mM *tph1a* morpholino solution were injected into the cell of fertilised eggs of the AB/AB strain at the one-cell stage (Fig. 11).

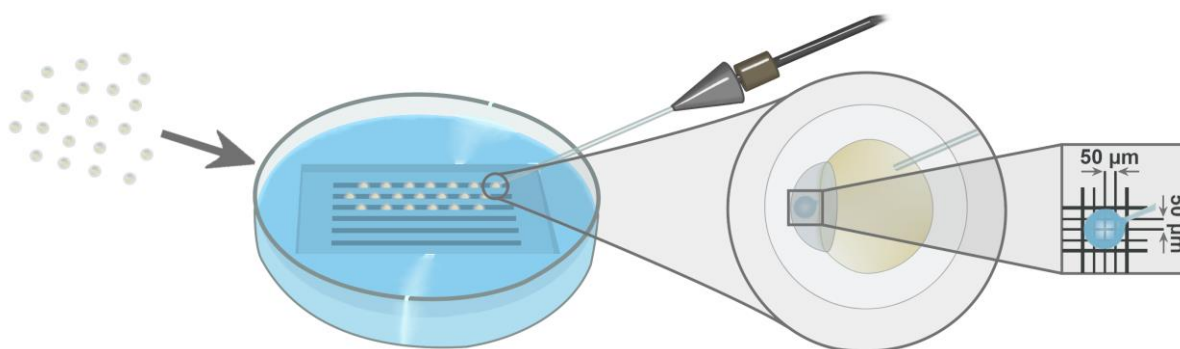


**Fig. 11: Scheme of microinjection setup.** Fertilised eggs (left) were aligned in an agarose mould (centre) and injected into the cell at the one-cell stage (right). Injected droplet size was measured using a hemocytometer (far right).

In case of the *fgf3* gene, the morpholino injections resulted in mRNAs with a partial and a complete inclusion of intron 2. Consequently, the mRNAs translated into two



nonsense amino acid sequences (Fig. 11B,C). Both sequences terminated at a premature stop causing a truncation of the respective Fgf3 protein (Fig. 11D). Results for both morpholinos targeting the *tph1a* gene are reported below (Chapter Results; Figs. 27, 28). To confirm the effects of the morpholinos on *fgf3* and *tph1a* complementary DNA (cDNA) was synthesised from isolated mRNA of injected embryos using the Revert Aid First Strand cDNA Synthesis Kit (Thermo Fisher Scientific). With the obtained cDNA a reverse transcriptase (RT)-PCR was performed using GoTaq polymerase (Promega). Subsequently, the PCR products were verified by Sanger sequencing (Eurofins). Uninjected embryos were stage-matched and used as control group. Alignments of amino acid sequences were performed with the alignment tool published in Di Tommaso et al. (2011).

### CRISPR/Cas9 strategy

Knock-out of *fgf3* and *tph1a* was achieved by establishing, then, applying the CRISPR/Cas9 technique. The online tool CHOPCHOP (Labun et al., 2016; 2019; Montague et al., 2014) was utilised to design two gRNAs for each gene. The gRNAs targeting the *fgf3* gene were located in exon 1 and exon 2 (Fig. 12; Table 5).

Table 5: Target sites, oligos and PCR primers for *fgf3* and *tph1a* CRISPR/Cas9 approach.

	<i>fgf3</i> exon 1 (5'-3')	<i>fgf3</i> exon 2 (5'-3')
<b>Target site</b>	GGGGTTTACGAGCACCTCGG	GGCAATCAAGGGACTGTTTT
<b>Oligo 1</b>	TAGGGGTTTACGAGCACCTCGG	TAGGCAATCAAGGGACTGTTTT
<b>Oligo 2</b>	AAACCCGAGGTGCTCGTAAACC	AAACAAAACAGTCCCTTGATTG
<b>Primer fwd</b>	AGCTTCTTGATCCGAGTTTGG	ATACGCTTTCAGACAAGGCAAT
<b>Primer rev</b>	GATCCGTCTATTTTCCCGTTTCG	CCCGACGTGACATAACACTTAC
	<i>tph1a</i> exon 2 (5'-3')	<i>tph1a</i> exon 4 (5'-3')
<b>Target site</b>	GGGAAAACACAACCGCAGCC	GGTAAAGTTATCCCACTTAC
<b>Oligo 1</b>	TAGGTAAAGTTATCCCACTTAC	TAGGGAAAACACAACCGCAGCC
<b>Oligo 2</b>	AAACGTAAGTGGGATAACTTTA	AAACGGCTGCGGTGTGTGTTTC
<b>Primer fwd</b>	AGGGTGAAGTGTCTTAAAGTGT	AGAGATGGAGAATGTGCCGT
<b>Primer rev</b>	CCTCACGTTACCTGGAAAAGC	AGCCAAGTCTGCAAAGTACT

Modified from Reuter et al. (2019).

In case of *tph1a*, exons 2 and 4 were targeted (Fig. 27; Table 5). Two DNA oligos were annealed and cloned into the vector DR274 (a kind gift from Keith Joung, Addgene plasmid #42250) which concluded the generation of the DNA templates for subsequent gRNA synthesis (Table 5). DNA vector templates were *in vitro* transcribed with T7 RNA polymerase (a generous gift from T. Ziegenhals and U. Fischer, Department of Biochemistry, Biocentre, University of Würzburg). Subsequent RNA extraction with Roti-Aqua-P/C/I (Roth) rendered ready-to-use gRNAs. In case of the *fgf3* gene, fertilised eggs of the AB/AB strain were injected into the cell at the one-cell stage with approximately 4.2 nl of CRISPR/Cas9 injection solution (Fig. 11). The solution contained 100 ng/μl gRNA 1, 125 ng/μl gRNA 2 and 300 ng/μl Cas9-NLS protein (*S. pyrogenes*, New England Biolabs). To verify whether the introduced gRNAs lead to insertion/deletion (indel) mutations in exon 1 and exon 2, respectively, both target sites were PCR amplified using GoTaq polymerase (Promega) (Fig. 12B; Table 5). Subsequent analysis of indel mutations was carried out by Sanger sequencing (Eurofins) (Fig. 12C). Embryos of the F<sub>0</sub> generation, i.e. injected with the CRISPR/Cas9 injection mix, were used for all CRISPR/Cas9 experiments. Uninjected embryos and embryos only injected with 300 ng/μl Cas9-NLS protein were stage-matched and served as control groups.

---

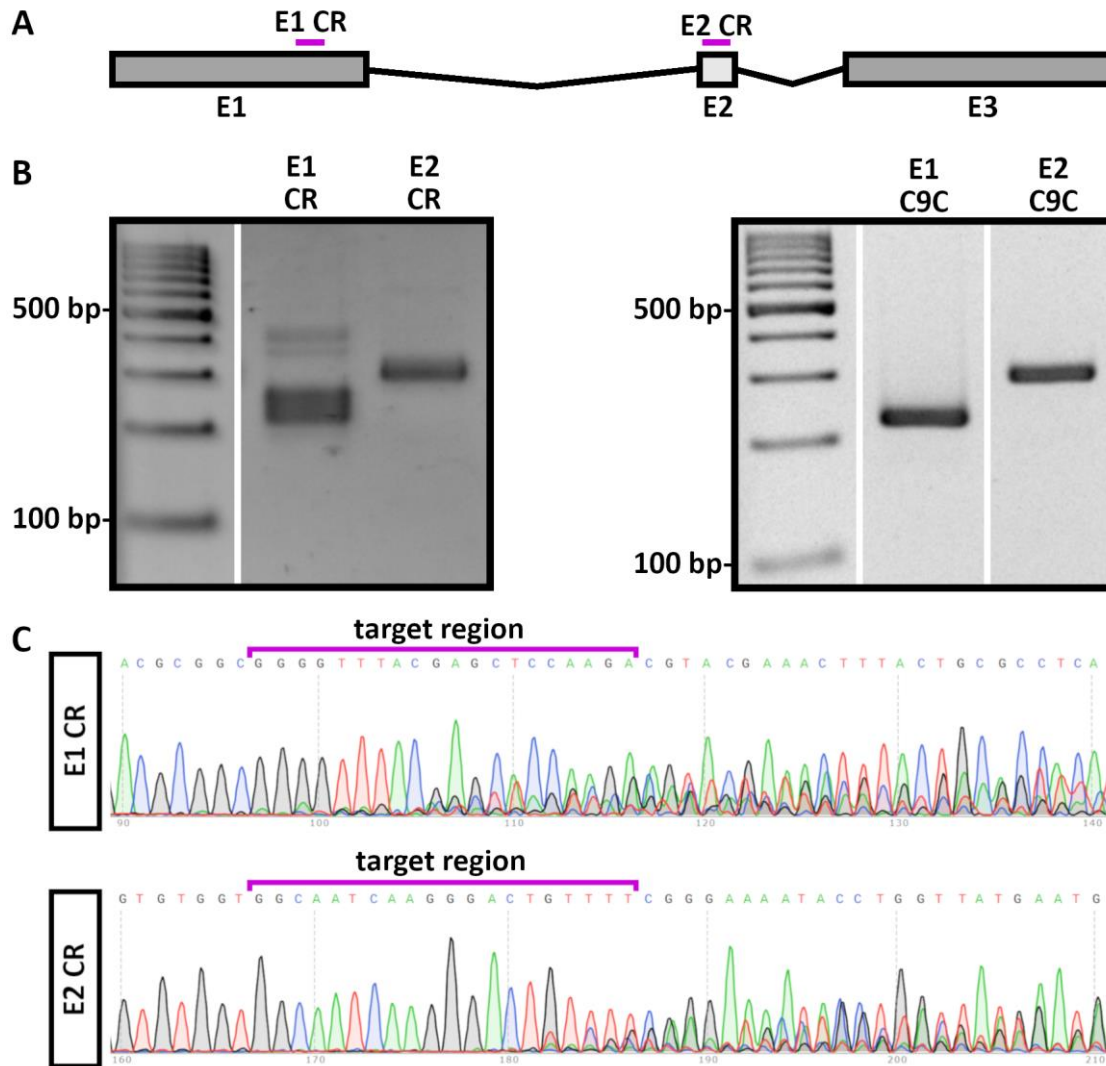


**Fig. 12: *fgf3* CRISPR/Cas9 knock-out efficiency and validation.** **A** Scheme of *fgf3* gene. Location of gRNA targets in exon 1 (E1 CR) and exon 2 (E2 CR) are depicted in magenta. **B** Genotyping results of two example embryos at 72 hpf by PCR. One embryo is injected with both gRNAs and Cas9 (left gel), the other control embryo is injected with Cas9 only (C9C) (right gel). Note multiple bands for E1 CR and E2 CR gRNA in CRISPR/Cas9 injected embryo (left gel). The control embryo shows single wildtype bands of amplified E1 and E2 target regions (E1 C9C: 224 bp, E2 C9C: 289 bp). **C** DNA sequencing traces of genotyping PCR. The embryo (same specimen as used for left gel in **B**) injected with E1 and E2 gRNAs revealed multiple traces in both target regions due to indel mutations. Modified from Reuter et al. (2019).

### Labelling proliferating cells in S phase

Embryos injected with the *fgf3* morpholino and uninjected control siblings were treated with 5-bromo-2'-deoxyuridine (BrdU, Sigma-Aldrich) to label all cells in S

phase at 36 hpf or 45 hpf. BrdU is a synthetic thymidine analogue which is incorporated into the DNA of replicating cells. For BrdU incorporation live embryos were treated with 10 mM BrdU in 15% DMSO in Danieau's solution. This BrdU pulse lasted for 20 min, during which the embryos were kept on ice. After several washes in 28°C warm Danieau's solution, embryos were either directly fixed for proliferation assays or raised until 72 hpf for cell fate assays. Immunohistochemistry was used for both assays to label BrdU-positive cells. Prior to immunohistochemistry, the epitope was revealed by an acid treatment. Thus, embryos were pre-treated with 10 µg/ml proteinase K (Roche), followed by the BrdU antigen retrieval in 2 N HCl for 1 h and neutralisation with 0.1 M borate buffer (pH 8.5) for 20 min.

## Cell death assays

### Acridine Orange

The cell death assay was carried out on live embryos using Acridine Orange. Embryos injected with *fgf3* morpholino and uninjected control siblings were treated at 24 hpf. Embryos were submerged in Danieau's solution containing 5 µg/ml Acridine Orange for 30 min at 28°C. Starting at this point, embryos were kept in darkness. Subsequent washes with warm Danieau's solution were directly followed by live imaging.

### Cleaved Caspase 3

*fgf3* morphants and uninjected control siblings fixed at 36 hpf were used for this cell death assay. Prior to cleaved caspase 3 (cCasp3) immunohistochemistry, the specimens were permeabilised in 100% acetone for 7 min at -20°C followed by a 50% MeOH in PBT treatment for 1 h at -20°C. Subsequently, washes in H<sub>2</sub>O were carried out. This concluded the preparations for immunohistochemistry.

---

## Immunohistochemistry

Only embryos processed for 5-HT and TH1 immunohistochemistry at 72 hpf and 4 dpf were dissected beforehand. The skin, eyes and jaw were removed for better antibody penetration during the immunohistochemical procedure. For all other antibody stainings embryos were not dissected.

The basic immunohistochemical procedure, which every embryo underwent, included a blocking step. One of two immuno blocking buffers was used depending on the antibody (Table 6). Incubation in the respective blocking buffer took either 1 or 2 h at room temperature. Subsequently, specimens were labelled with primary antibodies diluted in corresponding blocking buffers for 3 days at 4°C with slow shaking (Table 6). After several washes in PBT, immunoreactivity was revealed by incubation in secondary antibodies conjugated to Alexa Fluors. Secondary antibodies were diluted in the same blocking buffer used to dilute the primary antibody. The incubation period lasted 2 days at 4°C with slow shaking (Table 6). After several washes in PBT, embryos were stored in 80% glycerol in PBT and ready for imaging.

Table 6: Antibodies used for immunohistochemistry.

Antibody	Company	Host species	Clonality	Dilution	Cat. #	Blocking buffer
anti-5-HT	Sigma-Aldrich	rabbit	polyclonal	1:1000	S5545	1
anti-BrdU	antibodies-online	rat	monoclonal; clone: BU1-75	1:200	ABIN119313	2
anti-cCasp3	Cell Signalling	rabbit	polyclonal	1:500	9664	2
anti-pERK	Cell Signalling	rabbit	polyclonal	1:500	4370	2
anti-phH3	Millipore	rabbit	polyclonal	1:300	06-570	2
anti-TH1	Millipore	mouse	polyclonal	1:500	MAB318	1
Anti-rabbit IgG Alexa Fluor 488	Thermo Fisher Scientific	goat	polyclonal	1:1000	A-11034	
Anti-mouse IgG Alexa Fluor 568	Thermo Fisher Scientific	donkey	polyclonal	1:1000	A-10037	

### Whole-mount RNA *in situ* hybridisation

For whole-mount *in situ* hybridisation antisense RNA probes were synthesised by *in vitro* transcription of linearised plasmid DNA templates (Table 7).

Table 7: RNA probes used for whole-mount RNA *in situ* hybridisation.

Gene name	Gene abbreviation	Reference
<i>arginine vasopressin</i>	<i>avp</i>	Eaton et al. (2008)
<i>cortistatin</i>	<i>cort</i>	Devos et al. (2002)
<i>dual specificity phosphatase 1</i>	<i>dusp1</i>	this study
<i>dual specificity phosphatase 6</i>	<i>dusp6</i>	Tsang et al. (2004)
<i>ets variant 5b</i>	<i>etv5b</i>	Münchberg et al. (1999)
<i>fibroblast growth factor 3</i>	<i>fgf3</i>	Kiefer et al. (1996)
<i>fibroblast growth factor 8a</i>	<i>fgf8a</i>	Reifers et al. (1998)
<i>NK2 homeobox 4b</i>	<i>nkx2.4b</i>	Rohr and Concha (2000)
<i>oxytocin</i>	<i>oxl</i>	Unger and Glasgow (2003)
<i>tyrosine hydroxylase 2</i>	<i>th2</i>	Yamamoto et al. (2010)
Modified from Reuter et al. (2019).		

During this process the RNA, i.e. the uridine-5'-triphosphate (UTP) was labelled with digoxigenin (DIG) or fluorescein (fluo) using either a DIG or fluo labelling mix (Roche), respectively. Whole-mount RNA *in situ* hybridisations were largely performed as instructed in Thisse and Thisse (2008). For the procedure previously fixed and dehydrated embryos were transferred into a well plate where they were rehydrated and, subsequently, permeabilised with 10 µg/ml proteinase K (Roche) in PBT. The well plate was placed in a humid chamber, which was placed into a water bath heated to 65°C. The embryos were kept in the water bath at 65°C during the prehybridisation step lasting 1 h followed by overnight hybridisation with recycled probes, and during stringency washes on the next day. Hybridised transcripts were

labelled with anti-DIG (1:5000, Roche) or anti-fluo (1:2000, Roche) Fab fragments conjugated to alkaline phosphatase, which was necessary for subsequent colour precipitation. DIG labelled transcripts were precipitated with NBT/BCIP and fluo labelled transcripts with Fast Red tablets (Sigma-Aldrich) dissolved in respective buffers (see Annex, buffers). Firstly, transcripts of embryos processed for double RNA *in situ* hybridisation were labelled with an anti-fluo antibody revealed by Fast Red and secondly, with an anti-DIG antibody revealed by NBT/BCIP. A heat detachment of the anti-fluo antibody was carried out at 68°C for 2 h in PBT followed by incubation in the anti-DIG antibody. After PBT washes and fixation in 4% paraformaldehyde in PBT for 20 min the embryos were stored in 80% glycerol in PBT at 4°C.

### **Cryosections**

Following the *in situ* hybridisation procedure some embryos were cryo sectioned for histology. To cryoprotect the embryos they were incubated in 15% sucrose in PBS overnight. On the next day sucrose incubated embryos were embedded in 7.5% porcine skin gelatine (300 Bloom, Sigma-Aldrich) dissolved in 15% sucrose solution in PBS. After the gelatine had cured at 4°C, the resulting gelatine block was trimmed and immediately snap-frozen in 2-methylbutane, which was precooled in liquid nitrogen. This prevented the formation of ice crystals during the freezing process, which ensured a better tissue preservation. Subsequently, embryos were stored at -80°C. Frozen blocks were cut on a cryostat (Microm HM 500 OM). Frontal cryosections of embryo heads were collected on SuperFrost Plus slides (Thermo Fisher Scientific), rinsed in warm PBS, and prepared for imaging.

---

### 3D structural protein models of Fgf3

3D protein models were performed in collaboration with J. Kuper (Structural Biology, Rudolf-Virchow Centre for Experimental Research, University of Würzburg). To predict the structure of the zebrafish Fgf3 protein its amino acid sequence was sent to the Phyre2 server (Kelley et al., 2015). 155 residues of the entire Fgf3 sequence were modelled to the protein data bank entry 1IHK (Plotnikov et al., 2001) with a 100% confidence level. The modelled residues were subsequently used for structural analysis of wild type Fgf3 and two truncated Fgf3 isoforms. One isoform was derived from the *fgf3*<sup>l24l52</sup> mutation, the other resulted from *fgf3* morpholino injections (sequences: Fig. 10D). The three protein structures were modelled bound to a human FGF1 receptor, which was based on the protein data bank entry 3OJV (Beenken et al., 2012). PyMOL software (PyMOL Molecular Graphics System, version 2.0, Schrödinger, LLC) was used to visualise structures and the coot application (Emsley et al., 2010) for superpositions.

### Sample preparation, RNA library generation and analysis of the hypothalamic transcriptome

Sample preparation for RNA sequencing included the dissection of high quantities of hypothalami of homozygous wild type embryos (Tü/Tü) and homozygous *fgf3*<sup>l24l52</sup> mutants (in Tü/Tü background). The hypothalami were dissected at 3 and 7 dpf. The used wild type embryos were cousins to the homozygous mutants. In order to achieve this degree of kinship the wild type cousin embryos were the offspring of previously identified homozygous wild type adults. These wild type adults were in turn siblings to heterozygous adults, which gave birth to the homozygous mutant embryos used in this experiment. Homozygous *fgf3*<sup>l24l52</sup> mutant embryos were identified at 3 and 7 dpf

---



---

by their fused otoliths, which is the predominant phenotype (Herzog et al., 2004). Dissections were performed in petri dishes containing precooled slicing solution (Ma et al., 2015). Additionally, the petri dishes were put on ice to tranquilise the live embryos. Forceps were used to extract hypothalamic tissue. Extracted tissue was immediately preserved in RNAlater stabilisation solution (Qiagen), and stored at -80°C. The RNeasy Mini Kit (Qiagen) was used for RNA extractions. For each RNA sequencing sample dissected hypothalami were pooled to generate enough tissue to extract around 100 ng of RNA. Following this procedure, RNA for a total of 12 samples was extracted and pooled. These samples included three independent replicates for each experimental group. The experiment included a total of four groups (3 and 7 dpf wild type and mutant hypothalami).

The RNA libraries were created in cooperation with the Core Unit Systems Medicine of the University of Würzburg. The Illumina TruSeq stranded mRNA Sample Preparation Guide was used with 100 ng of input RNA and 15 PCR cycles to generate the RNA libraries. A total of 12 libraries were sequenced on an Illumina NextSeq 500 with a read length of 150 nt.

In collaboration with S. Kneitz (Physiological Chemistry, Biocentre, University of Würzburg) sequenced reads were mapped to the Ensembl *Danio rerio* genome version GRCz10 using the RNA-Seq aligner software STAR (Dobin et al., 2013). Expected read counts were calculated by the R package RNA-seq by Expectation Maximisation (RSEM) (Li and Dewey, 2011). Differentially expressed genes were detected using the Bioconductor/R package DESeq2 (Love et al., 2014).

Further analyses of hypothalamic gene expression focused on a selection of 82 genes relevant in the Fgf context (Table 8). Specifically, the selection included *fgf* genes, *fgf* receptor genes, Fgf-signalling pathway genes and Fgf downstream-target genes. The chosen Fgf-signalling pathway genes were mostly implicated in the Ras-Mapk pathway. This gene selection was compiled according to Itoh (2007), Ornitz and Itoh (2015), KEGG pathway mapping tool (Kanehisa, 2000) and zfin.org. Heat maps with dendrograms were visualised using R (package 'made4'). Genes were considered to

---

be expressed when they passed a base mean threshold of  $\geq 10$  in all four groups. Genes were considered to be differentially expressed when they passed a base mean threshold of  $\geq 10$  and a fold change threshold of  $\geq 1.5$  ( $\log_2 \text{FC} \geq 0.585$ ) in at least one of the three group comparisons that were carried out (wild type at 3 vs. 7dpf, wild type vs. mutant at 3 dpf, wild type vs. mutant at 7dpf).

Table 8: Selected Fgf-signalling pathway and target genes expressed in the hypothalamic transcriptome.

<i>pea3</i> -family, <i>fgf</i> , <i>fgfr</i> genes						
<i>etv1</i>	<i>fgf6a</i>	<i>fgf12a</i>	<i>fgf20b</i>			
<i>etv4</i>	<i>fgf6b</i>	<i>fgf12b</i>	<i>fgf21</i>			
<i>etv5a</i>	<i>fgf7</i>	<i>fgf13a</i>	<i>fgf22</i>			
<i>etv5b</i>	<i>fgf8a</i>	<i>fgf13b</i>	<i>fgf23</i>			
<i>fgf1a</i>	<i>fgf8b</i>	<i>fgf14</i>	<i>fgf24</i>			
<i>fgf1b</i>	<i>fgf9</i>	<i>fgf16</i>	<i>fgfr1a</i>			
<i>fgf2</i>	<i>fgf10a</i>	<i>fgf18a</i>	<i>fgfr1b</i>			
<i>fgf3</i>	<i>fgf10b</i>	<i>fgf18b</i>	<i>fgfr2</i>			
<i>fgf4</i>	<i>fgf11a</i>	<i>fgf19</i>	<i>fgfr3</i>			
<i>fgf5</i>	<i>fgf11b</i>	<i>fgf20a</i>	<i>fgfr4</i>			
Fgf-signalling pathway genes						
<i>araf</i>	<i>dusp3a</i>	<i>flrt3</i>	<i>kras</i>	<i>nf1b</i>	<i>rras2</i>	<i>tnip1</i>
<i>braf</i>	<i>dusp3b</i>	<i>frs2a</i>	<i>lamtor3</i>	<i>nras</i>	<i>shc1</i>	<i>tnip2</i>
<i>cnp1</i>	<i>dusp4</i>	<i>frs2b</i>	<i>map2k1</i>	<i>ptpn5</i>	<i>shc2</i>	
<i>cnp2</i>	<i>dusp5</i>	<i>frs3</i>	<i>map2k2a</i>	<i>raf1a</i>	<i>sos1</i>	
<i>cnp3</i>	<i>dusp6</i>	<i>gab1</i>	<i>map2k2b</i>	<i>raf1b</i>	<i>sos2</i>	
<i>cnp4</i>	<i>dusp7</i>	<i>grb2a</i>	<i>mapk1</i>	<i>rasa1a</i>	<i>spry1</i>	
<i>dusp1</i>	<i>dusp8a</i>	<i>grb2b</i>	<i>mapk3</i>	<i>rasa1b</i>	<i>spry2</i>	
<i>dusp10</i>	<i>flrt1a</i>	<i>hrasa</i>	<i>MRAS</i>	<i>rasa3</i>	<i>spry4</i>	
<i>dusp16</i>	<i>flrt1b</i>	<i>hrasb</i>	<i>mras</i>	<i>rasa4</i>	<i>syngap1a</i>	
<i>dusp2</i>	<i>flrt2</i>	<i>kl</i>	<i>nf1a</i>	<i>rras</i>	<i>syngap1b</i>	

Modified from Reuter et al. (2019).

### **Imaging, measurements, cell quantifications and figure preparation**

Prior to imaging of live embryos, they were mounted in 3% methylcellulose in Danieau's solution. Previously fixed embryos and sections were mounted in 80% glycerol in PBT. Images of live embryos were taken by a stereo microscope M205FA (Leica) with Leica Application Suit 3.8.0 (Leica). Fixed embryos were imaged with a light microscope Axiophot (Zeiss) and AxioVision Software. When fixed embryos had been processed for immunohistochemistry the images were taken with confocal microscopes Eclipse Ti (Nikon) or DMIRE SP2 system (Leica) with NIS Elements AR 3.22.15 (Nikon) or TCS (Leica) software, respectively.

Cell quantifications, area and length measurements were carried out using Fiji 1.8.0 imaging software (Schindelin et al., 2012) with the BioVoxxel Image Processing and Analysis Toolbox (Brocher, 2015). Cell quantifications were carried out double blinded utilising the Fiji point tool. Area measurements of the hypothalamic *nkx2.4b* expression domain were semi-automatically computed followed by manual validation and, if necessary, manual correction of the computed area. The body length of the embryos was measured manually as a straight line using the Fiji line tool. The beginning of the line marked the most anterior point and the end of the line marked the most posterior point of the body of the embryo.

During figure preparation background subtraction, and brightness and contrast adjustments were made to the entire image using Fiji 1.8.0 imaging software (Schindelin et al., 2012) with the BioVoxxel Image Processing and Analysis Toolbox (Brocher, 2015) and GIMP 2.10 (The GIMP Team). For confocal figure panels Z-stacks of confocal images were collapsed and represented as maximum intensity projections.

---

### Statistical analysis

Statistical analyses and graph design were performed with Rstudio 1.0.143 software (Rstudio, Inc.). Average and variance of experimental and control groups were represented by median and median absolute deviation (MAD) (Table 9). Normal distribution was analysed with the Shapiro-Wilk test. If the null hypothesis for normal distribution was accepted a parametric test would be used to evaluate the significance level. A non-parametric test would be used if the null hypothesis was rejected. Depending on group size either a two-sample t-test or a one-way ANOVA were run as parametric tests whereas a Mann-Whitney-U-test or a Kruskal-Wallis test were run as non-parametric tests. A parametric test followed a post-hoc test called Tukey's Honest Significance Differences for multiple group comparisons. In case of non-parametric data, the Nemenyi test served as a post-hoc test for multiple group comparisons. If the p-value was 0.05 or below the data would be considered significant. Significance levels were indicated in graphs as asterisks; one, two or three symbolising 0.05, 0.01 or 0.001, respectively.

---

## Results

### Characterisation of *fgf3* expression and impact on *etv5b* in the hypothalamus

Out of the 31 *fgf* genes found in zebrafish *fgf3* is not only reportedly expressed in the hypothalamus but also prominently represented in the caudal region (Herzog et al., 2004; Jackman et al., 2004; Liu et al., 2013; Reifers et al., 1998; Topp et al., 2008; Walshe and Mason, 2003). Moreover, caudal dopaminergic clusters of the hypothalamus show Fgf3 dependence during development (Koch et al., 2014). Serotonergic CSF-c cells form the largest cell cluster in the caudal hypothalamus and are intermingled with dopaminergic CSF-c cells known to be affected by Fgf3. Thus, Fgf3 may also play a role in the development of hypothalamic serotonergic CSF-c cells, especially, since the expression domain of *fgf3* may presumably overlap with serotonergic progenitors. Consequently, a detailed spatio-temporal expression analysis was carried out to determine the exact location of *fgf3* transcripts in relation to respective hypothalamic markers *rx3* and *emx2*, Fgf-signalling downstream target *etv5b* and feedback regulator *dusp6*. A time period between the 10 somites stage and 68 hpf was covered for the analysis focussing on 36 hpf and 68 hpf when serotonergic progenitors are most proliferating, and mature serotonergic CSF-c cells have become detectable, respectively (Bosco et al., 2013; Panula et al., 2010).

Generally, expression of *fgf3* in the hypothalamus was confirmed (Fig. 13) (Liu et al., 2013; Walshe and Mason, 2003). Specifically, the first cells expressing *fgf3* transcripts were observed in the presumptive hypothalamus at the 20 somites stage (Fig. 13A-D). At 30 hpf a similar expression pattern was revealed in the hypothalamic primordium (Fig. 13E,F). With advancing development, *fgf3* expression was confined to the caudal hypothalamus at 36 hpf and later (Fig. 13G,H,O,P). Further, double *in situ* hybridisation labellings at 30 and 36 hpf confirmed the caudally restricted expression

---

pattern of *fgf3* because it partially overlapped with the *emx2* expression pattern, which served as a caudal hypothalamic marker. Another double *in situ* hybridisation staining included the rostral hypothalamic marker *rx3* together with *fgf3*. Cells expressing *fgf3* were located more caudally compared to the rostral location of cells expressing *rx3*. Thus, no overlap between the expression patterns of the two genes was observed in the hypothalamus at 30 and 36 hpf further confirming the caudal position of *fgf3* expression (Fig. 13K-N). Later, at 68 hpf *fgf3* expression was even more restricted to cells located medially at the third ventricle (Fig. 13I,J,Q,R). Similarly, the Fgf-signalling downstream target *etv5b* and the feedback regulator *dusp6* were at first broadly expressed in the caudal hypothalamus at 36 hpf and later, at 68 hpf more confined (Fig. 13S-V). However, these transcripts were not limited to medially located cells at 68 hpf as opposed to cells expressing *fgf3*. Instead, *etv5b* and *dusp6* expressing cells were mediolaterally distributed along the posterior recess. *etv5b* expressing cells were located around the posterior recess whereas *dusp6* expressing cells were dorsally located above the posterior recess. To summarise, the observed hypothalamic expression of *fgf3* confirmed previous descriptions (Liu et al., 2013; Walshe and Mason, 2003). In the present study certain developmental stages relevant for serotonergic CSF-c cell ontogeny were analysed in greater detail, thus, expand the knowledge about hypothalamic *fgf3* expression. The hypothesis of *fgf3* being an important regulator in hypothalamic serotonergic CSF-c cell development possibly affecting early progenitor stages was continued to be investigated.

---

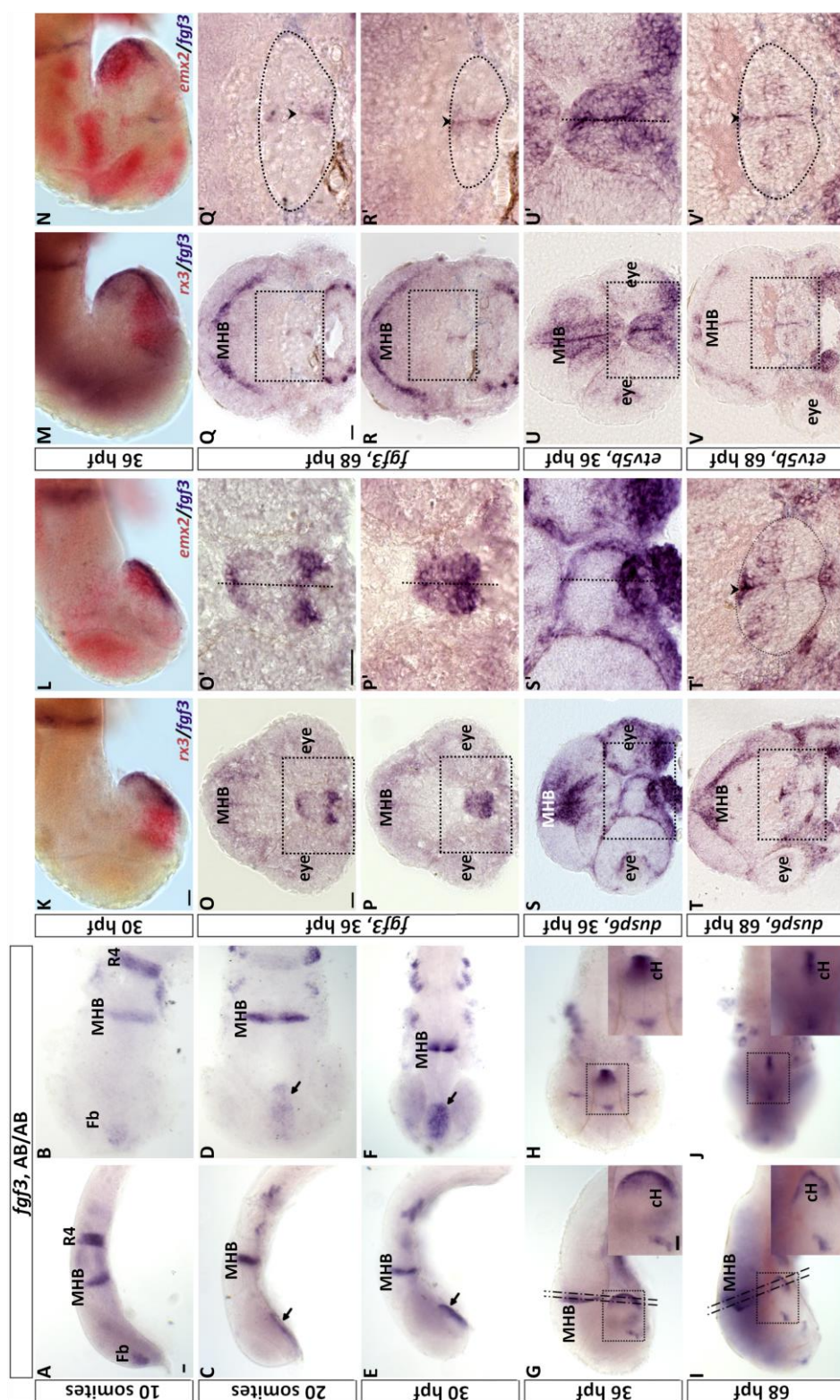


**Fig. 13: Spatio-temporal expression analysis of *fgf3* transcripts in the developing hypothalamus.** A, B *fgf3* transcripts are detectable in the forebrain (Fb), the mid- hindbrain boundary (MHB) and rhombomere 4 (R4) at the 10 somites stage. C–F *fgf3* expression in the hypothalamic primordium (arrows) at 20 somites and 30 hpf. G–J At 36 and 68 hpf *fgf3* transcripts are restricted to the caudal hypothalamus (cH). Left column shows lateral views and right column ventral views. Insets are high magnifications of boxed areas. Anterior to the left. K–N Double in situ hybridisation of *fgf3* and *rx3* or *emx2* at 30 and 36 hpf shows partial overlap of *fgf3* and *emx2* expression in the caudal hypothalamus. Anterior to the left. O–V 20 μm frontal cryosections at levels indicated in G and I of embryos stained for *fgf3*, *dusp6* and *etv5b* at 36 or 68 hpf. O'–V' High magnifications of boxed areas. Dashed lines in O', P', S' and U', and arrowheads in T', Q', R' and V' outline borders of caudal hypothalamus. Scale bars: 30 μm. Modified from Reuter et al. (2019).

The transcription factor *etv5b* belongs to the ETS-domain family and is a known downstream target of the intracellular Ras-Mapk pathway (Mason, 2007; Münchberg et al., 1999; Ornitz and Itoh, 2015; Raible and Brand, 2001; Roussigné and Blader, 2006). *etv5b* is activated by Fgf-signalling. Further, the Fgf ligand Fgf8a directly impacts on *etv5b* expression (Reifers et al., 1998; Roehl and Nüsslein-Volhard, 2001). This relationship has been investigated at embryonic stages in a general framework by loss-of-function and rescue experiments of *fgf8a*. In the context of hypothalamic serotonergic CSF-c cell development the relationship between Fgf-signalling and *etv5b* has been successfully demonstrated, yet the Fgf ligand regulating *etv5b*, thus, serotonergic CSF-c cell development remained undetermined (Bosco et al., 2013). However, Bosco et al. (2013) proposed an involvement of Fgf8a and/or Fgf3. Considering that *fgf8a* transcripts were only expressed in a few cells in the caudal hypothalamus at 36 hpf (Fig. 14A) (Reifers et al., 1998) as opposed to the broad expression pattern of *fgf3* (see above); Fgf3 appeared to be the more likely candidate in this particular context acting as the main Fgf ligand on serotonergic CSF-c cell development in the hypothalamus. Hence, Fgf3 was chosen for subsequent investigations. Therefore, the impact of Fgf3 on *etv5b* expression was analysed in *fgf3* morphants and in *fgf3*<sup>t24152</sup> mutants. This particular mutant allele was chosen because it is reported to be a null allele (amorph) (Herzog et al., 2004). The expression assays performed in *fgf3* impaired embryos at 36 hpf revealed that *etv5b* is indeed regulated by Fgf3 (Fig. 14B-G). *etv5b* transcripts were reduced in *fgf3*<sup>t24152</sup> mutants compared to wild type siblings (Fig. 14B-D). Moreover, homozygous mutants exhibited a more restricted expression pattern than heterozygous mutants suggesting a dose-dependent decline of *etv5b* expression. Additionally, the hypothalamic transcriptome analysis further confirmed these findings because homozygous mutants had lower read counts of *etv5b* transcripts than wild types both at 3 and 7 dpf (Fig. 14E). *etv5b* read counts did not transgress past the general thresholds applied to the transcriptome analysis, thus, are not included in Fig. 25, yet separately mentioned here. However, in *fgf3* morphants a similar decline of *etv5b* expression was observed as reported for *fgf3*<sup>t24152</sup> mutants (Fig.

---



14F,G). In summary, Fgf3 is partially regulating *etv5b* expression in the caudal hypothalamus during development. Notably, *etv5b* expression never ceased completely in the hypothalamus of mutants or morphants at 36 hpf nor in the transcriptome analysis at later stages. This may indicate that other Fgf ligands, possibly Fgf8a, are also regulating *etv5b* in the caudal hypothalamus.

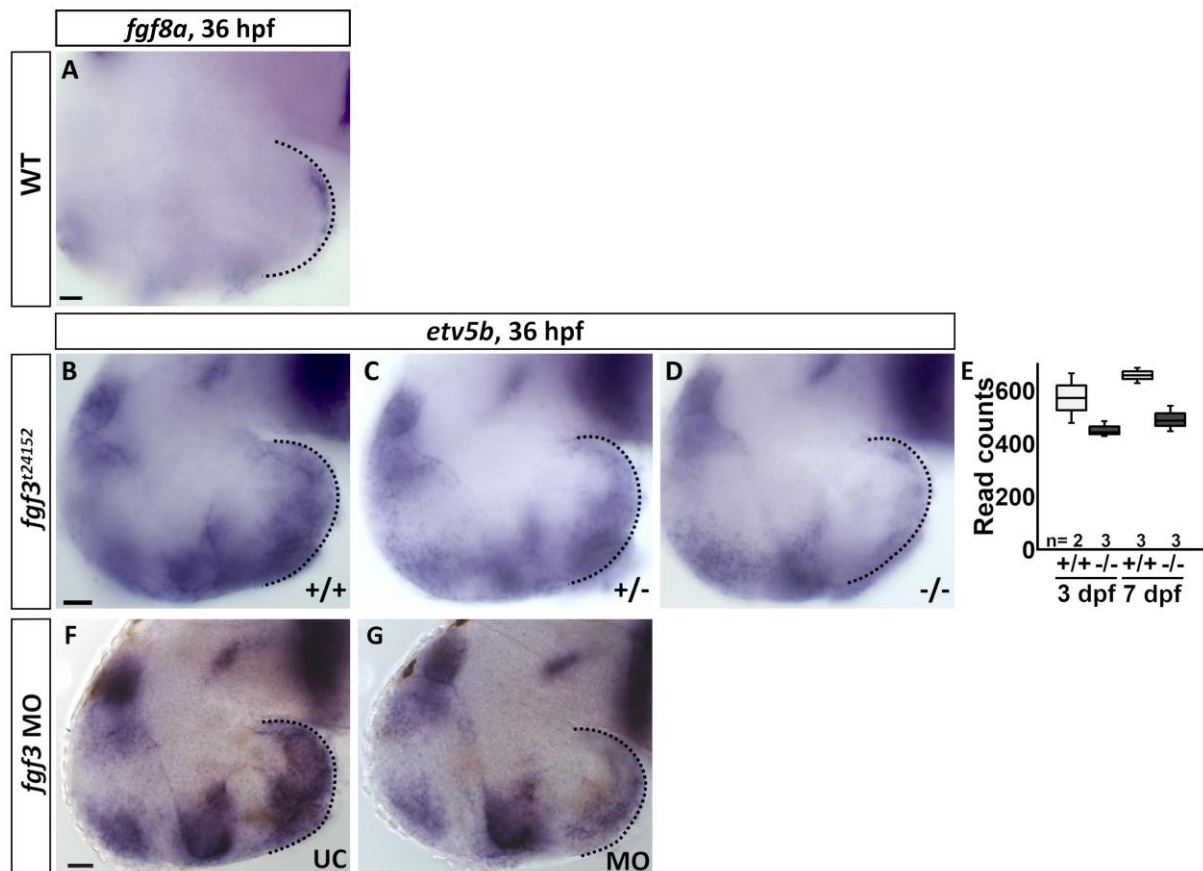


**Fig. 14:** Expression assays of *fgf8a* and *etv5b*. *etv5b* expression is reduced in the caudal hypothalamus of *fgf3<sup>t24152</sup>* mutants and *fgf3* morphants. **A** RNA *in situ* hybridisation of *fgf8a* at 36 hpf in wild types. **B-D, F, G** RNA *in situ* hybridisation of *etv5b* at 36 hpf in wild types (+/+), heterozygous (+/-) and homozygous (-/-) *fgf3<sup>t24152</sup>* mutant siblings, and uninjected controls (UC) and *fgf3* morphant (MO) siblings. **A-D, F, G** Light microscopic images depicting lateral views, anterior to the left. Dotted line indicates caudal hypothalamus. Scale bars: 30  $\mu$ m. **E** Read counts of *etv5b* transcripts generated by the transcriptome analysis of the hypothalamus of wild types (+/+) and homozygous (-/-) *fgf3<sup>t24152</sup>* mutants at 3 and 7 dpf. Tukey boxplots show median, 25–75% percentile, IQR whiskers and outliers. n=number of analysed replicates. Modified from Reuter et al. (2019).

### **Fgf3 regulates caudal hypothalamic monoaminergic CSF-c cell development**

Descriptive expression data pointed toward Fgf3 being a likely candidate involved in the generation of hypothalamic serotonergic CSF-c cells. Thus, functional investigations followed next. For functional studies three techniques to manipulate Fgf3 activity were applied. Analysis of monoaminergic CSF-c cell numbers followed in all three contexts. The first strategy included the *fgf3*<sup>t24152</sup> mutant. The *fgf3*<sup>t24152</sup> mutant has a G to A transition point mutation in the codon translated to tryptophan (W) at amino acid position 178 of 256 in wild types (Fig. 10D) (Herzog et al., 2004). The point mutation, however, introduces a stop codon leading to a premature end of translation after amino acid 177. Thereby, a truncated Fgf3 protein forms with 69% of the wild type amino acid sequence remaining. The second strategy was comprised of a morpholino-based knock-down of *fgf3* (Fig. 10). The splice-blocking morpholino lead to an inclusion of intron 2. As a consequence, a non-sense amino acid sequence was created during translation. The non-sense sequence started after amino acid 127, which is serine (S), the last wild type amino acid coded in exon 2 (Fig. 10D). Therefore, the Fgf3 amino acid sequence of morphants shared only 50% homology to the wild type amino acid sequence. After translation of the alternative sequence, eventually, a premature stop was introduced. The third strategy aimed to create a CRISPR/Cas9 knock-out for *fgf3* (Fig. 12). Hereby, indel mutations were generated due to error prone non-homologous end joining (Fig. 12C) (Hwang et al., 2013). The indel mutations result in a non-sense amino acid sequence or cause a premature end of translation. If a wild type amino acid sequence of *fgf3* was still translated it would have consisted of only a few residual wild type amino acids close to the N-terminal. Presumably, the short fragment may have been degraded. However, for the following experiments the F<sub>0</sub> generation was used as opposed to a stable line. The F<sub>0</sub> embryos were injected with a CRISPR/Cas9 cocktail probably causing an incomplete knock-out of *fgf3* with a

---

random mosaic loss-of-function of *fgf3* in many but not all cells of the embryo. Irrespective of the applied strategy, all embryos displayed comparable craniofacial and ear phenotypes at 72 hpf (Fig. 15). Loss of ceratobranchial cartilage leads to malformations of the ventral head skeleton, which were visible in embryos after *fgf3* impairment (Fig. 15A'-F'). Further, embryos had fused otoliths since Fgf3 impacts on anterior ear specification (Fig. 15A'-F') (Hammond and Whitfield, 2011; Herzog et al., 2004). Additionally, swim bladder inflation was disrupted (not shown).

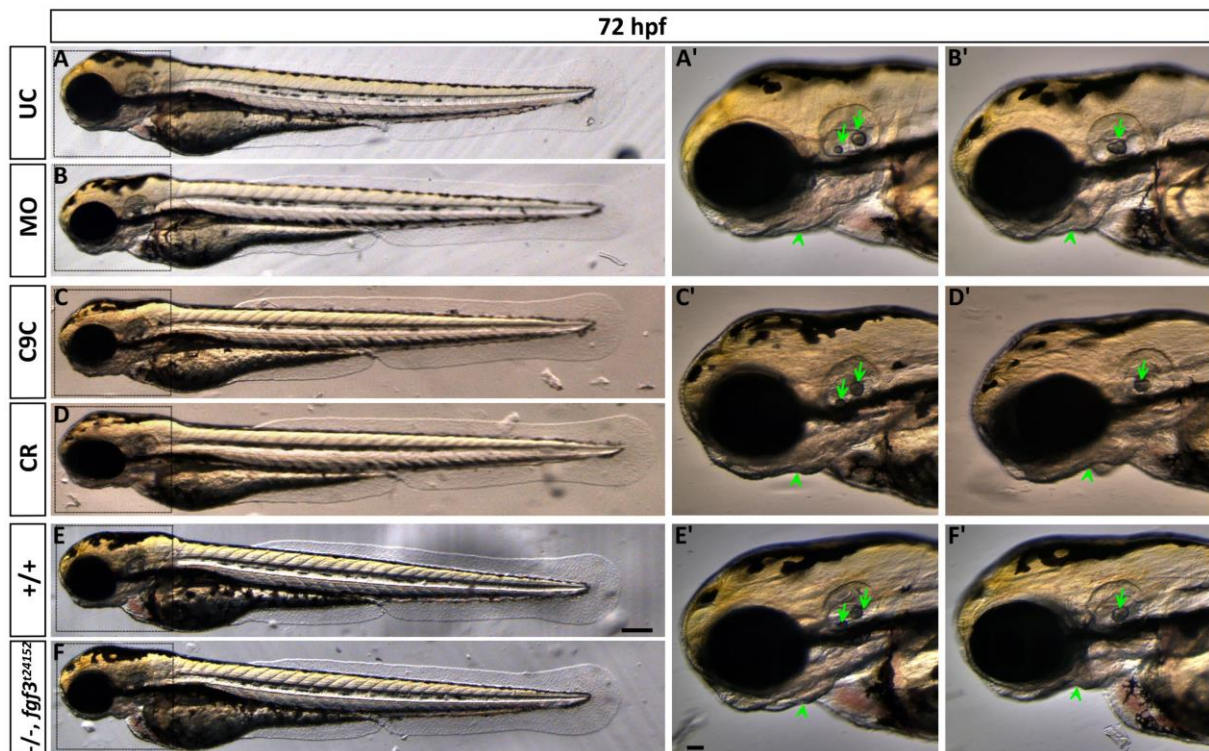


**Fig. 15: Morphological comparison of embryos after *fgf3* impairment highlights characteristic ear and craniofacial malformations.** A,B Morphology of uninjected control (UC) and *fgf3* morpholino injected (MO) siblings. C, D Morphology of Cas9 injected control (C9C) and *fgf3* CRISPR/Cas9 injected (CR) siblings. E, F Morphology of wild type (+/+) and homozygous *fgf3*<sup>t24152</sup> mutant (-/-) siblings. A-F Live images of embryos at 72 hpf. Areas in dashed boxes are magnified in A'-F'. Arrows point out otoliths, two in controls and one fused otolith in *fgf3* impaired embryos. Arrowheads depict lower jaw bone phenotype of *fgf3* impaired embryos compared to controls. Lateral views, anterior to the left. Scale bar in E: 100  $\mu$ m; in E': 50  $\mu$ m. Modified from Reuter et al. (2019).

The observed phenotypes confirmed previous descriptions of the *fgf3*<sup>t24152</sup> mutant (Hammond and Whitfield, 2011; Herzog et al., 2004) and emphasised the reproducibility between the three strategies. Notably, embryos were all similar in size and no additional morphological defects were observed (Figs. 15, 20J). Two cell death assays using Acridine Orange and cCasp3 as markers were performed at 24 and 36 hpf to examine possible side effects due to morpholino toxicity (Fig. 16). Both assays remained unobtrusive in morphants compared to wild types. Taken together, all three strategies to impair *fgf3* yielded similar phenotypes. Thus, the qualitative comparability between the three strategies was high establishing a firm foundation for subsequent investigations in the developing hypothalamus.

---

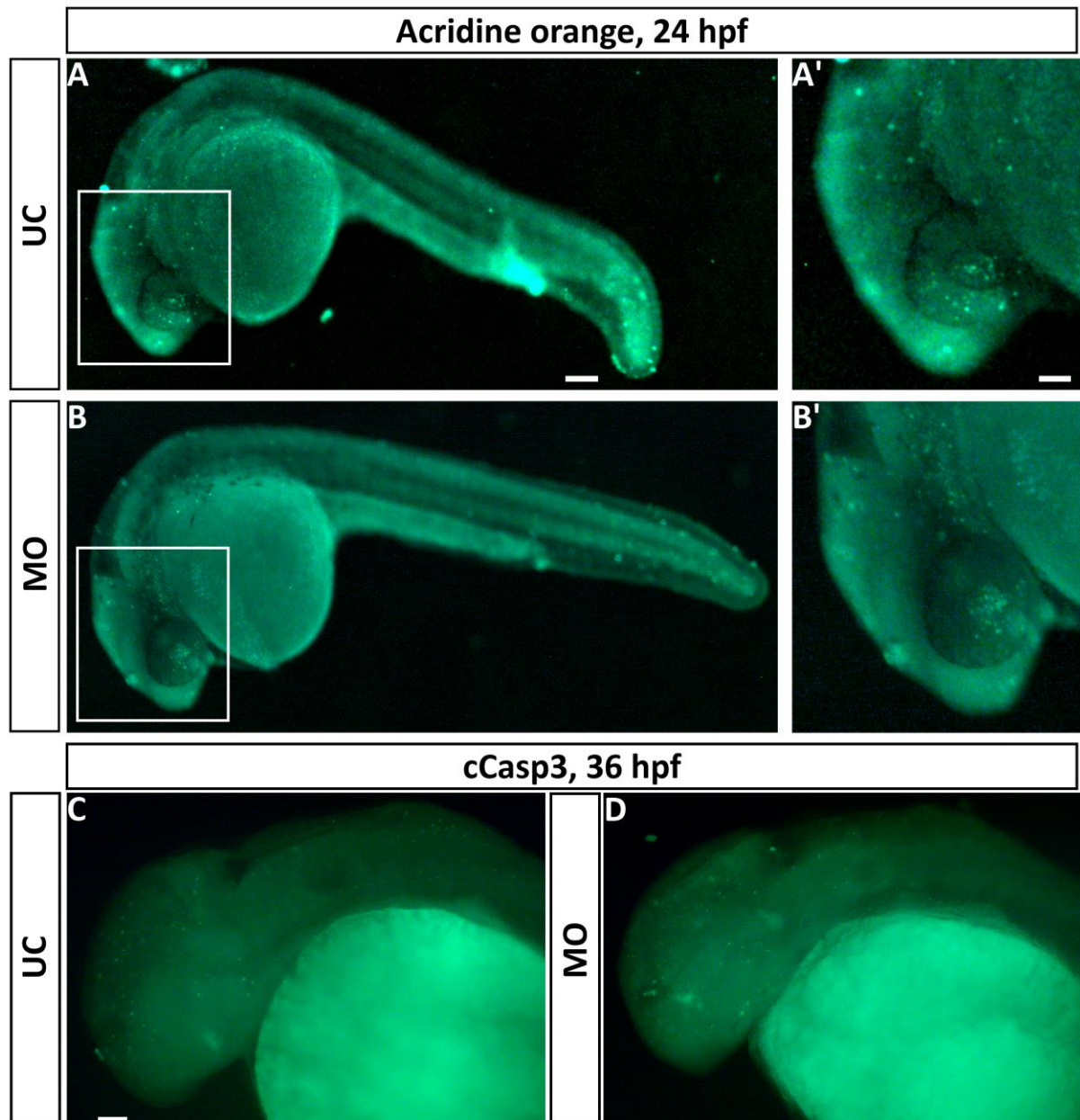


**Fig. 16: Cell death is unobtrusive in *fgf3* morphants at 24 and 36 hpf.** A, B Live images showing uninjected control (UC) and morphant (MO) siblings stained with Acridine Orange at 24 hpf. Boxed areas were magnified in A' and B'. C, D Uninjected control and morphant siblings were immunolabelled with Cleaved caspase 3 (cCasp3) at 36 hpf. Lateral views, anterior to the left. Scale bar in A: 100  $\mu$ m; in A' and C: 50  $\mu$ m. Acridine Orange assay performed by J. Jäckels. From Reuter et al. (2019).

To investigate the development of monoaminergic CSF-c cells in the hypothalamus all three strategies to impair *fgf3* were applied. Immunoreactive cells of the intermediate and caudal serotonergic clusters were quantified at 72 hpf and at 4 dpf. At 4 dpf only *fgf3* morphants were analysed. Starting around 62 hpf caudal serotonergic CSF-c cells



become mature (Bellipanni et al., 2002; Bosco et al., 2013; McLean and Fetcho, 2004; Panula et al., 2010). Until 72 hpf a well detectable and quantifiable cluster of caudal serotonergic CSF-c cells had developed that was even more prominent at 4 dpf. Serotonergic CSF-c cells were co-stained together with TH1-positive CSF-c cells at 72 hpf and 4 dpf to analyse catecholaminergic CSF-c cells of the hypothalamic field (Figs. 17, 18). As this region is populated by many catecholaminergic clusters (Fig. 7) (Rink and Wullimann, 2001) only the clusters closest to the caudal hypothalamus were quantified. These included cluster DC 4/5/6 located at the lateral recess close to the intermediate serotonergic cell cluster and cluster DC 7 located in the surrounding tissue of the posterior recess. The CSF-c cells of cluster DC 7 are intermingled with caudal serotonergic CSF-c cells (Kaslin and Panula, 2001; McLean and Fetcho, 2004; Rink and Wullimann, 2002). In addition to Th1, *th2* expressing cells labelled by *in situ* hybridisation were quantified in the caudal hypothalamus of morphants at 4 dpf. This developmental stage was chosen because *th2* is only expressed in a few cells at earlier stages in the caudal hypothalamus (Chen et al., 2009; Panula et al., 2010). The examined Th1 and *th2* clusters have been demonstrated to be dopaminergic (Filippi et al., 2007; Xavier et al., 2017; Yamamoto et al., 2010; 2011).

---

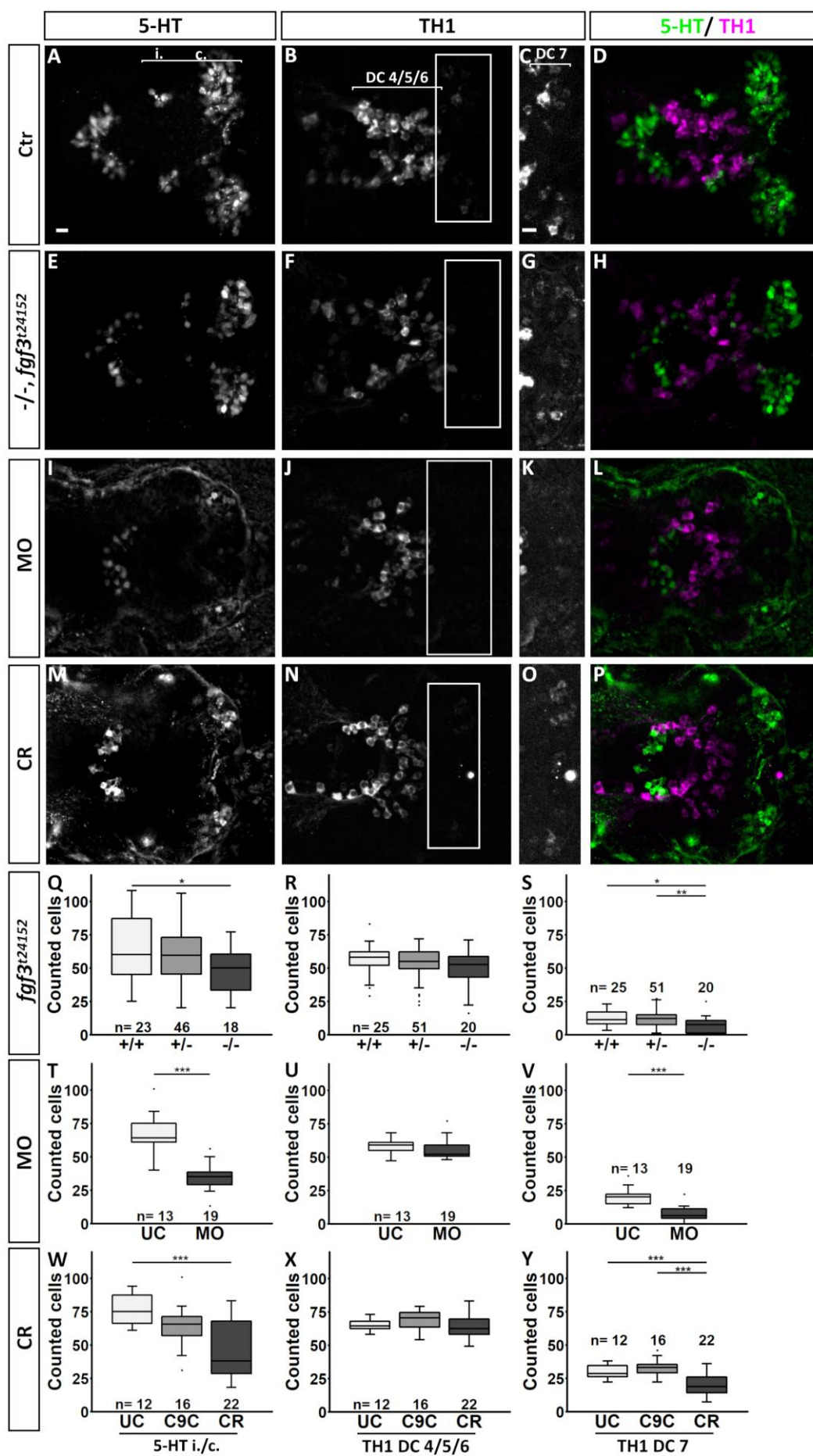
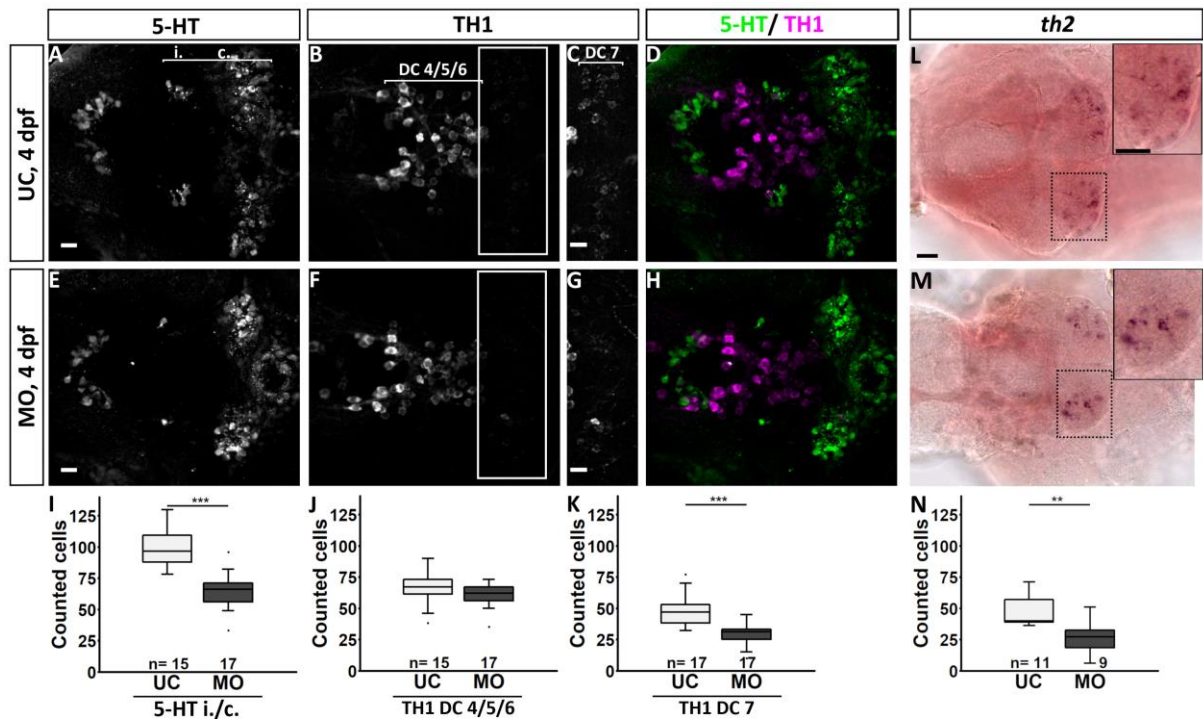


Fig. 17: See next page for legend.

**Fig. 17: Quantification of serotonergic and dopaminergic CSF-c cells of the caudal hypothalamic field at 72 hpf after *fgf3* manipulation** **A–P** Confocal maximum intensity projections (MIPs) of wild type controls (Ctr), homozygous *fgf3*<sup>t24152</sup> mutants (–/–), *fgf3* morphants (MO) and *fgf3* CRISPR/Cas9 embryos (CR) co-labelled with 5-HT (green) and TH1 (magenta) antibodies. Antibody stainings shown as single and merged channels. **A** Line indicates quantified intermediate (i.) and caudal (c.) serotonergic cell clusters. **B, C** Line indicates quantified dopaminergic cells in clusters DC 4/5/6 and DC 7, respectively. Boxed area in **B, F, J** and **N** is magnified in **C, G, K** and **O**, respectively, depicting TH1 positive cells of cluster DC 7 adjusted for brightness and contrast for better visualisation. Ventral views, anterior to the left. Scale bars: 10 µm. **Q–Y** Quantifications of 5-HT and TH1 immunoreactive cells in i./c. and DC 4/5/6 and DC 7 clusters of controls (+/+, UC, C9C) and related *fgf3* manipulated siblings (+/–, –/–, MO, CR). Tukey boxplots show median, 25–75% percentile, IQR whiskers and outliers. n=number of analysed individuals. +/–, heterozygous *fgf3*<sup>t24152</sup> mutants; UC, uninjected siblings; C9C, injected with Cas9 only. \*P>0.05, \*\*P>0.01, \*\*\*P>0.001. Data of *fgf3*<sup>t24152</sup> mutant experiments was pooled with previously generated data in Reuter (2015). Modified from Reuter et al. (2019).

Generally, the number of serotonergic CSF-c cells was significantly reduced in homozygous *fgf3*<sup>t24152</sup> mutants, *fgf3* morphants and *fgf3* CRISPR/Cas9 embryos at 72 hpf compared to respective wild type controls (Fig. 17). However, depending on the applied strategy the serotonergic phenotype varied in intensity as quantifications of immunoreactive serotonergic cells revealed. In detail, this meant that homozygous *fgf3*<sup>t24152</sup> mutants were missing 17% of serotonergic CSF-c cells compared to wild type siblings (Fig. 17Q; Table 9). *fgf3* morphants had 45% fewer cells than uninjected controls (Fig. 17T; Table 9). *fgf3* CRISPR/Cas9 embryos showed a reduction of 49% when compared to uninjected controls and 42% when compared to Cas9 injected controls. Hence, the loss of serotonergic CSF-c cells was most severe in *fgf3* CRISPR/Cas9 embryos and *fgf3* morphants. Out of the three strategies *fgf3*<sup>t24152</sup> mutants displayed the weakest serotonergic phenotype (Fig. 17W; Table 9). The serotonergic CSF-c cell number of intermediate and caudal hypothalamic clusters continued to be significantly reduced in *fgf3* morphants at 4 dpf (Fig. 18A,E,I; Table 9). The cell loss amounted to 33% compared to uninjected controls.





**Fig. 18: Quantification of 5-HT-, TH1- and *th2*-positive cells of the hypothalamic field at 4 dpf in *fgf3* morphants.** A–H Confocal MIPs of uninjected controls (UC) and *fgf3* morphants (MO) co-labelled with 5-HT (green) and TH1 (magenta) antibodies. Antibody stainings shown as single and merged channels. A Line indicates quantified intermediate (i.) and caudal (c.) serotonergic cell clusters. B, C Line indicates quantified dopaminergic cells in clusters DC 4/5/6 and DC 7, respectively. Boxed area in B and F is magnified in C and G, respectively, depicting TH1 positive cells of cluster DC 7 adjusted for brightness and contrast for better visualisation. Ventral views, anterior to the left. Scale bars: 10  $\mu$ m. L, M Light microscopic images depicting *th2* expression after *in situ* hybridisation in the caudal hypothalamus of UC and MO. Boxed areas are magnified in insets. Ventral views, anterior to the left. Scale bars in A, E, C, G: 10  $\mu$ m; in L: 30  $\mu$ m. I–K, N Quantifications of 5-HT, TH1 and *th2*-positive cells in the hypothalamic field clusters. Tukey boxplots show median, 25–75% percentile, IQR whiskers and outliers. n=number of analysed individuals. \* $P > 0.05$ , \*\* $P > 0.01$ , \*\*\* $P > 0.001$ . *fgf3* MO experiments/data generated by J. Jäckels (2017). Modified from Reuter et al. (2019).

The quantification of TH1 immunoreactive CSF-c cells of cluster DC 4/5/6 revealed similar cell numbers in controls and *fgf3* impaired embryos at 72 hpf (Fig. 17R,U,X; Table 9). In contrast, cluster DC 7 showed a significant reduction of dopaminergic CSF-c cells with all three approaches (Fig. 17S,V,Y; Table 9). Accordingly, homozygous *fgf3*<sup>t24152</sup> mutants lost 32% and *fgf3* morphants 70% of TH1-positive cells compared to respective control groups. Additionally, homozygous mutants lost 38% of TH1-positive cells compared to heterozygous siblings. In *fgf3* CRISPR/Cas9 embryos the cell reduction amounted to 35% compared to uninjected controls, and to 44% compared to

Cas9 injected controls. As already observed for the analysed serotonergic CSF-c cells *fgf3*<sup>t24152</sup> mutants displayed the weakest dopaminergic phenotype. Similar to the results at 72 hpf, at 4 dpf the dopaminergic CSF-c cell number of cluster DC 4/5/6 remained unaffected in *fgf3* morphants (Fig. 18B,F,J; Table 9). However, the reduction of dopaminergic CSF-c cells in cluster DC 7 of *fgf3* morphants continued at 4 dpf (Fig. 18C,G,K; Table 9). Morphants lacked 34% of cells compared to uninjected controls. Moreover, *th2* expressing cells located in the caudal hypothalamus close to TH1-positive cells of cluster DC 7 were also significantly decreased in *fgf3* morphants at 4 dpf (Fig. 18L,M,N; Table 9). Here, 33% of cells were missing in morphants compared to uninjected controls.

Summarising, *fgf3* impairment by three autonomous techniques rendered the same stable and previously reported ear, jaw and swim bladder phenotypes. Apart from the named defects, the overall morphology of the embryos was wild type-like. Thus, the observed effects in subsequent experiments were expected to be highly *fgf3* specific and qualitatively comparable between strategies. Hence, it came as no surprise that the investigation of monoaminergic CSF-c cells in the hypothalamic field consistently resulted in a cell loss with all three strategies. However, the intensity of the cell loss after *fgf3* impairment varied from strategy to strategy. Nonetheless, *Fgf3* dependence proved to be a specific effect among monoaminergic CSF-c cells of the caudal hypothalamus.

---

Table 9: Quantifications of analysed cell clusters in the hypothalamic field, and measurements of the *nkx2.4b* expression domain after *fgf3* impairment.

Fig.	17, 18						19		20, 21				21	22		23		26		
marker	5-HT		TH1			th2	oxt	avp	cort	nkx2.4b				Fish length	phH3	BrdU	5-HT	BrdU/5-HT	pErk	
area	i./c.		DC 4/5/6		DC 7	DC 7				ventral		lateral			cH	BrdU	i./c.	i./c.		
hpf	72	96	72	96	72	96	72	72	72	36	48	72	36	48	72	36	36	36-72	45-72	45-72
fgf3 morpholino	UC	64 ±11	59 ±4	67 ±6	20 ±5	47 ±9	40 ±4	127.5 ±9.5	57 ±4	37950 ±3352	36 ±27	48 ±26	72 ±40	36 ±27	48 ±23	72 ±24	109 ±16.5	87 ±6	98 ±21	25 ±43
	n	13	15	13	15	13	17	9	28	31	27	26	40	27	23	24	12	5	11	6
	MO	35 ±6	52 ±2	62 ±6	6 ±4	31 ±3	27 ±7	128 ±14	51 ±6	30840 ±3067	36 ±19	48 ±22	72 ±24	36 ±18	48 ±24	72 ±24	84.5 ±13.5	36 ±5	46 ±10	9 ±2.5
	n	19	17	19	17	19	17	11	24	25	19	22	24	18	24	24	12	4	15	6
p	4.6 e-06	2.0 e-06	0.191	0.19	1.2 e-05	9.5 e-06	0.001	n.s.	3.0 e-04	1.1 e-06	1.0 e-04	6.8 e-09	4.4 e-06	n.s.	n.s.	0.041 (0.862)	2.0 e-05	0.005	2.6 e-05	0.021
fgf3 <sup>124152</sup> mutation	+/+	60 ±22	58 ±6	11 ±4	-	-	-	27 ±4	86 ±10.5	28780 ±1832	28110 ±2861	42600 ±811	-	-	-	-	-	-	-	-
	n	23	25	-	25	-	-	14	20	12	17	10	-	-	-	-	-	-	-	-
	+/-	59.5 ±14	55 ±7	-	12 ±4	-	-	26 ±3	90 ±11	28310 ±2240	26390 ±1932	40870 ±1624	-	-	-	-	-	-	-	-
	n	46	51	-	51	-	-	38	26	41	36	34	18	-	-	-	-	-	-	-
	-/-	50 ±14.5	52.5 ±8.5	7.5 ±4.5	-	-	-	31 ±3	97 ±4	26950 ±1370	25160 ±1306	36670 ±1842	-	-	-	-	-	-	-	-
	n	18	20	-	20	-	-	19	15	16	11	20	19	-	-	-	-	-	-	-
	p	0.04	n.s.	-	0.0097	-	-	0.017	0.002	n.s.	0.076	0.038	3.7 e-08	-	-	-	-	-	-	-
	UC	75 ±12	64.5 ±3	28.5 ±4.5	-	-	-	-	-	-	-	-	-	-	-	-	-	-	-	-
fgf3 CRISPR/Cas9	n	12	12	-	12	-	-	-	-	-	-	-	-	-	-	-	-	-	-	-
	C9C	65.5 ±6	70.5 ±5.5	33 ±3.5	-	-	-	-	-	-	-	-	-	-	-	-	-	-	-	-
	n	16	16	-	16	-	-	-	-	-	-	-	-	-	-	-	-	-	-	-
	CR	38 ±16	62.5 ±5.5	18.5 ±6	-	-	-	-	-	-	-	-	-	-	-	-	-	-	-	-
n	22	12	-	12	-	-	-	-	-	-	-	-	-	-	-	-	-	-	-	
p	7.0 e-04	n.s.	-	1.3 e-07	-	-	-	-	-	-	-	-	-	-	-	-	-	-	-	-

Cell numbers and area sizes (pixels) displayed as median±MAD. p, p-values, determined by two-sample t-test, Mann-Whitney-U test, one-way ANOVA, or Kruskal-Wallis test. n, number of analysed individuals. C9C, Cas9 only injected control; cH, caudal hypothalamus; CR, CRISPR/Cas9 injected; MO, morphant; UC, uninjected control. Modified from Reuter et al. (2019)

### **Neuroendocrine cells expressing *avp* depend on Fgf3 whereas neuroendocrine cells expressing *oxl* and *cort* do not**

Due to the requirement of monoaminergic CSF-c cells for Fgf3 in the caudal hypothalamus the question whether the Fgf3 requirement is specific to monoaminergic CSF-c cells was subsequently addressed. To test this hypothesis three neuroendocrine cell markers *oxl*, *avp* and *cort* were chosen because they are expressed in close proximity to the monoaminergic clusters of the hypothalamic field (Devos et al., 2002; Eaton et al., 2008; Unger and Glasgow, 2003). Only a few genes of the regulatory network governing the development of these neuroendocrine cells are identified. Interestingly, the known genes regulate dopaminergic CSF-c cell development as well. Among them are *arnt1/sim1*, *otpa* and *otpb* (Eaton and Glasgow, 2006; 2007; Fernandes et al., 2013; Löhr et al., 2009). To test the alleged Fgf3 dependence *oxl*, *avp* and *cort* expression patterns were revealed by *in situ* hybridisation in *fgf3*<sup>l24152</sup> mutants and *fgf3* morphants at 72 hpf. Subsequently, stained cells in the hypothalamic field were quantified. *oxl* and *cort* clusters were independent of Fgf3 as cell numbers varied insignificantly between experimental and control groups (Fig. 19; Table 9). Taking a closer look at the quantified *oxl* cell numbers in *fgf3*<sup>l24152</sup> mutants (Fig. 19M): the statistical analysis of *oxl* cell quantifications suggested a significant difference between heterozygous and homozygous *fgf3*<sup>l24152</sup> mutants. However, the actual difference between this significant comparison and the statistical insignificant comparison between wild types and homozygous mutants amounted to an average of one cell (Table 9). This one-cell difference reflects the number of cells that the medians of wild types and heterozygous mutants diverged on average. The medians were 26 and 27 cells, respectively. The slight difference between the medians together with, generally, low variances in all three groups possibly caused the significant result between heterozygous and homozygous mutants rather than an actual biological difference due to *fgf3* impairment. Thus, it was concluded that the significance was in

---

---

this case a false positive result. Henceforth, *oxl* expressing cells were regarded to be independent of Fgf3. Additionally, this interpretation was supported by the *fgf3* morphant data.

However, an in all likelihood true positive result was observed for *avp* expressing cells. Quantifications showed that *avp* expressing cells were significantly reduced (Fig. 19E-H,O,P; Table 9). Precisely, homozygous *fgf3*<sup>t24152</sup> mutants were missing 16% of cells compared to wild types and 14% of cells compared to heterozygous *fgf3*<sup>t24152</sup> mutants. *fgf3* morphants lost 11% of cells compared to uninjected controls. Interestingly, the Fgf3-dependent *avp* cluster was most reduced at its caudal end whereas rostral *avp* expressing cells seemed to be less affected (Fig. 19E-H). This appeared to be another similarity to dopaminergic CSF-c cells in addition to the partial overlap of regulatory genes. The dopaminergic CSF-c cell cluster DC 7, the most caudal one in the hypothalamus, was affected by Fgf3 whereas the more anterior cluster DC4/5/6 was not (Figs. 17, 18) (Koch et al., 2014).

---

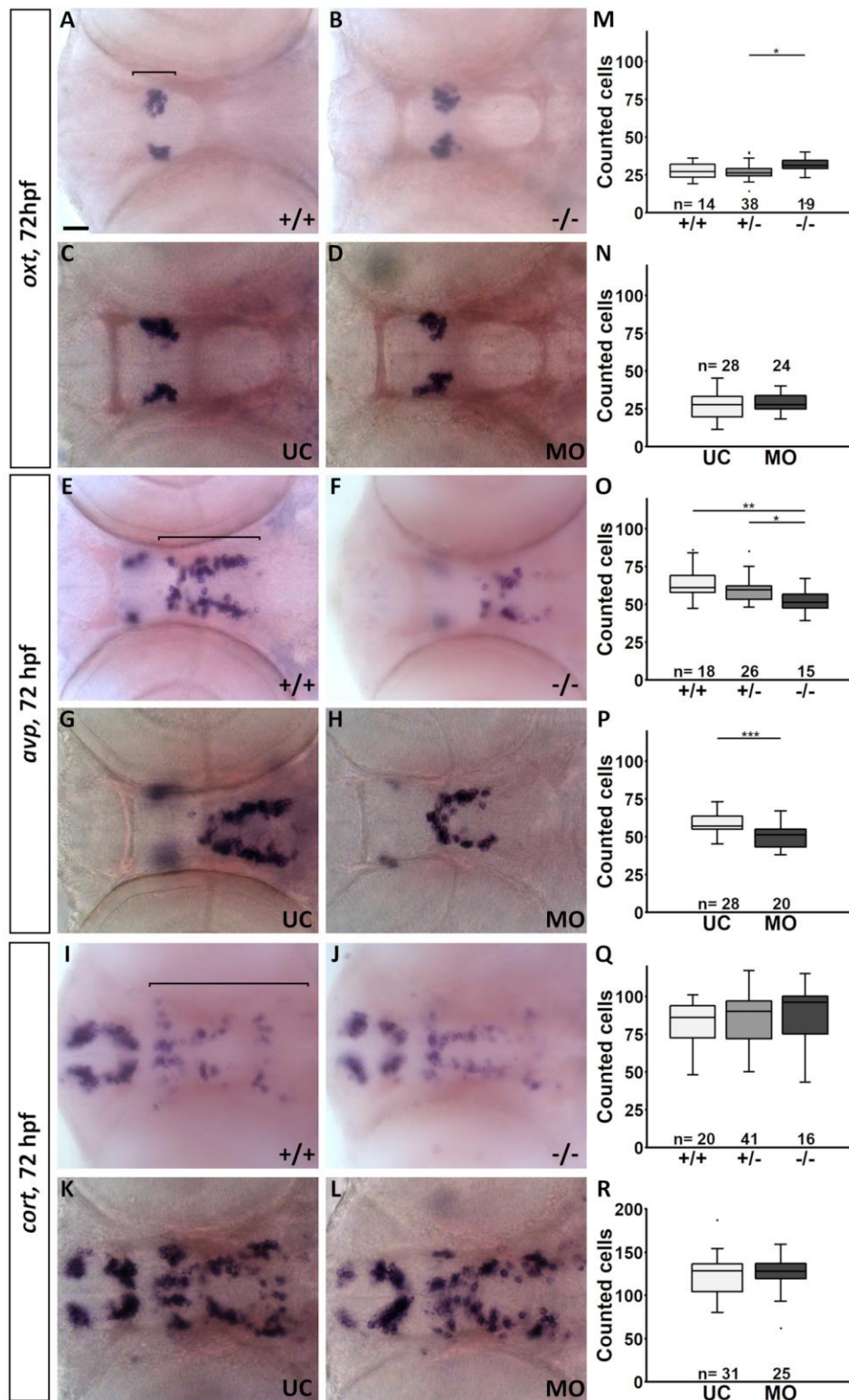


**Fig. 19:** Quantification of cells expressing *oxt*, *avp* and *cort* in the hypothalamic field of *fgf3*<sup>t24152</sup> mutants and *fgf3* morphants at 72 hpf. **A-L** Light microscopic images depicting *oxt*, *avp* and *cort* expression after *in situ* hybridisation in wild types (+/+), homozygous *fgf3*<sup>t24152</sup> mutants (-/-), *fgf3* morphants (MO) and uninjected controls (UC). Counted clusters are indicated by lines in **A**, **E**, and **I**. Ventral views, anterior to the left. Scale bar: 30  $\mu$ m. **M-R** Quantifications of *oxt*-, *avp*- and *cort*-positive cells in the hypothalamic field clusters of *fgf3*<sup>t24152</sup> mutants, *fgf3* morphants and respective control groups. Tukey boxplots show median, 25–75% percentile, IQR whiskers and outliers. n=number of analysed individuals. \*P>0.05, \*\*P>0.01, \*\*\*P>0.001. +/-, heterozygous *fgf3*<sup>t24152</sup> mutants. Data of *fgf3*<sup>t24152</sup> mutant experiments was pooled with previously generated data in Reuter (2015). *fgf3* MO experiments/data generated by J. Jäckels (2017). From Reuter et al. (2019).

### Impairment of *fgf3* leads to a smaller hypothalamus

The observed loss of monoaminergic and *avp* expressing cells after *fgf3* impairment lead to the investigation of the size of the hypothalamus. The hypothesis was postulated that the individual cell losses might culminate in an altogether smaller hypothalamus, which was tested next. To visualise the hypothalamus the expression domain of *nkx2.4b*, a frequently used hypothalamic marker (Rohr and Concha, 2000), was revealed by *in situ* hybridisation. Subsequently, area measurements of the expression domain were performed semi-automatically. The hypothalamus was measured from two sides. Measurements from a ventral viewpoint were conducted in *fgf3*<sup>t24152</sup> mutants and *fgf3* morphants. Measurements from a lateral perspective were carried out in *fgf3* morphants. Ventral and lateral hypothalamic sizes were determined in embryos at 36, 48 and 72 hpf. This enabled developmental comparisons between hypothalamic sizes when monoaminergic CSF-c cell proliferation and differentiation processes are active (Bosco et al., 2013). Generally, *fgf3* impairment did not qualitatively affect the structure of the *nkx2.4b* expression pattern neither ventrally nor laterally. Quantitatively, however, the size of the expression domain, thus, the size of the hypothalamus was significantly smaller from 36 to 72 hpf as ventral measurements suggested (Fig. 21). On the other hand, the lateral measurements in morphants showed only a significant size reduction at 36 hpf, yet no significant reduction at 48 and 72 hpf (Fig. 20). At 36 hpf the hypothalamus was 20% smaller in morphants compared to uninjected controls (Fig. 20A-I; Table 9). This ventrolateral discrepancy occurred most likely due to the changing shape of the hypothalamus during development from 36 to 72 hpf (Fig. 20K). Starting at 36 hpf, the hypothalamus had an oval ‘egg-like’ shape. Over the course of development until 72 hpf the ‘egg-like’ shape became broader and flatter, especially, at the caudal end of the hypothalamus. Therefore, the loss of cells and resulting size reduction was only visible from a ventral viewpoint at 48 and 72 hpf.

---



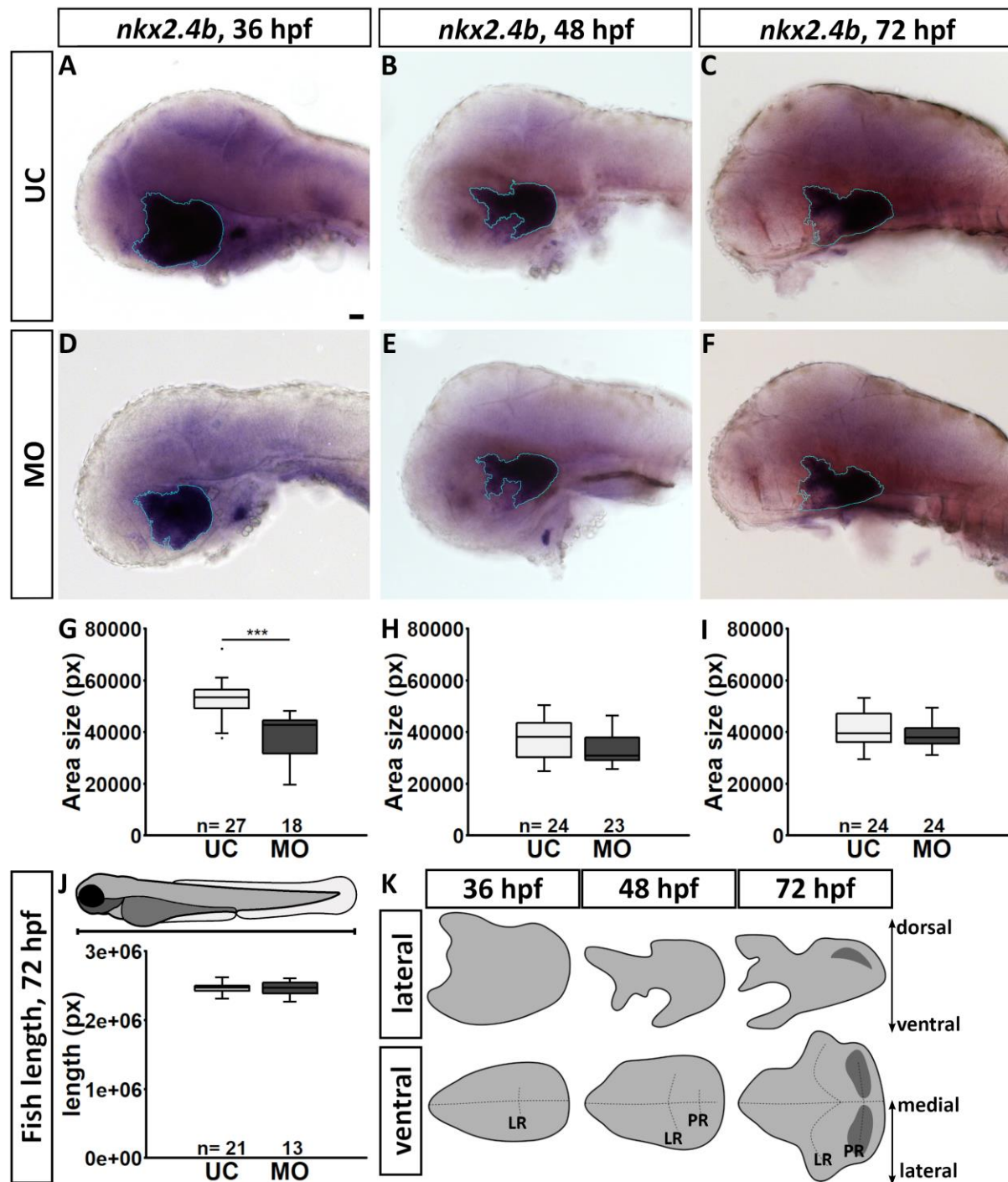


**Fig. 20: The shape of the *nkx2.4b* domain changes during development.** A-F Light microscopic images depicting *nkx2.4b* expression after *in situ* hybridisation *fgf3* morphants (MO) and uninjected controls (UC) at 36, 48 and 72 hpf. Area that was semi-automatically measured is highlighted in blue. Lateral views, anterior to the left. Scale bar: 30  $\mu$ m. G-I Area measurements (pixels) of the hypothalamus of *fgf3* MOs and UCs. J Total body length measurements of *fgf3* morphants at 72 hpf. Tukey boxplots show median, 25–75% percentile, IQR whiskers and outliers. n=number of analysed individuals. \* $P>0.05$ , \*\* $P>0.01$ , \*\*\* $P>0.001$ . K Scheme of lateral and ventral *nkx2.4b* domain emphasising shape changes over time from 36–72 hpf. Dark grey indicated position of caudal monoaminergic CSF-c cells around the posterior recess (PR). Dashed lines highlight the ventricular system of the hypothalamus including the lateral recess (LR) and the PR. *fgf3* MO injections and *in situ* hybridisations performed by J. Jäckels (2017). From Reuter et al. (2019).



At these developmental stages the lateral silhouette took on a flat shape, due to which the hypothalamus appeared to be unaffected in lateral measurements. Thus, changes in the shape of the developing hypothalamus omitted the effects of the cell loss from a lateral measuring position. However, the effects were revealed by the ventral measurements in *fgf3<sup>t24152</sup>* mutants and in *fgf3* morphants. Returning to the ventral analysis of the hypothalamus in *fgf3<sup>t24152</sup>* mutants: at 36 hpf homozygous *fgf3<sup>t24152</sup>* mutants exhibited a trend (6%) toward a smaller hypothalamus (Fig. 21M; Table 9). At 48 hpf the hypothalamus of homozygous *fgf3<sup>t24152</sup>* mutants was smaller by 11% compared to wild type controls, followed by an even greater reduction of 14% at 72 hpf compared to wild type siblings (Fig. 21N,O; Table 9). Further, at 72 hpf homozygous *fgf3<sup>t24152</sup>* mutants had a 10% smaller hypothalamus than heterozygous siblings. Expectedly, morphants displayed a stronger phenotype than mutants. Here, the hypothalamus was significantly reduced by 19, 16 and 15% at 36, 48 and 72 hpf, respectively, compared to respective uninjected controls (Fig. 21P-R; Table 9). This result was in line with the previously observed stronger monoaminergic phenotypes in morphants and, for sake of completeness, in CRISPR/Cas9 embryos compared to *fgf3<sup>t24152</sup>* mutants. To ensure that the smaller size of the hypothalamus was not a result of overall smaller morphants their body length was measured (Fig. 20J; Table 9). The analysis showed that morphants and uninjected controls had similar body lengths. Thus, the size reduction of the hypothalamus seemed to a specific effect caused by *fgf3* impairment.

Summarising, *fgf3* impairment lead to a reduction of monoaminergic CSF-c cells in caudal hypothalamic clusters that resulted in a smaller hypothalamic size. Since the hypothalamus was already smaller before serotonergic CSF-c cells were differentiated an early effect of *Fgf3* on serotonergic progenitors seemed likely. Due to the changing shape of the hypothalamus during development the size reduction was only visible from a ventral perspective.

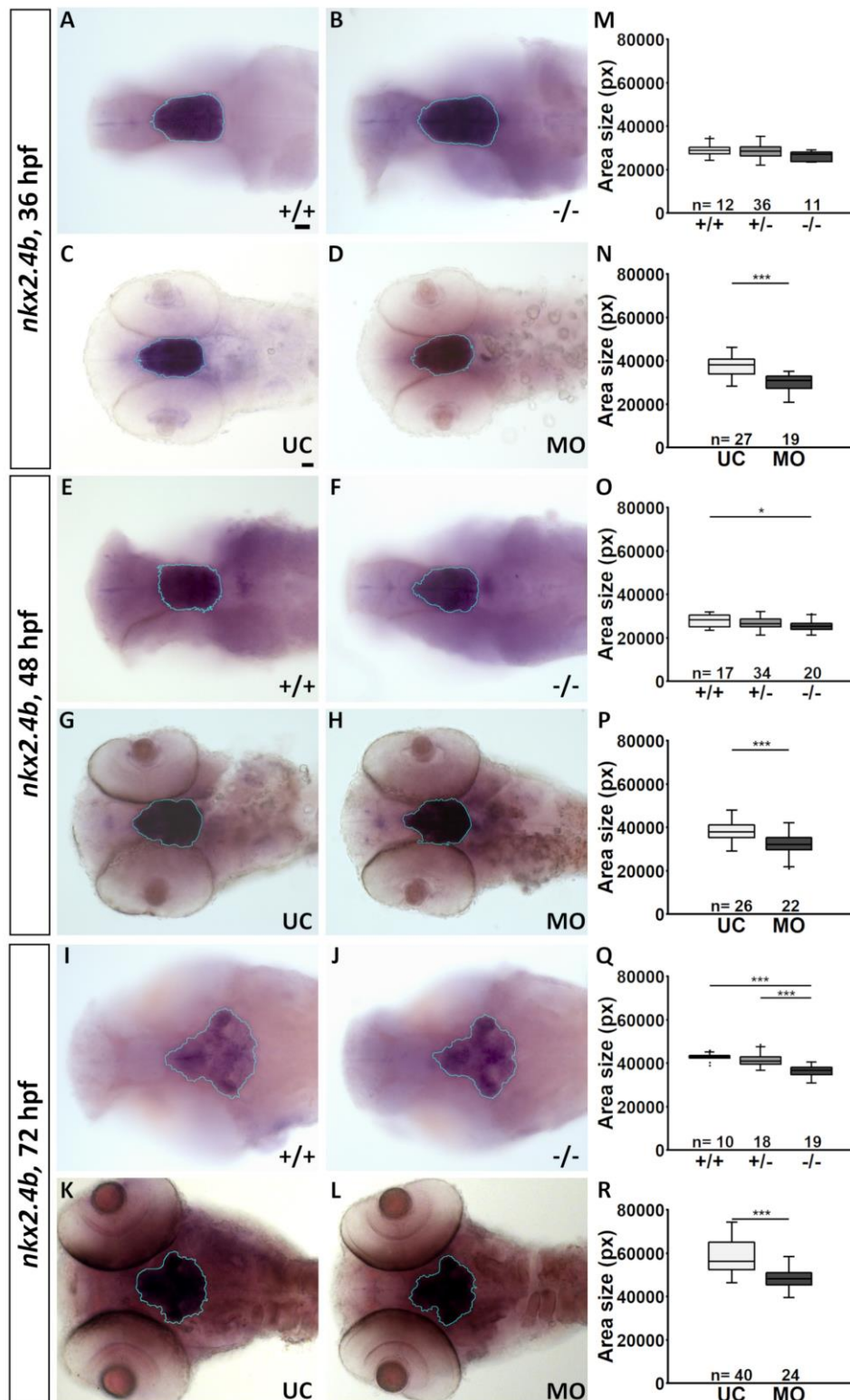


**Fig. 21: The hypothalamus of  $fgf3^{t24152}$  mutants and  $fgf3$  morphants is significantly smaller during development.** A-L Light microscopic images depicting  $nkx2.4b$  expression after *in situ* hybridisation in wild types (+/+), homozygous  $fgf3^{t24152}$  mutants (-/-),  $fgf3$  morphants (MO) and uninjected controls (UC) at 36, 48 and 72 hpf. Area that was semi-automatically measured is highlighted in blue. Ventral views, anterior to the left. Scale bars: 30  $\mu$ m. **M-R** Area measurements (pixels) of the hypothalamus of  $fgf3^{t24152}$  mutants,  $fgf3$  morphants and respective control groups. Tukey boxplots show median, 25–75% percentile, IQR whiskers and outliers. n=number of analysed individuals. \* $P>0.05$ , \*\* $P>0.01$ , \*\*\* $P>0.001$ . +/-, heterozygous  $fgf3^{t24152}$  mutants. *In situ* hybridisation stainings in  $fgf3^{t24152}$  mutants were pooled with previously obtained stainings in Reuter (2015).  $fgf3$  MO experiments performed by J. Jäckels (2017). Modified from Reuter et al. (2019).

---

### **Fgf3 ensures proliferation, survival and serotonergic lineage commitment of caudal hypothalamic cells**

Comparing to the literature, *fgf3* expression preceded *tph1a* expression and 5-HT immunoreactivity of caudal hypothalamic clusters by several hours (Bellipanni et al., 2002; Bosco et al., 2013). Adding to this was the finding that the hypothalamus was already smaller at stages when monoaminergic CSF-c cells were still immature precursors. Together, this data argued for an early impact of Fgf3 on monoaminergic progenitors. A second possibility was that the cell loss caused by the absence (or reduction) of Fgf3 activity could have entailed an increase of cell death in the caudal hypothalamus. A third possibility was a cell fate change of monoaminergic CSF-c cells. Subsequently, these three hypotheses concerning the functional impact of Fgf3 on the development of hypothalamic monoaminergic progenitors were explored in the context of the caudal serotonergic clusters. The analysis tools included a proliferation, cell death and cell fate assay, all of which were carried out in *fgf3* morphants (Figs. 22, 23).

The proliferation assay was performed at 36 hpf. BrdU and phospho histone 3 (phH3) were used as S and M phase markers, respectively (Fig. 22A-F). The anti-phH3 antibody detects phosphorylation of histone 3 at serine 10 (Goto et al., 1999; Hendzel et al., 1997). The process of phosphorylation correlates with the process of chromatin condensation at the beginning of the M phase of the cell cycle. Immunohistochemistry was followed by cell quantifications of BrdU- and phH3-positive cells in the caudal hypothalamus. Quantifications of BrdU-positive cells in the caudal hypothalamus revealed a significant reduction of cells by 23% in morphants compared to uninjected controls (Fig. 22G; Table 9). phH3-positive cells were not affected in *fgf3* morphants compared to uninjected controls (Fig. 22H; Table 9). This may be due to the short period that cells are in M phase, which makes detection of phH3-positive cells harder. It could also be that the S phase of the cell cycle was more affected by *fgf3* impairment

---

than the M phase. Still, these findings showed that fewer cells were proliferating in the caudal hypothalamus of *fgf3* morphants at 36 hpf.

At the same time cCasp3 immunohistochemistry revealed a significant increase of cell death by 95% in the caudal hypothalamus of *fgf3* morphants at 36 hpf (Fig. 22I-K; Table 9) Uninjected siblings had almost no cCasp3-positive cells in this region. As reported above the overall cell death observed in whole-mount morphants rendered a similar impression as the cell death observed in uninjected siblings (Fig. 16). Additionally, morphants had similar body lengths as uninjected siblings (Fig. 20J; Table 9). Together, this suggested that the increased cell death in the caudal hypothalamus was, firstly, specific to this region and, secondly, a consequence of *fgf3* knock-down rather than a methodological constraint attributed to morpholino toxicity or off-target effects.

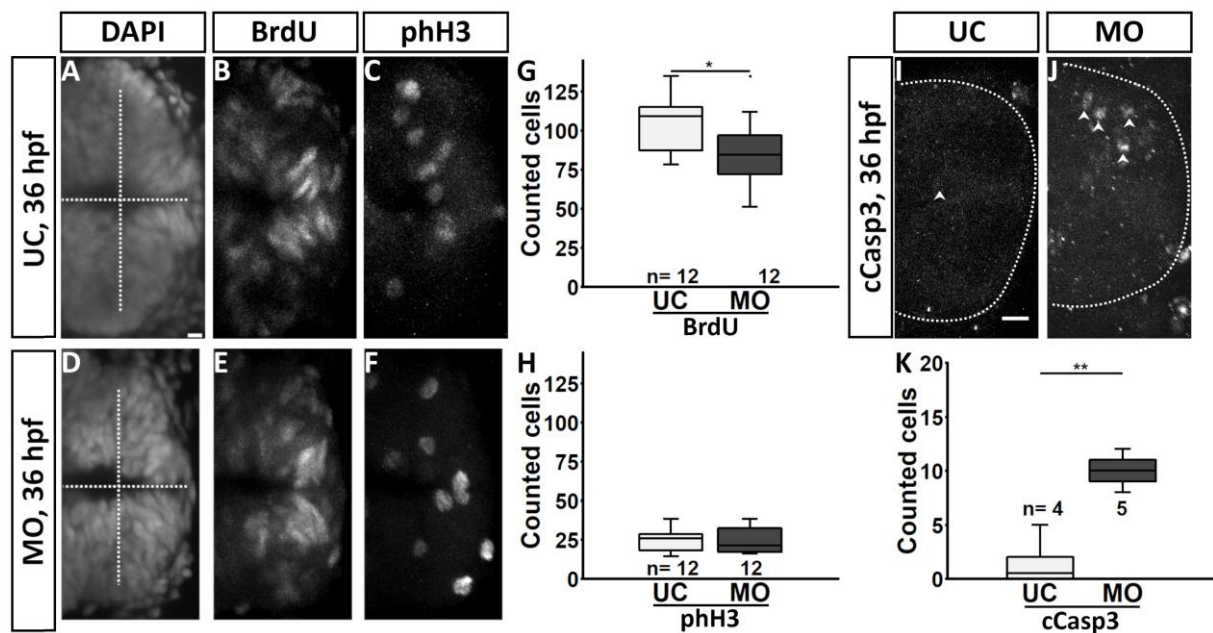


**Fig. 22: Cell proliferation is reduced, and cell death is increased in the caudal hypothalamus of *fgf3* morphants at 36 hpf.** A-F, I, J Confocal MIPs of uninjected control (UC) and *fgf3* morphant (MO) siblings at 36 hpf immunolabelled for BrdU and phospho-histone H3 (pH3) and counterstained with DAPI, or immunolabelled for cleaved caspase 3 (cCasp3). Dashed lines indicate ventricle with posterior recess in A and D, or caudal morphological boarder of the hypothalamus in I and J. J Arrow heads indicate examples of cCasp3-positive cells. Anterior to the left, ventral views. Scale bars = 10  $\mu$ m. G, H, K Quantifications of BrdU, pH3 and cCasp3-positive cells. Tukey boxplots showing median, 25-75% percentile, IQR whiskers and outliers. n = number of analysed individuals. From Reuter et al. (2019).

---

Following the analysis of cell proliferation and cell death assays, the cell fate of serotonergic progenitors was investigated next. The cell fate assay served as a tool to determine whether the changes in proliferation observed for the entire caudal hypothalamic cell population included proliferating progenitors that would later follow the serotonergic lineage. Thus, embryos were pulsed with BrdU at 36 hpf or at 45 hpf followed by a chase period until 72 hpf and subsequent processing for 5-HT and BrdU immunohistochemistry. The chase period allowed the embryo to grow, which allowed cells to divide and multiply. Due to the BrdU pulse at 36 hpf all replicating, i.e. proliferating cells at this time point incorporated the thymidine analogue into their DNA. Subsequent divisions of those cells would distribute the BrdU-DNA evenly from mother to daughter cells until the end of the chase period at 72 hpf or until these cells entered postmitotic differentiation. Meanwhile, around 62 hpf caudal serotonergic CSF-c cells were starting to mature. Until 72 hpf a well identifiable cluster of caudal serotonergic CSF-c cells developed. Immunohistochemistry for BrdU and 5-HT allowed the visualisation and quantification of double positive cells. The identification of double positive cells suggested that these now (at 72 hpf) serotonergic CSF-c cells were ‘relatives’ of progenitors once proliferating at 36 hpf. Thus, this method allowed to trace a cells’ developmental history back in time. The process was analogous for the cells that were pulsed with BrdU at 45 hpf (Fig. 23A-N). 5-HT immunoreactive and double positive BrdU/5-HT cells were quantified in intermediate and caudal serotonergic clusters of *fgf3* morphants. The serotonergic phenotype was confirmed in all morphants whether pulsed at 36 or 45 hpf. Morphants pulsed at 36 hpf showed a cell loss of 59% and morphants pulsed at 45 hpf lost 53% of serotonergic CSF-c cells compared to respective uninjected control groups (Fig. 23O,Q; Table 9). The number of double positive BrdU/5-HT cells was reduced at 72 hpf following a pulse at either 36 or 45 hpf. Morphants pulsed at 36 hpf had 64% fewer BrdU/5-HT-positive cells and morphants that had received a pulse at 45 hpf lost 38% of double positive cells compared to respective uninjected siblings (Fig. 23P,R; Table 9). Firstly, these findings confirm that

---

a portion of caudal hypothalamic progenitors that proliferated at either 36 or 45 hpf were developing into serotonergic CSF-c cells. Secondly, caudal serotonergic progenitors need Fgf3 at 36 and 45 hpf to commit to the serotonergic lineage.

Together, these findings suggest that Fgf3 has multiple roles during the development of the caudal hypothalamus. It ensures that hypothalamic progenitors keep proliferating and surviving, thus, enables them to commit to the correct cell lineage as demonstrated for serotonergic CSF-c cells.

---

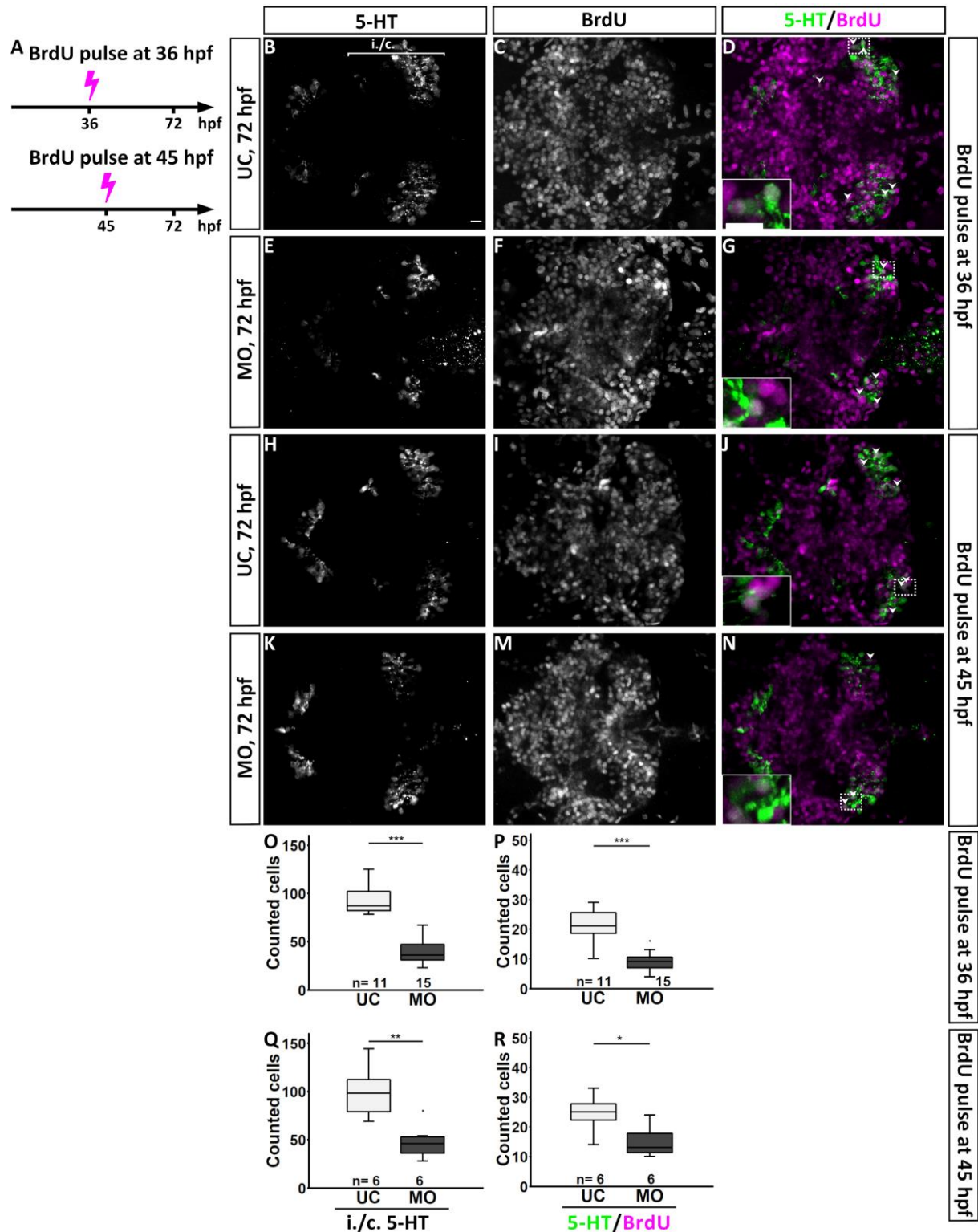


**Fig. 23: Serotonergic progenitors of the caudal hypothalamus depend on *fgf3* during development.** **A** Scheme depicting the time of BrdU pulses at 36 or 45 hpf followed by a chase period until 72 hpf when embryos were processed for immunohistochemistry. **B-N** Confocal MIPs of uninjected control (UC) and *fgf3* morphant (MO) siblings at 72 hpf immunolabelled for 5-HT and BrdU. Antibody stainings shown as single and merged channels. **B** Line indicates intermediate (i.) and caudal (c.) serotonergic cell clusters. **D, G, J, N** Inlays are high magnifications of dashed boxes depicting examples of double positive cells with arrow heads. Anterior to the left, ventral views. Scale bar = 10  $\mu$ m. **O-Q** Quantifications of 5-HT immunoreactive and double positive BrdU/5-HT cells in MOs and UCs. Tukey boxplots showing median, 25-75% percentile, IQR whiskers and outliers. n = number of analysed individuals.



### **Impaired Fgf3 isoforms of mutants and morphants are probably still able to interact with Fgf receptors**

As stated several times throughout the course of these paragraphs *fgf3*<sup>t24152</sup> mutants displayed weaker phenotypes than was generally expected and specifically when compared to *fgf3* morphants and CRISPR/Cas9 embryos. Thus, the capability of the truncated Fgf3 isoforms to correctly fold and bind to a receptor was investigated. Thereby, the severity of the *fgf3*<sup>t24152</sup> mutation and the *fgf3* morpholino on the Fgf3 protein itself should be understood. 3D models of the wild type Fgf3 protein and its two impaired isoforms were generated bound to an FGF1 receptor (performed by J. Kuper (Structural Biology, Rudolf-Virchow Centre for Experimental Research, University of Würzburg)). All three-resulting ligand-receptor 3D models were subsequently compared (Fig. 24). As highlighted in the previously performed Fgf3 alignment, *fgf3*<sup>t24152</sup> mutants possessed a longer remaining wild type sequence than *fgf3* morphants – 70% compared to 50%, respectively (see Fig. 10D). The 3D models predicted that both impaired Fgf3 isoforms were structurally less stable and complete, thus, more prone to be degraded than wild type Fgf3. In case of *fgf3*<sup>t24152</sup> mutants, the Fgf3 protein was able to fold. Thus, Fgf3 could still bind to the receptor because the majority of receptor interaction sites remained intact (Fig. 24B). As expected, the structure of the predicted Fgf3 isoform resulting from the *fgf3* morpholino knock-down was less preserved than the Fgf3 structure affected by the *fgf3*<sup>t24152</sup> mutation (Fig. 24C). Therefore, morpholino Fgf3 was likely less inclined to interact with the receptor. It was plausible that this was the reason why morphants exhibited stronger phenotypes than *fgf3*<sup>t24152</sup> mutants. These results also indicated that the *fgf3*<sup>t24152</sup> mutation lead only to a partial loss-of-function of Fgf3.

---



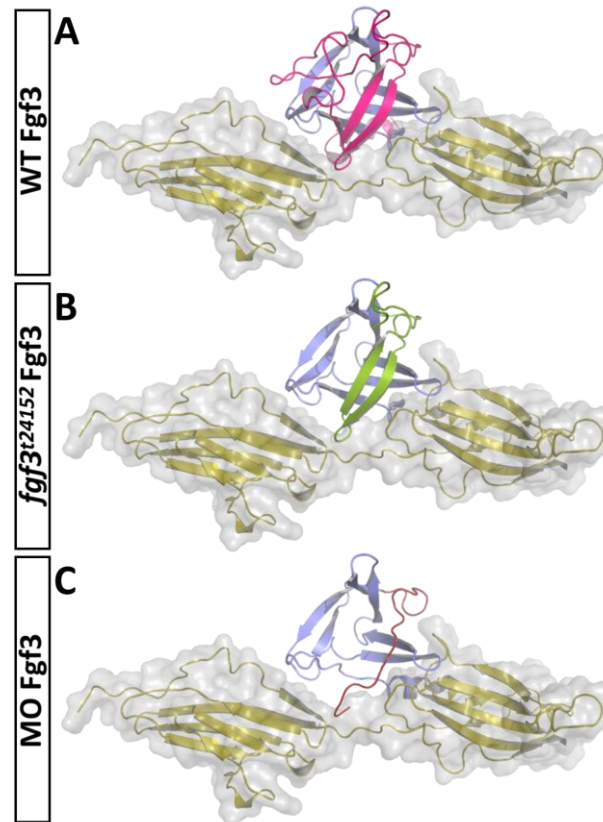


**Fig. 24: Fgf3 protein models of wild type,  $fgf3^{t24152}$  mutant and  $fgf3$  morphant isoforms bound to a FGF1 receptor.** **A-C** Ribbon representations of Fgf3 models. **A** Modelled zebrafish Fgf3 (blue and pink) bound to an FGF1 receptor (yellow). The affected part of the protein by the  $fgf3^{t24152}$  mutation or the  $fgf3$  morpholino is coloured in pink. **B** The deleted region of the  $fgf3^{t24152}$  mutation is omitted. The remaining part (green) reflects the sequence still translated in  $fgf3^{t24152}$  mutants but lacking in  $fgf3$  morphants. Note, this isoform still folds, thus, if the variant stays partially folded receptor binding would still be possible since most of the interfaces with the FGF1 receptor would stay intact. **C** Model of the morpholino knock-down. The non-sense sequence is coloured in red. In comparison to the  $fgf3^{t24152}$  mutant model it lacks more structural elements, hence, a correct folding and residual receptor interactions are less likely. 3D protein models generated by J. Kuper (Structural Biology, Rudolf-Virchow Centre for Experimental Research, University of Würzburg). From Reuter et al. (2019).

### The analysed genes of the hypothalamic transcriptome display small expression alterations after *fgf3* impairment

The three major categories, into which Fgf ligands can be sorted, are canonical, intracellular or endocrine ligands (Ornitz and Itoh, 2015). Each category has subfamilies with several members that, in turn, activate intracellular signalling pathways that impact on a multitude of genes. Fgf3 is only one of these ligands and

belongs to the canonical category. Hence, it was hypothesised that previously overlooked Fgfs in the hypothalamus could compensate for the *Fgf3* loss-of-function. Compensatory mechanisms could account for the fact that some monoaminergic CSF-c and *avp* expressing cells remained after *fgf3* impairment. This hypothesis was tested by performing a transcriptome analysis on data obtained from the RNA sequencing of dissected hypothalami of homozygous *fgf3*<sup>l24152</sup> mutants and wild type cousins at 3 and 7 dpf (Fig. 25A) (in collaboration with S. Kneitz (Physiological Chemistry, Biocentre, University of Würzburg)). The analysis focussed only on genes in the context of Fgf-signalling including ligands, receptors, pathway components and downstream targets. 31-known zebrafish *fgf* genes were investigated. As a result, additional transcripts of overlooked *fgf* genes were found to be expressed in the hypothalamus of wild types and mutants (Fig. 25B; Table 8). Three *fgf* genes – *fgf3*, *fgf4*, *fgf8a* – identified in the transcriptome analysis were already known to be expressed in the developing hypothalamus (Herzog et al., 2004; Jackman et al., 2004; Liu et al., 2013; Reifers et al., 1998). Another 13 *fgf* genes were detected including *fgf2*, *fgf6a*, *fgf8b*, *fgf11b*, *fgf12a*, *fgf12b*, *fgf13a*, *fgf13b*, *fgf14*, *fgf18a*, *fgf18b*, *fgf20a* and *fgf24*. Thus, a total of 16 *fgf* genes was expressed in the hypothalamus. Strikingly, the only *fgf* gene found to be upregulated (that was passing the defined thresholds) in mutants at 3 and 7 dpf was *fgf3*. Hence, partial loss of *fgf3* function triggered a self-compensatory mechanism. However, at 7 dpf mutants showed an up- or downregulation of *fgf11b* or *fgf24*, respectively, compared to wild types of the same age (Fig. 25C). The other detected *fgfs* were not passing a 1.5-fold change threshold.

Of the five *fgf* receptors five were expressed in the hypothalamus in all four groups (Fig. 25B). Comparing the 3 and 7 dpf wild type stages *fgfr2*, *fgfr3* and *fgfr4* were downregulated later in development at 7 dpf (Fig. 25C). Differential expression of the *fgf* receptors was not observed in mutants compared to wild types.

The ETS-domain transcription factors are activated by Fgf-signalling acting via the intracellular Ras-Mapk pathway (Mason, 2007; Ornitz and Itoh, 2015). *etv1*, *etv4*, *etv5a* and *etv5b* were selected for the analysis and all four were found to be expressed in the

---

hypothalamus (Fig. 25B). Exclusively, *etv5a* passed the defined fold change threshold, thus, was the only analysed ETS gene upregulated in wild types at 7dpf compared to wild types at 3 dpf (Fig. 25C). Similar to the *fgf* receptors, the four ETS genes were not differentially expressed in mutants compared to wild types.

62 Fgf-signalling pathway genes were chosen for the transcriptome analysis. Therein, a focus was placed on genes of the Ras-Mapk pathway and known regulators. Out of these 62 genes 56 expressed transcripts in the hypothalamus in all groups (Table 8; Fig. 25D). When comparing 3-day-old mutants and wild types none of the 56 genes were differentially expressed (Fig. 25E). At 7 dpf, however, *dusp1*, *dusp2* and *dusp5* were downregulated in mutants (Fig. 25E).

Summarising, the analysis of the hypothalamic transcriptome revealed that 16 *fgf* genes were expressed in the hypothalamus of zebrafish. Three of the 16 Fgf ligands were previously known to be active in the developing hypothalamus (Herzog et al., 2004; Jackman et al., 2004; Liu et al., 2013; Reifers et al., 1998). Only *fgf3*, *fgf11b* and *fgf24* were differentially regulated in *fgf3<sup>t24152</sup>* mutants. *fgf3* seemed to act in a self-compensatory capacity. Furthermore, the analysed Fgf-signalling pathway and downstream target genes were moderately altered in *fgf3<sup>t24152</sup>* mutants. Among them were *dusp1*, *dusp2*, *dusp5* and *etv5a*. This suggested that either minor compensatory mechanisms are at work in *fgf3<sup>t24152</sup>* mutants and/or the Fgf3 protein of *fgf3<sup>t24152</sup>* mutants is still partly functional, thus, rendering milder effects.

---

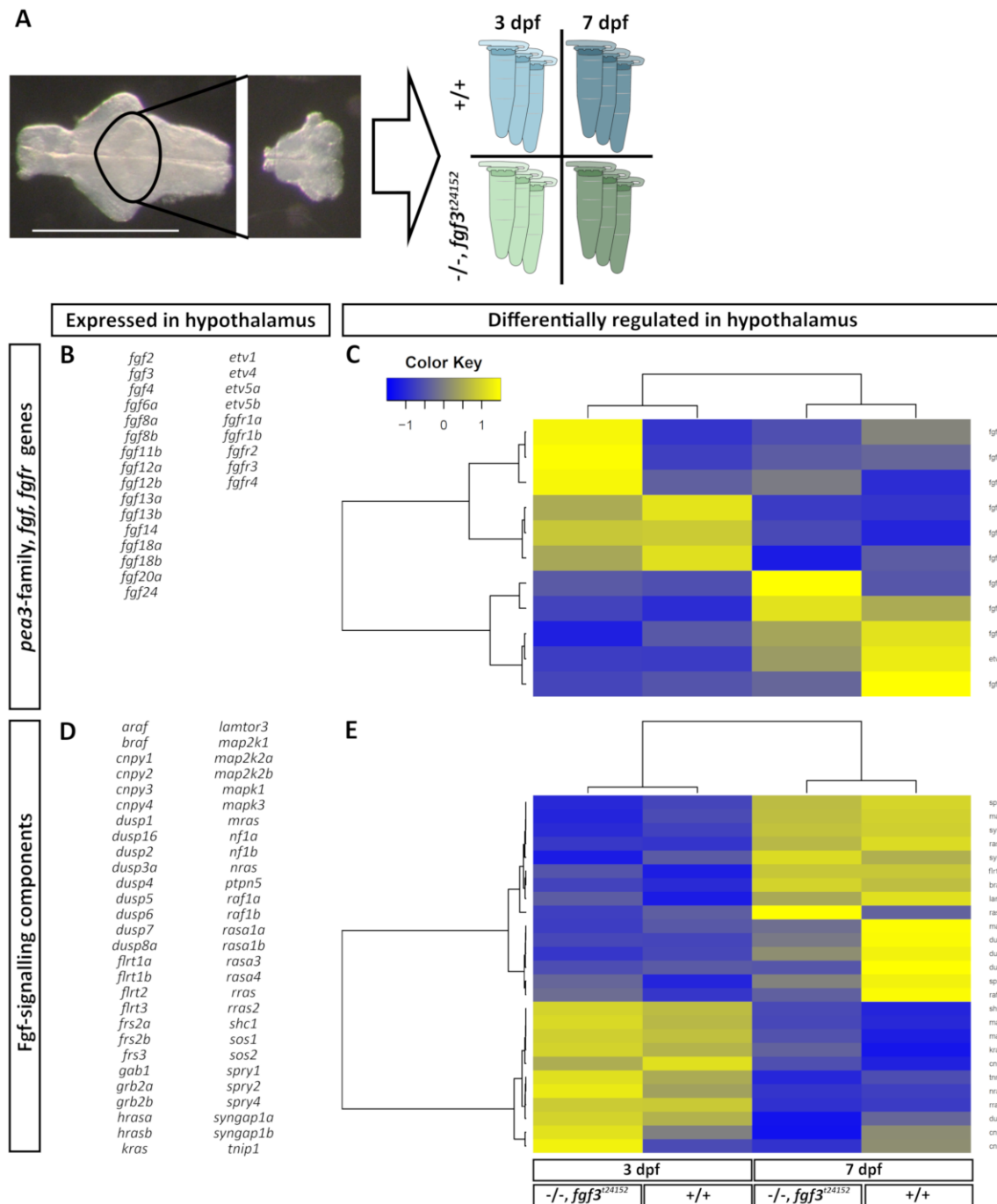


**Fig. 25: Hierarchical clustering analysis of Fgf-signalling pathway components and downstream targets in the hypothalamus of *fgf3*<sup>t24152</sup> mutants and wild types at 3 and 7 dpf. A** Scheme of sample preparation for RNA sequencing. Light microscopic images show the dissected hypothalamic field (ventral views, anterior to the left) of wildtypes (+/+, blue tubes) and *fgf3*<sup>t24152</sup> mutants (-/-, green tubes) at 3 (light tubes) and 7 dpf (dark tubes). The amount of tubes in each group depicts the number of collected replicates resulting in a total of 12 samples processed for RNA sequencing. Scale bar = 500  $\mu$ m **B, D** List of *fgfs*, *fgfrs*, Fgf-signalling target genes and Fgf-signalling pathway genes (D) expressed (base mean  $\geq 10$ ) in the hypothalamus of -/- and +/+. *shc2* is the only displayed gene not passing the base mean threshold in the 3 dpf -/- group. **C, E** Heat maps of differentially regulated (base mean  $\geq 10$ , fold change  $\geq 1.5$ ) *fgfs*, *fgfrs* and Fgf-signalling target genes (C) and Fgf-signalling pathway genes (E) in the hypothalamus of -/- and +/+. Columns depict z-scores of mean values of analysed replicates of each group and rows depict individual genes. Colour key shows z-score ranging from  $\geq -1.5$  to  $\leq 1.5$ . Colour intensity represents expression level of a gene in one group with blue or yellow indicating low or high expression. Heat maps were generated in collaboration with S. Kneitz (Physiological Chemistry, Biocentre, University of Würzburg). From Reuter et al. (2019).

---

Subsequently, two *dusp* feedback regulators of the Fgf-signalling pathway were investigated in more detail by *in situ* hybridisation in *fgf3* morphants at 36 hpf (Fig. 26A-D). The stage was chosen due to its relevance for hypothalamic serotonergic development. Based on the transcriptome data *dusp1* and *dusp 6* were chosen even though *dusp6* did not pass the fold change threshold. However, *dusp6* is known to negatively regulate the Ras-Mapk pathway by dephosphorylating active Map kinases (Thisse and Thisse, 2005). Recapitulating the result of the transcriptome analysis *dusp1* was downregulated in *fgf3*<sup>t24152</sup> mutants at 7 dpf (Fig. 26A,B). Generally, few *dusp1* expressing cells were observed in the hypothalamus of wild types and morphants at 36 hpf after *in situ* hybridisation (Fig. 26A). Morphants seemed to have even fewer *dusp1* expressing cells in the caudal hypothalamus than uninjected controls. On the other hand, *dusp6* was prominently expressed in the hypothalamus, yet no visible cell reduction was noted in *fgf3* morphants compared to wild types at 36 hpf (Fig. 26C,D). Taken together, the negative feedback regulators *dusp1* and *dusp6* appeared to be mildly downregulated after *fgf3* impairment.

To further substantiate this finding, it was hypothesised that if the inhibitors were truly downregulated after *fgf3* impairment the Map kinases might be more active. To test this p44/42 Mapk (Erk1/2) (pErk) immunohistochemistry was performed on *fgf3* morphants at 36 hpf and pErk-positive cells were quantified in the caudal hypothalamus (Fig. 26E-G). The analysis showed an increase of pErk-positive cells by 75% in morphants compared to wild type siblings. However, due to the generally low number of pErk-positive cells and a large variation this result was not significant, thus, represented only a trend. Nonetheless, this strong trend suggested that *fgf3* impairment lead to a downregulation of certain *dusp* genes, which in turn seemed to lead to increase of phosphorylated Map kinase-positive cells in the caudal hypothalamus.

---

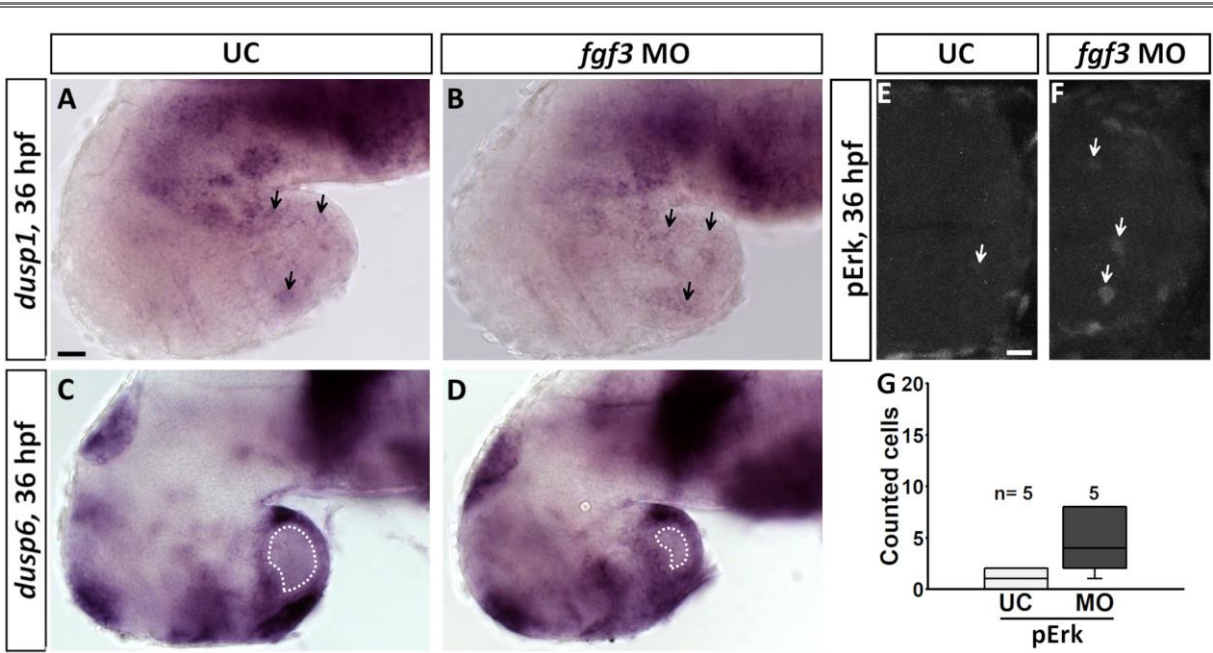


**Fig. 26:** Expression of negative feedback regulators and pErk-positive cells is mildly altered in the caudal hypothalamus of *fgf3* morphants. **A-D** Light microscopic pictures of *in situ* hybridisation for *dusp1* and *dusp6* performed in uninjected control (UC) and *fgf3* morphant (MO) siblings at 36 hpf. Arrows depict areas where *dusp1* is weaker expressed in MOs than in UCs. The *dusp6* expression pattern appears of similar quality in MOs and UCs, however, the *dusp6* negative domain in the caudal hypothalamus is smaller in MOs indicated by dashed line. Lateral views, anterior to the left. Scale bar = 30  $\mu$ m. **E, F** Confocal MIPs of uninjected control (UC) and *fgf3* morphant (MO) siblings at 36 hpf immunolabelled for pErk. Arrows indicate pErk-positive cells in the caudal hypothalamus. Ventral views, anterior to the left. Scale bar = 10  $\mu$ m. **G** Quantification of pErk-positive cells for MOs and UCs. Modified from Reuter et al. (2019).

***tph1a* impairment strategies to explore the function of serotonergic CSF-c cells in the hypothalamus**

The final phase of this project switches from the development of monoaminergic clusters in the hypothalamus to the function of mature hypothalamic serotonergic CSF-c cells. Studies regarding this particular subject are scarce. The best gene to target for subsequent experiments was *tph1a* since it is essential for the synthesis of 5-HT in the hypothalamic clusters. Apart from the hypothalamus, *tph1a* is transiently expressed in the spinal cord and in the pineal gland. It is known that serotonergic intraspinal neurons of the spinal cord have an impact on locomotion behaviour (Montgomery et al., 2016; 2018). However, some hypothalamic CSF-c cells could

---

represent deep encephalic photoreceptors (Vigh and Vigh-Teichmann, 1998). To investigate the function of hypothalamic serotonergic CSF-c cells two strategies to impair *tph1a* were applied including a CRISPR/Cas9 knock-out and a morpholino-based knock-down. For the knock-out two target sites were chosen; one in exon 2 and the other at the end of exon 4 (Fig. 27A; Table 5). For both target sites gRNAs were subsequently designed according to the protocol (see Annex). For the knock-down two morpholinos were designed (Gene Tools) targeting splice donor sites at exon 3 (E3) and 4 (E4) (Fig. 27A; Table 4). Both morpholinos were validated. E3 morpholino injections resulted in an inclusion of intron 3 (Fig. 27B). This result was confirmed twice by RT-PCR and Sanger sequencing for the upper cDNA product of E3 morpholino injected embryos at 24 hpf (upper band E3 MO 24 hpf in Fig. 27B). However, during one experimental run the gDNA-PCR of this DNase treated sample revealed a product with roughly the same size as the wild type splice product (UC 5dpf in Fig. 27B). This was unusual since the gDNA product size would have been 1462 bp long in case of an incomplete digest of gDNA. As the revealed product was smaller, the preparation of cDNA was continued by reverse transcriptase treatment. As expected, DNA sequencing of the cDNA product (upper band E3 MO 24 hpf Fig. 27B) revealed a correctly spliced cDNA of the exon 2-exon 3 boundary and a complete inclusion of intron 3 followed by the remaining sequence of exon 4. Thus, it was concluded that the E3 morpholino was working and the observed product amplification following the gDNA-PCR was not impacting on the morpholino validation process in a relevant manner. As a consequence of the morpholino application, a frame shift was introduced, which lead to the translation of a nonsense amino acid sequence followed by a premature stop after amino acid 144 (F). Thus, after application of the E3 morpholino 29% of the wild type sequence remained intact (Figs. 27B, 28).

---

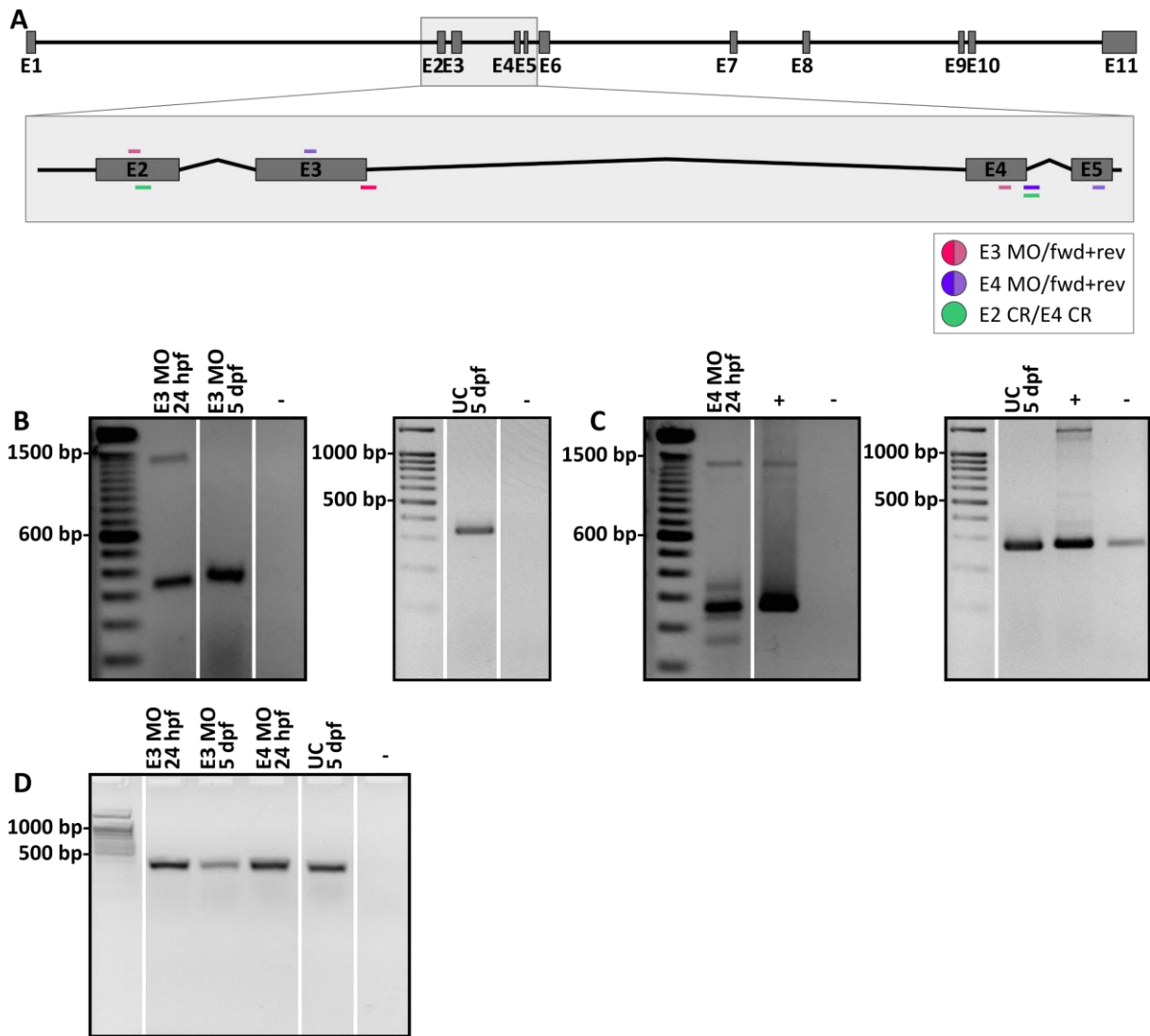


**Fig. 27: Validation of *tph1a* morpholino knock-down and *tph1a* CRISPR/Cas9 target sites.** **A** Scheme of *tph1a* gene and magnification of target region for morpholinos and CRISPR/Cas9. Locations of splice morpholino target sites in exon 3 (E3 MO) and exon 4 (E4 MO) indicated in magenta and purple, respectively. Forward (fwd) and reverse (rev) primers detecting morphant splice forms correspond to the colour of the respective morpholino. CRISPR/Cas9 target sites in exon 2 (E2 CR) and exon 4 (E4 CR) are indicated in green. **B** RT-PCR products of *tph1a* E3 morphants (MO) at 24 hpf and 5 dpf, uninjected control (UC) siblings at 5 dpf and water control (-). *tph1a* E3 MO band at 1335 bp suggests an inclusion of intron 3. Band of UC at 343 bp. Respective bands were verified by Sanger sequencing. **C** RT-PCR products of *tph1a* E4 morphants (MO) at 24 hpf and uninjected control (UC) siblings at 5 dpf, positive (+) and water control (-). *tph1a* E4 morphant bands at 333 bp and 158 bp suggest both an inclusion of intron 4 and an exclusion of exon 4, respectively. Band of UC at 259 bp. Sanger sequencing of respective bands was inconclusive except for UC band which was verified. **D**  $\beta$ -actin RT-PCR products of samples used in **B** and **C**.



Injecting with the E4 morpholino revealed an inclusion of intron 4 and an exclusion of exon 4 (Fig. 27C). Both results could not be validated by Sanger sequencing, thus, should be repeated in a new experimental run. In case the Sanger sequencing had confirmed the observed effects after RT-PCR amplification, the E4 morpholino would have had the following repercussions on *tph1a* translation (Figs. 27B, 28): the amino acid sequence containing intron 4 would have resulted in a nonsense sequence and a premature stop. Thus, 36% of the wild type sequence would have remained. The exon 4 exclusion would have resulted in a nonsense sequence followed by a premature stop leaving 29% of the wild type sequence intact.

Summarising, the gRNAs for a *tph1a* CRISPR/Cas9 knock-out were designed and synthesised. *tph1a* knock-down with the E3 morpholino was successfully validated and rendered reliable results. The E4 morpholino showed also the expected effects, however, these results should be verified by Sanger sequencing before starting future experiments. Thus, there are potentially two but surely one morpholino to achieve a knock-down of *tph1a*. Both strategies are ready to explore the function of hypothalamic serotonergic CSF-c cells.

---

Tph1a WT	1	MYSSKSDGPRRGRSFD SMNLGLTLEEKQLNNEMNKSAFTKIEENKDNKTE	50
Tph1a E3MO	1	MYSSKSDGPRRGRSFD SMNLGLTLEEKQLNNEMNKSAFTKIEENKDNKTE	50
Tph1a E4MO InIn	1	MYSSKSDGPRRGRSFD SMNLGLTLEEKQLNNEMNKSAFTKIEENKDNKTE	50
Tph1a E4MO ExEx	1	MYSSKSDGPRRGRSFD SMNLGLTLEEKQLNNEMNKSAFTKIEENKDNKTE	50
		*****	
Tph1a WT	51	SSETGRAAVVFLSKNEVGGLVKALKLFQENHVNLVHIESRKSRRNSEFE	100
Tph1a E3MO	51	SSETGRAAVVFLSKNEVGGLVKALKLFQENHVNLVHIESRKSRRNSEFE	100
Tph1a E4MO InIn	51	SSETGRAAVVFLSKNEVGGLVKALKLFQENHVNLVHIESRKSRRNSEFE	100
Tph1a E4MO ExEx	51	SSETGRAAVVFLSKNEVGGLVKALKLFQENHVNLVHIESRKSRRNSEFE	100
		*****	
Tph1a WT	101	IFVDCDSNREQLHEIIQLLRKHVNVVEMDAPDNRLPEES <b>E</b> MENVPWFPPK	150
Tph1a E3MO	101	IFVDCDSNREQLHEIIQLLRKHVNVVEMDAPDNRLPEES <b>G</b> MNVF*-----	144
Tph1a E4MO InIn	101	IFVDCDSNREQLHEIIQLLRKHVNVVEMDAPDNRLPEES <b>E</b> MENVPWFPPK	150
Tph1a E4MO ExEx	101	IFVDCDSNREQLHEIIQLLRKHVNVVEMDAPDNRLPEES <b>G</b> IQQCLSQKK	150
		***** : :	
Tph1a WT	151	ISDLDKCANRVLMYGSDLDADHPGFKDNVYRKRKYFADLAMSYKHGDPI	200
Tph1a E3MO		-----	
Tph1a E4MO InIn	151	ISDLDKCANRVLMYGSDLDADHPVSGI*-----	177
Tph1a E4MO ExEx		*-----	
		-----	
Tph1a WT	201	PRIEFTEEEVKTWGVVFRELNKLYPSHACREYLKNLPLLIKHCDSDREDNI	250
Tph1a E3MO		-----	
Tph1a E4MO InIn		-----	
Tph1a E4MO ExEx		-----	
		-----	
Tph1a WT	251	PQLEDVSRFLKERTGFTIRPVAGYLSPRDFLAGLAFRVFHCTQYVRHSSD	300
Tph1a E3MO		-----	
Tph1a E4MO InIn		-----	
Tph1a E4MO ExEx		-----	
		-----	
Tph1a WT	301	PLYTPEPDTCHHELLGHVPLLAEPSFAQFSQEIGLASLGASDDSIQKLATC	350
Tph1a E3MO		-----	
Tph1a E4MO InIn		-----	
Tph1a E4MO ExEx		-----	
		-----	
Tph1a WT	351	YFFTVEFGLCKQEGKLRAYGAGLLSSISELKHALSGNARILPFDPNVTCK	400
Tph1a E3MO		-----	
Tph1a E4MO InIn		-----	
Tph1a E4MO ExEx		-----	
		-----	
Tph1a WT	401	QECIIITTFQDVYFMSDSFEEAKVKMREFAKTIKRPFSVRYNPYTQSVDVL	450
Tph1a E3MO		-----	
Tph1a E4MO InIn		-----	
Tph1a E4MO ExEx		-----	
		-----	
Tph1a WT	451	KDTSINNVEELRHELDIIGDALSRNLKQLGV	483
Tph1a E3MO		-----	
Tph1a E4MO InIn		-----	
Tph1a E4MO ExEx		-----	

**Fig. 28: Amino acid sequence alignment of wild type and splice morpholino products Tph1a.** Exon 3 morpholino (E3 MO) leads to an inclusion of intron 3, thus, a short nonsense sequence is translated after amino acid 138 (S) followed by a premature stop after amino acid 144 (F). Hence, only 29% of the wild type sequence remain after knock-down with E3 MO. After exon 4 morpholino (E4 MO) application an inclusion of intron 4 (In In) and exclusion of exon 4 (Ex Ex) occur. The intron inclusion leads to a nonsense sequence after amino acid 172 (P) and a premature stop after amino acid 177 (I) leaving 36% of the wild type sequence intact. The exon exclusion introduces a nonsense sequence after amino acid 138 (S) coming to a premature stop after amino acid 150 (K). 29% of the wild type amino acid remain intact the same percentage as after E3 MO application. Red amino acid highlights last translated amino acid of exon 3. Purple (amino acids 60-128) and light blue (amino acids 144-365) lines indicate catalytic domains of *tph1a* (Bellipanni et al., 2002).

## Summary chart of results

Table 10: Summary of results of statistically analysed experiments.

Fig.	14	17, 18							19			20, 21							22	
marker region	<i>etv5b</i>	5-HT		TH1				<i>th2</i>	<i>oxl</i>	<i>avp</i>	<i>cort</i>	<i>nkx2.4b</i>				Fish length	pH 3	Brd U		
hp	36	i/c.		DC 4/5/6		DC 7		DC 7				ventral		lateral						
	36	72	96	72	96	72	96	96	72	36	36	36	48	72	36	48	72	72	36	36
<i>fgf3</i> morpholino	↓	↓	↓	-	-	↓	↓	↓	-	↓	-	↓	↓	↓	↓	-	-	-	-	↓
<i>fgf3</i> <sup>24/52</sup> mutation	+/-	↓							-	-	-	-	-	-						
	-/-	↓	↓		↓				-	↓	-	Trend	↓	↓						
<i>fgf3</i> CRISPR/Cas9		↓			↓															

Fig.	22	23				26	25											
marker region	cCas p3 Hyp	5-HT		BrdU/ 5-HT		pErk	<i>fgf3</i>		<i>fgf11a</i>		<i>fgf24</i>		<i>dusp1</i>		<i>dusp2</i>		<i>dusp5</i>	
hp	36	36-72	45-72	36-72	45-72	36	72	168	72	168	72	168	72	168	72	168	72	168
<i>fgf3</i> morpholino	↑	↓	↓	↓	↓	Trend												
<i>fgf3</i> <sup>24/52</sup> mutation	-/-					↑	↑	↑	-	↑	-	↓	-	↓	-	↓	-	↓

Comparisons drawn to wild types; ↓, decrease/downregulation; ↑, increase/upregulation; -, no change; empty field, no data available

## Discussion

For a summary of results see Table 10.

In the present work the ligand Fgf3 is identified and validated as a critical factor for the development of serotonergic and dopaminergic CSF-c as well as *avp* expressing cells in the hypothalamus of zebrafish. Fgf-signalling via the ligand Fgf3 is particularly important for caudal hypothalamic development. It is demonstrated that Fgf-signalling influences lineage specification processes in the secondary prosencephalon well beyond initial patterning and regionalisation events of gastrulation and primary neurulation. Further, the transcriptome of the hypothalamic region is sequenced and used to investigate Fgf3-signalling pathway components and downstream targets. The findings suggest a self-regulatory mechanism of Fgf3 with minor alterations of regulatory pathway components. Moreover, the availability of the hypothalamic transcriptome poses an opulent source of reference for future investigations of hypothalamic development and function. Together, this thesis provides new insights into the development of the hypothalamic posterior recess region of zebrafish, thereby, contributing to the understanding of the evolution of the vertebrate hypothalamus.

### **Caudal hypothalamic Fgf3 regulates the expression of the ETS-domain transcription factor *etv5b* in the developing hypothalamus**

The Fgf-signalling pathway is important in a variety of processes such as cell motility, cell survival, cell proliferation and differentiation, stress response and Fgf-feedback inhibition (Itoh, 2007; Itoh and Ornitz, 2011; Mason, 2007; Ornitz and Itoh, 2015; Thisse and Thisse, 2005; Tsai et al., 2011). Fgf-signalling has been shown to act via the ETS-domain transcription factor family of which *etv5b* is a member (Münchberg et al., 1999;

---

---

Roussigné and Blader, 2006; Reifers et al., 1998; Roehl and Nüsslein-Volhard, 2001; Raible and Brand, 2001). In zebrafish the development of serotonergic CSF-c cells in the caudal hypothalamus requires Fgf-signalling via *etv5b* (Bosco et al., 2013). To identify the Fgf ligand/s responsible for serotonergic CSF-c cell ontogeny in the hypothalamus two *fgfs* – *fgf3* and *fgf8a* – were considered as possible candidates because of the location of both expression domains in relation to hypothalamic serotonergic CSF-c cells (Kaslin and Panula, 2001; Lillesaar, 2011; McLean and Fetcho, 2004). Of these two ligands a role of *Fgf3* is known in dopaminergic CSF-c cell generation of the caudal hypothalamic cluster DC 7 (Koch et al., 2014). In addition, *fgf8a* is only expressed in a few cells in the caudal hypothalamus whereas expression of *fgf3* is much more prominent (Herzog et al., 2004; Liu et al., 2013; Reifers et al., 1998; Reuter et al., 2019). Therefore, *fgf3* is the main focus of this thesis. This does not exclude that *Fgf8a* or any other Fgf ligand expressed in the hypothalamus may be important for the development of hypothalamic cell populations. Focussing on *fgf3*, at early developmental stages *fgf3* expressing cells are broadly distributed in the putative hypothalamus. As development advances, *fgf3* expression is confined to the caudal hypothalamus. Here, expression is restricted to medial cells flanking the dorsal and ventral sides of the third ventricle. The position of *fgf3* expression in the caudal hypothalamus is in close vicinity or may partly overlap with serotonergic progenitors at 36 hpf or differentiated serotonergic CSF-c cells at 68 hpf and later stages. A strong indicator for Fgf-signalling in this region is the fact that Fgf ligands, receptors, downstream targets and feedback inhibitors are expressed during embryonic development and adulthood in zebrafish (Bosco et al., 2013; Herzog et al., 2004; Liu et al., 2013; Raible and Brand, 2001; Reifers et al., 1998; Reuter et al., 2019; Roehl and Nüsslein-Volhard, 2001; Topp et al., 2008). At developmental stages preceding 36 hpf expression domains of, e.g. *etv4*, *etv5a*, *etv5b* and *dusp6* coincide largely with the *fgf3* expression domain (Fig. 13P,S,U) (Bosco et al., 2013). At 36 hpf and later stages *etv4*, *etv5a*, *etv5b* and *dusp6* continue to be broadly expressed along the medio-lateral axis covering the whole width of the posterior recess. In contrast, *fgf3* is expressed in medial

---

cells around the third ventricle but not along the posterior recess (Fig. 13Q,R,V) (Bosco et al., 2013). The regulation of these targets might be achieved in a dose-dependent manner as a result of an extracellular Fgf3 gradient. The relative position, at which the target cell is exposed to the gradient in space and time, may impact on transcription factor activity. This argues in favour of Fgf3 acting as a morphogen to regulate downstream targets and feedback signals (Bökel and Brand, 2013; Ornitz and Itoh, 2015). This study provides evidence for a link between Fgf3 and the Fgf-signalling downstream target *etv5b*. In order to impact on *etv5b* expressing cells Fgf3 may cross through the extracellular space utilising the modes of signal distribution known from volume transmission (Agnati et al., 2006; De-Miguel and Fuxe, 2012; Fuxe et al., 2007). The direct mechanism, by which the Fgf3 ligand reaches the target cell, remains elusive. After an extracellular morphogen gradient has formed it is interpreted by the target cell. The mechanism used for interpretation has been investigated for Fgf8 in zebrafish and includes endocytic uptake and lysosomal targeting processes regulated by the ubiquitin ligase Cbl (Nowak et al., 2011). After the gradient has been interpreted by the target cell, downstream genes of Fgf-signalling are activated. Even though this mechanism has not been investigated in the present study, the dependence of cells expressing *etv5b* on Fgf3 is clearly observable in *fgf3*<sup>t24152</sup> mutants and *fgf3* morphants. Both impairment strategies lead to the detection of fewer *etv5b* expressing cells in the caudal hypothalamus.

Taken together, during development of the caudal hypothalamus Fgf3 is a crucial Fgf ligand regulating *etv5b* expression. At later developmental stages after 36 hpf Fgf3 is presumed to be secreted by cells surrounding the third ventricle. Due to the location of cells expressing transcripts of downstream targets, Fgf3 likely acts as a morphogen. Therefore, Fgf3 may communicate with more laterally located target cells that are expressing other ETS-domain transcription factor targets and feedback regulators. It cannot be excluded that other Fgf ligands have an impact on *etv5b* expression. The identity of such ligands remains to be uncovered in the hypothalamus, a possible candidate being Fgf8a (Reifers et al., 1998; Roehl and Nüsslein-Volhard, 2001).

---

### **Monoaminergic CSF-c and *avp* expressing cells of the caudal hypothalamus are highly dependent on Fgf3 activity**

The monoaminergic system of the CNS is a versatile yet common feature among vertebrates. Synthesising monoaminergic cells universally share certain biosynthesis genes throughout vertebrates (Table 2) (Anichtchik et al., 2006; Filippi et al., 2007; Kaslin and Panula, 2001; Pelletier et al., 2001; Wen et al., 2008; Yamamoto et al., 2011). Thus, monoaminergic cells might share other similarities such as signalling pathways and transcription factors during development. A factor that is shared by two monoaminergic systems is *fezf2*, a component of the Wnt-signalling pathway (Jeong et al., 2007; Levkowitz et al., 2003; Rink and Guo, 2004). The transcription factor impacts on hypothalamic dopaminergic and serotonergic cell ontogeny. The impact of *fezf2* seems to be restricted to only the hypothalamic monoaminergic clusters not affecting monoaminergic clusters of other regions. Separate cell clusters of one monoamine can also rely on different regulatory genetic networks during development. Investigations of the present study and others (Bosco et al., 2013) regarding hypothalamic serotonergic cell development suggest that the hypothalamic serotonergic gene regulatory network consists of different factors than those known for the raphe network (see Figs. 8, 29) (Deneris and Gaspar, 2018; Deneris and Wyler, 2012; Flames and Hobert, 2011; Jeong et al., 2006; Kiyasova and Gaspar, 2011; Levkowitz et al., 2003; Lillesaar et al., 2007; McLean and Fetcho, 2004; Norton et al., 2005; Teraoka et al., 2004; Rink and Guo, 2004; Wang et al., 2013). Focussing on the development of serotonergic clusters in the hypothalamus, most hypothalamic serotonergic CSF-c progenitors are proliferating at 36 hpf (Bosco et al., 2013; McLean and Fetcho, 2004; Panula et al., 2010). By 62 hpf the first mature 5-HT synthesising CSF-c cells have developed in the intermediate and caudal clusters. *etv5b* regulates the proliferation of hypothalamic serotonergic progenitors (Bosco et al., 2013), and itself is dependent on Fgf3 as demonstrated above. To investigate the effect of Fgf3 on serotonergic CSF-c cells and

---

to test the hypothesis that *Fgf3* acts via *etv5b* in this context, *fgf3* has been impaired. As a result of manipulating *Fgf3* the number of serotonergic CSF-c cells is reduced leading to the conclusion that hypothalamic serotonergic CSF-c cells depend on *Fgf3*. The reduction is observable with each of the applied mutant, morphant and CRISPR/Cas9 strategies rendering the cell reduction a stable effect attributed to *fgf3* impairment. Despite the significant decline of serotonergic CSF-c cells the intermediate and caudal serotonergic clusters are never completely lost. Similar observations have been made in experiments using *etv5b* morphants (Bosco et al., 2013). Taken together, it appears that the hypothalamic and raphe serotonergic clusters rely on two individual developmental networks. This impression should be further investigated by finding more candidates, active during hypothalamic serotonergic development. The need for two networks governing raphe and hypothalamic serotonergic development could be due to the neuroanatomical regions that these cells are part of. Therefore, it is hypothesised that serotonergic clusters have different gene regulatory networks according to the respective CNS regions, the clusters are located in. This does not exclude that two or more members of the same gene family may play a role in serotonergic cell ontogeny of several clusters, as discussed below.

The investigations also included dopaminergic clusters. Dopaminergic CSF-c cells of clusters DC 4/5/6 and DC 7 are located in the caudal hypothalamic field where they are intermingled with intermediate and caudal serotonergic CSF-c cells, respectively (Kaslin and Panula, 2001; McLean and Fetcho, 2004; Rink and Wullimann, 2001). To test whether dopaminergic and serotonergic CSF-c cells have a mutual requirement for *Fgf3* in this region, TH1-positive cell clusters DC4/5/6 and DC 7 have been quantified after *fgf3* impairment. All three strategies used for *fgf3* impairment show a cell reduction of cluster DC 7, which is located most caudally. Thus, cluster DC 7 depends on *Fgf3*. Further, *th2* expressing cells of the caudal hypothalamus depend on *Fgf3* as well. In contrast, CSF-c cells of cluster DC 4/5/6 are not affected by *fgf3* impairment. These findings confirm previous ones using the *fgf3*<sup>t24152</sup> mutant to show that TH1-positive cells of cluster DC 7 depend on *Fgf3* while TH1-positive cells of

---



---

cluster DC 4/5/6 are independent (Koch et al., 2014). Contrary to this, when using *etv5b* morphants both clusters show no reduction of TH1-positive cells (Bosco et al., 2013). To account for the reduction but never complete loss of caudal monoaminergic clusters multiple scenarios are conceivable: firstly, certain serotonergic and dopaminergic CSF-c cells are independent of *Fgf3/Etv5b*; secondly, the applied impairment approaches result in a partial reduction yet not complete loss of *fgf3/Fgf3* (*etv5b*) activity; thirdly, other *Fgfs* compensate for the loss of *fgf3/Fgf3* which is sufficient for the remaining cells to develop and commit to the respective cell lineage. These points are discussed in greater detail below.

To address the question whether the observed *Fgf3* dependence is specific to monoaminergic CSF-c cells in the caudal hypothalamus three neuroendocrine cell markers including *oxt*, *avp* and *cort* have been analysed. All three peptide hormones are expressed in cells located in close proximity to the investigated monoaminergic clusters (Devos et al., 2002; Eaton et al., 2008; Unger and Glasgow, 2003). Cell numbers for *oxt* and *cort* expressing cells are unaffected in the examined hypothalamic clusters of *fgf3<sup>t24152</sup>* mutants and *fgf3* morphants. Similarly, *oxt* and *cort* expressing cells show no quantitative difference in *etv5b* morphants (Bosco et al., 2013). Therefore, it can be concluded that both populations are independent of *Fgf3* and *Etv5b*. However, cells expressing the third peptide hormone *avp* are reduced in hypothalamic clusters of *fgf3<sup>t24152</sup>* mutants and *fgf3* morphants, thus, *avp* expressing cells depend of *Fgf3*. Notably, the *avp* cluster is most reduced at its caudal end whereas rostral *avp* expressing cells seem to be less affected (Fig. 19E-H). This appears to be a similarity to dopaminergic CSF-c cells that are affected in the caudal-most hypothalamic cluster (DC 7) but not in a more anterior cluster (DC 4/5/6) (Koch et al., 2014; Reuter et al., 2019). Moreover, during proliferation dopaminergic CSF-c and *avp* expressing progenitors rely on the transcription factors *otpa* and *otpb* (Fernandes et al., 2013), which is an example for the dependence of different cell lineages on common factors during development. Interestingly, *avp* expressing cell numbers are not influenced by *etv5b* knock-down (Bosco et al., 2013). Additionally, when using a GFP-reporter line to

---

label *avp*-positive cells no cell number variations are reported in the hypothalamus of *fgf3*<sup>t24152</sup> mutants and wild types at 4 dpf (Liu et al., 2013). However, it appears that the *avp* expressing cell population analysed in the present study consists of only a few GFP-positive cells at 4 dpf in Liu et al. (2013). Hence, comparisons of both studies and possible conclusions derived thereof should be drawn carefully with this aspect in mind.

Summarising, monoaminergic CSF-c and *avp* cell ontogeny requires Fgf3 in such a manner that the most caudally located cell clusters have the highest requirement for Fgf3. This argues for a caudo-rostral gradient of Fgf3 dependence. Differences during the development of these three lineages (5-HT, TH1, *avp*) lie in their requirement for Etv5b (Bosco et al., 2013). The serotonergic CSF-c clusters are the only population showing Etv5b dependence. However, dopaminergic and *avp* populations may require another ETS-domain transcription factor activated by Fgf3. Possible candidates are *etv4* and *etv5a* since their transcripts are present in the hypothalamus (see Fig. 25; Bosco et al. (2013), Münchberg et al. (1999), Raible and Brand (2001), Roehl and Nüsslein-Volhard (2001), Roussigné and Blader (2006)). Finally, only clusters located in the caudal hypothalamus are affected by Fgf3 or Etv5b, which is supported by the reduced size of the caudal *nkx2.4b* expression domain (discussed below). Thus, it can be speculated that the two factors – Fgf3 and Etv5b – take part in generating the posterior recess region, which is a feature of teleosts and absent in, e.g. placental mammals (Xavier et al., 2017; Xie and Dorsky, 2017). This hypothesis is based on the concept that ‘hypothalamic compartments or modules’ are generated based on species-specific developmental programmes that can be either gained or lost during evolution (Xie and Dorsky, 2017). Another region of the hypothalamus could potentially represent another module, to which this concept might apply. This module is the tuberal/anterior hypothalamus, a region that is present in teleosts and mammals (Muthu et al., 2016). The formation of the tuberal/anterior hypothalamus largely seems to depend on Shh and Rx3. Both factors negatively affect dopaminergic clusters DC 1 and 2 and the anterior *avp* expressing cells. The tuberal/ anterior hypothalamic module

---

---

is abutting the posterior recess region and *fgf3* expression domain therein. Together, both modules express different factors (Shh/Rx3 and Fgf3/Etv5b) that affect the same cell lineages (DA, *avp*). This supports the concept that the developmental programme of a module A is responsible for the generation of the cell lineage clusters therein. If an abutting module B is lost or gained during evolution, by this logic, cell clusters of module A are unaffected even if module B shares clusters belonging to the same cell lineage. In addition, this would serve as a hypothesis to explain the variations in the gene regulatory networks between monoaminergic clusters. As this study together with Bosco et al. (2013) and Rink and Guo (2004) point out, the hypothalamic serotonergic gene regulatory network is as unique and tailored to the hypothalamic clusters as the raphe network is to the raphe serotonergic cells. Nonetheless, even if particular genes are not shared certain gene families might be. This is the case for the ETS-domain transcription factor family, which *pet1* and *etv5b* are part of, even though both factors exercise different functions during serotonergic development (Bosco et al., 2013; Lillesaar et al., 2007): *pet1* is active in differentiating raphe cells shortly before they are 5-HT immunoreactive; *etv5b* impacts on proliferating hypothalamic serotonergic progenitors. For future studies of monoaminergic cell development, a look at the gene family level might render suitable candidate genes that regulate the cell ontogeny of other serotonergic clusters even if the specific function may vary from cluster to cluster. It can be speculated that the additional genome duplication event of teleosts (Furutani-Seiki and Wittbrodt, 2004; Meyer and Schartl, 1999) might have facilitated the gene divergence between clusters. The genome duplication event enlarged the pool of genes of teleosts, which may have enabled genes of the same family to regionally specialise and/or functionalise. The hypothesised effects of the genome duplication within the framework of gained or lost modules/compartments might have created a foundation (enlarged gene pool), which has led to the neuroanatomical differences between the caudal hypothalamus of teleosts and placental mammals. Functionally, the *th2*-positive cells of the caudal hypothalamus of zebrafish are implicated in swimming behaviour (McPherson et al., 2016). Thus, it is

---

possible that the caudal hypothalamus of teleosts exercises different functions than the mammalian caudal hypothalamus.

### **Fgf3 regulates the proliferation of serotonergic progenitors in the caudal hypothalamus**

Dopaminergic and serotonergic CSF-c cells form large cell clusters in the caudal hypothalamus. By losing a portion of these cells after *fgf3* impairment the size of the hypothalamus may consequently be reduced. Indeed, this is the case as measurements of the *nkx2.4b* expression domain confirm at 72 hpf, a time point when serotonergic and dopaminergic CSF-c cells prominently cover the caudal hypothalamus (Bellipanni et al., 2002; Panula et al., 2010). Notably, the hypothalamus is already smaller at earlier developmental stages when monoaminergic CSF-c cells are still undifferentiated precursors. This may suggest an early impact of Fgf3 on monoaminergic progenitors when they are still proliferating. Favouring this hypothesis is the fact that *Etv5b* is similarly early involved in the proliferation process of serotonergic progenitor cells by maintaining the progenitor pool (Bosco et al., 2013). Thus, the proliferation of hypothalamic cells has been analysed after *fgf3* impairment at 36 hpf, a time point when the majority of serotonergic progenitors proliferates (Bosco et al., 2013). Globally, proliferating cells of the caudal hypothalamus are significantly reduced at 36 hpf. In addition, caudal hypothalamic cell death is increased at this stage. Such an early effect on cell death could deplete the caudal hypothalamic progenitor pool, hence, fewer cells would mature at later stages. Thus, this could explain the decreased hypothalamic size at all investigated stages after *fgf3* impairment. Strengthening this statement is that the global cell death appears to be at comparable levels in *fgf3* impaired and wild type embryos at 24 and 36 hpf. The overall growth and morphology of *fgf3*<sup>t24152</sup> mutants, *fgf3* CRISPR/Cas9 embryos and, especially, *fgf3* morphants is wild type-like apart from the ear, jaw and swim bladder phenotypes. This underlines that

---

the increase of cell death in the caudal hypothalamus is a specific effect. While the reduction of proliferating cells and simultaneous increase of cell death are consequences that influence all developing cells in the caudal hypothalamus, the next step focuses on specific effects of *fgf3* impairment on caudal serotonergic progenitors. The cell fate assay demonstrates that caudal serotonergic progenitors need Fgf3 at 36 and 45 hpf to commit to a serotonergic lineage. In summary, the proliferation of caudal hypothalamic cells is regulated by Fgf3. Among the affected cells are caudal serotonergic progenitors. The increase of hypothalamic cell death may be a secondary effect of progenitors not being able to follow their typical cell cycle programme. Therefore, early effects on proliferating progenitors have later repercussions on caudal serotonergic CSF-c cells. This together with the absence of dopaminergic and *avp* expressing cells can account for the smaller size of the hypothalamus. Thus, the following updated model of the gene regulatory network of hypothalamic serotonergic, dopaminergic CSF-c and *avp* expressing cells is proposed:

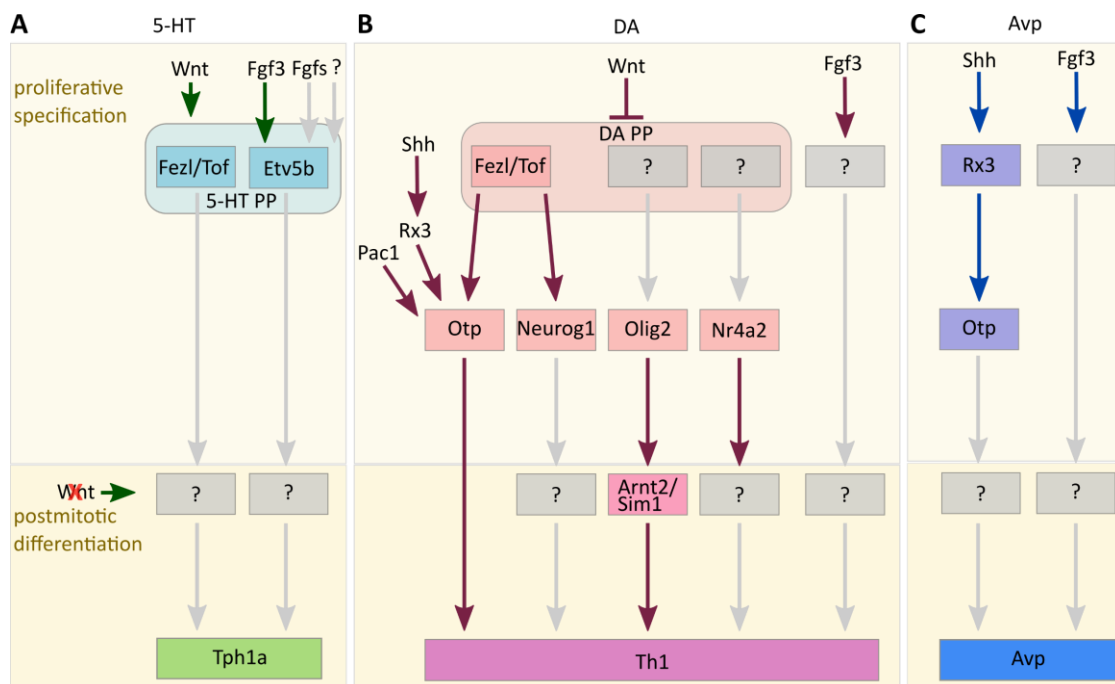


**Fig. 29: Gene regulatory networks of the hypothalamus.** A-C Updated schemes of the gene regulatory networks governing the development of serotonergic, dopaminergic and *avp* expressing cells. Grey boxes indicate one or multiple unknown factors. PP, progenitor pool. Based on Alunni et al. (2013), Bosco et al. (2013), Fernandes et al. (2013), Koch et al. (2014), Löhr et al. (2009), Muthu et al. (2016), Reuter et al. (2019), Rink and Guo (2004) and Wang et al. (2013).

### **Assessing the effects of the three *fgf3* impairment strategies on Fgf3 activity in the hypothalamus**

As discussed above each of the applied strategies to impair *fgf3* (mutant, morpholino, CRISPR/Cas9) lead to a significant reduction of monoaminergic CSF-c cells. In the least severe case, the loss of serotonergic CSF-c cells amounts to 17% on average in *fgf3*<sup>t24152</sup> mutants. In the most severe case, this entails an average reduction of serotonergic CSF-c cells by 49% observed in *fgf3* CRISPR/Cas9 embryos. Yet monoaminergic CSF-c cells of the caudal hypothalamus never disappear completely irrespective of the used strategy. The following explanations may account for this: firstly, in each of the strategies Fgf3 may still be active after impairment; secondly, specifically due to the weak hypothalamic phenotypes in *fgf3*<sup>t24152</sup> mutants, the *fgf3*<sup>t24152</sup> mutant allele may not be a null allele, thus, Fgf3 may still activate downstream signalling; thirdly, compensatory mechanisms by other Fgf ligands or Fgf3 itself may account for the remaining monoaminergic cells; fourthly, some of the remaining monoaminergic CSF-c cells are not depending on Fgf3 during development.

Regarding the first two explanations, the 3D models of the Fgf3 proteins from the *fgf3*<sup>t24152</sup> mutant and morpholino knock-down sequences suggest that both truncated isoforms are less stable and complete. Thus, they may be more prone to be recognised by the cell's degradation system. Moreover, both isoforms are potentially less inclined to interact with receptors due to the truncation. The stability and interaction potential are most compromised in *fgf3* morphants. However, as this strategy represents a transient knock-down wild type transcripts will still be present in morphants. For this reason, morphants cannot exhibit a complete loss-of-function phenotype. Herzog et al. (2004) reported that the nonsense *fgf3*<sup>t24152</sup> mutation is likely to be amorphic, which leads to a truncated Fgf3 protein with a complete loss of activity. The *fgf3*<sup>t26212</sup> and *fgf3*<sup>t24149</sup> mutations are reported to be hypomorphic with a residual Fgf3 activity of less than 1% (Herzog et al., 2004). This interpretation is based on results of RNA

---

---

overexpression experiments by comparing effects of mutant and wild type *fgf3* mRNA injections on neurectoderm formation. Injections with *fgf3*<sup>t24152</sup> mRNA caused no dorsalisation of the embryo or posteriorisation of the neurectoderm, which would be expected effects upon injection of active *fgf3* mRNA. Thus, the lack of potency of the *fgf3*<sup>t24152</sup> mRNA is emphasised. Especially, when comparing the results to the *fgf3*<sup>t26212</sup> and *fgf3*<sup>t24149</sup> mRNA injections, both of which cause a mild dorsalisation and posteriorisation. Hence, Herzog et al. (2004) come to the conclusion that the *fgf3*<sup>t24152</sup> mutation is likely to be amorphic. Accordingly, in the present thesis homozygous mutants have been expected to provide stronger hypothalamic phenotypes in general as well as compared to *fgf3* morphants. Together with the 3D model and the characterisation of hypothalamic phenotypes this study comes to the conclusion that the *fgf3*<sup>t24152</sup> mutation is not amorphic as previously suggested but rather hypomorphic. Thus, *fgf3*<sup>t24152</sup> mutants as *fgf3* morphants do not exhibit a complete loss-of-function phenotype. For the CRISPR/Cas9 strategy one gRNA targets exon 1 of the *fgf3* gene. The exact location of the target site is 153 base pairs downstream of the start codon. Thus, in the most severe scenario the indel mutations would introduce a premature stop causing a loss of ~80% of the wild type amino acid sequence. However, in this study embryos of the F<sub>0</sub> generation, i.e. embryos injected with an *fgf3* CRISPR/Cas9 cocktail are analysed. Generally, CRISPR/Cas9 F<sub>0</sub> generations are affected by various indel mutations caused by the error prone non-homologous end joining-mediated repair (Hwang et al., 2013). In addition, F<sub>0</sub> embryos have a random mosaic distribution of mostly mutated but also unmutated cells. Consequently, the analysed embryos display phenotypes of varying severity compared to the rather stable phenotypes exhibited by *fgf3*<sup>t24152</sup> mutants and *fgf3* morphants. Some individuals show an almost complete loss of the caudal serotonergic clusters. These cases are accompanied by a drastic reduction of the caudal hypothalamic size. Thus, Fgf3 function appears to be strongly impaired if not lost completely in these embryos (compare Fig. 17M,P). In light of these observations, using a stable, i.e. nonmosaic *fgf3* CRISPR/Cas9 knock-out line in future studies will yield more consistent phenotypes rendering a complete loss

---

of caudal serotonergic CSF-c cells or even of the entire posterior recess region possible scenarios.

Regarding the third possibility that other Fgf ligands may compensate for Fgf3 when its activity is impaired: in search of possible candidates compensating for Fgf3, 16 *fgf* ligands are expressed in the hypothalamus according to the hypothalamic transcriptome analysis performed in this thesis. The only canonical *fgf* ligand being upregulated at both investigated developmental stages is *fgf3* itself, which argues for a self-compensatory mechanism. *fgf11b* is upregulated in mutants at 7 dpf but not 3 dpf. It is an orthologue to the human FGF11, which belongs to the intracellular subfamily and as such does not interact with Fgf receptors but voltage gated sodium channels (Ornitz and Itoh, 2015). Further, a mild upregulation of *fgf8a* is observed even though the predefined thresholds are not passed. *fgf8a* expressing cells have been detected by *in situ* hybridisation in the caudal hypothalamus but they are spatially more restricted than *fgf3* expressing cells (see Fig. 14A and Reifers et al. (1998)). This may account for *fgf8a* not passing the thresholds in the transcriptome analysis. Fgf-signalling pathway components such as feedback regulators and downstream targets are moderately affected in *fgf3*<sup>t24152</sup> mutants. At 7 dpf three *dusp* genes (*dusp1*, *dusp2*, *dusp5*) are found to be downregulated. All three genes belong to the same subfamily constituting negative feedback regulators of Map kinases located in the nucleus (Kondoh and Nishida, 2007). Additionally, *dusp6* a feedback regulator of a different subfamily, which is located in the cytoplasm where it regulates Erk1/2 (Tsang et al., 2004). *dusp6* has not passed the thresholds in the transcriptome analysis but is mildly downregulated as well. These findings are supported by *in situ* hybridisations of *dusp1* and *dusp6* in *fgf3* morphants, which have been conducted at 36 hpf when serotonergic progenitors proliferate most (Bosco et al., 2013). Moreover, analysis of pErk1/2-positive cells in the caudal hypothalamus of *fgf3* morphants has been carried out at the same developmental stage. The slight increase of pErk1/2-positive cells corroborates that subtle expression changes of feedback regulators may already be sufficient to affect the targets of these feedback regulators in the hypothalamus.

---



The fourth possibility that certain monoaminergic CSF-c cells of the caudal hypothalamic clusters are not depending on *Fgf3* can mostly be speculated about. However, the caudal serotonergic clusters are known to be affected by *fezf2* and Wnt signalling during development (see Fig. 29) (Rink and Guo, 2004; Wang et al., 2013). It will be a task for future studies to investigate whether *Fgf3* and *Fezf2* (Wnt) rely on each other or act independently on either the same or different hypothalamic serotonergic CSF-c cells.

Summarising, a partial reduction of *Fgf3* function leads to mild alterations of the *Fgf*-signalling pathway at multiple levels according to the hypothalamic transcriptome analysis of *fgf3*<sup>t24152</sup> mutants. A self-compensatory mechanism of *fgf3* and a compensation by other *fgf* ligands may be at work as suggested by the upregulation of *fgf3* and *fgf8a*, the latter of which is only mildly upregulated. In addition, slightly altered expression of *Erk1/2*, feedback regulators and downstream targets is noted. In future investigations it will be interesting to see if the observed effects may be more substantial in a hypothalamic transcriptome analysis of a stable *fgf3* CRISPR/Cas9 knock-out line. It is possible that some serotonergic CSF-c cells rely on other factors besides *Fgf3*. It is equally possible that all serotonergic CSF-c cells of the caudal hypothalamus will be lost in an *fgf3* CRISPR/Cas9 stable line since they are already mostly gone in some individuals of the CRISPR/Cas9 F<sub>0</sub> generation.

### **First steps toward understanding the functions of serotonergic CSF-c cells of the hypothalamus**

The development of hypothalamic serotonergic CSF-c cells is the main focus of the present study. However, to uncover the function of hypothalamic serotonergic CSF-c cells once they have matured is an essential step to expand the knowledge about the largest serotonergic population found in the zebrafish CNS (Lillesaar and Gaspar, 2019). At this point, it can only be speculated about alleged functions of serotonergic

CSF-c cells. They may play a role in circadian rhythmicity (Vigh and Vigh-Teichmann, 1998). This hypothesis is based on the observation that some hypothalamic CSF-c cells may represent deep encephalic photoreceptors. Since this may potentially include serotonergic CSF-c cells, this hypothesis should be investigated. Further, roles in mechanosensation and pH sensation have recently been demonstrated for hypothalamic and spinal cord CSF-c cells (Djenoune et al., 2014; Jalalvand et al., 2018). In zebrafish spinal cord CSF-c cells are implicated in locomotion (Böhm et al., 2016; Fidelin et al., 2015; Montgomery et al., 2016; 2018; Orts-Del'Immagine and Wyart, 2017). Even though some of these roles seem to be specific functions of the spinal cord similar roles for caudal hypothalamic serotonergic CSF-c cells should be investigated. In order to examine any possible function serotonergic CSF-c cells might have (Howe et al., 2013) the *tph1a* CRISPR/Cas9 knock-out and morpholino strategy will be valuable resources. In the present work first steps to generate a knock-out have been undertaken and two morpholinos have been tested with respect to their efficiency. Thus, the basis is created to investigate the function of hypothalamic serotonergic CSF-c cells.

---

## Conclusion

In conclusion, this thesis identifies Fgf3 as a prominent Fgf ligand in the caudal hypothalamus of zebrafish (Herzog et al., 2004). Therein, Fgf3 regulates the development of monoaminergic CSF-c (Koch et al., 2014) and *avp* expressing cells. Most interestingly, the requirement of Fgf3 by these cells follows a caudo-rostral gradient with a higher dependence on Fgf3 by caudally located cells. Moreover, the ETS-domain transcription factor *etv5b*, a downstream target of Fgf-signalling, is demonstrated to be under the control of Fgf3. With regard to serotonergic CSF-c cell development, it is shown that *fgf3* is expressed several hours before *tph1a* and 5-HT (Bellipanni et al., 2002; Bosco et al., 2013). This together with the fact that the *nkx2.4b* expression domain is already smaller before mature serotonergic CSF-c cells develop argues for an early impact of Fgf3 on the proliferation of serotonergic progenitors. This hypothesis is supported by the universal decrease of proliferating cells in the hypothalamus and simultaneous increase of cell death. Complementary cell fate experiments confirm that proliferating serotonergic progenitors need Fgf3 to commit to the serotonergic lineage. These results support earlier findings stating that hypothalamic serotonergic progenitors require Fgf-signalling via *etv5b* for proper proliferation (Bosco et al., 2013). Additionally, the transcriptome analysis of the hypothalamus reveals that 16 transcripts of Fgf ligands are expressed at developmental stages. In addition to Fgf3 all other 15 Fgf ligands constitute potential candidates to be tested with regard to their involvement in hypothalamic monoaminergic development as well as hypothalamic development in general. Further, the transcriptome analysis provides evidence for a self-compensatory mechanism of *fgf3* since *fgf3* expression is upregulated as a consequence of its own impairment. In addition, Fgf-signalling pathway components such as *dusp1*, *dusp2*, *dusp5*, *dusp6* and Erk1/2 appear to be mildly affected after *fgf3* impairment. To sum up, Fgf3-signalling is demonstrated to be of critical importance during hypothalamic

---

development impacting on caudal serotonergic, dopaminergic CSF-c and *avp* expressing cells. In addition, two strategies are set up to determine the function of hypothalamic serotonergic CSF-c cells by knock-out of the biosynthesis enzyme *tph1a*. The presented findings of this thesis contribute to understand the evolution of the vertebrate hypothalamus by revealing parts of the developmental programme governing the emergence of the posterior recess region of the hypothalamus.

The establishment of a stable *fgf3* CRISPR/Cas9 line provides the basis for future *fgf3* experiments. This will reveal the impact of a complete loss of Fgf3 activity on caudal hypothalamic development including effects on proliferation and differentiation of serotonergic CSF-c cells. Further, a stable line would provide the opportunity to re-sequence the hypothalamic transcriptome in a complete loss-of-function background, thus, presumably providing stronger and clearer results regarding differential gene expression as opposed to the results obtained by using *fgf3*<sup>t24152</sup> mutants. This will facilitate the identification of new candidate genes that depend on Fgf3 and are involved in the serotonergic and caudal hypothalamic gene regulatory network. Especially, if the sequencing will be performed at, e.g. 72 hpf and at earlier developmental stages, e.g. 36 or 48 hpf when serotonergic progenitors proliferate and differentiate. The already existing hypothalamic transcriptome of wild types can be used for gene comparisons in a spatiotemporal manner. This transcriptome brings the benefit of highlighting a specific set of genes active at a certain time point within a restricted space – the hypothalamus. Comparing two developmental time points when hypothalamic genes are active lends the possibility to understand how the development and maintenance of the hypothalamus is regulated over time. An optogenetic approach to manipulate hypothalamic Fgf3 activity only at developmental stages when serotonergic progenitors proliferate and differentiate will further refine the impact of Fgf3 on serotonergic neurogenesis in the hypothalamus. In addition, the impact of other transduction pathways on serotonergic development should be investigated as well. Wnt-signalling via *fezf2* or Shh-signalling via *rx3* and targets

---

thereof present a starting point. Comparing and analysing gene family members of factors that are known to have an impact on, e.g. raphe serotonergic clusters or hypothalamic dopaminergic clusters may provide new candidates involved in hypothalamic serotonergic cell ontogeny. The named approaches can also be used to analyse any other candidate gene likely to be involved in hypothalamic development and function. Thus, at some point developmental programmes might be revealed that lead to the development of individual hypothalamic ‘modules’.

Uncovering the function of serotonergic CSF-c cells in the caudal hypothalamus will be another future task. This can be achieved by establishing a stable *tph1a* CRISPR/Cas9 line. As performed for *fgf3* in this study, a morphological characterisation of the phenotypes displayed by *tph1a* knock-out mutants will be required. A behavioural characterisation should be conducted as well. Possible starting points present behaviours that 5-HT and the hypothalamus impact on, thus, may suggest a link between the two. Mechanosensation and pH sensation could be two more functions hypothalamic serotonergic CSF-c cells have. Another possible connection may exist between hypothalamic serotonergic CSF-c cells and deep brain photoreceptors. Thus, circadian rhythmicity could be investigated in *tph1a* knock-outs by expression analysis of opsins and other members of the phototransduction pathway.

---

## References

- Affaticati, P., Yamamoto, K., Rizzi, B., Bureau, C., Peyri  ras, N., Pasqualini, C., Demarque, M., Vernier, P. (2015). Identification of the optic recess region as a morphogenetic entity in the zebrafish forebrain. *Sci Rep*, 8738.
- Agduhr, E. (1922).   ber ein zentrales Sinnesorgan bei den Vertebraten. *Z. Anat. Entwickl. Gesch.* **3-6**, 223–360.
- Agnati, L. F., Fuxe, K., Zoli, M., Ozini, I., Toffano, G., Ferraguti, F. (1986). A correlation analysis of the regional distribution of central enkephalin and beta-endorphin immunoreactive terminals and of opiate receptors in adult and old male rats. Evidence for the existence of two main types of communication in the central nervous system. *Acta Physiol Scand.* **2**, 201–207.
- Agnati, L. F., Leo, G., Zanardi, A., Genedani, S., Rivera, A., Fuxe, K., Guidolin, D. (2006). Volume transmission and wiring transmission from cellular to molecular networks. *Acta Physiol (Oxf)*. **1-2**, 329–344.
- Alunni, A., Coolen, M., Foucher, I., Bally-Cuif, L. (2013). Neurogenesis in Zebrafish. In *Patterning and Cell Type Specification in the Developing CNS and PNS* (Ed.: Rubenstein, J. L.; Rakic, P.), pp. 645–677: Elsevier Science.
- Anichtchik, O., Sallinen, V., Peitsaro, N., Panula, P. (2006). Distinct structure and activity of monoamine oxidase in the brain of zebrafish (*Danio rerio*). *J. Comp. Neurol.* **5**, 593–610.
- Appel, B., Korzh, V., Glasgow, E., Thor, S., Edlund, T., Dawid, I. B., Eisen, J. S. (1995). Motoneuron fate specification revealed by patterned LIM homeobox gene expression in embryonic zebrafish. *Development*. **12**, 4117–4125.
- Araya, C., Ward, L. C., Girdler, G. C., Miranda, M. (2016). Coordinating cell and tissue behavior during zebrafish neural tube morphogenesis. *Dev. Dyn.* **3**, 197–208.
- Baeuml, S. W., Biechl, D., Wullimann, M. F. (2019). Adult *islet1* expression outlines ventralized derivatives along zebrafish neuraxis. *Front Neuroanat*, 19.
- Bak, M., Fraser, S. E. (2003). Axon fasciculation and differences in midline kinetics between pioneer and follower axons within commissural fascicles. *Development*. **20**, 4999–5008.
- Ballion, B., Branchereau, P., Chapron, J., Viala, D. (2002). Ontogeny of descending serotonergic innervation and evidence for intraspinal 5-HT neurons in the mouse spinal cord. *Developmental Brain Research*. **1**, 81–88.
- Bally-Cuif, L., Hammerschmidt, M. (2003). Induction and patterning of neuronal development, and its connection to cell cycle control. *Current Opinion in Neurobiology*. **1**, 16–25.
- Beccari, L., Marco-Ferreres, R., Bovolenta, P. (2013). The logic of gene regulatory networks in early vertebrate forebrain patterning. *Mechanisms of Development*. **2-3**, 95–111.
- Beenken, A., Eliseenkova, A. V., Ibrahim, O. A., Olsen, S. K., Mohammadi, M. (2012). Plasticity in interactions of fibroblast growth factor 1 (FGF1) N terminus with FGF receptors underlies promiscuity of FGF1. *J Biol Chem*. **5**, 3067–3078.
- Bellipanni, G., Rink, E., Bally-Cuif, L. (2002). Cloning of two *tryptophan hydroxylase* genes expressed in the diencephalon of the developing zebrafish brain. *Mechanisms of Development*, S215-S220.
- Bertrand, N., Castro, D. S., Guillemot, F. (2002). Proneural genes and the specification of neural cell types. *Nat. Rev. Neurosci.* **7**, 517–530.
- Biran, J., Tahor, M., Wincer, E., Levkowitz, G. (2015). Role of developmental factors in hypothalamic function. *Front Neuroanat*, 47.
- Blader, P., Fischer, N., Gradwohl, G., Guillemot, F., Str  hle, U. (1997). The activity of Neurogenin1 is controlled by local cues in the zebrafish embryo. *Development*. **22**, 4557–4569.
- Blechman, J., Borodovsky, N., Eisenberg, M., Nabel-Rosen, H., Grimm, J., Levkowitz, G. (2007). Specification of hypothalamic neurons by dual regulation of the homeodomain protein Orthopedia. *Development*. **24**, 4417–4426.
- Blin, M., Norton, W., Bally-Cuif, L., Vernier, P. (2008). NR4A2 controls the differentiation of selective dopaminergic nuclei in the zebrafish brain. *Mol Cell Neurosci.* **4**, 592–604.

- 
- Boettger, T., Knoetgen, H., Wittler, L., Kessel, M. (2001). The avian organizer. *Int J Dev Biol.* **1**, 281–287.
- Böhm, U. L., Prendergast, A., Djenoune, L., Nunes Figueiredo, S., Gomez, J., Stokes, C., Kaiser, S., Suster, M., Kawakami, K., Charpentier, M. et al. (2016). CSF-contacting neurons regulate locomotion by relaying mechanical stimuli to spinal circuits. *Nat Commun*, 10866.
- Bökel, C., Brand, M. (2013). Generation and interpretation of FGF morphogen gradients in vertebrates. *Curr Opin Genet Dev.* **4**, 415–422.
- Borodovsky, N., Ponomaryov, T., Frenkel, S., Levkowitz, G. (2009). Neural protein Olig2 acts upstream of the transcriptional regulator Sim1 to specify diencephalic dopaminergic neurons. *Dev. Dyn.* **4**, 826–834.
- Bosco, A., Bureau, C., Affaticati, P., Gaspar, P., Bally-Cuif, L., Lillesaar, C. (2013). Development of hypothalamic serotonergic neurons requires Fgf signalling via the ETS-domain transcription factor Etv5b. *Development.* **2**, 372–384.
- Branton, W. D., Mayeri, E., Brownell, P., Simon, S. B. (1978). Evidence for local hormonal communication between neurones in Aplysia. *Nature.* **5666**, 70–72.
- Briscoe, J., Ericson, J. (1999). The specification of neuronal identity by graded Sonic Hedgehog signalling. *Semin Cell Dev Biol.* **3**, 353–362.
- Brocher, J. *The BioVoxel Image Processing and Analysis Toolbox*. EuBIAS-Conference, Paris, FRA, 2015.
- Brustein, E., Chong, M., Holmqvist, B., Drapeau, P. (2003). Serotonin patterns locomotor network activity in the developing zebrafish by modulating quiescent periods. *J Neurobiol.* **3**, 303–322.
- Candy, J., Collet, C. (2005). Two tyrosine hydroxylase genes in teleosts. *Biochim Biophys Acta.* **1**, 35–44.
- Carlberg, M. (1992). Localization of dopamine in the freshwater hydrozoan *Hydra attenuata*. *Cell and Tissue Research.* **3**, 601–607.
- Chen, Y.-C., Priyadarshini, M., Panula, P. (2009). Complementary developmental expression of the two tyrosine hydroxylase transcripts in zebrafish. *Histochem Cell Biol.* **4**, 375–381.
- Chen, Y.-C., Semenova, S., Rozov, S., Sundvik, M., Bonkowsky, J. L., Panula, P. (2016). A novel developmental role for dopaminergic signaling to specify hypothalamic neurotransmitter identity. *J. Biol. Chem.* **42**, 21880–21892.
- Cheng, C. W., Yan, C. H. M., Choy, S. W., Hui, M. N. Y., Hui, C.-C., Cheng, S. H. (2007). Zebrafish homologue *irx1a* is required for the differentiation of serotonergic neurons. *Dev. Dyn.* **9**, 2661–2667.
- Chitnis, A. B., Kuwada, J. Y. (1990). Axonogenesis in the brain of zebrafish embryos. *J Neurosci.* **6**, 1892–1905.
- Christenson, J. G., Dairman, W., Udenfriend, S. (1972). On the identity of DOPA decarboxylase and 5-hydroxytryptophan decarboxylase. *Proc. Natl. Acad. Sci. U.S.A.* **2**, 343–347.
- Concha, M. L., Adams, R. J. (1998). Oriented cell divisions and cellular morphogenesis in the zebrafish gastrula and neurula. *Development.* **6**, 983–994.
- Craven, S. E., Lim, K.-C., Ye, W., Engel, J. D., Sauvage, F. de, Rosenthal, A. (2004). Gata2 specifies serotonergic neurons downstream of sonic hedgehog. *Development.* **5**, 1165–1173.
- Cunningham, J. A., Liu, A. G., Bengtson, S., Donoghue, P. C. J. (2017). The origin of animals. *Bioessays.* **1**, 1–12.
- Dahlström, A., Fuxe, K. (1964). Evidence for the existence of monoamine neurons in the central nervous system: I. Demonstration of monoamines in the cell bodies of brain stem neurons. *Acta Physiol Scand Suppl*, Vol.62, Suppl 232:1–52.
- del Corral, R. D., Breitzkreuz, D. N., Storey, K. G. (2002). Onset of neuronal differentiation is regulated by paraxial mesoderm and requires attenuation of FGF signalling. *Development.* **7**, 1681.
- Delaune, E., Lemaire, P., Kodjabachian, L. (2005). Neural induction in *Xenopus* requires early FGF signalling in addition to BMP inhibition. *Development.* **2**, 299–310.
- De-Miguel, F. F., Fuxe, K. (2012). Extrasynaptic neurotransmission as a way of modulating neuronal functions. *Front Physiol*, 16.
- Deneris, E., Gaspar, P. (2018). Serotonin neuron development. *Wiley Interdiscip Rev Dev Biol.* **1**.
-

- Deneris, E. S., Wyler, S. C. (2012). Serotonergic transcriptional networks and potential importance to mental health. *Nat. Neurosci.* **4**, 519–527.
- Descarries, L., Alain, B., Watkins, K. C. (1975). Serotonin nerve terminals in adult rat neocortex. *Brain Research.* **3**, 563–588.
- Descarries, L., Mechawar, N. (2000). Ultrastructural evidence for diffuse transmission by monoamine and acetylcholine neurons of the central nervous system. In *Volume transmission revisited* (Ed.: Agnati, L. F.), pp. 27–47. Amsterdam: Elsevier.
- Devos, N., Deflorian, G., Biemar, F., Bortolussi, M., Martial, J. A., Peers, B., Argenton, F. (2002). Differential expression of two somatostatin genes during zebrafish embryonic development. *Mechanisms of Development.* **1–2**, 133–137.
- Di Tommaso, P., Moretti, S., Xenarios, I., Orobittg, M., Montanyola, A., Chang, J.-M., Taly, J.-F., Notredame, C. (2011). T-Coffee: a web server for the multiple sequence alignment of protein and RNA sequences using structural information and homology extension. *Nucleic Acids Research. Web Server issue*, W13–7.
- Ding, Y.-Q., Marklund, U., Yuan, W., Yin, J., Wegman, L., Ericson, J., Deneris, E., Johnson, R. L., Chen, Z.-F. (2003). *Lmx1b* is essential for the development of serotonergic neurons. *Nat. Neurosci.* **9**, 933–938.
- Djenoune, L., Khabou, H., Joubert, F., Quan, F. B., Nunes Figueiredo, S., Bodineau, L., Del Bene, F., Burcklé, C., Tostivint, H., Wyart, C. (2014). Investigation of spinal cerebrospinal fluid-contacting neurons expressing PKD2L1. *Front Neuroanat*, 26.
- Dobin, A., Davis, C. A., Schlesinger, F., Drenkow, J., Zaleski, C., Jha, S., Batut, P., Chaisson, M., Gingeras, T. R. (2013). STAR. *Bioinformatics.* **1**, 15–21.
- Dono, R. (2003). Fibroblast growth factors as regulators of central nervous system development and function. *Am J Physiol Regul Integr Comp Physiol.* **4**, R867–81.
- Duncan, R. N., Xie, Y., McPherson, A. D., Taibi, A. V., Bonkowsky, J. L., Douglass, A. D., Dorsky, R. I. (2016). Hypothalamic radial glia function as self-renewing neural progenitors in the absence of Wnt/ $\beta$ -catenin signaling. *Development.* **1**, 45–53.
- Eaton, J. L., Glasgow, E. (2006). The zebrafish bHLH PAS transcriptional regulator, single-minded 1 (*sim1*), is required for isotocin cell development. *Dev. Dyn.* **8**, 2071–2082.
- Eaton, J. L., Glasgow, E. (2007). Zebrafish orthopedia (*otp*) is required for isotocin cell development. *Dev Genes Evol.* **2**, 149–158.
- Eaton, J. L., Holmqvist, B., Glasgow, E. (2008). Ontogeny of *vasotocin*-expressing cells in zebrafish: selective requirement for the transcriptional regulators *orthopedia* and *single-minded 1* in the preoptic area. *Dev. Dyn.* **4**, 995–1005.
- Emsley, P., Lohkamp, B., Scott, W. G., Cowtan, K. (2010). Features and development of *Coot*. *Acta Crystallogr D Biol Crystallogr.* Pt **4**, 486–501.
- Erspamer, V., Vialli, M. (1937). Ricerche sul secreto delle cellule enterocromaffini. *Zeitschrift für Zellforschung (Zeitschrift für Zellforschung und Mikroskopische Anatomie).* **1**, 81–99.
- Fernandes, A. M., Beddows, E., Filippi, A., Driever, W. (2013). Orthopedia transcription factor *otpa* and *otpb* paralogous genes function during dopaminergic and neuroendocrine cell specification in larval zebrafish. *PLoS ONE.* **9**, e75002.
- Fidelin, K., Djenoune, L., Stokes, C., Prendergast, A., Gomez, J., Baradel, A., Del Bene, F., Wyart, C. (2015). State-dependent modulation of locomotion by GABAergic spinal sensory neurons. *Curr Biol.* **23**, 3035–3047.
- Filby, A. L., Paull, G. C., Hickmore, T. F. A., Tyler, C. R. (2010). Unravelling the neurophysiological basis of aggression in a fish model. *BMC Genomics.* **1**, 498.
- Filippi, A., Dürr, K., Ryu, S., Willaredt, M., Holzschuh, J., Driever, W. (2007). Expression and function of *nr4a2*, *lmx1b*, and *pitx3* in zebrafish dopaminergic and noradrenergic neuronal development. *BMC Dev Biol*, 135.
- Fitzpatrick, P. F. (1999). Tetrahydropterin-dependent amino acid hydroxylases. *Annu Rev Biochem*, 355–381.
- Flames, N., Hobert, O. (2011). Transcriptional control of the terminal fate of monoaminergic neurons. *Annu Rev Neurosci*, 153–184.



- 
- Fredriksson, R., Schiöth, H. B. (2005). The repertoire of G-protein-coupled receptors in fully sequenced genomes. *Mol Pharmacol.* **5**, 1414–1425.
- Furutani-Seiki, M., Wittbrodt, J. (2004). Medaka and zebrafish, an evolutionary twin study. *Mechanisms of Development.* **7-8**, 629–637.
- Fuxe, K., Dahlström, A., Höistad, M., Marcellino, D., Jansson, A., Rivera, A., Diaz-Cabiale, Z., Jacobsen, K., Tinner-Staines, B., Hagman, B. et al. (2007). From the Golgi-Cajal mapping to the transmitter-based characterization of the neuronal networks leading to two modes of brain communication. *Brain Res Rev.* **1**, 17–54.
- Gaspar, P., Cases, O., Maroteaux, L. (2003). The developmental role of serotonin. *Nature Reviews Neuroscience.* **12**, 1002.
- Gaspar, P., Lillesaar, C. (2012). Probing the diversity of serotonin neurons. *Philos. Trans. R. Soc. Lond., B, Biol. Sci.* **1601**, 2382–2394.
- Gilbert, S. F. (2014). *Developmental biology*, Sunderland, MA, USA: Sinauer Associates, Inc. Publishers.
- Goto, H., Tomono, Y., Ajiro, K., Kosako, H., Fujita, M., Sakurai, M., Okawa, K., Iwamatsu, A., Okigaki, T., Takahashi, T. et al. (1999). Identification of a novel phosphorylation site on histone H3 coupled with mitotic chromosome condensation. *J Biol Chem.* **36**, 25543–25549.
- Götz, M., Huttner, W. B. (2005). The cell biology of neurogenesis. *Nat. Rev. Mol. Cell Biol.* **10**, 777–788.
- Grandel, H., Kaslin, J., Ganz, J., Wenzel, I., Brand, M. (2006). Neural stem cells and neurogenesis in the adult zebrafish brain. *Dev. Biol.* **1**, 263–277.
- Gutknecht, L., Kriegebaum, C., Waider, J., Schmitt, A., Lesch, K.-P. (2009). Spatio-temporal expression of tryptophan hydroxylase isoforms in murine and human brain. *Eur Neuropsychopharmacol.* **4**, 266–282.
- Haddon, C., Smithers, L., Schneider-Maunoury, S., Coche, T., Henrique, D., Lewis, J. (1998). Multiple delta genes and lateral inhibition in zebrafish primary neurogenesis. *Development.* **3**, 359–370.
- Hammond, K. L., Whitfield, T. T. (2011). Fgf and Hh signalling act on a symmetrical pre-pattern to specify anterior and posterior identity in the zebrafish otic placode and vesicle. *Development.* **18**, 3977–3987.
- Hashimoto, H., Yabe, T., Hirata, T., Shimizu, T., Bae, Y.-k., Yamanaka, Y., Hirano, T., Hibi, M. (2000). Expression of the zinc finger gene *fez-like* in zebrafish forebrain. *Mechanisms of Development.* **1-2**, 191–195.
- Hauptmann, G., Gerster, T. (2000). Regulatory gene expression patterns reveal transverse and longitudinal subdivisions of the embryonic zebrafish forebrain. *Mechanisms of Development.* **1**, 105–118.
- Hay-Schmidt, A. (2000). The evolution of the serotonergic nervous system. *Proc Biol Sci.* **1448**, 1071–1079.
- Hendricks, T., Francis, N., Fyodorov, D., Deneris, E. S. (1999). The ETS domain factor Pet-1 is an early and precise marker of central serotonin neurons and interacts with a conserved element in serotonergic genes. *J Neurosci (The Journal of neuroscience: the official journal of the Society for Neuroscience).* **23**, 10348–10356.
- Henzel, M. J., Wei, Y., Mancini, M. A., van Hooser, A., Ranalli, T., Brinkley, B. R., Bazett-Jones, D. P., Allis, C. D. (1997). Mitosis-specific phosphorylation of histone H3 initiates primarily within pericentromeric heterochromatin during G2 and spreads in an ordered fashion coincident with mitotic chromosome condensation. *Chromosoma.* **6**, 348–360.
- Herrick, C. J. (1910). The morphology of the forebrain in amphibia and reptilia. *J. Comp. Neurol. Psychol.* **5**, 413–547.
- Herzog, W., Sonntag, C., von der Hardt, S., Roehl, H. H., Varga, Z. M., Hammerschmidt, M. (2004). Fgf3 signaling from the ventral diencephalon is required for early specification and subsequent survival of the zebrafish adenohypophysis. *Development.* **15**, 3681–3692.
- His, W. (1888). Zur Geschichte des Gehirns. In *Abhandlungen der mathematisch-physischen Classe der königlich sächsischen Gesellschaft der Wissenschaften* (Ed.: Hirzel, S.), pp. 342 - 392, II Bl. Leipzig.
- Hökfelt, T. (1984). Distributional map of tyrosine hydroxylase immunoreactive neurons in the rat brain. In *Classical transmitters in the CNS 2/1* (Ed.: Björklund, A.; Hökfelt, T.), pp. . Amsterdam: Elsevier.
- Holzschuh, J., Ryu, S., Aberger, F., Driever, W. (2001). Dopamine transporter expression distinguishes dopaminergic neurons from other catecholaminergic neurons in the developing zebrafish embryo. *Mechanisms of Development.* **1-2**, 237–243.
-

- 
- Howe, K., Clark, M. D., Torroja, C. F., Torrance, J., Berthelot, C., Muffato, M., Collins, J. E., Humphray, S., McLaren, K., Matthews, L. et al. (2013). The zebrafish reference genome sequence and its relationship to the human genome. *Nature*. **7446**, 498–503.
- Hoyer, D., Hannon, J. P., Martin, G. R. (2002). Molecular, pharmacological and functional diversity of 5-HT receptors. *Pharmacology Biochemistry and Behavior*. **4**, 533–554.
- Hwang, W. Y., Fu, Y., Reyon, D., Maeder, M. L., Tsai, S. Q., Sander, J. D., Peterson, R. T., Yeh, J.-R. J., Joung, J. K. (2013). Efficient genome editing in zebrafish using a CRISPR-Cas system. *Nat Biotechnol*. **3**, 227–229.
- Itoh, N. (2007). The Fgf Families in Humans, Mice, and Zebrafish: Their Evolutional Processes and Roles in Development, Metabolism, and Disease. *Biol. Pharm. Bull.* **10**, 1819–1825.
- Itoh, N., Ornitz, D. M. (2011). Fibroblast growth factors: from molecular evolution to roles in development, metabolism and disease. *J Biochem*. **2**, 121–130.
- Jäckels, J. (2017). Morphological evaluations of the hypothalamus after a morpholino-based *fgf3* loss-of-function in developing zebrafish. Bachelor thesis, University of Würzburg, Würzburg.
- Jackman, W. R., Draper, B. W., Stock, D. W. (2004). Fgf signaling is required for zebrafish tooth development. *Dev. Biol.* **1**, 139–157.
- Jacob, J., Ferri, A. L., Milton, C., Prin, F., Pla, P., Lin, W., Gavalas, A., Ang, S.-L., Briscoe, J. (2007). Transcriptional repression coordinates the temporal switch from motor to serotonergic neurogenesis. *Nat. Neurosci.* **11**, 1433–1439.
- Jacob, J., Storm, R., Castro, D. S., Milton, C., Pla, P., Guillemot, F., Birchmeier, C., Briscoe, J. (2009). Insm1 (IA-1) is an essential component of the regulatory network that specifies monoaminergic neuronal phenotypes in the vertebrate hindbrain. *Development*. **14**, 2477–2485.
- Jalalvand, E., Robertson, B., Tostivint, H., Löw, P., Wallén, P., Grillner, S. (2018). Cerebrospinal fluid-contacting neurons sense pH changes and motion in the hypothalamus. *J Neurosci*. **35**, 7713–7724.
- Jalalvand, E., Robertson, B., Wallén, P., Grillner, S. (2016). Ciliated neurons lining the central canal sense both fluid movement and pH through ASIC3. *Nat Commun*, 10002.
- Jenkins, T. A., Nguyen, J. C. D., Polglaze, K. E., Bertrand, P. P. (2016). Influence of tryptophan and serotonin on mood and cognition with a possible role of the gut-brain Axis. *Nutrients*. **1**.
- Jensen, P., Farago, A. F., Awatramani, R. B., Scott, M. M., Deneris, E. S., Dymecki, S. M. (2008). Redefining the serotonergic system by genetic lineage. *Nat. Neurosci.*, 417 EP -.
- Jeong, J.-Y., Einhorn, Z., Mathur, P., Chen, L., Lee, S., Kawakami, K., Guo, S. (2007). Patterning the zebrafish diencephalon by the conserved zinc-finger protein Fezl. *Development*. **1**, 127–136.
- Jeong, J.-Y., Einhorn, Z., Mercurio, S., Lee, S., Lau, B., Mione, M., Wilson, S. W., Guo, S. (2006). Neurogenin1 is a determinant of zebrafish basal forebrain dopaminergic neurons and is regulated by the conserved zinc finger protein Tof/Fezl. *Proc. Natl. Acad. Sci. U.S.A.* **13**, 5143–5148.
- Kanehisa, M. S. G. (2000). KEGG. *Nucleic Acids Research*. **1**, 27–30.
- Kapsimali, M., Caneparo, L., Houart, C., Wilson, S. W. (2004). Inhibition of Wnt/Axin/beta-catenin pathway activity promotes ventral CNS midline tissue to adopt hypothalamic rather than floorplate identity. *Development*. **23**, 5923–5933.
- Kaslin, J., Panula, P. (2001). Comparative anatomy of the histaminergic and other aminergic systems in zebrafish (*Danio rerio*). *J. Comp. Neurol.* **4**, 342–377.
- Keller, P. J., Schmidt, A. D., Wittbrodt, J., Stelzer, E. H. K. (2008). Reconstruction of zebrafish early embryonic development by scanned light sheet microscopy. *Science*. **5904**, 1065–1069.
- Kelley, L. A., Mezulis, S., Yates, C. M., Wass, M. N., Sternberg, M. J. E. (2015). The Phyre2 web portal for protein modeling, prediction and analysis. *Nat Protoc*, 845 EP -.
- Kiefer, P., Strähle, U., Dickson, C. (1996). The zebrafish Fgf-3 gene: cDNA sequence, transcript structure and genomic organization. *Gene*. **2**, 211–215.
-

- 
- Kim, S.-H., Shin, J., Park, H.-C., Yeo, S.-Y., Hong, S.-K., Han, S., Rhee, M., Kim, C.-H., Chitnis, A. B., Huh, T.-L. (2002). Specification of an anterior neuroectoderm patterning by Frizzled8a-mediated Wnt8b signalling during late gastrulation in zebrafish. *Development*. **19**, 4443–4455.
- Kimmel, C. B., Ballard, W. W., Kimmel, S. R., Ullmann, B., Schilling, T. F. (1995). Stages of embryonic development of the zebrafish. *Dev. Dyn.* **3**, 253–310.
- Kimmel, C. B., Hatta, K., Eisen, J. S. (1991). Genetic control of primary neuronal development in zebrafish. *Development*. **Supplement 2**, 47–57.
- Kimmel, C. B., Warga, R. M., Schilling, T. F. (1990). Origin and organization of the zebrafish fate map. *Development*. **4**, 581–594.
- Kiyasova, V., Gaspar, P. (2011). Development of raphe serotonin neurons from specification to guidance. *Eur. J. Neurosci.* **10**, 1553–1562.
- Koch, P., Löhr, H. B., Driever, W. (2014). A mutation in *cnot8*, component of the Ccr4-not complex regulating transcript stability, affects expression levels of developmental regulators and reveals a role of Fgf3 in development of caudal hypothalamic dopaminergic neurons. *PLoS ONE*. **12**, e113829.
- Kolmer, W. (1921). Das „Sagittalorgan“ der Wirbeltiere. *Z. Anat. Entwickl. Gesch.* **3-6**, 652–717.
- Kondoh, K., Nishida, E. (2007). Regulation of MAP kinases by MAP kinase phosphatases. *Biochim Biophys Acta*. **8**, 1227–1237.
- Koshida, S., Shinya, M., Nikaido, M., Ueno, N., Schulte-Merker, S., Kuroiwa, A., Takeda, H. (2002). Inhibition of BMP activity by the FGF signal promotes posterior neural development in zebrafish. *Dev. Biol.* **1**, 9–20.
- Köster, R. W., Fraser, S. E. (2001). Direct imaging of in vivo neuronal migration in the developing cerebellum. *Current Biology*. **23**, 1858–1863.
- Kudoh, T., Wilson, S. W., Dawid, I. B. (2002). Distinct roles for Fgf, Wnt and retinoic acid in posteriorizing the neural ectoderm. *Development*. **18**, 4335–4346.
- Kuhlenbeck, H. (1973). *The Central Nervous System of Vertebrates, Vol. 3/II: Overall Morphologic Pattern*, Basel: S. Karger.
- Labun, K., Montague, T. G., Gagnon, J. A., Thyme, S. B., Valen, E. (2016). CHOPCHOP v2. *Nucleic Acids Research*. **W1**, W272–6.
- Labun, K., Montague, T. G., Krause, M., Torres Cleuren, Y. N., Tjeldnes, H., Valen, E. (2019). CHOPCHOP v3. *Nucleic Acids Research*. **W1**, W171–W174.
- Landolt, E. (1871). Beitrag zur Anatomie der Retina vom Frosch, Salamander und Triton. *Archiv f. mikrosk. Anatomie*. **1**, 81–100.
- Lau, B., Breaud, S., Huang, Y., Lin, E., Guo, S. (2006). Dissociation of food and opiate preference by a genetic mutation in zebrafish. *Genes Brain Behav.* **7**, 497–505.
- Lee, J. E., Wu, S.-F., Goering, L. M., Dorsky, R. I. (2006). Canonical Wnt signaling through Lef1 is required for hypothalamic neurogenesis. *Development*. **22**, 4451–4461.
- Léger, S., Brand, M. (2002). Fgf8 and Fgf3 are required for zebrafish ear placode induction, maintenance and inner ear patterning. *Mechanisms of Development*. **1**, 91–108.
- Lekven, A. C., Thorpe, C. J., Waxman, J. S., Moon, R. T. (2001). Zebrafish *wnt8* Encodes two Wnt8 proteins on a bicistronic transcript and is required for mesoderm and neurectoderm patterning. *Dev Cell*. **1**, 103–114.
- Levkowitz, G., Zeller, J., Sirotkin, H. I., French, D., Schilbach, S., Hashimoto, H., Hibi, M., Talbot, W. S., Rosenthal, A. (2003). Zinc finger protein too few controls the development of monoaminergic neurons. *Nat. Neurosci.* **1**, 28–33.
- Lewis, K. E., Eisen, J. S. (2003). From cells to circuits. *Prog Neurobiol.* **6**, 419–449.
- Li, B., Dewey, C. N. (2011). RSEM. *BMC Bioinformatics*. **1**, 323.
- Lillesaar, C. (2011). The serotonergic system in fish. *J. Chem. Neuroanat.* **4**, 294–308.
- Lillesaar, C., Gaspar, P. (2019). Serotonergic Neurons in Vertebrate and Invertebrate Model Organisms (Rodents, Zebrafish, *Drosophila melanogaster*, *Aplysia californica*, *Caenorhabditis elegans*). In *Serotonin* (Ed.: Pilowsky, P. M.), pp. 49–80. London: Elsevier Academic Press.
-

- Lillesaar, C., Stigloher, C., Tannhäuser, B., Wullmann, M. F., Bally-Cuif, L. (2009). Axonal projections originating from raphe serotonergic neurons in the developing and adult zebrafish, *Danio rerio*, using transgenics to visualize raphe-specific *pet1* expression. *J. Comp. Neurol.* **2**, 158–182.
- Lillesaar, C., Tannhäuser, B., Stigloher, C., Kremmer, E., Bally-Cuif, L. (2007). The serotonergic phenotype is acquired by converging genetic mechanisms within the zebrafish central nervous system. *Dev. Dyn.* **4**, 1072–1084.
- Liu, F., Pogoda, H.-M., Pearson, C. A., Ohyama, K., Löhr, H., Hammerschmidt, M., Placzek, M. (2013). Direct and indirect roles of Fgf3 and Fgf10 in innervation and vascularisation of the vertebrate hypothalamic neurohypophysis. *Development*. **5**, 1111–1122.
- Livesey, F. J., Cepko, C. L. (2001). Vertebrate neural cell-fate determination. *Nature Reviews Neuroscience*. **2**, 109.
- Löhr, H., Ryu, S., Driever, W. (2009). Zebrafish diencephalic A11-related dopaminergic neurons share a conserved transcriptional network with neuroendocrine cell lineages. *Development*. **6**, 1007–1017.
- Love, M. I., Huber, W., Anders, S. (2014). Moderated estimation of fold change and dispersion for RNA-seq data with DESeq2. *Genome Biol.* **12**, 550.
- Lowery, L. A., Sive, H. (2004). Strategies of vertebrate neurulation and a re-evaluation of teleost neural tube formation. *Mechanisms of Development*. **10**, 1189–1197.
- Luo, G. R., Chen, Y., Li, X. P., Liu, T. X., Le, W. D. (2008). Nr4a2 is essential for the differentiation of dopaminergic neurons during zebrafish embryogenesis. *Mol Cell Neurosci.* **2**, 202–210.
- Lupo, G., Harris, W. A., Lewis, K. E. (2006). Mechanisms of ventral patterning in the vertebrate nervous system. *Nature Reviews Neuroscience*. **2**, 103–114.
- Ma, Y., Juntti, S. A., Hu, C. K., Huguenard, J. R., Fernald, R. D. (2015). Electrical synapses connect a network of gonadotropin releasing hormone neurons in a cichlid fish. *Proc. Natl. Acad. Sci. U.S.A.* **12**, 3805–3810.
- Manger, P. R., Fahringer, H. M., Pettigrew, J. D., Siegel, J. M. (2002). The distribution and morphological characteristics of serotonergic cells in the brain of monotremes. *Brain Behav Evol.* **5**, 315–332.
- Maroon, H., Walshe, J., Mahmood, R., Kiefer, P., Dickson, C., Mason, I. (2002). Fgf3 and Fgf8 are required together for formation of the otic placode and vesicle. *Development*. **9**, 2099–2108.
- Mason, I. (2007). Initiation to end point: the multiple roles of fibroblast growth factors in neural development. *Nat. Rev. Neurosci.* **8**, 583–596.
- Mathieu, J., Barth, A., Rosa, F. M., Wilson, S. W., Peyri  ras, N. (2002). Distinct and cooperative roles for Nodal and Hedgehog signals during hypothalamic development. *Development*. **13**, 3055–3065.
- Maximino, C., Brito, T. M. de, da Silva Batista, A. W., Herculano, A. M., Morato, S., Gouveia, A. (2010). Measuring anxiety in zebrafish. *Behavioural Brain Research*. **2**, 157–171.
- Mayeri, E., Rothman, B. S., Brownell, P. H., Branton, W. D., Padgett, L. (1985). Nonsynaptic characteristics of neurotransmission mediated by egg-laying hormone in the abdominal ganglion of *Aplysia*. *J Neurosci.* **8**, 2060–2077.
- McLean, D. L., Fetcho, J. R. (2004). Ontogeny and innervation patterns of dopaminergic, noradrenergic, and serotonergic neurons in larval zebrafish. *J. Comp. Neurol.* **1**, 38–56.
- McPherson, A. D., Barrios, J. P., Luks-Morgan, S. J., Manfredi, J. P., Bonkowsky, J. L., Douglass, A. D., Dorsky, R. I. (2016). Motor Behavior Mediated by Continuously Generated Dopaminergic Neurons in the Zebrafish Hypothalamus Recovers after Cell Ablation. *Curr Biol.* **2**, 263–269.
- Meyer, A., Schartl, M. (1999). Gene and genome duplications in vertebrates: the one-to-four (-to-eight in fish) rule and the evolution of novel gene functions. *Current Opinion in Cell Biology*. **6**, 699–704.
- Montague, T. G., Cruz, J. M., Gagnon, J. A., Church, G. M., Valen, E. (2014). CHOPCHOP. *Nucleic Acids Research. Web Server issue*, W401–7.
- Montgomery, J. E., Wahlstrom-Helgren, S., Wiggin, T. D., Corwin, B. M., Lillesaar, C., Masino, M. A. (2018). Intrapinal serotonergic signaling suppresses locomotor activity in larval zebrafish. *Dev Neurobiol.*
- Montgomery, J. E., Wiggin, T. D., Rivera-Perez, L. M., Lillesaar, C., Masino, M. A. (2016). Intrapinal serotonergic neurons consist of two, temporally distinct populations in developing zebrafish. *Dev Neurobiol.* **6**, 673–687.

- 
- Moret, F., Guiland, J.-C., Coudouel, S., Rochette, L., Vernier, P. (2004). Distribution of tyrosine hydroxylase, dopamine, and serotonin in the central nervous system of amphioxus (*Branchiostoma lanceolatum*). *J. Comp. Neurol.* **1**, 135–150.
- Moroz, L. L., Kohn, A. B. (2016). Independent origins of neurons and synapses. *Philos. Trans. R. Soc. Lond., B, Biol. Sci.* **1685**, 20150041.
- Mueller, T., Wullimann, M. (2015). *Atlas of Early Zebrafish Brain Development: A Tool for Molecular Neurogenetics*: Elsevier Science.
- Müller, F., Albert, S., Blader, P., Fischer, N., Hallonet, M., Strähle, U. (2000). Direct action of the nodal-related signal cyclops in induction of sonic hedgehog in the ventral midline of the CNS. *Development*. **18**, 3889–3897.
- Münchberg, S. R., Ober, E. A., Steinbeisser, H. (1999). Expression of the Ets transcription factors *erm* and *pea3* in early zebrafish development. *Mechanisms of Development*. **2**, 233–236.
- Muñoz-Sanjuán, I., Brivanlou, A. H. (2002). Neural induction, the default model and embryonic stem cells. *Nat. Rev. Neurosci.* **4**, 271–280.
- Muthu, V., Eachus, H., Ellis, P., Brown, S., Placzek, M. (2016). Rx3 and Shh direct anisotropic growth and specification in the zebrafish tuberal/anterior hypothalamus. *Development*. **14**, 2651–2663.
- Nagy, J. I., Dudek, F. E., Rash, J. E. (2004). Update on connexins and gap junctions in neurons and glia in the mammalian nervous system. *Brain Res Brain Res Rev.* **1–3**, 191–215.
- Nakamura, K., Sugawara, Y., Sawabe, K., Ohashi, A., Tsurui, H., Xiu, Y., Ohtsuji, M., Lin, Q. S., Nishimura, H., Hasegawa, H. et al. (2006). Late developmental stage-specific role of tryptophan hydroxylase 1 in brain serotonin levels. *J. Neurosci.* **2**, 530–534.
- Nichols, D. E., Nichols, C. D. (2008). Serotonin receptors. *Chem Rev.* **5**, 1614–1641.
- Nieuwkoop, P. D. (1952). Activation and organization of the central nervous system in amphibians. Part III. Synthesis of a new working hypothesis. *J. Exp. Zool.* **1**, 83–108.
- Norton, W., Bally-Cuif, L. (2010). Adult zebrafish as a model organism for behavioural genetics. *BMC Neuroscience*. **1**, 90.
- Norton, W., Folchert, A., Bally-Cuif, L. (2008). Comparative analysis of serotonin receptor (HTR1A/HTR1B families) and transporter (*slc6a4a/b*) gene expression in the zebrafish brain. *J. Comp. Neurol.* **4**, 521–542.
- Norton, W. H., Mangoli, M., Lele, Z., Pogoda, H.-M., Diamond, B., Mercurio, S., Russell, C., Teraoka, H., Stickney, H. L., Rauch, G.-J. et al. (2005). Monorail/Foxa2 regulates floorplate differentiation and specification of oligodendrocytes, serotonergic raphé neurones and cranial motoneurons. *Development*. **4**, 645–658.
- Nowak, M., Machate, A., Yu, S. R., Gupta, M., Brand, M. (2011). Interpretation of the FGF8 morphogen gradient is regulated by endocytic trafficking. *Nat Cell Biol.* **2**, 153–158.
- Ornitz, D. M., Itoh, N. (2015). The Fibroblast Growth Factor signaling pathway. *Wiley Interdiscip Rev Dev Biol.* **3**, 215–266.
- Orr, H. (1887). Contribution to the embryology of the lizard; With especial reference to the central nervous system and some organs of the head; together with observations on the origin of the vertebrates. *J. Morphol.* **2**, 311–372.
- Orts-Del'Immagine, A., Wyart, C. (2017). Cerebrospinal-fluid-contacting neurons. *Curr Biol.* **22**, R1198–R1200.
- Oulion, S., Bertrand, S., Escriva, H. (2012). Evolution of the FGF Gene Family. *Int J Evol Biol*, 298147.
- Panula, P., Chen, Y.-C., Priyadarshini, M., Kudo, H., Semenova, S., Sundvik, M., Sallinen, V. (2010). The comparative neuroanatomy and neurochemistry of zebrafish CNS systems of relevance to human neuropsychiatric diseases. *Neurobiol. Dis.* **1**, 46–57.
- Patel, C. K., Rodriguez, L. C., Kuwada, J. Y. (1994). Axonal outgrowth within the abnormal scaffold of brain tracts in a zebrafish mutant. *J Neurobiol.* **4**, 345–360.
- Pattyn, A., Simplicio, N., van Doorninck, J. H., Goridis, C., Guillemot, F., Brunet, J.-F. (2004). Ascl1/Mash1 is required for the development of central serotonergic neurons. *Nat. Neurosci.*, 589 EP -.
- Pattyn, A., Vallstedt, A., Dias, J. M., Sander, M., Ericson, J. (2003). Complementary roles for Nkx6 and Nkx2 class proteins in the establishment of motoneuron identity in the hindbrain. *Development*. **17**, 4149–4159.
-

- 
- Peitsaro, N., Kaslin, J., Anichtchik, O. V., Panula, P. (2003). Modulation of the histaminergic system and behaviour by alpha-fluoromethylhistidine in zebrafish. *J. Neurochem.* **2**, 432–441.
- Pelletier, I., Bally-Cuif, L., Ziegler, I. (2001). Cloning and developmental expression of zebrafish GTP cyclohydrolase I. *Mechanisms of Development.* **1**, 99–103.
- Pierre, J., Repérant, J., Ward, R., Vesselkin, N. P., Rio, J. P., Miceli, D., Kratskin, I. (1992). The serotonergic system of the brain of the lamprey, *Lampetra fluviatilis*: An evolutionary perspective. *J. Chem. Neuroanat.* **3**, 195–219.
- Plotnikov, A. N., Eliseenkova, A. V., Ibrahim, O. A., Shriver, Z., Sasisekharan, R., Lemmon, M. A., Mohammadi, M. (2001). Crystal structure of fibroblast growth factor 9 reveals regions implicated in dimerization and autoinhibition. *J Biol Chem.* **6**, 4322–4329.
- Pownall, M. E., Tucker, A. S., Slack, J. M., Isaacs, H. V. (1996). *eFGF*, *Xcad3* and Hox genes form a molecular pathway that establishes the anteroposterior axis in *Xenopus*. *Development.* **12**, 3881.
- Puelles, L. (2019). Survey of midbrain, diencephalon, and hypothalamus neuroanatomic terms whose prosomeric definition conflicts with columnar tradition. *Front Neuroanat.* **20**.
- Puelles, L., Rubenstein, J. L. R. (2003). Forebrain gene expression domains and the evolving prosomeric model. *Trends Neurosci.* **9**, 469–476.
- Puelles, L., Rubenstein, J. L. R. (2015). A new scenario of hypothalamic organization: rationale of new hypotheses introduced in the updated prosomeric model. *Front Neuroanat.*
- Puelles, L., Rubenstein, J. L.R. (1993). Expression patterns of homeobox and other putative regulatory genes in the embryonic mouse forebrain suggest a neuromeric organization. *Trends Neurosci.* **11**, 472–479.
- Raible, F., Brand, M. (2001). Tight transcriptional control of the ETS domain factors *Erm* and *Pea3* by Fgf signaling during early zebrafish development. *Mechanisms of Development.* **1-2**, 105–117.
- Ramón y Cajal, S. (1909). *Histologie du système nerveux de l'homme & des vertébrés*, Paris: Maloine.
- Rapport, M. M., Green, A. A., Page, I. H. (1948). Serum vasoconstrictor (Serotonin). *J. Biol. Chem.* **3**, 1243–1251.
- Reifers, F., Bohli, H., Walsh, E. C., Crossley, P. H., Stainier, D. Y., Brand, M. (1998). Fgf8 is mutated in zebrafish *acerebellar (ace)* mutants and is required for maintenance of midbrain-hindbrain boundary development and somitogenesis. *Development.* **13**, 2381–2395.
- Reuter, I. (2015). The role of Fgf3 during generation of hypothalamic serotonergic neurons - studies of the zebrafish *lia* mutant. Master thesis, University of Würzburg, Würzburg.
- Reuter, I., Jäckels, J., Kneitz, S., Kuper, J., Lesch, K.-P., Lillesaar, C. (2019). Fgf3 is crucial for the generation of monoaminergic cerebrospinal fluid contacting cells in zebrafish. *Biol Open.*
- Rink, E., Guo, S. (2004). The *too few* mutant selectively affects subgroups of monoaminergic neurons in the zebrafish forebrain. *Neuroscience.* **1**, 147–154.
- Rink, E., Wullmann, M. F. (2001). The teleostean (zebrafish) dopaminergic system ascending to the subpallium (striatum) is located in the basal diencephalon (posterior tuberculum). *Brain Research.* **1-2**, 316–330.
- Rink, E., Wullmann, M. F. (2002). Development of the catecholaminergic system in the early zebrafish brain: an immunohistochemical study. *Developmental Brain Research.* **1**, 89–100.
- Roehl, H., Nüsslein-Volhard, C. (2001). Zebrafish *pea3* and *erm* are general targets of FGF8 signaling. *Current Biology.* **7**, 503–507.
- Rohr, K. B., Barth, K. A., Varga, Z. M., Wilson, S. W. (2001). The Nodal Pathway Acts Upstream of Hedgehog Signaling to Specify Ventral Telencephalic Identity. *Neuron.* **2**, 341–351.
- Rohr, K. B., Concha, M. L. (2000). Expression of *nk2.1a* during early development of the thyroid gland in zebrafish. *Mechanisms of Development.* **1-2**, 267–270.
- Ross, L. S., Parrett, T., Easter, S. S. (1992). Axonogenesis and morphogenesis in the embryonic zebrafish brain. *J Neurosci.* **2**, 467–482.
- Roussigné, M., Blader, P. (2006). Divergence in regulation of the PEA3 family of ETS transcription factors. *Gene Expr. Patterns.* **8**, 777–782.
-

- Russek-Blum, N., Gutnick, A., Nabel-Rosen, H., Blechman, J., Staudt, N., Dorsky, R. I., Houart, C., Levkowitz, G. (2008). Dopaminergic neuronal cluster size is determined during early forebrain patterning. *Development*. **20**, 3401–3413.
- Ryan, J. F., Pang, K., Schnitzler, C. E., Nguyen, A.-D., Moreland, R. T., Simmons, D. K., Koch, B. J., Francis, W. R., Havlak, P., Smith, S. A. et al. (2013). The genome of the ctenophore *Mnemiopsis leidyi* and its implications for cell type evolution. *Science*. **6164**, 1242592.
- Ryu, S., Mahler, J., Acampora, D., Holzschuh, J., Erhardt, S., Omodei, D., Simeone, A., Driever, W. (2007). Orthopedia homeodomain protein is essential for diencephalic dopaminergic neuron development. *Curr Biol*. **10**, 873–880.
- Sako, H., Kojima, T., Okado, N. (1986). Immunohistochemical study on the development of serotonergic neurons in the chick. *J. Comp. Neurol.* **1**, 61–78.
- Sallinen, V., Sundvik, M., Reenilä, I., Peitsaro, N., Khrustalyov, D., Anichtchik, O., Toleikyte, G., Kaslin, J., Panula, P. (2009a). Hyperserotonergic phenotype after monoamine oxidase inhibition in larval zebrafish. *J. Neurochem.* **2**, 403–415.
- Sallinen, V., Torkko, V., Sundvik, M., Reenilä, I., Khrustalyov, D., Kaslin, J., Panula, P. (2009b). MPTP and MPP+ target specific aminergic cell populations in larval zebrafish. *J. Neurochem.* **3**, 719–731.
- Schindelin, J., Arganda-Carreras, I., Frise, E., Kaynig, V., Longair, M., Pietzsch, T., Preibisch, S., Rueden, C., Saalfeld, S., Schmid, B. et al. (2012). Fiji: an open-source platform for biological-image analysis. *Nat. Methods*. **7**, 676–682.
- Schneider, H., Fritzky, L., Williams, J., Heumann, C., Yochum, M., Pattar, K., Noppert, G., Mock, V., Hawley, E. (2012). Cloning and expression of a zebrafish 5-HT(2C) receptor gene. *Gene*. **2**, 108–117.
- Shepherd, G. M. (2015). *Foundations of the Neuron Doctrine: 25th Anniversary Edition*: Oxford University Press.
- Sherrington, C. S. (1906). *The Integrative action of the nervous system*: Yale University Press.
- Shinya, M., Eschbach, C., Clark, M., Lehrach, H., Furutani-Seiki, M. (2000). Zebrafish Dkk1, induced by the pre-MBT Wnt signaling, is secreted from the prechordal plate and patterns the anterior neural plate. *Mechanisms of Development*. **1**, 3–17.
- Shontz, E. C., Souders, C. L., Schmidt, J. T., Martyniuk, C. J. (2018). Domperidone upregulates dopamine receptor expression and stimulates locomotor activity in larval zebrafish (*Danio rerio*). *Genes Brain Behav.* **4**, e12460.
- Smeets, W. J., González, A. (2000). Catecholamine systems in the brain of vertebrates. *Brain Res Brain Res Rev.* **2-3**, 308–379.
- Spemann, H., Mangold, H. (1924). Über Induktion von Embryonalanlagen durch Implantation artfremder Organisatoren. *Archiv f mikr Anat u Entwicklungsmechanik*. **3-4**, 599–638.
- Stern, C. D. (2005). Neural induction. *Development*. **9**, 2007–2021.
- Stigloher, C., Chapouton, P., Adolf, B., Bally-Cuif, L. (2008). Identification of neural progenitor pools by E(Spl) factors in the embryonic and adult brain. *Brain Research Bulletin*. **2-4**, 266–273.
- Storey, K. G., Goriely, A., Sargent, C. M., Brown, J. M., Burns, H. D., Abud, H. M., Heath, J. K. (1998). Early posterior neural tissue is induced by FGF in the chick embryo. *Development*. **3**, 473.
- Strähle, U., Lam, C. S., Ertzer, R., Rastegar, S. (2004). Vertebrate floor-plate specification. *Trends in Genetics*. **3**, 155–162.
- Streit, A., Stern, C. D. (1999). Establishment and maintenance of the border of the neural plate in the chick. *Mechanisms of Development*. **1-2**, 51–66.
- Teraoka, H., Russell, C., Regan, J., Chandrasekhar, A., Concha, M. L., Yokoyama, R., Higashi, K., Take-Uchi, M., Dong, W., Hiraga, T. et al. (2004). Hedgehog and Fgf signaling pathways regulate the development of *tphR*-expressing serotonergic raphe neurons in zebrafish embryos. *J Neurobiol.* **3**, 275–288.
- Tessmar-Raible, K., Raible, F., Christodoulou, F., Guy, K., Rembold, M., Hausen, H., Arendt, D. (2007). Conserved Sensory-Neurosecretory Cell Types in Annelid and Fish Forebrain. *Cell*. **7**, 1389–1400.
- Thisse, B., Thisse, C. (2005). Functions and regulations of fibroblast growth factor signaling during embryonic development. *Dev. Biol.* **2**, 390–402.
- Thisse, C., Thisse, B. (2008). High-resolution in situ hybridization to whole-mount zebrafish embryos. *Nat Protoc.* **1**, 59–69.

- Thöny, B., Auerbach, G., Blau, N. (2000). Tetrahydrobiopterin biosynthesis, regeneration and functions. *Biochem. J.* **1**, 1–16.
- Topp, S., Stigloher, C., Komisarczuk, A. Z., Adolf, B., Becker, T. S., Bally-Cuif, L. (2008). Fgf signaling in the zebrafish adult brain: association of Fgf activity with ventricular zones but not cell proliferation. *J. Comp. Neurol.* **4**, 422–439.
- Tropepe, V., Sive, H. L. (2003). Can zebrafish be used as a model to study the neurodevelopmental causes of autism? *Genes, Brain and Behavior.* **5**, 268–281.
- Tsai, P.-S., Brooks, L. R., Rochester, J. R., Kavanaugh, S. I., Chung, W. C. J. (2011). Fibroblast growth factor signaling in the developing neuroendocrine hypothalamus. *Front Neuroendocrinol.* **1**, 95–107.
- Tsang, M., Maegawa, S., Kiang, A., Habas, R., Weinberg, E., Dawid, I. B. (2004). A role for MKP3 in axial patterning of the zebrafish embryo. *Development.* **12**, 2769–2779.
- Ueda, S., Nojyo, Y., Sano, Y. (1984). Immunohistochemical demonstration of the serotonin neuron system in the central nervous system of the bullfrog, *Rana catesbeiana*. *Anatomy and Embryology.* **3**, 219–229.
- Ueda, S., Takeuchi, Y., Sano, Y. (1983). Immunohistochemical demonstration of serotonin neurons in the central nervous system of the turtle (*Clemmys japonica*). *Anatomy and Embryology.* **1**, 1–19.
- Ugrumov, M. V., Proshlyakova, E. V., Sapronova, A. (1989). Development of the hypothalamic 5-hydroxytryptamine system during ontogenesis in rats. *Neuroscience.* **1**, 127–131.
- Umbricco, D., Anttil, M., Descarries, L. (1990). Serotonin-immunoreactive neurons in the cnidarian *Renilla koellikeri*. *J. Comp. Neurol.* **2**, 167–178.
- Unger, J. L., Glasgow, E. (2003). Expression of isotocin-neurophysin mRNA in developing zebrafish. *Gene Expression Patterns.* **1**, 105–108.
- van Doorninck, J. H., van der Wees, J., Karis, A., Goedknecht, E., Engel, J. D., Coesmans, M., Rutteman, M., Grosveld, F., Zeeuw, C. I. de (1999). GATA-3 is involved in the development of serotonergic neurons in the caudal raphe nuclei. *J. Neurosci.* **12**, RC12.
- Varga, Z. M., Amores, A., Lewis, K. E., Yan, Y. L., Postlethwait, J. H., Eisen, J. S., Westerfield, M. (2001). Zebrafish smoothed functions in ventral neural tube specification and axon tract formation. *Development.* **18**, 3497–3509.
- Vernier, P. (2017). The brains of teleost fishes. In *Evolution of nervous systems* (Ed.: Kaas, J. H.), pp. 59–75. Kidlington, Oxford, United Kingdom: Academic Press is an imprint of Elsevier.
- Versteeg, R. I., Serlie, M. J., Kalsbeek, A., La Fleur, S. E. (2015). Serotonin, a possible intermediate between disturbed circadian rhythms and metabolic disease. *Neuroscience*, 155–167.
- vigh, B., Teichmann, I., Aros, B. (1969). Das Paraventricularorgan und das Liquorkontakt-Neuronensystem. *Verh Anat Ges*, 683–688.
- Vigh, B., Manzano e Silva, M. J., Frank, C. L., Vincze, C., Czirok, S. J., Szabó, A., Lukáts, A., Szél, A. (2004). The system of cerebrospinal fluid-contacting neurons. Its supposed role in the nonsynaptic signal transmission of the brain. *Histol Histopathol.* **2**, 607–628.
- Vigh, B., Vigh-Teichmann, I. (1998). Actual problems of the cerebrospinal fluid-contacting neurons. *Microsc. Res. Tech.* **1**, 57–83.
- Walshe, J., Mason, I. (2003). Unique and combinatorial functions of Fgf3 and Fgf8 during zebrafish forebrain development. *Development.* **18**, 4337–4349.
- Wang, X., Kopinke, D., Lin, J., McPherson, A. D., Duncan, R. N., Otsuna, H., Moro, E., Hoshijima, K., Grunwald, D. J., Argenton, F. et al. (2013). Wnt signaling regulates postembryonic hypothalamic progenitor differentiation. *Dev Cell.* **3**, 624–636.
- Wang, Y., Takai, R., Yoshioka, H., Shirabe, K. (2006). Characterization and expression of serotonin transporter genes in zebrafish. *Tohoku J Exp Med.* **3**, 267–274.
- Ware, M., Hamdi-Rozé, H., Dupé, V. (2014). Notch signaling and proneural genes work together to control the neural building blocks for the initial scaffold in the hypothalamus. *Front Neuroanat*, 140.
- Warga, R. M., Nüsslein-Volhard, C. (1999). Origin and development of the zebrafish endoderm. *Development.* **4**, 827–838.



- 
- Webb, S. E., Miller, A. L. (2006). Ca<sup>2+</sup> signaling and early embryonic patterning during the blastula and gastrula periods of zebrafish and *Xenopus* development. *Biochimica et Biophysica Acta (BBA) - Molecular Cell Research*. **11**, 1192–1208.
- Wen, L., Wei, W., Gu, W., Huang, P., Ren, X., Zhang, Z., Zhu, Z., Lin, S., Zhang, B. (2008). Visualization of monoaminergic neurons and neurotoxicity of MPTP in live transgenic zebrafish. *Dev. Biol.* **1**, 84–92.
- Wilson, S. I., Edlund, T. (2001). Neural induction. *Nat. Neurosci.*, 1161–1168.
- Wilson, S. I., Graziano, E., Harland, R., Jessell, T. M., Edlund, T. (2000). An early requirement for FGF signalling in the acquisition of neural cell fate in the chick embryo. *Curr Biol.* **8**, 421–429.
- Wilson, S. W., Houart, C. (2004). Early steps in the development of the forebrain. *Dev Cell.* **2**, 167–181.
- Woo, K., Fraser, S. E. (1995). Order and coherence in the fate map of the zebrafish nervous system. *Development*. **8**, 2595–2609.
- Wullmann, M. F. (2009). Secondary neurogenesis and telencephalic organization in zebrafish and mice. *Integr Zool.* **1**, 123–133.
- Wullmann, M. F., Puelles, L. (1999). Postembryonic neural proliferation in the zebrafish forebrain and its relationship to prosomeric domains. *Anatomy and Embryology*. **4**, 329–348.
- Wullmann, M. F., Rupp, B., Reichert, H. (1996). *Neuroanatomy of the Zebrafish Brain: A Topological Atlas*, Basel: Birkhäuser Basel.
- Xavier, A. L., Fontaine, R., Bloch, S., Affaticati, P., Jenett, A., Demarque, M., Vernier, P., Yamamoto, K. (2017). Comparative analysis of monoaminergic cerebrospinal fluid-contacting cells in *Osteichthyes* (bony vertebrates). *J. Comp. Neurol.* **9**, 2265–2283.
- Xie, Y., Dorsky, R. I. (2017). Development of the hypothalamus. *Development*. **9**, 1588–1599.
- Yamamoto, K., Bloch, S. (2017). Overview of brain evolution: Lobe-Finned Fish vs. Ray-Finned Fish. In *Evolution of the Brain, Cognition, and Emotion in Vertebrates* (Ed.: Watanabe, S.; Hofman, M. A.; Shimizu, T.), pp. 3–33. Tokyo: Springer Japan.
- Yamamoto, K., Fontaine, R., Pasqualini, C., Vernier, P. (2015). Classification of dopamine receptor genes in vertebrates: nine subtypes in osteichthyes. *Brain Behav Evol.* **3-4**, 164–175.
- Yamamoto, K., Ruuskanen, J. O., Wullmann, M. F., Vernier, P. (2010). Two tyrosine hydroxylase genes in vertebrates: New dopaminergic territories revealed in the zebrafish brain. *Mol Cell Neurosci.* **4**, 394–402.
- Yamamoto, K., Ruuskanen, J. O., Wullmann, M. F., Vernier, P. (2011). Differential expression of dopaminergic cell markers in the adult zebrafish forebrain. *J. Comp. Neurol.* **3**, 576–598.
- Yamamoto, K., Vernier, P. (2011). The evolution of dopamine systems in chordates. *Front Neuroanat*, 21.
-

## Appendix

### Abbreviations

5-HIAA	5-Hydroxyindoleacetic acid	hpf	Hours post fertilization
5-HT	5-Hydroxytryptamine	<i>htr</i>	<i>5-HT receptor</i>
5-HTP	5-hydroxytryptophan	Hyb	Hybridisation buffer
AB	Antibody	buffer	
AO	Acridine Orange	indel	Insertion/ deletion
<i>arnt2</i>	<i>aryl-hydrocarbon receptor nuclear translocator 2</i>	<i>insm1</i>	<i>insulinoma-associated 1a</i>
<i>ascl1</i>	<i>achaete-scute family bHLH transcription factor 1</i>	<i>irx1a</i>	<i>iroquois homeobox 1a</i>
<i>avp</i>	<i>arginine vasopressin</i>	ISH	<i>In situ</i> hybridisation
BMP	Bone morphogenic protein	L-DOPA	L-3,4-dihydroxyphenylalanine
BrdU	Bromodesoxyuridine	<i>lef1</i>	<i>lymphoid enhancer-binding factor 1</i>
BSA	Bovine serum albumin	LiCl	Lithium chloride
cAMP	Cyclic adenosine monophosphate	<i>lmx1b</i>	<i>LIM homeobox transcription factor 1, beta</i>
cCasp3	Cleaved Caspase 3	<i>mao</i>	<i>monoamine oxidase</i>
cDNA	Complementary DNA	Mapk	Mitogen-activated protein kinase
CNS	Central nervous system	MeOH	Methanol
<i>cort</i>	<i>cortistatin (somatostatin 3)</i>	MIPs	Maximum intensity projections
( <i>sst3</i> )		NaOAc	Sodium acetat
CSF	Cerebrospinal fluid	<i>neurod1</i>	<i>neuronal differentiation 1</i>
CSF-c	Cerebrospinal fluid-contacting	<i>nkx2.2</i>	<i>NK2 homeobox 2</i>
<i>cyp2</i>	<i>cytochrome P450, family 2</i>	<i>nkx2.4b</i>	<i>NK2 homeobox 4b</i>
DA	dopamine	( <i>nkx2.1a</i> )	
Ddc	Dopamine decarboxylase	<i>nkx6.1</i>	<i>NK6 homeobox 1</i>
<i>ddc</i>	<i>dopa decarboxylase</i>	<i>nr4a2</i>	<i>nuclear receptor subfamily 4, group A, member 2</i>
DIG	Digoxigenin	<i>nr5a1</i>	<i>nuclear receptor subfamily 5, group A, member 1</i>
DOPAC	3,4-Dihydroxyphenylacetic acid	NSS	Normal sheep serum
dpf	days post fertilization	nTPOC	Nucleus of the dorsolateral tract of the postoptic commissure
<i>drd</i>	<i>dopamine receptor D</i>	o/n	Overnight
<i>dusp1, 2, 5, 6</i>	<i>dual specificity phosphatase 1, 2, 5, 6</i>	<i>olig2</i>	<i>oligodendrocyte lineage transcription factor 2</i>
E3	Exon 3	<i>otp</i>	<i>orthopedia homeobox a</i>
E4	Exon 4	<i>otx2</i>	<i>orthodenticle homeobox 2</i>
EtOH	Ethanol	<i>oxt</i>	<i>oxytocin</i>
<i>fev (pet1)</i>	<i>FEV transcription factor, ETS family member</i>	PBS	Phosphate buffered saline
<i>fezf2 (fezl, tof)</i>	<i>FEZ family zinc finger 2</i>	PBT	Phosphate buffered saline with Tween 20
Fgf	Fibroblast growth factor	PCNA	Proliferating cell nuclear antigen
fluo	fluorescein	PFA	Paraformaldehyde
<i>foxa2</i>	<i>forkhead box A2</i>	phH3	Phospho Histone 3
Fwd	Forward	PK	Proteinase K
GABA	γ-Aminobutyric acid	Rev	Reverse
<i>gata2, 3</i>	<i>GATA binding protein 2, 3</i>	RT	Room temperature
<i>gch1</i>	<i>GTP cyclohydrolase 1</i>	RT-PCR	Reverse transcriptase – Polymerase chain reaction
gDNA	Genomic DNA	<i>rx(3)</i>	<i>retinal homeobox gene (3)</i>
gRNA	Guide RNA		
<i>hoxb1</i>	<i>homeobox B1</i>		

Shh	Sonic hedgehog	TE	TRIS EDTA buffer
<i>sim1</i>	<i>SIM bHLH transcription factor 1</i>	TGFβ	Transforming growth factor beta
<i>slc18a2</i>	<i>solute carrier family 18 member 2</i>	<i>th1, 2</i>	<i>tyrosine hydroxylase 1, 2</i>
( <i>vmat2</i> )	( <i>vesicular monoamine transporter 2</i> )	<i>tph1a, 1b, 2</i>	<i>tryptophan hydroxylase 1a, 1b, 2</i>
<i>slc6a3</i>	<i>solute carrier family 6 member 3</i>	TPOC	dorsolateral tract of the postoptic commissure
( <i>dat</i> )	( <i>dopamine transporter</i> )	UTP	Uridine-5'-triphosphate
<i>slc6a4a</i>	<i>solute carrier family 6 member 4a</i>	<i>vax</i>	<i>ventral anterior homeobox</i>
( <i>serta</i> )	( <i>serotonin transporter a</i> )	w/o	Without
<i>slc6a4b</i>	<i>solute carrier family 6 member 4b</i>	Wnt	Wingless-related integration site
( <i>sertb</i> )	( <i>serotonin transporter b</i> )		

## Recipes and protocols

### Solutions and buffers

#### 1 M NaCl – 500 ml final volume:

29.22 g NaCl  
Fill up to 500 ml ddH<sub>2</sub>O  
autoclave

#### 5 M NaCl – 500 ml final volume:

146.11 g NaCl  
Fill up to 500 ml ddH<sub>2</sub>O  
autoclave

#### 1 M KCl – 500 ml final volume:

37.28 g KCl  
Fill up to 500 ml ddH<sub>2</sub>O  
autoclave

#### 1 M MgSO<sub>4</sub> – 500 ml final volume:

Gram depend on amount of hydrates  
  
autoclave

#### 1 M Ca(NO<sub>3</sub>)<sub>2</sub> – 500 ml final volume:

118.08 g Ca(NO<sub>3</sub>)<sub>2</sub> · 4 H<sub>2</sub>O  
Fill up to 500 ml ddH<sub>2</sub>O  
autoclave

#### 1 M HEPES, pH 7.4 – 500 ml final volume:

119.16 g C<sub>8</sub>H<sub>18</sub>N<sub>2</sub>O<sub>4</sub>S (HEPES)  
Fill up to 500 ml ddH<sub>2</sub>O  
autoclave

#### Danieau's solution – 1 l final volume:

17.4 ml 1 M NaCl  
210 µl 1 M KCl  
120 µl 1 M MgSO<sub>4</sub>  
180 µl 1 M Ca(NO<sub>3</sub>)<sub>2</sub>  
1.5 ml 1 M HEPES, pH 7.4  
Fill up to 1 l ddH<sub>2</sub>O  
autoclave  
1 ml 0.1% Methylene blue

#### 10x (2 mM) PTU – 500 ml final volume:

304.44 mg PTU  
Fill up to 500 ml ddH<sub>2</sub>O  
Keep dark, wrap in aluminium foil  
Working solution: 1x PTU

#### 0.5 M EDTA, pH 8.0 – 500 ml final volume:

93.05 g EDTA · 2H<sub>2</sub>O  
~10 g NaOH tablets  
Fill up to 400 ml ddH<sub>2</sub>O  
Adjust pH to 8.0 NaOH  
EDTA will not go into solution until pH is ~8.0  
Fill up to 500 ml ddH<sub>2</sub>O

#### 20x SSC, pH 7.0 – 500 ml final volume:

87.65 g NaCl  
44.1 g Sodium citrate · 2 H<sub>2</sub>O  
Fill up to 450 ml ddH<sub>2</sub>O  
Adjust pH to 8.0 NaOH  
Fill up to 500 ml ddH<sub>2</sub>O  
autoclave

#### 20x PBS – 1 l final volume:

160 g NaCl  
4 g KCl  
28.8 g Na<sub>2</sub>HPO<sub>4</sub>  
4.8 g KH<sub>2</sub>PO<sub>4</sub>  
Fill up to 1 l ddH<sub>2</sub>O  
autoclave

#### 1x PBT – 1 l final volume:

50 ml 20x PBS  
Fill up to 1 l ddH<sub>2</sub>O  
autoclave  
5 ml 20% Tween 20

**4% PFA – 200 ml final volume:**

200 ml PBS  
Boil PBS in microwave  
8 g PFA  
Slowly add PFA, no more heat  
Shake vigorously until PFA is dissolved,  
store aliquots at -20°C

**20% Tween 20 – final volume 200 ml:**

40 ml Tween 20  
Fill up to 200 ml ddH<sub>2</sub>O

**1 M Tris, pH 7.4 – 100 ml final volume:**

12.11 g Tris base  
Fill up to 80 ml ddH<sub>2</sub>O  
Adjust pH to 7.4 37% HCl  
Fill up to 100 ml ddH<sub>2</sub>O  
autoclave

**TE buffer, pH 8.0 – 50 ml final volume:**

500 µl 1 M Tris, pH 7.4  
100 µl 0.5 M EDTA, pH 8.0  
Fill up to 40 ml ddH<sub>2</sub>O  
Adjust pH to 8.0 37% HCl  
Fill up to 50 ml ddH<sub>2</sub>O

**1 M Tris, pH 9.4 – 100 ml final volume:**

12.11 g Tris base  
Fill up to 80 ml ddH<sub>2</sub>O  
Adjust pH to 9.4 37% HCl  
Fill up to 100 ml ddH<sub>2</sub>O  
autoclave

**0.5 M citric acid, pH 6.0 – 100 ml final volume:**

Grams depend on amount of hydrates  
Adjust pH to 6.0 37% HCl  
Fill up to 100 ml ddH<sub>2</sub>O  
autoclave

**LB agar – 400 ml final volume:**

16 g LB medium  
400 ml ddH<sub>2</sub>O  
autoclave

**LB medium – 400 ml final volume:**

10 g LB medium  
400 ml ddH<sub>2</sub>O  
autoclave

**50 mg/ml ampicillin stock – 20 ml final volume:**

1 g ampicillin  
Fill up to 20 ml ddH<sub>2</sub>O  
Sterile filter  
Store 1 ml aliquots at -20°C

**10 mg/ml kanamycin stock:**

Store 1 ml aliquots at -20°C

**100 µg/ml Amp plates – 400 ml final volume:**

Boil 400 ml LB agar  
Let cool down to ~40°C  
Add 800 µl 50 mg/ml ampicillin  
Pour into petri dishes, let become solid, then store at 4°C

**50 µg/ml KAN plates – 400 ml final volume:**

Boil 400 ml LB agar  
Let cool down to ~40°C  
Add 2 ml 10 mg/ml kanamycin  
Pour into petri dishes, let become solid, then store at 4°C

**10x TBE buffer (stock) – 5 l final volume:**

520 g Tris base  
275 g Boric acid  
200 ml 0.5 M EDTA, pH 8.0  
Fill up to 5 l ddH<sub>2</sub>O  
Working solution: 1x TBE

**50x TAE buffer (stock) – 1 l final volume:**

242 g Tris base  
57.1 ml Glacial acetic acid  
100 ml 0.5 M EDTA, pH 8.0  
Fill up to 1 l ddH<sub>2</sub>O  
Working solution: 1x TAE

**6x gel loading dye (stock) – 10 ml final volume:**

25 ml Bromphenol blue

25 ml Xylene cyanol FF

4 g sucrose

Fill up to 10 ml ddH<sub>2</sub>O

Working solution: dilute 1:2 in TBE or TAE

**DNA ladder mix:**

1 volume (100 µl) DNA ladder

1 volume (100 µl) 6x gel loading dye

4 volumes (400 µl) ddH<sub>2</sub>O, RNase-free

---

## Genotyping by PCR

### Generating gDNA

- Only use embryos stored in 100% MeOH for at least 24 h
- Use PCR tubes and place one embryo in each tube
- Remove all remaining MeOH w/o losing embryo
- Dry embryos in tubes without lid in PCR machine with open lid:
  - 95°C pause
  - 95°C 5 min
  - 10°C pause
- Handle PCR tubes very carefully to avoid losing embryos
- Add 12.5 µl TE buffer with 200µg/ml PK to each tube
- Incubate embryos in tubes (lids on) in PCR machine with closed lid:
  - 55°C pause
  - 55°C 4 h
  - 95°C 10 min
  - 10°C pause
- Add 37.5 µl ddH<sub>2</sub>O, RNase-free to a final volume of 50 µl to each tube
- Store gDNA at -20°C

### Genotyping

- Work on ice
- Prepare two PCR reaction mixes for a single embryo:

#### Reaction mix 1:

2.5 µl	10x HiDi buffer
0.5 µl	dNTPs
0.5 µl	<u>wild type fwd primer</u>
0.5 µl	rev primer
0.25 µl	HiDi polymerase
18.75 µl	ddH <sub>2</sub> O, RNase-free

#### Reaction mix 2:

2.5 µl	10x HiDi buffer
0.5 µl	dNTPs
0.5 µl	<u>mutant fwd primer</u>
0.5 µl	rev primer
0.25 µl	HiDi polymerase
18.75 µl	ddH <sub>2</sub> O, RNase-free

#### PCR programme:

95°C pause  
 95°C 2 min  
 95°C 15 sec ↓  
 61°C 10 sec  
 72°C 30 sec x34 cycles  
 10°C pause

- Run gel: 1.5% agarose in TAE, 4 µl loading dye + 12.5 µl PCR product, 120V, 35 min

## Injections

- Prepare needles (Harvard Apparatus Capillaries 1.0 OD x 0.58 ID x 100 L mm) and an injection plate with 1.2% agarose in blue Danieau's solution
- Prepare 4-5  $\mu$ l injection solution by diluting the morpholino stock with water to the desired injection concentration
- Add 3  $\mu$ l injection solution into the injection needle
- Inject embryo into the cell

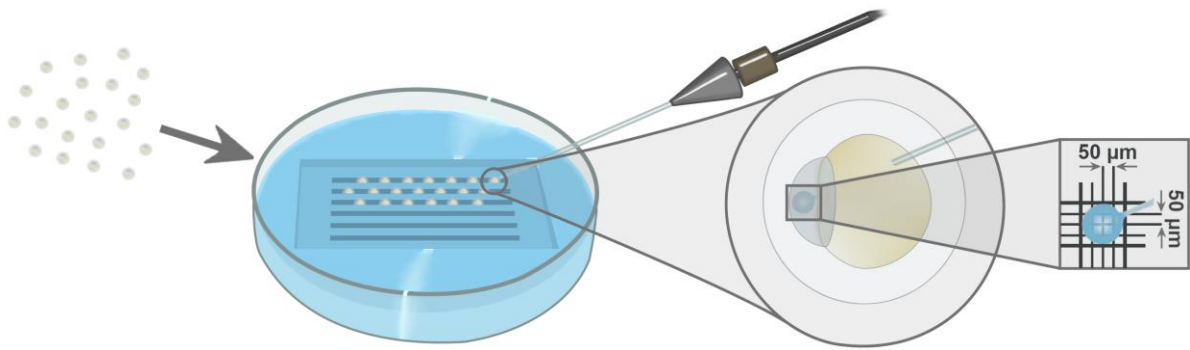


**Fig. 30: Scheme of microinjection setup.** Fertilised eggs (left) were aligned in an agarose mould (centre) and injected into the cell at the one-cell stage (right). Injected droplet size was measured using a hemocytometer (far right).



## Morpholino validation

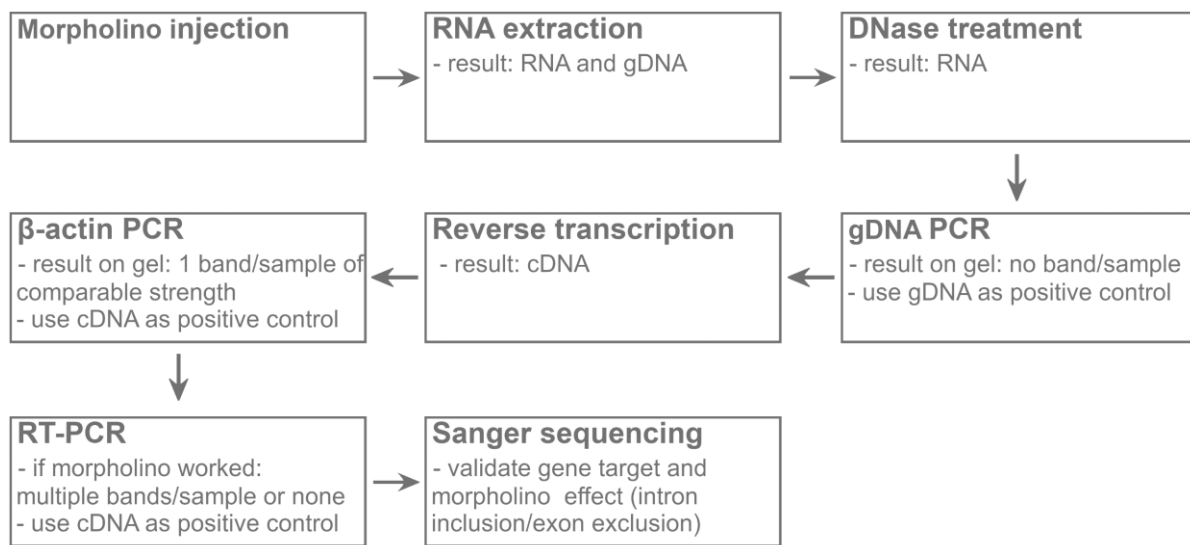


Fig. 31: Flow chart for morpholino validation.

## RNA extraction

- Pool 5 embryos per condition and stage for extraction in one tube, remove Danieau's solution
- Add 500 µl TRIZOL and incubate embryos for 5 min (samples can be stored at -20°C for a few days, if possible continue directly with homogenisation)
- Homogenise embryos with syringe (BD discardit II 2 ml) and needle (Neoinject 23G 1¼ "0.6 x 30 mm)
- Add 100 µl chloroform (100 µl chloroform/ 500 µl Trizol) and shake vigorously for 15 sec., then incubate for 3 min at RT
- Centrifuge at 12000 g for 15 min at 4°C
- Transfer upper phase to a new tube and add 500 µl 100% isopropanol, shake vigorously and incubate for 10 min at RT
- Remove supernatant and wash pellet with 500 µl 75% EtOH (in H<sub>2</sub>O) to remove proteins
- Centrifuge at 12000 g for 5 min at 4°C
- Remove supernatant and wash pellet for second time with 500 µl 75% EtOH (in H<sub>2</sub>O)
- Centrifuge at 12000 g for 5 min at 4°C

- Remove supernatant as much as possible, let pellet air dry and dissolve in 20 µl ddH<sub>2</sub>O (if RNA yield is high dilute to 50 µl (add 30 µl)). If difficult to dissolve incubate for 10 min at 57°C.
- From now on keep RNA on ice
- (- Run gel to verify RNA quality, 1% agarose in TAE, 120V, 25 min)
- Use 1 µl for NanoDrop measurement:
  - If 230 peak is too high, reprecipitate sample:
    - Add 1 / 10 of the total volume of 4 M LiCl (2 µl → 20 µl total volume)
    - Add 3x the total volume of 100% EtOH (60 µl → 20 µl total volume)
    - Mix and keep at -20°C o/n
    - Centrifuge at 12000 g for 15 min at 4°C
    - Remove supernatant, let pellet air dry and dissolve in 20 µl ddH<sub>2</sub>O
- Store RNA at -80°C

#### **DNase treatment –DNase I recombinant, RNase-free (10 U/µl) (Roche)**

- Work on ice
 

Reaction mix:	
XX µl	1-2 µg RNA
1 µl	10x incubation buffer
0.5 µl	DNase I (10 U)
0.25 µl	RiboLock
Fill up to 10 µl with ddH <sub>2</sub> O, RNase-free	
- Incubate for 20 min at 37°C
- Add 1.6 µl 50 mM EDTA to stop DNase reaction
- Incubate for 10 min at 75°C

#### **gDNA PCR – GoTaq DNA polymerase (Promega)**

- Work on ice
 

Reaction mix:		PCR programme:		
5 µl	10x green buffer	95°C	pause	
2 µl	MgCl <sub>2</sub> (25 mM)	95°C	2 min	
0.5 µl	dNTPs (10 mM)	95°C	1 min	↓
0.5 µl	fwd primer (10 µM)	XX°C	30 sec	x34 cycles
0.5 µl	rev primer (10 µM)	72°C	1 min for 1kb	
0.25 µl	GoTaq polymerase	72°C	7 min	
15.25 µl	ddH <sub>2</sub> O, RNase-free	10°C	pause	
1 µl	DNase treated sample			
- Use gDNA as positive control
- Run gel: 1% agarose in TAE, 120 V, 50 min, 15 µl direct-to-gel PCR product
  - No bands should be visible in samples, only band visible in positive control

## Reverse transcription

- Work on ice
  - Add to 9 µl DNase treated RNA:
  - 1 µl Oligo dT (100 µM)
  - 1.5 µl ddH<sub>2</sub>O, RNase-free
- Incubate for 5 min at 65°C
  - Continue to add:
  - 4 µl 5x reaction buffer
  - 0.5 µl RNase inhibitor 40 U/µl (RiboLock)
  - 2 µl dNTPs (10 mM)
- Incubate for 2 min at 42°C
  - Continue to add:
  - 1 µl Reverse transcriptase
- Incubate for 50 min at 42°C followed by 10 min at 70°C
- cDNA can be stored at -20°C

## β-actin PCR

- Work on ice
- Run gel: 1.5% agarose in TAE, 120 V, 40 min, 15 µl direct-to-gel PCR product, 4.5 µl 100 bp ladder

## RT-PCR

- Work on ice
 

Reaction mix:		PCR programme:		
10 µl	10x green buffer	95°C	pause	
4 µl	MgCl <sub>2</sub> (25 mM)	95°C	2 min	
1 µl	dNTPs (10 mM)	95°C	1 min	↓
1 µl	fwd primer (10 µM)	XX°C	30 sec	x34 cycles
1 µl	rev primer (10 µM)	72°C	1 min for 1kb	
0.5 µl	GoTaq polymerase	72°C	7 min	
30.5 µl	ddH <sub>2</sub> O, RNase-free	10°C	pause	
2 µl	cDNA			
- Run gel: 1% agarose in TAE, 120 V, 50 min
  - divide 50 µl reaction mix equally in 4 gel pockets
    - Allows to directly excise, pool and gel extract bands of equal size
- Purify with GenElute Gel Extraction Kit (Sigma-Aldrich)
  - Elute in warm 40 µl ddH<sub>2</sub>O, RNase-free, incubate for 1 min then spin down
  - Elute again with spun down eluate
- Send excised and purified bands for Sanger sequencing (Eurofins, LGC genomics)
  - Blast sequences in ensembl against zebrafish genome

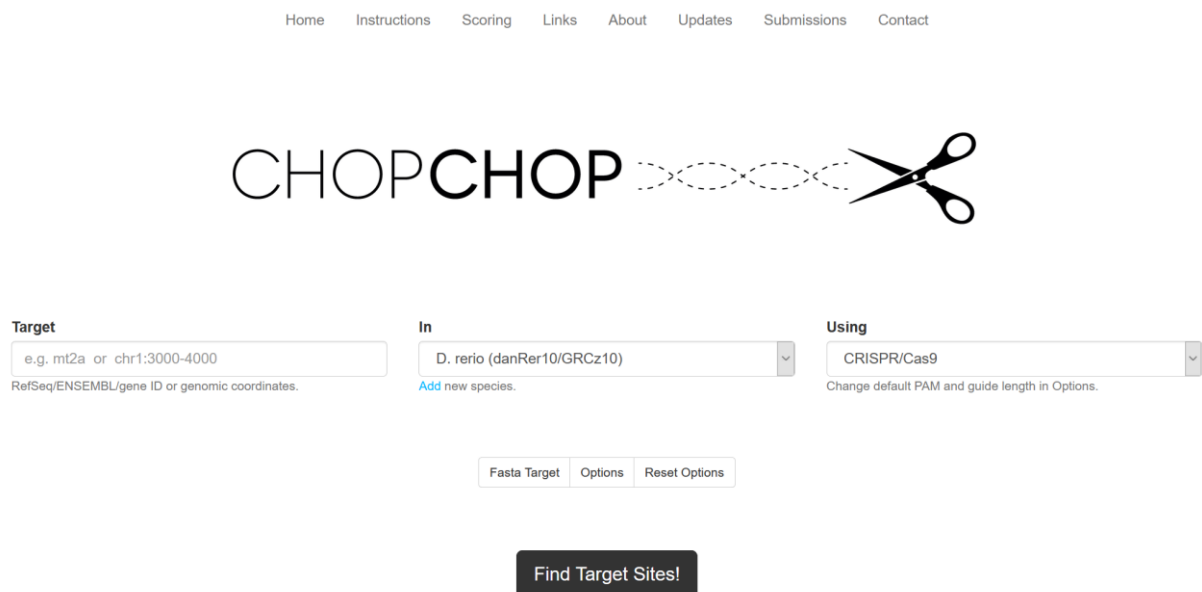
## CRISPR/Cas9 strategy

## CRISPR guideRNAs (gRNA)

**Target site and gRNA design**

Find potential target regions using Chop Chop (<http://chopchop.cbu.uib.no/>)

(2<sup>nd</sup> option: ZiFit <http://zifit.partners.org/ZiFiT/>) (find how-to-use guide under: Additional Info)



The screenshot shows the ChopChop web interface. At the top, there is a navigation bar with links: Home, Instructions, Scoring, Links, About, Updates, Submissions, and Contact. Below this is the 'CHOPCHOP' logo, which includes a stylized DNA double helix and a pair of scissors. The main form has three input fields: 'Target' (with a placeholder 'e.g. mt2a or chr1:3000-4000' and a note 'RefSeq/ENSEMBL/gene ID or genomic coordinates.'), 'In' (a dropdown menu showing 'D. rerio (danRer10/GRCz10)' with a link 'Add new species.'), and 'Using' (a dropdown menu showing 'CRISPR/Cas9' with a note 'Change default PAM and guide length in Options.'). Below these fields are three buttons: 'Fasta Target', 'Options', and 'Reset Options'. At the bottom center is a large black button labeled 'Find Target Sites!'.

Fig. 32: Screenshot of ChopChop web page. (Labun et al., 2016; Labun et al., 2019; Montague et al., 2014)

- Target: Type in gene or gene ID
- In: Choose organism (D.rerio (danRer10/GRCz10))
- Using: CRISPR/Cas9
- Open Options → Cas9 Tab → check boxes indicated in yellow, leave the rest as is

General
Cas9
Primers

sgRNA length without PAM:

**PAM-3':**

☒ NGG
☐ NAG
☐ NGA
☐ NRG (R = A or G)
☐ NNAGAAW (W = A or T)
☐ NNNNGMTT (M = A or C)
☐ NNGRRT (R = A or G)

☐ Custom PAM:

**Method for determining off-targets in the genome:**

☒ Off-targets with up to  mismatches in protospacer ([Hsu et al., 2013](#))
☐ Off-targets may have no more than  mismatches in the protospacer seed region ([Cong et al., 2013](#))

**Efficiency score:**

☐ Doench et al. 2014 - only for NGG PAM
☐ Doench et al. 2016 - only for NGG PAM
☐ Chari et al. 2015 - only NGG and NNAGAAW PAM's in hg19 and mm10
☒ Xu et al. 2015 - only for NGG PAM
☐ Moreno-Mateos et al. 2015 - only for NGG PAM
☐ G20

**5' requirements for sgRNA:**

☐ GN or NG
☒ GG
☐ No requirements

**Self-complementarity (Thyme et al.):**

☒ Check for self-complementarity
☒ I intend to replace the leading nucleotides with "GG"
☒ Check for complementarity versus backbone:
☒ Standard backbone
☐ Extended backbone
☐ Custom backbone:

Fig. 33: Screenshot of ChopChop web page. (Labun et al., 2016; Labun et al., 2019; Montague et al., 2014)

- Hit ,Find Target Sites!'

## Result page:

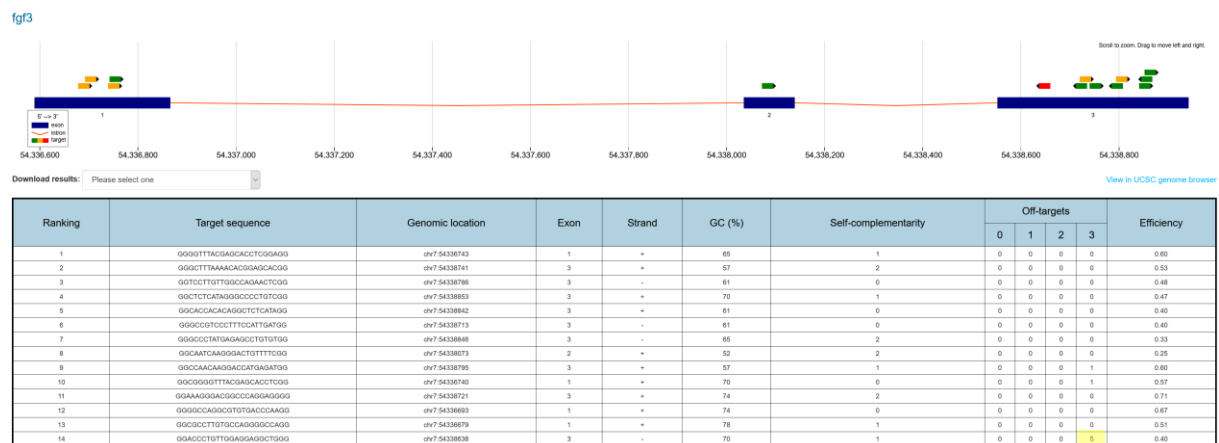


Fig. 34: Screenshot of ChopChop web page, *fgf3* gene example. (Labun et al., 2016; Labun et al., 2019; Montague et al., 2014)

- Map of gene with location of target sequences (Code: green = great target, Yellow = medium, Red=bad)
- Table: ranks targets according to efficiency
  - o Uses an algorithm for calculation, considering Off-targets (weight strongest), Self-complementarity and GC Content
- Off-Target column: Values underneath heading (0,1,2,3) categorise found off-targets in off-targets with 0 mismatched bases, 1 mism. base, 2 mism. Bases, 3 mism. Bases
  - o Yellow box E.g.: For target seq no.14, 5 off-targets were found each with 3 mismatches
- Choose a target by navigating to target site indicated on map or table and click on it

## Target site page:

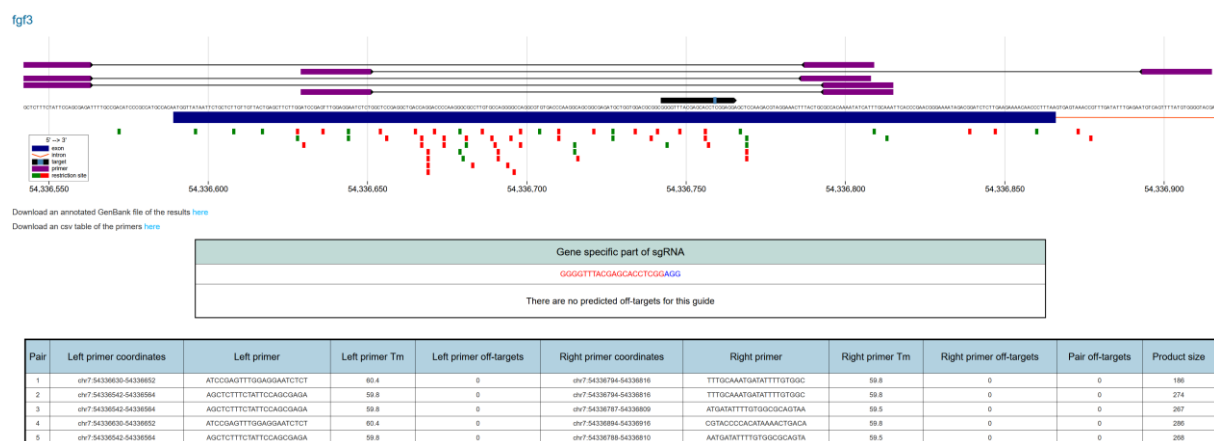


Fig. 35: Screenshot of ChopChop web page, *fgf3* gRNA target site example. (Labun et al., 2016; Labun et al., 2019; Montague et al., 2014)

- Map: black-blue= target site close-up
  - Purple = forward/reverse primer locations suggested for later sequencing  
DON'T confuse with target site oligos, these you must design yourself
- sgRNA target (red) with PAM sequence (blue) attached at 3' end (exclude PAM for oligo design!)
- Table with primer suggestions for sequencing
- Optional: ENSEMBL Blast of target sequence; include PAM seq for Blast

### ***gRNA oligo design (manually)***

- Oligo 1: Use target seq as template, Oligo 1= upper DNA strand (5'-3')
- Oligo 2: write complementary seq to target seq, Oligo 2= lower DNA strand (3'-5')
- Additional bases for correct ligation into cloning vector DR274 (blue, BsaI restriction sites)
  - Bases for Oligo 1: 5' TAGG 3', TAGG part of T7 promotor sequence (see DR274)
  - Bases for Oligo 2: 5' AAAC 3' CAAA part of gRNA scaffold sequence (see DR274)

Target seq (5'-3')	GGGGTTTACGAGCACCTCGG
Oligo 1 (5'-3')	TAGGGGTTTACGAGCACCTCGG
Oligo 2 (3'-5')	CCCCAAATGCTCGTGGAGCCAAA

- Order oligos

## gRNA – Oligo annealing. Cloning. Transcription.

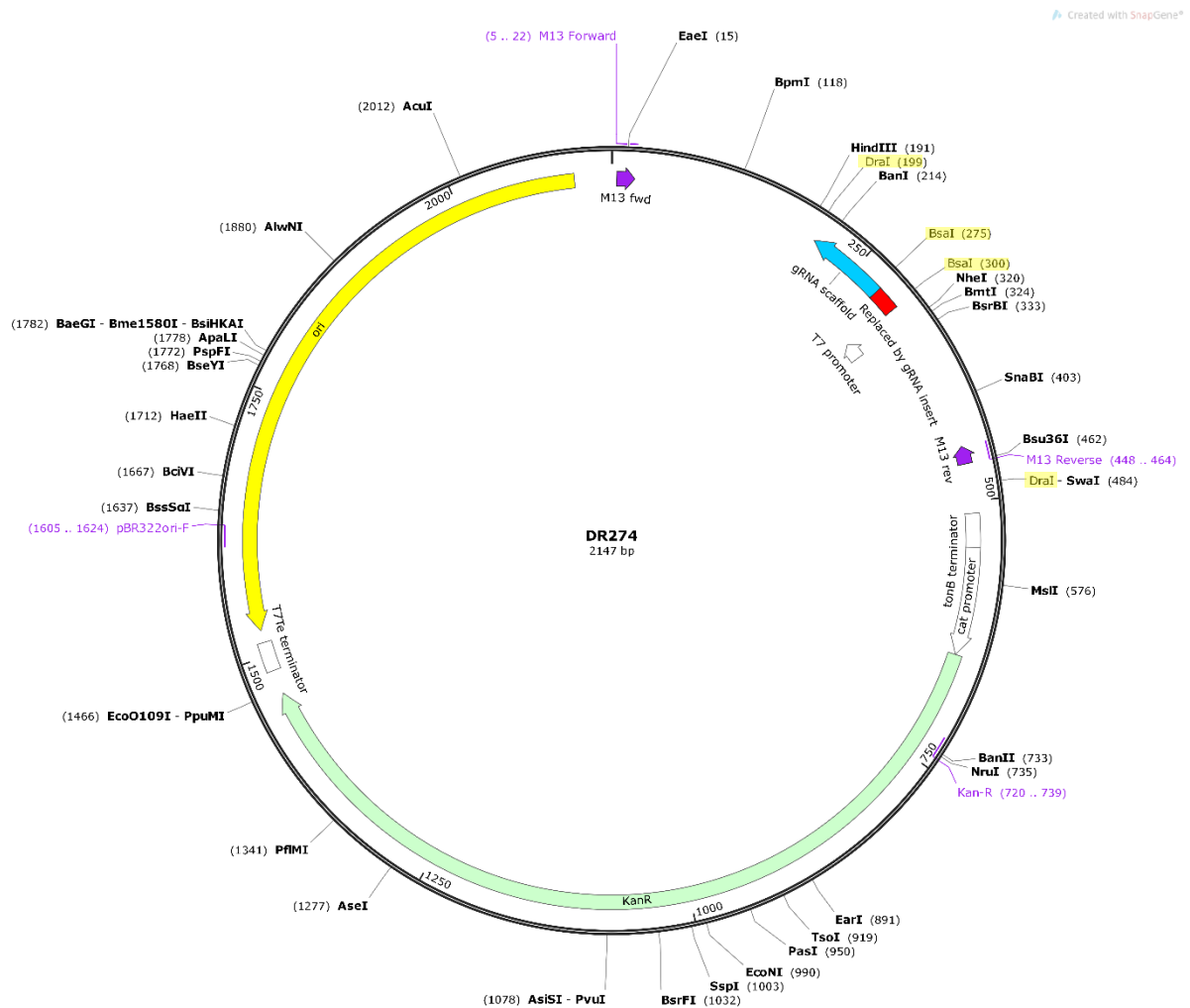


Fig. 36: Vector: pDR274 (<http://www.addgene.org/42250/>)

## Optional:

- Transformation, midi, glycerol stock of DR274 for storage



**DR274 linearisation**

Thermo:		NEB:	
1 µg	pDR274 plasmid	1 µg	pDR274 plasmid
5 µl	Buffer G (10x, green)	5 µl	NEB buffer 4
1 µl	Bsal (10 U/µl)	2 µl	Bsal (5U, NEB, high fidelity)
		0.5 µl	BSA (bovine serum albumin, NEB)
Fill up to 50 µl	dH <sub>2</sub> O	Fill up to 50 µl	dH <sub>2</sub> O

- Incubate for 2 h at 37°C
- Heat inactivate for 20 min at 65°C
- Check linearisation on gel: 0.8% agarose (in TAE), 2 µl lin. Vector, 1kb ladder, 120 V, 40 min
  - o Don't forget unlinearised vector as control
  - o Split remaining 48 µl of linearisation reaction evenly in 3 pockets; for better yields after gel extraction
- Cut band at 2100 bp and pool cut bands in case 3 pockets were used
- Purify with GenElute Gel Extraction kit
  - o Elute in 40 µl dH<sub>2</sub>O
    - Check on gel: 0.8% agarose (in TAE), 5 µl lin. Vector, 1kb ladder, 120 V, 40min
    - if unlinearised plasmid DNA was removed completely
    - Reason: later: unlinearised and ligated vector sizes cannot be distinguished,  
Only 25 bp difference

**Oligo annealing**

- Dilute ordered gRNA oligos in dH<sub>2</sub>O and incubate 30 min at 37°C
  - o Oligo stocks: 100 µM (in dH<sub>2</sub>O)  
10 µM (in dH<sub>2</sub>O) for annealing reaction
- 50 µl oligo annealing reaction for ligation into DR274 (in PCR tubes):

Invitrogen:		NEB:	
3 µl	Oligo 1 (10 µM)	3 µl	Oligo 1 (10 µM)
3 µl	Oligo 2 (10 µM)	3 µl	Oligo 2 (10 µM)
10 µl	T4 DNA ligase reaction buffer (5x)	4 µl	T4 DNA ligase reaction buffer (NEB)
34 µl	dH <sub>2</sub> O	39 µl	dH <sub>2</sub> O

- Write PCR programme that starts at 95°C and goes down in 5°C/ 2 min steps to 25°C

- PCR programme:

95°C Pause  
 95°C 2 min  
 90°C 2 min  
 85°C 2 min  
 ....  
 25°C 2 min  
 10°C pause

- Store at -20°C
- Dilute reaction 1:40 after annealing is completed:

Invitrogen  
 2 µl Annealed oligos (1.2 µM)  
 78 µl dH<sub>2</sub>O

For NEB ligation:  
 5 µl Annealed oligos (1.2 µM)  
 45 µl dH<sub>2</sub>O

- Final annealed oligo concentration: 30 nM (Invitrogen) / 120 nM (NEB)
- Use this dilution for ligation

### ***Oligo ligation into DR274. Transformation. DNA sequencing.***

- Prepare 4 ligation mixes (20 µl reaction volume each):

Invitrogen:					NEB				
Mix	A	B	C	Ctr	A	B	C	Ctr	
pDR274 (Linearised, gel purified)	1.5 µl	2.6 µl	4 µl	2.6 µl	0.5 µl	1 µl	1.5 µl	1 µl	
annealed Oligos (30nM)	1 µl	2 µl	3 µl	-	3.5 µl	3 µl	2.5 µl	-	
T4 DNA Ligase Puffer (NEB)	4 µl	4 µl	4 µl	4 µl	0.5 µl	0.5 µl	0.5 µl	0.5 µl	
T4 DNA Ligase	0.5 µl	0.5 µl	0.5 µl	0.5 µl	0.5 µl	0.5 µl	0.5 µl	0.5 µl	
dH <sub>2</sub> O	13 µl	10.9 µl	8.5 µl	7.1 µl	-	-	-	-	

- Incubate for 1h at 24°C (NEB: 2 hours at RT)

### **Transformation into competent bacteria Dh5α:**

Invitrogen: 20 µl Ligation mix  
 100 µl Competent bacteria

NEB: 5 µl Ligation mix  
 75 µl Competent bacteria

- Incubate 30 min on ice  
 90 sec at 42°C  
 2 min on ice
- Add 1 ml LB-Medium
- Incubate for 1.5 h at 37°C with shaking
- Centrifuge bacteria at max 2000 g for 5 min, discard 920 µl supernatant

- Resuspend pellet in remaining 200 µl
- Plate bacteria on Kanamycin plates (KAN):
  - distribute one mix to 2 plates with 180 µl and 20 µl
  - DR274 has only KAN resistance no ampicillin resistance

Colony Screen per PCR (because clones are almost always positive ones and discrimination between uncut vector and linearised plasmid is not possible)

-	Picked colony	95°C	Pause	
5 µl	PCR reaction buffer (5x)	95°C	5 min	
2 µl	MgCl <sub>2</sub> (50 mM)	95°C	1 min	
1 µl	dNTPs (10 mM)	XX°C	30 sec	
1 µl	M13 fwd primer	72°C	1 min	x34 cycles
1 µl	Oligo1 = rev primer	72°C	7 min	
0.25 µl	Go taq	10°C	pause	
14.75 µl	dH <sub>2</sub> O			

- Pick one colony with pipette tip, streak on KAN plate with grid then dip tip into PCR mix. As positive control pick one colony of control plate; incubate KAN plate with grid at 37°C
- Check on gel: 1.5% agarose (in TAE), 12 µl PCR product, 100 bp ladder, 120 V, 45 min
  - Fragment size of positive colonies: 298 bp
- Grow o/n culture of positive colonies (with gRNA insert) in LB medium
- Make midi preps
- but keep 800 µl of o/n culture for glycerol stocks. Sequence clones after midi
  - Use M13 fwd primer (M13-21 primer (Eurofins standard primer))
- Check sequencing result:
  - If positive: cloned oligo sequence right after T7 promotor sequence  
 5'- **TAATACGACTCACTATA** – **Oligo sequence** -3'
  - If negative: Oligo sequence is missing and instead blue sequence is found  
 5'- **TAATACGACTCACTATA** – **ggagagaccgagagagggtctca**-3'
- Don't forget glycerol stocks for DR274-gRNA vector when sequencing is positive

### ***Linearisation of ligated vector***

Thermo:

5 µg	pDR274-oligo plasmid
5 µl	Tango buffer (10x, yellow)
1 µl	DraI (10 U, Thermo)
Fill up to 50 µl	dH <sub>2</sub> O

NEB:

5 µg	DR274-oligo plasmid
5 µl	CutSmart buffer
1 µl	DraI (10 U, NEB)
Fill up to 50 µl	dH <sub>2</sub> O

- Incubate for 1.5 h at 37°C
- Heat inactivate for 20 min at 65°C
- Check linearisation on gel: 0.8% agarose (in TAE), 5 µl sample, 1kb ladder, 120 V, 40 min
  - Don't forget unlinearised vector as control
  - If linearisation worked:
    - Band at 285 bp contains T7 promotor site and gRNA target+scaffold site (DraI cuts plasmid twice)
  - Split remaining 45 µl of linearisation reaction evenly in three pockets, cut 285 bp bands and pool them for better yields after gel extraction
- Purify with GenElute Gel Extraction kit, elute in 40 µl dH<sub>2</sub>O
  - *This step is necessary to avoid transcription of any unlinearised plasmid DNA. Otherwise RNA transcribed from unlinearised plasmid will cloud the real yield of transcribed gRNA which is very short compared to RNA strand from unlinearised plasmid.*

### ***In vitro transcription into gRNA and purification***

150 ng	285 bp template DNA
5 µl	T7 transcription buffer (10x)
10 µl	NTPs (5x) (not dNTPs)
2.5 µl	DTT (Dithiothreitol) (0.1 M)
2.5 µl	T7 RNA polymerase
Fill up to 50 µl	dH <sub>2</sub> O

Recipes (by biochemistry Thomas):

5x NTPs:		For 100 µl:	
Component	Final conc	Stock c.	Vol (µl)
ATP	25 mM	100 mM	25 µl
CTP	25 mM	100 mM	25 µl
GTP	40 mM	100 mM	40 µl
UTP	10 mM	100 mM	10 µl

DTT = 'deprotecting' agent for thiolated DNA

- Incubate for 1h at 37°C
- Add 1 µl of DNaseI (RNase free, Roche) and incubate for 10 min at 37°C
- No heat inactivation if phenol/chloroform extraction used for purification; DNase will be inactivated/ removed by P/C extraction
- Check for white precipitate at bottom of tube, indicator for successful reaction. Precipitate is pyrophosphate which dissociated from NTPs in order to form RNA strand

10x T7 transcription buffer:		For 50 ml:	
component	Final conc	Stock c.	Vol (ml)
Tris-HCl pH 7.9	400 mM	1 M	12.8
Tris-base		1 M	7.2
spermidine	10 mM	0.5 M	1
MgCl <sub>2</sub> (6 H <sub>2</sub> O)	260 mM	salt	2.64 g
Triton X 100	0.1%		0.05
dH <sub>2</sub> O			To 50

---

**Purification - Phenol/ Chloroform extraction**

- *Make sure to use Phenol:Chloroform:Isoamylalcohol (in water → pH 4.5, Roth) for RNA extraction*
    - *Do not use Roti Phenol (Roth, TE buffered → pH 7.5) → only for DNA extraction!*
    - *Phenol pH importance for extraction:*
      - *low pH for RNA: DNA is enriched in protein interphase and organic phase, leads to less DNA contamination of aqueous phase for RNA extraction*
      - *High pH for DNA: partitioning of DNA into organic phase is suppressed. Leads to accumulation of both RNA and DNA in aqueous phase*
  - Add 1 volume (50 µl) of P:C:I solution to transcription reaction (50 µl), mix vigorously
  - Centrifuge for 5 min at max. speed
  - Transfer aqueous (upper) phase to new Eppi
  - Add 1 volume of chloroform (for RNA extraction), mix vigorously
  - Centrifuge for 5 min at max. speed
  - Transfer aqueous (upper) phase to new Eppi
  - Precipitate RNA by adding 1 Volume of 100% isopropanol, mix vigorously
  - Incubate mix at -20°C for 1h
  - Centrifuge for 15 min at max. speed at 4°C
  - Carefully remove supernatant
  - Wash pellet in 100% EtOH
  - Centrifuge for 10 min at max. speed at 4°C
  - Carefully remove supernatant
  - Dry pellet at 42°C, check regularly (don't incubate for longer than 10 min)
  - Resuspend pellet in 25 µl dH<sub>2</sub>O (RNase free)
    - If pellet doesn't dissolve, incubate for 30 sec at 42°C
  - Measure concentration at nanodrop
    - If concentration is high make working stock dilution of 250 ng/µl
  - Store stock solution at -80°C and working stock at -20°C
  - Check RNA on gel: 1% agarose (in TAE), 100 bp ladder, 120 V, 40 min
-

---

2 µl	working stock RNA
5 µl	dH <sub>2</sub> O (RNase free)
1 µl	6x DNA loading dye

- Expected RNA product size: ~103 bp

#### Optional: Option 1) Lithium Chloride (LiCl) precipitation

is a convenient and effective way to remove unincorporated nucleotides and most proteins. Lithium chloride precipitation, however, does not precipitate transfer RNA and may not efficiently precipitate RNAs smaller than 300 nucleotides. Also, the concentration of RNA should be at least 0.1 µg/µL to assure efficient precipitation. To precipitate from mMESSAGE mMACHINE® reactions that are thought to have relatively low yields of RNA, do not dilute the transcription reaction with water prior to adding the LiCl Precipitation Solution the first substep below.

- Stop the reaction and precipitate the RNA by adding 30 µL Nuclease-free Water and 30 µL LiCl Precipitation Solution
- mix thoroughly. Chill for ≥30 min at –20°C
- Centrifuge at 4°C for 15 min at maximum speed to pellet the RNA.
- Carefully remove the supernatant. Wash the pellet once with ~1 mL 70% ethanol, and recentrifuge to maximize removal of unincorporated nucleotides
- Carefully remove the 70% ethanol, and resuspend the RNA in a solution or buffer† appropriate for your application. Determine the RNA concentration and store frozen at –20°C or –80°C
- Measure concentration (1µl) and check on gel (2µl RNA mit 7µl ddH<sub>2</sub>O and 1µl RNA loading buffer (Ambion); incubate 10min at 80°C before loading on gel)

#### Option 2: RNeasy Kit (Qiagen)

---

## Cas9 mRNA synthesis

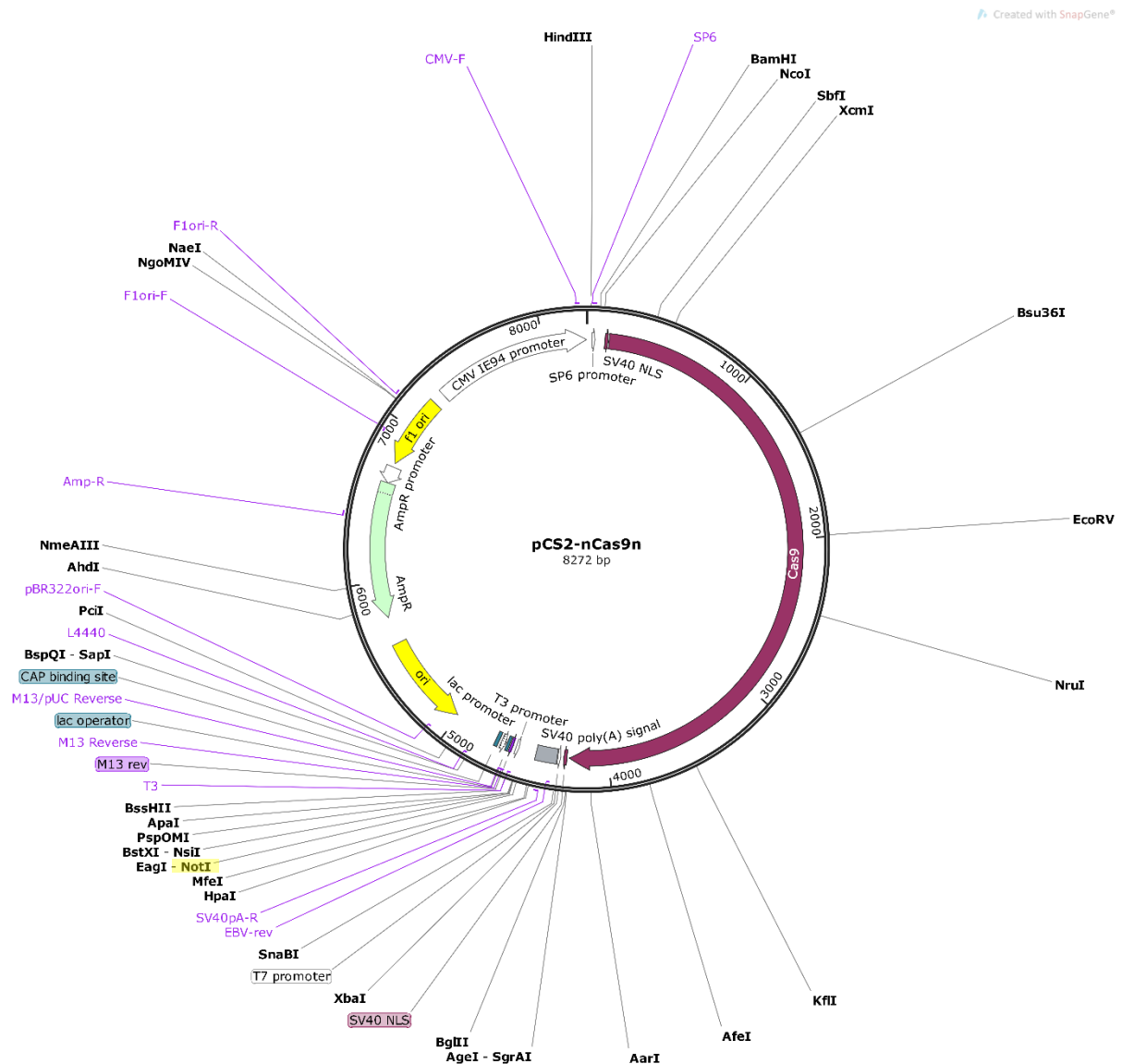


Fig. 37: Vektor pCS2-nCas9n by Wentz and Chen (<http://www.pnas.org/content/110/34/13904>); Addgene (<http://www.addgene.org/47929/>)

**Advantages: Sp6 Promoter for mMessage mMachine Kit; PolyA tail already present**

Optional:

- Transformation, midi, glycerol stock of pCS2-nCas9n for storage

**pCS2-nCas9n linearisation**

Thermo:		NEB:	
5 µg	pCS2-nCas9n	5 µg	pCS2-nCas9n
5 µl	Buffer O (10x, orange)	5 µl	Cut-Smart buffer (NEB)
0.5 µl	NotI (10 U/µl)	0.5 µl	NotI (5U, NEB)
Fill up to 50 µl	dH <sub>2</sub> O	Fill up to 50 µl	dH <sub>2</sub> O

- Incubate o/n (but at least 2h) at 37°C
- Heat inactivate for 15 min at 65°C
- Check linearisation on gel: 0.8% agarose (in TAE), 2 µl lin. Vector, 1kb ladder, 120 V, 40 min
  - Don't forget unlinearised vector as control
    - If linearisation worked: Band at 8272 bp
- Prepare 2<sup>nd</sup> gel for gel extraction:
  - 0.8% agarose (in TAE), 1kb ladder, 120 V, 40 min
  - split 45 µl of linearisation reaction evenly in pockets, cut 8272 bp bands and pool them for better yields after gel extraction
- Purify with GenElute Gel Extraction kit, elute in 40 µl dH<sub>2</sub>O
  - *This step is necessary to avoid transcription of any unlinearised plasmid DNA. Otherwise RNA transcribed from unlinearised plasmid will cloud the real yield of transcribed gRNA which is very short compared to RNA strand from unlinearised plasmid.*

**In vitro transcription into Cas9 mRNA**

Use SP6 mMessage mMachine Kit (Invitrogen):

2 µl	SP6 RNA polymerase
1 µg	Linearised pCS2-nCas9n
(1 µl	RNase inhibitor)
2 µl	10x Reaction buffer
10 µl	2x NTP/CAP
Fill up to 20 µl	dH <sub>2</sub> O

Pipette from bottom up and keep reaction buffer at RT; rest on ice; RNase inhibitor not part of Invitrogen protocol, therefore, optional

- Incubate for 2h at 37°C
- Add 1 µl of DNaseI (RNase free, Roche) and incubate for 15 min at 37°C



---

**Purification - Phenol/ Chloroform extraction**

- *Make sure to use Phenol:Chloroform:Isoamylalcohol (in water → pH 4.5, Roth) for RNA extraction*
    - *Do not use Roti Phenol (Roth, TE buffered → pH 7.5) → only for DNA extraction!*
    - *Phenol pH importance for extraction:*
      - *low pH for RNA: DNA is enriched in protein interphase and organic phase, leads to less DNA contamination of aqueous phase for RNA extraction*
      - *High pH for DNA: partitioning of DNA into organic phase is suppressed. Leads to accumulation of both RNA and DNA in aqueous phase*
  - Add 30 µl dH<sub>2</sub>O (RNase free) to reaction mix
  - Add 1 volume (50 µl) of P:C:I solution to transcription reaction (50 µl), mix vigorously
  - Centrifuge for 5 min at max. speed
  - Transfer aqueous (upper) phase to new Eppi
  - Add 1 volume of chloroform (for RNA extraction), mix vigorously
  - Centrifuge for 5 min at max. speed
  - Transfer aqueous (upper) phase to new Eppi
  - Precipitate RNA by adding 1 Volume of 100% isopropanol, mix vigorously
  - Incubate mix at -20°C for 1h
  - Centrifuge for 15 min at max. speed at 4°C
  - Carefully remove supernatant
  - Wash pellet in 100% EtOH
  - Centrifuge for 10 min at max. speed at 4°C
  - Carefully remove supernatant
  - Dry pellet at 42°C, check regularly (don't incubate for longer than 10 min)
  - Resuspend pellet in 25 µl dH<sub>2</sub>O (RNase free)
    - If pellet doesn't dissolve, incubate for 30 sec at 42°C
  - Measure concentration at nanodrop
    - If concentration is high make working stock dilution
  - Store stock solution at -80°C and working stock at -20°C
-

- 
- Check RNA on gel: 1% agarose (in TAE), 1 kb ladder, 120 V, 40 min

2 µl	working stock RNA
5 µl	dH <sub>2</sub> O (RNase free)
1 µl	6x DNA loading dye

Optional:

- Option 1: RNeasy Kit (Qiagen)
- Option 2: Lithium Chloride (LiCl) precipitation

is a convenient and effective way to remove unincorporated nucleotides and most proteins. Lithium chloride precipitation, however, does not precipitate transfer RNA and may not efficiently precipitate RNAs smaller than 300 nucleotides. Also, the concentration of RNA should be at least 0.1 µg/µL to assure efficient precipitation. To precipitate from mMESSAGE mMACHINE® reactions that are thought to have relatively low yields of RNA, do not dilute the transcription reaction with water prior to adding the LiCl Precipitation Solution the first substep below.

- Stop the reaction and precipitate the RNA by adding 30 µL Nuclease-free Water and 30 µL LiCl Precipitation Solution
  - mix thoroughly. Chill for ≥30 min at –20°C
  - Centrifuge at 4°C for 15 min at maximum speed to pellet the RNA.
  - Carefully remove the supernatant. Wash the pellet once with ~1 mL 70% ethanol, and recentrifuge to maximize removal of unincorporated nucleotides
  - Carefully remove the 70% ethanol, and resuspend the RNA in a solution or buffer† appropriate for your application. Determine the RNA concentration and store frozen at –20°C or –80°C
  - Measure concentration (1µl) and check on gel (2µl RNA mit 7µl ddH<sub>2</sub>O and 1µl RNA loading buffer (Ambion); incubate 10min at 80°C before loading on gel)
-

---

## Microinjections

Cas9 mRNA injection mix:		Cas9 protein (M0646T, NEB) injection mix	
400 ng/μl	Cas9 mRNA	300 ng/μl	Cas9 protein (NEB)
25-100 ng/μl	gRNA	25-100 ng/μl	gRNA
Fill up to 5 μl	dH <sub>2</sub> O (RNase free)	Fill up to 5 μl	dH <sub>2</sub> O (RNase free)

- Try both 25 and 100 ng/μl gRNA concentrations to start with
- Adjust water in case of coinjection of several gRNAs
- Always prepare a Cas9 control injection mix w/o gRNA
- Inject at 1 cell stage into the cell not into the yolk
- Fix embryos for functional control at 3dpf or later in 4% PFA, store at -20°C in 100% MeOH

## Functional control

### *PK treatment*

- Use embryos in 100% MeOH or do MeOH row
- Place embryos into PCR tubes (1 embryo/ tube)
- Remove as much MeOH as possible
- Dry embryos by incubating 5 min at 95°C
  - *The cover was removed from the PCR tubes and the lid of the thermocycler was left open, to allow the MeOH to evaporate.*
- Add 12.5 μl TE buffer containing 200 μg/ ml PK
- Incubate for 4h at 55°C and heat inactivate for 10 min at 95°C using a thermocycler.
- Add 37.5 μl dH<sub>2</sub>O (final volume 50 μl)
- Store gDNA at -20°C

### **Genotyping - PCR reaction**

- Choose primers from ChopChop suggestions flanking the target site (small product sizes)
-

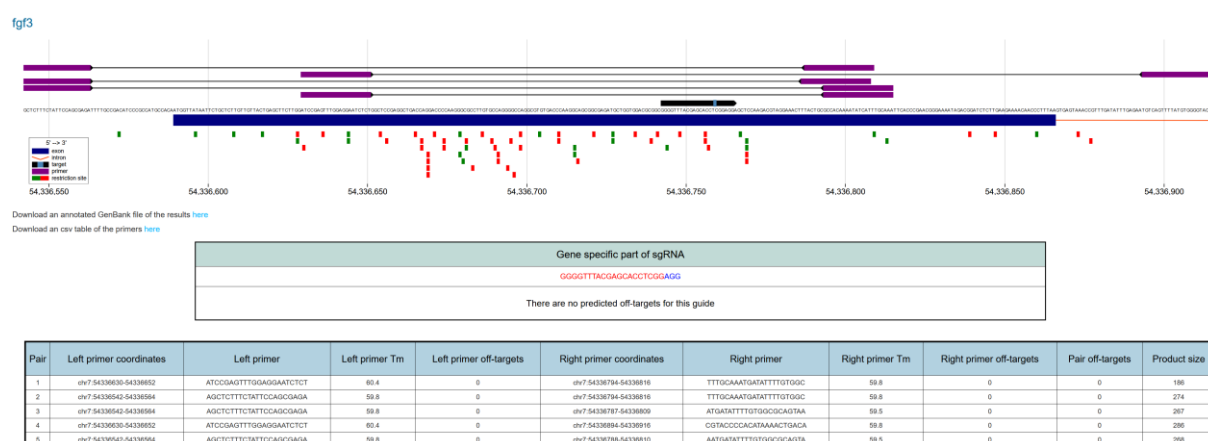


Fig. 38: Screenshot of ChopChop web page, *fgf3* gRNA target site example. (Labun et al., 2016; Labun et al., 2019; Montague et al., 2014)

Promega Go taq: 95°C Pause  
 3 µl gDNA 95°C 2 min  
 10 µl 10x reaction buffer 95°C 1 min  
 3 µl MgCl<sub>2</sub> (50 mM) 30 sec  
 1 µl dNTPs (10 mM) 72°C 30 sec x35 cycles  
 1 µl Fwd primer (10 µM) 72°C 7 min  
 1 µl Rev primer (10 µM) 10°C pause  
 0.25 µl Go taq  
 30.75 µl dH<sub>2</sub>O

- Check PCR reaction on gel: 3% high resolution agarose (3:1 NuSieve Lonza) (in TBE), 10 µl product, 100 bp ladder, 120 V, 1 h 30 min
  - o Special agarose allows discrimination between In/ Del bands
  - o Expected are bands which are ~25 bp bigger or smaller than WT band due to In/ Dels

## BrdU labelling

- Prepare 10 mM BrdU solution one day prior to BrdU pulse:
    - BrdU takes time to dissolve
    - Use heat block at 37°C with shaking
    - Weigh 15 mg BrdU (B5002, Sigma-Aldrich) for 5 ml final solution
    - Prepare 15% DMSO in Danieau's solution (w/o methylene blue)
    - Add 1 ml 15% DMSO to tube containing 15 mg BrdU and incubate on heat block with shaking for at least 5 min
    - Transfer supernatant (no undissolved BrdU) to Falcon tube
    - Add 1 ml 15% DMSO to undissolved BrdU and repeat procedure until BrdU is completely dissolved (do not exceed 5 ml)
    - Fill up to 5 ml final volume with 15% DMSO and store at 4°C for no longer than one night
    - Keep 50 ml Danieau's solution at 28°C o/n in incubator to warm up
  - Next day:
    - Dechorionate embryos
    - Add ice cold BrdU solution into small petri dish. Keep dish on ice
    - Carefully add dechorionated embryos without adding too much fluid to BrdU solution
    - Incubate for 20 min on ice
    - Transfer embryos (and as little BrdU solution as possible) to petri dish (not on ice) containing 28°C warm Danieau's solution and rinse embryos a few times with warm Danieau's solution
    - Let embryos recover in Danieau's solution for 20 min at 28°C
    - Fix or leave in incubator for chase period
-

### Acridine Orange staining

- Prepare 1000x stock solution of 5 mg/ml Acridine Orange (AO) in ddH<sub>2</sub>O and store at RT. Protect from light by wrapping Falcon tube in aluminium foil
- Dechorionate embryos
- Add 5 µl AO stock solution to 5 ml Danieau's solution (w/o methylene blue) in small petri dish, swirl to mix
- Transfer embryos to AO solution without adding too much fluid
- Wrap small petri dish in aluminium foil and incubate embryos in darkness for 30 min at RT
- Transfer embryos (and as little AO solution as possible) to big petri dish containing Danieau's solution and rinse embryos a few times with warm Danieau's solution. Work fast to prevent bleaching in light
- Image live embryos immediately under GFP filter
- Use 3% methylcellulose to immobilise embryos during imaging

50 ml 3% methylcellulose:

To 25 ml	Danieau's solution
Add 1.5 g	methylcellulose
And 25 ml	Danieau's solution

- Keep on shaker at 4°C o/n or longer, dissolves very slowly
  - When dissolved store at 4°C
-

## Immunohistochemistry

### 5-HT/TH1 whole-mount immunohistochemistry

- Start with embryos stored in 100% MeOH
- Rehydrate embryos in reverse MeOH row in PBT
 

75%	MeOH	1x	5 min
50%	MeOH	1x	5 min
25%	MeOH	1x	5 min
100%	PBT	2x	5 min
- Embryos at 72 hpf or older: Dissect brain free of skin, eyes and jaw to allow better penetration of reagents; remove yolk to mount embryos easier for imaging
- Incubate in blocking buffer for 2 h at room temperature with slow shaking
 

Blocking buffer 1– 50 ml final volume:			
5 ml	2% NSS		
100 mg	BSA - Albumin Fraction V		
	(PanReac AppliChem, A1391)		
Fill up to 50 ml	PBT		
- Incubate in primary AB in blocking buffer for 3 days at 4°C in darkness with slow shaking
 

α-5-HT	rabbit:	1:1000
α-TH1	mouse:	1:500
- Wash 4x 5 min in PBT with slow shaking
- Keep dark from now on: Incubate in secondary AB in blocking buffer for 2 days at 4°C with slow shaking
 

α-rabbit IgG Alexa Fluor 488:	1:1000
α-mouse IgG Alexa Fluor 568:	1:1000
- Wash 6x 5 min in PBT with slow shaking
- Store in 80% glycerol in PBT at 4°C

## BrdU whole-mount immunohistochemistry

## Special solutions to prepare for this protocol:

2 N HCl - 25 ml final volume:		0.1 M sodium tetraborate, pH 8.5 – 500 ml final volume:	
Water before acid!!		190.69 g	Na <sub>2</sub> B <sub>4</sub> O <sub>7</sub> · 10 H <sub>2</sub> O
Add ~15 ml	ddH <sub>2</sub> O to falcon tube	Fill up to 500 ml	H <sub>2</sub> O
4.16 ml	HCl 37% (12 M)		
Fill up to 25 ml	ddH <sub>2</sub> O		

- Start with embryos stored in 100% MeOH
- Rehydrate embryos in reverse MeOH row in PBT
 

75%	MeOH	1x	5 min
50%	MeOH	1x	5 min
25%	MeOH	1x	5 min
100%	PBT	2x	5 min
- Embryos at 72 hpf or older: Dissect brain free of skin, eyes and jaw to allow better penetration of reagents; remove yolk to mount embryos easier for imaging
- Permeabilise embryos in 10 µg/ml proteinase K in PBT:
 

36 hpf	20 min
72 hpf (dissected)	25 min
- Wash 1x quickly and 2x, 5 min in PBT
- Refix in 4% PFA for no longer than 20 min
- Washes: Do not invert the tube – not at all! Embryos will stick to the wall, let them stick and gently remove and apply solutions.
 

100%	ddH <sub>2</sub> O	3x	quickly
2 N	HCl	2x	quickly
- Incubate in 2 N HCl for 1 h to denature DNA, thereby, exposing the BrdU epitope
- Remove 2 N HCl solution and neutralise with 0.1 M sodium tetraborate buffer, pH 8.5 for 20 min
- Wash 4x 5 min in PBT
- Incubate in blocking buffer for 1 h at room temperature with slow shaking
 

Blocking buffer 2– 50 ml final volume:	
Add DMSO to PBT before NSS and BSA otherwise NSS will denature	
Add ~30 ml	PBT
1% (500 µl)	DMSO
5 ml	2% NSS
100 mg	BSA - Albumin Fraction V (PanReac AppliChem, A1391)
- Incubate in primary AB in blocking buffer for 3 days at 4°C in darkness with slow shaking



---

Apply AB pairs together: BrdU/phH3 or BrdU/5-HT

$\alpha$ -5-HT	rabbit:	1:1000
$\alpha$ -BrdU	rat:	1:200
$\alpha$ -phH3	rabbit:	1:300

- Wash 5x 10 min in PBT with slow shaking
- Keep dark from now on: Incubate in secondary AB in blocking buffer for 2 days at 4°C with slow shaking

$\alpha$ -rabbit IgG Alexa Fluor 488:	1:1000
$\alpha$ -mouse IgG Alexa Fluor 568:	1:1000

- Wash 5x 10 min in PBT with slow shaking
  - Store in 80% glycerol in PBT at 4°C
-

## cCasp3 whole-mount immunohistochemistry

- Start with embryos stored in 100% MeOH
  - Directly transfer embryos from 100% MeOH to 100% acetone and incubate for 7 min at -20°C
  - Rehydrate embryos in 50% MeOH in PBT for 1 h at -20°C
  - Wash 1x quickly in H<sub>2</sub>O and 4x 5 min in PBT
  - Block with blocking buffer for 1 h at RT with slow shaking
    - Blocking buffer 2– 50 ml final volume:
    - Add DMSO to PBT, only then NSS, BSA
    - otherwise NSS will denature
    - Add ~30 ml PBT
    - 1% (500 µl) DMSO
    - 5 ml 2% NSS
    - 100 mg BSA - Albumin Fraction V
    - (PanReac AppliChem, A1391)
  - Incubate in primary AB in blocking buffer for 3 days at 4°C with slow shaking
    - α-cCasp3 rabbit: 1:500
  - Wash 4x 5 min in PBT
  - Keep dark from now on: Incubate in secondary AB in blocking buffer for 2 days at 4°C in darkness with slow shaking
    - α-rabbit IgG Alexa Fluor 488: 1:1000
  - Wash 4x 5 min in PBT
  - Store in 80% glycerol in PBT at 4°C
-

---

## pErk whole-mount immunohistochemistry

- Start with embryos stored in 100% MeOH
  - Directly transfer embryos from 100% MeOH to 100% acetone and incubate for 7 min at -20°C
  - Rehydrate embryos in 50% MeOH in PBT for 1 h at -20°C
  - Wash 1x quickly in H<sub>2</sub>O and 4x 5 min in PBT
  - Incubate in blocking buffer for 1 h at RT with slow shaking
    - Blocking buffer – 50 ml final volume:
      - Add DMSO to PBT before NSS and BSA otherwise NSS will denature
      - Add ~30 ml PBT
      - 1% (500 µl) DMSO
      - 5 ml 2% NSS
      - 100 mg BSA - Albumin Fraction V (PanReac AppliChem, A1391)
  - Incubate in primary AB in blocking buffer for 3 days at 4°C with slow shaking
    - α-pErk rabbit: 1:500
  - Wash 4x 5 min in PBT
  - Keep dark from now on: Incubate in secondary AB in blocking buffer for 2 days at 4°C in darkness with slow shaking
    - α-rabbit IgG Alexa Fluor 488: 1:1000
  - Wash 4x 5 min in PBT
  - Store in 80% glycerol in PBT at 4°C
-

DIG/fluor labelling of RNA probe for *in situ* hybridisation

- Start with plasmid DNA of mini/ midi prep
- Linearisation of plasmid:
 

	Linearisation mix – work on ice	
~5 µg	DNA	
2.5 µl	Restriction enzyme (10U/µl)	
5 µl	10x buffer	
Fill up to 50 µl	ddH <sub>2</sub> O, RNase-free	
- Mix and spin down
- Incubate for 2 h at 37°C in heat block
- Check linearisation on gel before stopping the reaction
  - 1% agarose in TAE, 2 µl lin. vector, 1 µl unlinearised plasmid as control, 1kb ladder, 120 V, 40 min
- Purify linearised DNA with GenElute PCR Clean-up Kit (Sigma-Aldrich)
  - Elute in 40 µl warm (65°C) ddH<sub>2</sub>O, RNase-free; incubate H<sub>2</sub>O in column for 2 min, then spin down and re-elute with spun down product to increase yield
  - Alternative: Phenol-Chloroform extraction
    - Fill up linearisation mix to 200 µl with ddH<sub>2</sub>O, RNase-free
    - Add 100 µl Roti-Phenol and 100 µl chloroform
    - Vortex and centrifuge for 5 min at maximum speed
    - Transfer upper, aqueous phase to new tube
    - Add 100 µl chloroform
    - Vortex and centrifuge for 5 min at maximum speed
    - Transfer upper, aqueous phase to new tube (note transferred volume, ~ 190 µl)
    - Add  $\frac{1}{10}$  of volume (19 µl) 3 M NaOAc and 2x the volume (380 µl) 100% EtOH
 

3 M NaOAc – 10 ml final volume	
2.46 g	NaOAc
Fill up to 10 ml	ddH <sub>2</sub> O, RNase-free
    - Precipitate at -20°C minimum 2 h better o/n
    - Centrifuge for 15 min at 4°C at maximum speed

- 
- Remove supernatant and wash pellet with 100 µl 75% EtOH
    - Centrifuge for 15 min at 4°C at maximum speed
    - Dry pellet and resuspend in 20 µl ddH<sub>2</sub>O, RNase-free
    - Measure on NanoDrop or check on gel: 1% agarose in TAE, 5 µl lin., purified vector, 1kb ladder, 120 V, 40 min
  - *In vitro* transcription and RNA probe labelling
    - Reaction mix – work on ice
      - 2 µl 10x transcription buffer
      - 2 µl DIG or fluo RNA labelling mix (Roche)
      - 0.5 µl RNase inhibitor
      - 2 µl Linearised, purified vector DNA
      - 11.5 µl ddH<sub>2</sub>O, RNase-free
      - 1 µl RNA polymerase (T7, T3 or SP6)
    - Mix and spin down
    - Incubate for 2 h at 37°C in heat block
    - Add 1 µl DNase I recombinant, RNase-free (Roche)
    - Mix and spin down
    - Incubate for 30 min at 37°C
  - Purification of RNA probe by precipitation
    - Add 30 µl TE buffer, pH 8.0; now total volume is 50 µl
    - Add  $\frac{1}{10}$  of volume (5 µl) 4 M LiCl and 3x the volume (150 µl) 100% EtOH
      - 4 M LiCl – final volume 10 ml
      - 1.70 g LiCl
      - Fill up to 10 ml ddH<sub>2</sub>O, RNase-free
      - Aliquot into 1.5 ml tubes
    - 
    - Precipitate at -20°C o/n
    - Centrifuge for 15 min at 4°C at maximum speed
    - Remove supernatant and wash pellet with 100 µl 75% EtOH
    - Centrifuge for 15 min at 4°C at maximum speed
    - Dry pellet and resuspend in 40 µl ddH<sub>2</sub>O, RNase-free
    - Check on gel: 1% agarose in TAE, 3 µl probe to 0.5 µl loading dye, 100 bp ladder, 120 V, 10 min
    - Store RNA probe at -80°C
-

Whole-mount RNA *in situ* hybridisation

## Day 1

- Heat water bath to 65°C
- Start with embryos stored in 100% MeOH
- Rehydrate embryos in reverse MeOH row in PBT
 

75%	MeOH	1x	5 min
50%	MeOH	1x	5 min
25%	MeOH	1x	5 min
100%	PBT	2x	5 min
- Embryos at 4 dpf or older: Dissect brain free of skin, eyes and jaw to allow better penetration of reagents; remove yolk to mount embryos easier for imaging
- Transfer embryos into 24 well plate
  - o From now on be careful not to dry out embryos by removing too much solution, leave rather more than too few fluid in well!!!
- Permeabilise embryos in 10 µg/ml proteinase K (PK) in PBT:
 

<10 somites	no PK, continue with PFA
10-20 somites	3 min
24-28 hpf	5 min
28-32 hpf	10 min
32-36 hpf	15 min
36-48 hpf	20 min
48-58 hpf	25 min
58-72 hpf	30 min
72 hpf	40 min
Dissected brains ≥4 dpf	no PK, continue with PFA
Dissected adult brains	45 min
- Wash 2x 2 min in PBT, no shaking, fragile embryos after PK treatment
- Refix in 4% PFA for 20 min, no shaking
- Wash 4x 5 min in PBT with slow shaking
- Prepare and store hybridisation buffers at -20°C

Hybridisation buffer – 50 ml final volume

32.5 ml	Formamide
12.5 ml	20x SSC
100 µl	Heparin 5000U/ml
250 mg	Torlua yeast RNA
250 µl	20% Tween 20
250 µl	0.5 M citric acid, pH 6.0
Fill up to 50 ml	ddH <sub>2</sub> O

Hybridisation wash buffer (-RNA and Heparin) – 50 ml final volume

For stringency washes on Day 2

32.5 ml	Formamide
12.5 ml	20x SSC
250 µl	20% Tween 20
250 µl	0.5 M citric acid, pH 6.0
Fill up to 50 ml	ddH <sub>2</sub> O

- Prehybridisation in 500 µl hybridisation buffer (hyb buffer) for 1 h at 65°C with slow shaking
  - o Put 24 well plate with embryos in hyb buffer into humid chamber (plastic box with wet paper), then place chamber into water bath
- Hybridisation with antisense RNA probe: Dilute and keep probes on ice before application. Use 1 µl probe/100 µl hyb buffer, apply 300 µl/well. Incubate o/n at 65 °C with slow shaking.
- Prepare solutions for stringency washes on Day 2, keep o/n in water bath
  - o use hybridisation wash buffer (-RNA and heparin)

## Day 2

- Recycle probes and store at -20°C to reuse in next ISH
- Stringency washes with slow shaking:
 

75% hyb buffer: 25% 2x SSC	65°C	10 min
50% hyb buffer: 50% 2x SSC	65°C	10 min
25% hyb buffer: 75% 2x SSC	65°C	10 min
2x SSC (5 ml 20x SSC to 45 ml H <sub>2</sub> O)	65°C	10 min
0.05x SSC (250 µl 2x SSC to 10 ml H <sub>2</sub> O)	65°C	2x 30 min
0.05x SSC: 50% PBT	RT	5 min
100% PBT	RT	2x 5 min
- Incubate in blocking buffer for 1 h at RT with slow shaking
 

Blocking buffer – 50 ml final volume:		
1 ml	2% NSS	
100 mg	BSA - Albumin Fraction V	
	(PanReac AppliChem, A1391)	
Fill up to 50 ml	PBT	
- Incubate in primary AB in blocking buffer for 2 h at RT with slow shaking (or o/n at 4°C)
 

Single ISH		Double ISH	
α-DIG-AP	1:5000	α-fluo-AP	1:2000
- Wash in PBT 3x 5 min, 6x 10 min and o/n at 4°C with slow shaking

## Single ISH - Day 3

- Prepare fresh NTMT solution every time and keep on ice, redo if solution turns out milky or cloudy, NTMT must be crystal clear
 

NTMT – 50 ml final volume:	
5 ml	1 M Tris-base, pH 9.5
2.5 ml	1 M MgCl <sub>2</sub>
1 ml	5 M NaCl
250 µl	20% Tween 20
Fill up to 50 ml	ddH <sub>2</sub> O

- Switch from PBT to NTMT: remove as much PBT from well w/o embryos drying, apply a little bit of NTMT, remove NTMT directly and reapply fresh NTMT, do not switch PBT to NTMT in more than 2 wells at the same time. Like this precipitation of NTMT is avoided.
- Wash 3x 10 min in NTMT at RT with slow shaking
- From now on keep 24 well plate dark, wrap in aluminium foil
- Prepare fresh NBT/BCIP solution every time and keep on ice and dark, wrapped in aluminium foil

NBT/BCIP solution – 10 ml final volume:  
 Keep dark and on ice, wrap in aluminium foil  
 10 ml NTMT  
 200 µl NBT/BCIP stock solution

- Reveal transcripts with NBT/BCIP solution at RT: apply 500 µl NBT/BCIP solution/ well. Exchange NBT/BCIP solution regularly and monitor staining intensity carefully
- Wash in PBT, 4x 5 min at RT and o/n at 4°C

#### Single ISH - Day 4

- Post-fix in 4% PFA for 20 min at RT with slow shaking
- Wash 4x 5 min in PBT with slow shaking
- Store in 80% glycerol in PBT at 4°C

#### Double ISH - Day 3

- Prepare either Domingo's buffer or 0.1 M Tris buffer (both work):

Domingo's buffer, pH 8.2 – 100 ml final volume	0.1 M Tris buffer, pH 8.2 – 100 ml final volume
8 ml 5 M NaCl	1.21 g Tris base
1.21 g Tris base	0.1% (100 µl) 20% Tween 20
Fill up to 100 ml ddH <sub>2</sub> O	Fill up to 100 ml ddH <sub>2</sub> O

- Dissolve 1 Fast Red tablet in 10 ml of one buffer, keep solution dark, wrap in aluminium foil
  - o After dissolving tablet sterile filter Fast Red solution!
- Switch from PBT to Domingo's or Tris buffer: remove as much PBT from well w/o embryos drying, apply a little bit of buffer, remove buffer directly and reapply fresh buffer, do not switch PBT to buffer in more than 2 wells at the same time. Like this precipitation is avoided.
- Wash 3x 10 min in Domingo's or Tris buffer at RT with slow shaking
- From now on keep 24 well plate dark, wrap in aluminium foil



- Reveal transcripts with Fast Red solution at RT: apply 500 µl Fast Red solution/ well. Exchange Fast Red solution regularly and monitor staining intensity carefully, almost overstain sample with Fast Red because staining will fade during washes and DIG staining is very intense
- Wash 4x 5 min in PBT at RT
- Detach  $\alpha$ -fluor AB by incubating 2 h at 65°C in water bath (with 24 well plate in humid chamber) or heat block (in tubes)
  - Alternative: detach AB by incubating 3x 10 min in 0.1 M Glycine, pH 2.0
 

0.1 M Glycine, pH 2.0 – 100 ml final volume:	
0.75 g	glycine
80 ml	H <sub>2</sub> O
Adjust pH with	37% HCl
Fill up to 100 ml	ddH <sub>2</sub> O
- Incubate in blocking buffer (recipe Day 2) for 1 h at RT with slow shaking
- Incubate in primary AB in blocking buffer for 2 h at RT with slow shaking (or o/n at 4°C)
 

Double ISH	
$\alpha$ -DIG-AP	1:5000
- Wash in PBT 3x 5 min, 6x 10 min and o/n at 4°C with slow shaking

#### Double ISH – Day 4

- Prepare fresh NTMT solution every time and keep on ice, redo if solution turns out milky or cloudy, NTMT must be crystal clear
 

NTMT – 50 ml final volume:	
5 ml	1 M Tris-base, pH 9.5
2.5 ml	1 M MgCl <sub>2</sub>
1 ml	5 M NaCl
250 µl	20% Tween 20
Fill up to 50 ml	ddH <sub>2</sub> O
- Switch from PBT to NTMT: remove as much PBT from well w/o embryos drying, apply a little bit of NTMT, remove NTMT directly and reapply fresh NTMT, do not switch PBT to NTMT in more than 2 wells at the same time. Like this precipitation of NTMT is avoided.
- Wash 3x 10 min in NTMT at RT with slow shaking
- Prepare fresh NBT/BCIP solution every time and keep on ice and dark, wrapped in aluminium foil
 

NBT/BCIP solution – 10 ml final volume:	
Keep dark and on ice, wrap in aluminium foil	
10 ml	NTMT
200 µl	NBT/BCIP stock solution

- Reveal transcripts with NBT/BCIP solution at RT: apply 500 µl NBT/BCIP solution/ well. Exchange NBT/BCIP solution regularly and monitor staining intensity carefully to not overstain sample thereby hiding Fast Red staining
- Wash in PBT, 4x 5 min at RT and o/n at 4°C

#### **Double ISH – Day 5**

- Post-fix in 4% PFA for 20 min at RT with slow shaking
  - Wash 4x 5 min in PBT with slow shaking
  - Store in 80% glycerol in PBT at 4°C
-

---

## Cryosections

- Start with embryos in tube containing PBT
  - Wash 1x 5 min in PBS
  - Wash 1x 5 min in 15% sucrose solution (store at 4°C for short while)
    - 15% sucrose solution – final volume 50 ml
    - 7.5g sucrose
    - Fill up to 50 ml PBS
    - Do not autoclave, sucrose will be precipitated as caramel
  - Cryoprotect embryos in 15% sucrose solution o/n at 4°C
  - Prepare gelatine-sucrose solution:
    - Gelatine - sucrose solution – final volume 100 ml
    - 7.5 % (7.5 g) gelatine 300 Bloom
    - 15% sucrose (15 g) sucrose
    - Fill up to 50 ml PBS
    - Dissolve at 65°C (water bath), store 50 ml aliquots at -20°C
  - Coat small plastic weighing pan in 100% glycerol (1 drop is sufficient)
  - Warm up gelatine-sucrose solution in water bath
  - Fill up half of weighing pan with liquid gelatine-sucrose, cool down at 4°C until gelatine-sucrose is solid
  - Keep gelatine-sucrose solution in water bath at ~40°C not warmer
  - Add cryoprotected embryo to solid gelatine-sucrose in weighing pan
    - keep weighing pan under binocular cool by placing on precooled metal block
  - Remove all excess sucrose solution around embryo with paper towel and position embryo parallel to one edge in the middle of the weighing pan
  - Fill up rest of weighing pan with warm gelatine-sucrose solution
  - Carefully transfer weighing pan at 4°C, check if embryo is still in position if not correct position
  - Cut small cork squares, one for each block of gelatine
  - Pour 300 ml 2-methylbutane into beaker and place beaker in tank with liquid nitrogen, cool down until 2-methylbutane starts freezing on the bottom of the beaker (white spots), work under hood!!
  - Once gelatine has become solid, remove gelatine from weighing pan and cut out a rectangular block containing the embryo
-

- Glue embryo in block perpendicular to cork square with tissue tek, mark ventral side of embryo on cork for cutting later since embryo will not be visible after snap freezing
  - Use long forceps to dip cork square with glued on gelatine block into 2-methylbutane for 10 sec, recycle 2-methylbutane
  - Transfer block immediately at -20°C for short term storage (<1 h)
  - Store long term at -80°C (~2-3 weeks)
  
  - When cryosectioning transport gelatine blocks in dry ice to avoid melting
    - immediately place blocks into cryostat
    - take knife, brushes, old forceps, SuperFrost slides, tissue tek and pencil and place and cool knife, brushes, slides, and forceps in cryostat
  - Keep cryostat box at -29°C and object temperature at -25°C
  - Cut 20 µm sections
  - After block is in position for cutting, wait 30 min before starting the cutting to allow block to properly cool down
-

---

## Sample preparation for RNA sequencing

- Prepare slicing solution and keep at 4°C:

Slicing solution - final volume 1 l		
234 mM	80.1 g	sucrose
11 mM	1.98 g	D-glucose
2.5 mM	2.5 ml	1 M KCl
1.25 mM	172.5 mg	NaH <sub>2</sub> PO <sub>4</sub>
0.5 mM	73.5 mg	CaCl <sub>2</sub>
2 mM	2 ml	1 M MgSO <sub>4</sub>
26 mM	2.18 g	NaHCO <sub>3</sub>
Fill up to 1 l		ddH <sub>2</sub> O

Do not autoclave, sucrose will be precipitated as caramel

- Place small petri dish with slicing solution in big petri dish filled with ice to keep solution cool and embryos tranquilised during dissections
    - o Use a second small/big petri dish and transfer dissected brain over to this one to dissect hypothalamus in fresh medium. Like this contaminations from other parts of the embryos are avoided
  - Add 50 µl RNA later stabilisation solution to tube to collect and store hypothalamic tissue in
  - Add embryo to ice cold slicing solution, wait 1 min before dissecting
  - Dissect whole brain then cut off hypothalamus with super fine forceps
  - Extract dissected hypothalamus using capillary with suction pommel at the end
  - Transfer to tube with RNAlater
  - Collect at least 30 hypothalami/tube for sufficient quantity (~100 ng) after RNA extraction
  - Store tissue in RNAlater at -80°C
  - RNA extraction with RNeasy Mini Kit (Qiagen)
    - o Follow Qiagen manual – animal tissue
    - o Use needle (20 G 1½ (0.9x40 mm) Braun) and syringe to homogenise
    - o Elute in 40 µl ddH<sub>2</sub>O, RNase-free, reapply eluate and spin down spin down again to increase yield
-

## Publication list

**Reuter I., Jäckels J., Kneitz S., Kuper J., Lesch K.-P., & Lillesaar C.** (2019). Fgf3 is crucial for the generation of monoaminergic cerebrospinal fluid contacting cells in zebrafish. *Biology open*

**Reuter I., Knaup S., Romanos M., Lesch K.-P., Drepper C., & Lillesaar C.** (2016). Developmental exposure to acetaminophen does not induce hyperactivity in zebrafish larvae. *Journal of neural transmission (Vienna, Austria: 1996)*, 123(8), 841–848

---

## Curriculum Vitae

---







### **Acknowledgement/ Danksagung [ger]**

Die letzten Jahre und die vorliegende Arbeit, als Produkt dieser Zeit, wären ohne Rat, Unterstützung, sowie viele helfende Hände und Köpfe nicht möglich gewesen. Dafür möchte ich mich gerne bedanken.

Allen voran bei meinem Thesiskomitee:

Bei meinem Erstbetreuer Prof. Lesch, für die bereitwillige Übernahme dieser Aufgabe, sowie die fachlichen Ratschläge und finanzielle Unterstützung, die für das Gelingen dieser Arbeit unerlässlich waren.

Bei Dr. Lillesaar, ohne deren essentielle Betreuung es diese Arbeit nicht geben würde; für die Möglichkeit das Projekt nach der Masterarbeit in ihrer Gruppe weiterführen und soweit das in der Wissenschaft erreichbar ist, zu einem Abschluss bringen zu können. Ich bedanke mich für die Offenheit und Geduld mit denen meine Fragen diskutiert oder beantwortet wurden, sowie die Gestaltungsfreiheit in dieser Zeit. Sei sie experimenteller, geistiger oder zeitlicher Natur gewesen.

Bei Prof. Scharrtl und Prof. Romanos, für die Mitgliedschaft in meinem Thesiskomitee und wissenschaftliche Ratschläge und Ideen; Prof. Scharrtl danke ich für die Übernahme als Zweitgutachter und das Bereitstellen der Räumlichkeiten wie Labor, Büro und fish facility.

Für den Großteil der Finanzierung dieser Arbeit durch das Doktorandenstipendium danke ich der GSLS, sowie für das Kursangebot und den organisatorischen Rahmen in Form des Doktorandenprogramms.

Dank gilt auch allen ehemaligen und jetzigen Mitarbeitenden der AG Lillesaar und der Lehrstühle physiologische Chemie und molekulare Psychiatrie, sowie den Fischen.

---

Insbesondere bedanke ich mich bei meinen Kollaborationspartnern Dr. Kneitz und Dr. Kuper, deren Beiträge für wichtige Erkenntnisse in dieser Arbeit gesorgt haben. Bei Jana möchte ich mich für ihre tatkräftige Unterstützung bei der Durchführung von essentiellen Versuchen bedanken.

Außerdem bedanke ich mich bei Carina, Teresa, Jana, Freddy, Moritz und Lina für Kaffeepausen, Zuhören, Zuarbeiten, Zudenken, Freizeit, eine gehörige Portion Humor und noch so viel mehr; Kriterien, die ich sehr schätze und maßgeblich das Gelingen dieser Arbeit beeinflusst haben – positiv, versteht sich.

Danke an das Kompetenzteam aus Raum B236 – Barbara, Martina, Janine und Verena. Es war ein unvergessliches Fest; danke, dass ihr mitgefeiert, gefiebert und gepanzert habt.

Zuletzt gilt mein Dank allen Freunden, den bereits erwähnten und besonders auch denen, die unerwähnt bleiben sollen, sowie meiner Familie und Eltern. Das dieses Unterfangen durchgeführt und in diesem Abschluss gipfeln konnte, ist eurer Unterstützung zu verdanken. Ihr seid Teil meines Fundamentes, das durch euch stabil bleibt, egal woher oder wie stark der Wind auch weht.

Danke!

---

### **Affidavit [en]**

I hereby confirm that my thesis entitled 'Development and function of monoaminergic systems in the brain of zebrafish' is the result of my own work. I did not receive any help or support from commercial consultants. All sources and/or materials applied are listed and specified in the thesis.

Furthermore, I confirm that this thesis has not yet been submitted as part of another examination process neither in identical nor in similar form.

Place, Date

Signature

### **Eidesstattliche Erklärung [ger]**

Hiermit erkläre ich an Eides statt, die Dissertation ‚Entwicklung und Funktion monoaminerger Systeme im Zebrafischgehirn‘ eigenständig, d.h. insbesondere selbstständig ohne Hilfe eines kommerziellen Promotionsberaters, angefertigt und keine anderen als die von mir angegebenen Quellen und Hilfsmittel verwendet zu haben.

Ich erkläre außerdem, dass die Dissertation weder in gleicher noch in ähnlicher Form bereits in einem anderen Prüfungsverfahren vorgelegen hat.

Ort, Datum

Unterschrift

---